fire

Special Issue Reprint

Cable and Electrical Fires

Edited by
Ying Zhang, Xiaoyu Ju, Xianjia Huang and Fuchao Tian

mdpi.com/journal/fire

MDPI

Cable and Electrical Fires

Cable and Electrical Fires

Guest Editors

Ying Zhang
Xiaoyu Ju
Xianjia Huang
Fuchao Tian

MDPI

Basel • Beijing • Wuhan • Barcelona • Belgrade • Novi Sad • Cluj • Manchester

Guest Editors

Ying Zhang
School of Safety Science and Emergency Management
Wuhan University of Technology
Wuhan
China

Xiaoyu Ju
State Key Laboratory of Fire Science
University of Science and Technology of China
Hefei
China

Xianjia Huang
Joint Laboratory of Nuclear Power Plant Fire Safety
Guangzhou Institute of Industry Research Co. Ltd.
Guangzhou
China

Fuchao Tian
State Key Laboratory of Coal Mine Disaster Prevention and Control
China Coal Technology and Engineering Group Shenyang Research Institute
Shenyang
China

Editorial Office
MDPI AG
Grosspeteranlage 5
4052 Basel, Switzerland

This is a reprint of the Special Issue, published open access by the journal *Fire* (ISSN 2571-6255), freely accessible at: https://www.mdpi.com/journal/fire/special_issues/WR1GFAP389.

For citation purposes, cite each article independently as indicated on the article page online and as indicated below:

Lastname, A.A.; Lastname, B.B. Article Title. *Journal Name* **Year**, *Volume Number*, Page Range.

ISBN 978-3-7258-2515-8 (Hbk)
ISBN 978-3-7258-2516-5 (PDF)
https://doi.org/10.3390/books978-3-7258-2516-5

Cover image courtesy of Ying Zhang

Contents

About the Editors

Ying Zhang

Ying Zhang, Ph.D., is a professor in the School of Safety Science and Emergency Management, Wuhan University of Technology, Wuhan, China. He studied Safety Science and Technology at the University of Science and Technology (China) and received his PhD (2012) from there. In 2015, he was named "the Hong Kong Scholar" and received a researcher position in the Hong Kong Polytechnic University (2016-2018). His research over the past few years has focused on electrical fires, including ignition and flame spread behaviors. He is also interested in the thermal safety of new energy utilization, such as with lithium-ion batteries (LIB) and photovoltaic fire safety.

Xiaoyu Ju

Xiaoyu Ju, Ph.D., is a professor in the State Key Laboratory of Fire Science at the University of Science and Technology of China. He has been awarded a research grant supported by the Chinese Academy of Sciences and started his career at USTC in 2023. In 2024, he was named as "Outstanding Young Scholar" by the National Natural Science Foundation of China (NSFC) and was promoted to a professor position. He has been focusing on fire dynamics in wildland and wildland–urban interface (WUI) fires over the past few years, including flame spread, fire whirl, firebrands, and fire emissions. He is also interested in photovoltaic fire safety and lithium-ion battery (LIB) safety. Prof. Ju has co-authored over 30 journal papers and reported his research in ISOC, IAFSS, AOSFST, ISSM, and at several other international conferences. One of his publications on flame flickering inhibition (Phys. Rev. Appl. 19 (2023) 014060) has been featured in well-known media such as the New Scientist and on APS News (front page).

Xianjia Huang

Xianjia Huang, Ph.D., is the team leader of the Joint Laboratory of Nuclear Power Plant Fire Safety, Guangzhou Institute of Industrial Technology, Guangzhou, China. His research focuses on fire safety in nuclear power plants, and is responsible for developing fire protection design software, including the fire design tools for calculating the heat release rate of cable fires (named as MOFIS-C) and zone-model fire simulations (named as MOFIS-Z). These two tools have both been approved by the Office of Nuclear Regulation, British New Reactors Division—Generic Design Assessment: Step 4 Assessment of Internal Hazards for the UK HPR 1000 Reactor—and have been successfully applied in nuclear engineering in China. He obtained a PhD in Safety Science and Engineering from the University of Science and Technology of China in 2012. He has published 19 SCI-indexed papers in fire-related fields and been granted nine invention patents as the primary inventor.

Fuchao Tian

Fuchao Tian, Ph.D., is the chief scientist at the China Coal Technology and Engineering Group (CCTEG) and the chief engineer of the Experimental Center at Shenyang Research Institute, and serves as a member of the editorial boards of both the Journal of China Coal Society and the Journal of China University of Mining & Technology. He is devoted to the prevention and control of fire and gas coupling disasters, and he has also excelled in the research and development of experimental instruments, as well as the transformation of scientific and technological innovations and achievements. He obtained a PhD in Safety Science and Engineering from China University of Mining and Technology (Beijing) in 2010.

His contributions have been widely recognized through the publication of 18 SCI/EI-indexed papers, the authorization of 24 invention patents, and the formulation and revision of two national and industrial standards.

fire

MDPI

Review

Research Progress on the Fire Characteristics of Electric Cables and Wires

Feiyang Yu, Shijie Wang, Kaixuan Tang, Yifan Lin, Shasha Wang * and Ying Zhang *

School of Safety Science and Emergency Management, Wuhan University of Technology, Wuhan 430070, China; yufeiyang@whut.edu.cn (F.Y.); wsj518@163.com (S.W.); kaixuant@whut.edu.cn (K.T.); lyf2@whut.edu.cn (Y.L.)
* Correspondence: wshasha2020@whut.edu.cn (S.W.); yzhang@whut.edu.cn (Y.Z.)

Abstract: With the development of the social economy and the improvement of electrification, cables and wires play an important role in people's lives and industrial development. Meanwhile, the large-scale laying of cables has also made them a fire hazard that cannot be ignored in land construction such as residential buildings, utility tunnels, nuclear power plants, refineries, marine systems such as submarines and ships, and airborne systems such as spacecrafts and aircrafts. In this work, studies on fire the characteristics of cables and wires over the last decades have been reviewed. Based on different experimental forms and objects (laboratory wires and commercial cables), this paper summarizes the theories of the fire dynamics in wire combustion, including the models of ignition and flame propagation, the criteria for blowing off and quenching, and the critical conditions for dripping behavior. The effects of materials, layouts, and environments on wire combustion phenomena such as airflow, ambient pressure, oxygen, gravity, and orientation angle have been discussed in detail according to the theories of heat transfer and combustion. In addition, test standards and studies on the fire behavior and release of toxic gases of commercial cables have also been fully described. Through the summary of the above content, it is expected to build a preliminary theoretical framework and future research directions for researchers in the field of cable fires.

Keywords: fire characteristics; cable; laboratory wire; fire models

Citation: Yu, F.; Wang, S.; Tang, K.; Lin, Y.; Wang, S.; Zhang, Y. Research Progress on the Fire Characteristics of Electric Cables and Wires. *Fire* **2024**, *7*, 186. https://doi.org/10.3390/fire7060186

Academic Editor: Grant Williamson

Received: 24 April 2024
Revised: 16 May 2024
Accepted: 20 May 2024
Published: 30 May 2024

1. Introduction

In the face of the current socio-economic development situation, the demand for cables in the fields of electric power transportation and information transmission is increasing, especially in power supply systems, nuclear power stations, utility tunnel systems, and other industrial and mining enterprises. The use of cables is significant. As the lifeblood of national power and communication, the large number of combustible components contained in the cable itself make it a fire safety hazard. According to the U.S. Fire Administration statistics, the estimate of residential building fires due to electrical malfunction was over 20,000 per year for the 10-year period of 2012 to 2021 [1]. In the event of a fire in a place where a large number of cables are laid, the potential hazards brought by it are mainly manifested in the following aspects [2,3]:

- First, the cable sheath and insulating materials are flammable, which can be ignited in high-temperature situations;
- Secondly, under good ventilation conditions, cable fires can accelerate their spread along the cables. Due to the fact that cables are mostly connected to important places, once a fire spreads to important places, the loss is significant;
- Third, the burning process of cables can release toxic and corrosive gases such as hydrogen chloride and carbon monoxide, which can cause significant damage to people and equipment;
- Fourth, the process of cable burning is often accompanied by a large amount of smoke, greatly affecting the escape and rescue work.

Since the cable fire accident of the Browns Ferry nuclear power plant in 1975, scholars have gradually begun to pay attention to the fire characteristics of cables, but have been more inclined to industrial testing. Until the early 1980s, Bakhman et al. [4,5] began to use PMMA and PE-wrapped copper and glass rods as simplified laboratory wires to study the phenomenon of wire combustion. After that, Fernandez-Pello et al. [6] used a thermogravimetric analyzer and an experimental apparatus consisting of a gas-fired radiant panel, a specimen holder frame to study the ignition delay time and flame propagation rate of several different wires under different external radiation effects. They classified these types of wires into fire risk levels based on their combustion performance and flame propagation ability. At the same time, Tewarson, A. et al. [7] and Babauskas, V. et al. [8] also conducted studies on the fire behavior and test methods of commercial cables. During this period, few scholars used the method proposed by Bakhman to study the combustion behavior of wires until the late 1990s. Since 1998, domestic and foreign scholars have re-used laboratory wires to conduct a large number of studies on the ignition [8–17], propagation [18–75], extinction [18–25], and dripping [18,20,21,33,45,48,50,52,71,76,77] behaviors of wires, as well as the impact of environmental factors and wire configuration in wire combustion. In addition to the bench-scale laboratory wire fire tests and the small-scale commercial cable tests such as the FPA (fire propagation apparatus) and cone calorimeter mentioned above, medium- and large-scale experiments also run through the development of cable fire research, providing many simulation methods and empirical formulas for real-world cable fire behavior [2,3,78–112]. The above-mentioned studies will be elaborated in Sections 2 and 3.

After decades of development, research on the behavior of cable and wire fires has yielded significant results. Therefore, this work will systematically summarize the research results of many scholars over the past decades based on different experimental scales and experimental objects in the hope of establishing a relatively complete research framework and summarizing the issues to be resolved.

2. Wire Combustion Characteristics

In wire fire experiments, coaxial peeled wires or self-made wires are widely used, which are only composed of an insulating layer and a wire core. Commonly used insulation and wire core materials are polyethylene (PE), ethylene-tetrafluoro-ethylene (ETFE) and copper (Cu), iron (Fe), nickel–chromium alloy (NiCr), aluminum (Al), and stainless steel (SS).

The research on wire fires is usually divided into different categories according to its development process: ignition, flame propagation, melt and drip, extinction. Therefore, the above research sites are reviewed separately in the following paragraphs, and the effects of environmental factors and wire configurations on different combustion processes are also discussed.

2.1. Ignition

Compared with other polymer fuels, due to the unique nature of the wire core, there are three ignition models for wires:

(1) Piloted ignition under external heat sources like other fuels [113];
(2) Spontaneous combustion of the insulation layer caused by overcurrent [8,13,14,16];
(3) Arc ignition [114].

2.1.1. Piloted Ignition by External Heating

The external heat source ignition process is usually as follows: The external heat source heats the insulation. When the insulation surface temperature rises to the pyrolysis temperature, the surface precipitates the pyrolysis gas and mixes with the air. As the mixture reaches the ignition limit, it is ignited when encountering a hot surface, hot spot, spark, or flame. The typical external heat source ignition phenomenon is shown in Figure 1. As shown in Figure 1, for different insulation materials, there are differences in the form of

the flame after piloted ignition. The flame of polyethylene insulation after being ignited by an external heat source is usually presented as a candle-like stable flame, while it is presented as a multi-point jet flame with insulation shrinkage and swelled for polyvinyl chloride insulation. This is because the surface of PVC insulation will be charred when it is heated, while PE insulation will not. A similar combustion phenomenon was found in Gong's research [115], reporting that the PVC sheath under external heating swelled and shrank under five stages before being ignited: inert, fluctuation, rapid swelling, shrinkage, end stable, and a flame appearing as a jet flame.

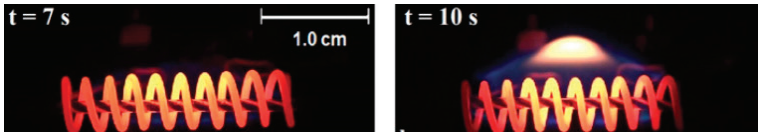

Figure 1. Ignition phenomenon of the NiCr-PE wire (d_c = 0.7 mm, δ_p = 0.15 mm). Reprinted from Ref. [15] with the permission of Elsevier.

There are usually three heat transfer protocols in the piloted ignition process of wire due to external heating:

(1) The external radiation directly heats the insulation layer, and the core acts as a heat sink [15,34,116];
(2) External radiation directly heats the core, and the core acts as heat source [10,15];
(3) Internal Joule heat and external radiation joints heat the insulation [12,75].

Under this ignition mode, the following assumptions can be made [15]:

(1) The contact thermal resistance between the insulation layer and the wire core are ignored;
(2) The materials are isotropic;
(3) The phase transitions and deformations are ignored;
(4) The radial heat transfer is ignored.

Based on the above assumptions, a one-dimensional heat transfer model can be established. The energy conservation equation of the insulation and the core are as follows [117]:

$$\rho_c c_c A_c \frac{\partial T_c}{\partial t} = k_c A_c \frac{\partial^2 T_c}{\partial x^2} + \dot{q}_j' - \dot{q}_{cp}' \quad (1)$$

$$\rho_p c_p A_p \frac{\partial T_p}{\partial t} = k_p A_p \frac{\partial^2 T_p}{\partial x^2} + 2\pi r_p \dot{q}_{er}'' + \dot{q}_{cp}' \quad (2)$$

where x is along the wire axis, and ρ, c, A, T, and k are the density, specific heat, cross-section area, temperature, and thermal conductivity, respectively. The subscripts p and c represent the insulation and the metal core. $\dot{q}_j'$ represents the Joule heating, which can be calculated by $\dot{q}_j' = I^2 R$. $\dot{q}_{cp}'$ represents the heat conduction between the core and the wire. $\dot{q}_{er}''$ represents the external radiation heat flux. The dot and apostrophe of the physical quantities mentioned in this article indicate only the variable in time and space.

The three heat transfer protocols have different boundary conditions, and the forms of Equations (1) and (2) will also change.

For protocol (1), Joule heat needs to be removed first, and secondly, the core acts as a heat sink, so the heat conduction value is negative. In this case, the energy required for pyrolysis and ignition comes from the net heat flux, which is the external heat flux minus the heat conduction of the insulation to the core. When the external heat source with

length L is heated locally, there is a critical heat flux for the piloted ignition of the wire as follows [15,75]:

$$\dot{q}''_{er,crt} = \dot{q}''_{loss} + \frac{r_c}{L}(T_{ig} - T_\infty)\sqrt{\frac{2h_p k_c}{r_p}} \quad (3)$$

where T_{ig} and T_∞ represent the ignition temperature and the wire balance temperature. $\dot{q}''_{loss}$ represents the heat loss from the wire surface in the heating zone.

When the external heating is global, the prediction model of ignition delay time under the global external heating can be derived by referring to the classical thermally thin solid ignition model [10,113] as follows:

$$t_{ig} = t_{py} + t_{mix} + t_{chem} \approx t_{py} = \frac{\sum(\rho cA)(T_{py} - T_\infty)}{\dot{q}''_{net}} \quad (4)$$

where $\sum(\rho cA) = (\rho cA)_c + (\rho cA)_p$, T_{py} is the pyrolysis temperature of the insulation, and $\dot{q}''_{net}$ is the net heat flux. t_{py}, t_{mix}, and t_{chem} represent the pyrolysis time, the mixing time, and the gas-phase chemical time, respectively. If there is a piloted source such as a laser spark, electrical spark, flame, or hot surface that is close to the gas mixture, t_{mix} and t_{chem} are usually much smaller than t_{py}. Hence, the ignition delay time of the piloted ignition is usually characterized by the pyrolysis time, while the gas-phase kinetic effects can be ignored.

As for Protocols (2) and (3), the difference mainly lies in the source of the net heat flux. For the former, $\dot{q}''_{net}$ mainly comes from the difference between the heat conduction of the core and the heat loss of the outer surface of the insulation, while for the latter, it is from the joint heating of the internal and external heat sources.

Figure 2 shows two examples (external coil heat and external radiation with laser spark) of the ignition delay time changing with the external heating [10,15]. As shown in Figure 2, the core material, insulation size, internal current, external heat flux, and environment conditions (oxygen and gravity conditions) all affect the ignition delay time of the wire.

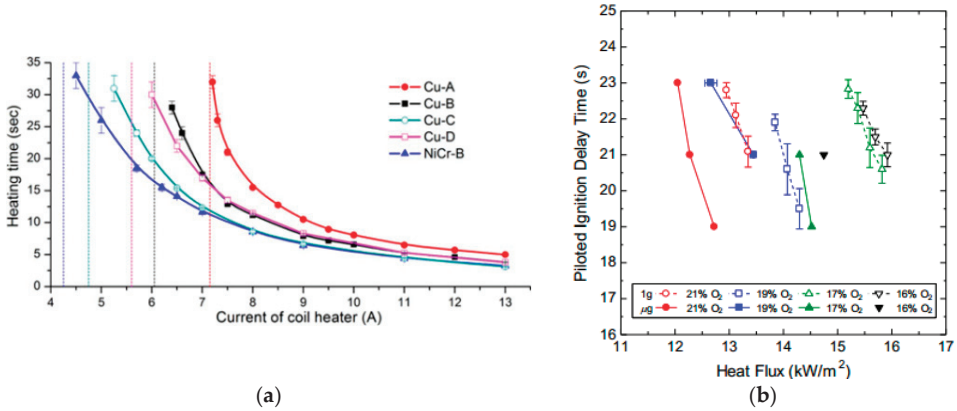

(**a**) (**b**)

Figure 2. Ignition characteristics under external heating. (**a**) External coil heat (A, B, C, D represent the wires with different diameters and insulation thickness). Reprinted from Ref. [15] with the permission of Elsevier; (**b**) external radiation with laser spark. Reprinted from Ref. [10] with the permission of Elsevier.

It is obvious and common sense that with the increase of external heat flux, the piloted ignition delay time will be significantly reduced. However, at a high heat flux, it will gradually stabilize, and when the core is energized, the increase in current will reduce the critical ignition heat flux to a certain extent. Additionally, piloted ignition will be

more difficult to achieve, and the ignition delay time will be longer for the wire with the higher thermal conductivity core, larger diameter, and thinner insulation [15]. This can be explained by Equations (3) and (4). As for the gravity and oxygen concentration, microgravity and a high oxygen concentration significantly increase the risk of wire fire. The mechanisms of influence will be discussed at the end of Section 2.1.2.

2.1.2. Overcurrent Ignition

Overcurrent ignition caused by short circuit and overload is another important model, which may be more in line with the actual wire and cable fire. When excess current passes through the core, considerable Joule heat is generated. Under the significant amount of Joule heat, the core is rapidly heated to show a red-hot glow. The heat generated by the core is transferred to the insulation through thermal conduction, and the insulation rapidly heats up to the melting temperature and further heats up to the pyrolysis temperature. The pyrolysis gas is produced at the interface between the core and the insulation. After the gas mixes with air (released after the insulation is melted and broken for PE insulation [8,16], bursting jetting from the bubble containing volatile compounds after the insulation breakdown for FEP insulation [11], released after the swelled insulation breakdown for PVC [115]), the mixture oxidizes and exotherms, which eventually leads to gas-phase thermal explosion [118,119], spontaneous ignition, or assisted ignition by the exposed high-temperature core [120].

The research on wire overcurrent ignition started from a series of combustion studies in microgravity to improve the fire safety of spacecrafts. Kong and his team [17,121–124] were pioneers in the study of overcurrent ignition. Different from previous microgravity combustion experiments, Kong et al. adopted a functional simulation method to make the Grashoff number ($Gr = \beta g \Delta T L^3 / v^3$) of the environment the same as that of the microgravity environment by adjusting the pressure and the height of the passage in the ground conditions so as to simulate the buoyancy level of the microgravity environment. The focus of their studies was to achieve pre-ignition characteristics of energized wire (the law of temperature evolution before ignition, the characteristics of flue gas transport, and the ignition delay time) that were similar to that in microgravity via functional simulation. During the same period, Fujita and Shimizu et al. [13,14,16] conducted studies on short-term overcurrent ignition and long-term sustained overcurrent ignition in a microgravity environment achieved using tower drop and parabolic flight, respectively. Based on their research results, as shown in Figure 3, it can be found that there are significant differences in the ignition behavior of wires under microgravity and normal gravity conditions due to the absence of buoyancy-induced convection. In a microgravity environment, when a short-term overcurrent is introduced, the ignition point usually occurs on the surface of the wire core and then develops into a tubular flame around the wire core, shown in Figure 4. However, for a long-term overload current supply under normal gravity, the ignition point is usually far away from the wire. However, it was found that this phenomenon can also be observed for a short-term and small overcurrent under microgravity conditions in a subsequent study [120]. But the former phenomenon is unique to microgravity environments. Additionally, another phenomenon that is unique to microgravity environments is that ignition can occur after the current supply ends; that is, delayed ignition.

It is found that for both Studies by Kong's and Fujita's research teams on overcurrent ignition of polymer-insulated wires under microgravity conditions, the fire risk of wires under microgravity conditions is higher than that in normal gravity. As shown in Figure 5, because of the elimination of the nature convection in microgravity, which results in a longer residence time of the flammable mixture and a reduction in heat loss (compared with the normal gravity environment, there is no natural convection heat loss), the ignition limit (current and limit oxygen concentration) is more extensive in microgravity than in normal gravity.

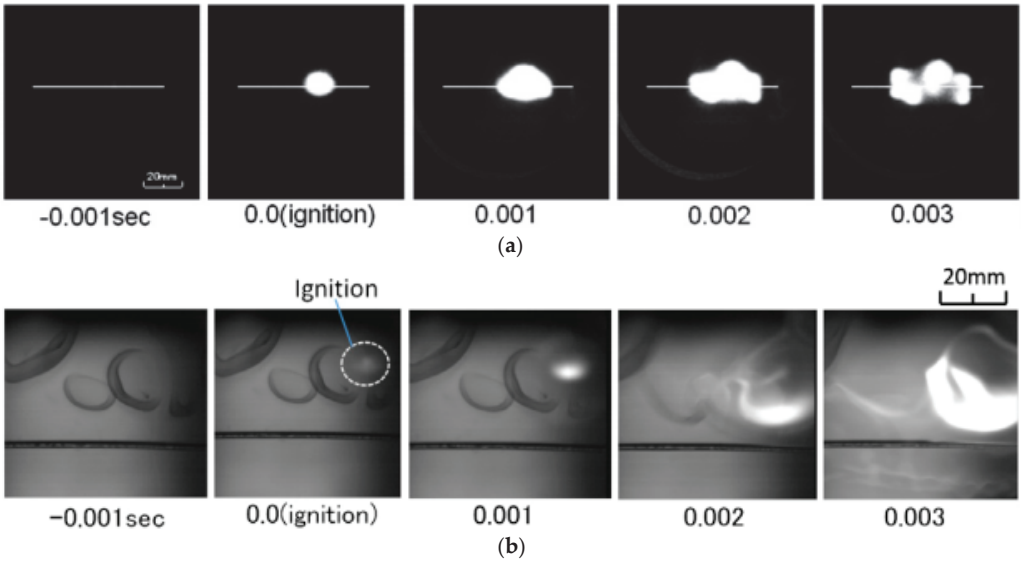

Figure 3. Ignition behavior. Reprinted from Ref. [16] with the permission of Elsevier. (**a**) Short-term excess current in microgravity; (**b**) continuous excess current in $0.8G_0$.

Figure 4. Tubular flame. Reprinted from Ref. [16] with the permission of Elsevier.

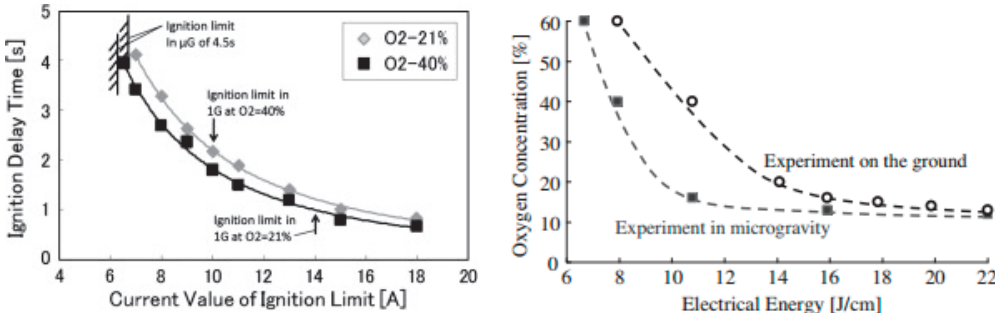

Figure 5. (**a**) Current value of ignition limit. Reprinted from Ref. [16] with the permission of Elsevier; (**b**) the limit oxygen concentration under microgravity and normal gravity conditions. Reprinted from Ref. [14] with the permission of Elsevier.

In addition to microgravity studies, other scholars have also studied the effects of airflow environment [8], pressure [11], and inclination angles [125] under normal gravity conditions on the ignition of wires under overcurrent conditions. These studies all show that the gas-phase kinetic effects cannot be ignored for the ignition behavior of wires under overcurrent conditions. Meanwhile, due to the large amount of Joule heat brought by the

overcurrent, the pyrolysis time is greatly reduced compared with the external heat source, which is comparable to the mixing time and chemical reaction time. This means that all the three times of Equation (4) need to be considered.

For overcurrent ignition, t_{py} will be changed to the following equation:

$$t_{py} = \frac{\sum(\rho c A)(T_{py} - T_\infty)}{\dot{q}''_j - \dot{q}''_{loss}} \tag{5}$$

t_{mix} can be calculated as follows [126]:

$$t_{mix} \approx \frac{\delta_{BD}^2}{D_g} \approx \frac{\lambda^3}{h^2 D_g} \approx \frac{(\rho c k)_g}{Le \times h^2} \tag{6}$$

where D_g and δ_{BD} represent the diffusion coefficient and boundary layer thickness. Le is the Lewis number. h is nature convective heat transfer coefficient, which should be changed to the mixed convective heat transfer coefficient if there is external airflow.

The gas-phase chemical time t_{chem} consists of two parts: chemical induction time and chemical reaction time:

$$t_{chem} = t_{in} + t_r \tag{7}$$

t_{in} can be expressed as follows [113,127]:

$$t_{in} = -\frac{1}{4a} \ln\ [1 - \frac{4c(2-\beta)}{e^2(1-\beta^2)} \frac{c_{p,g} R T_{sp}^2 a}{A_0 \Delta H_R \rho_g n W_o X_{O_2} X_f}] \tag{8}$$

where c is a proportionality constant, E is the gaseous reaction activation energy, n is the reaction order, A is the pre-exponential factor, and β is coefficient and calculated as $\beta = T_{sp} c_{p,g} / X_f \Delta H_R$. T_{sp} is the spontaneous temperature. ΔH_R is the reaction heat, and X represents the volume fraction.

t_R can be expressed as follows [113]:

$$t_R = \frac{0.623 k T}{\alpha(E/RT) A \Delta H_R e^{-E/RT}} \tag{9}$$

It can be seen from Equations (3)–(9) that changes in gravity, pressure, oxygen concentration, air flow, and tilt angle affect different components of the ignition delay time. For example, convective heat loss is positive with the heat transfer coefficient h, which is positive with $Gr^{1/3}$. Due to $Gr \propto p^2$, $\dot{q}''_{loss} \propto h \propto p^{2/3}$. With the decreasing ambient pressure p, the pyrolysis time t_{py} decreases according to Equation (5).

2.1.3. Arc Ignition

Arc failures can be induced in several ways [128–130]: (1) when the surface of the cable insulation layer forms a conductive path due to carbonization, moisture, pollution, and other factors, a high-temperature arc may be formed on the surface of the cable insulation layer; (2) the high temperature generated by the fire or the formed arc will cause the surrounding air to ionize, and the conductive gas may lead to the formation of a new arc once it is in contact with other circuits; (3) the high temperature generated by fire or the formed arc will lead to the pyrolysis of the insulation layer, reducing its insulation and eventually leading to the formation of an arc. The arc temperature is about 6500 K at the lowest current of the arc and gradually rises to tens of thousands of Kelvin at a high current [131], which is much higher than the ignition temperature of any polymer.

Previous research on arc faults usually focuses on the detection method of arc faults. Only a few scholars have studied the arc ignition characteristics of wires and cables. Currently, two methods are usually adopted to study the ignition and thermal characteristics of wire arcs: arc fault simulation [70,114,132,133] and overload-induced arc [134,135], as shown in Figure 6.

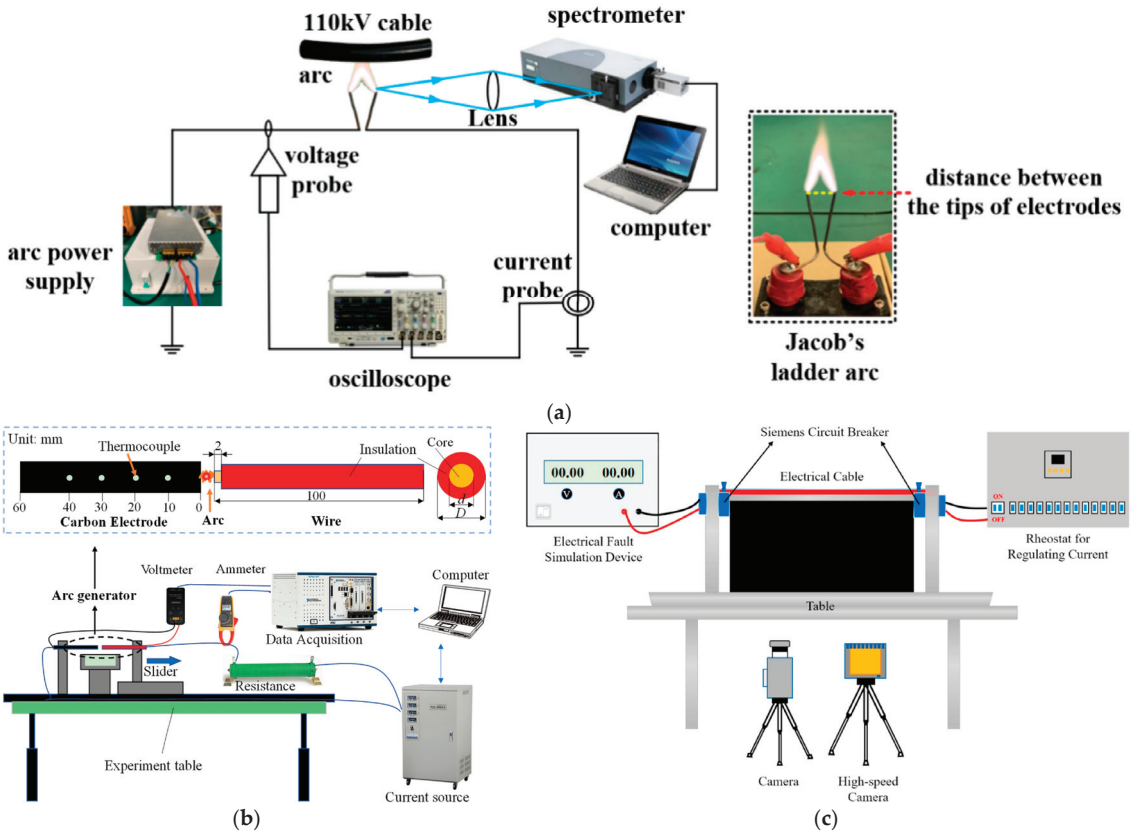

Figure 6. Arcing mode. (**a**) Jacob's ladder arc. Ref. [70]; (**b**) series arc generator by fixed electrode and movable electrode. Reprinted from Ref. [114] with the permission of Elsevier; (**c**) overload-induced arc. Reprinted from Ref. [135] with the permission of Elsevier.

The two experimental methods have their own characteristics. For the former, the thermal behavior and ignition behavior under the action of a continuous arc can be studied. For the latter, we can study the ignition characteristics of an open arc caused by a direct current. It can be confirmed that for both modes, a Joule heating effect and arc ignition effect exist simultaneously. For arc fault simulation, the ignition and non-ignition heat transfer models are shown in Figure 7. The model satisfies the following assumptions [132]: (1) Both the carbon electrode and polymer sheath are isotropic, meet the properties of thermally thin materials, and ignore the contact thermal resistance. (2) The thermal inertia of the polymer sheath is much smaller than that of the carbon electrode. (3) The deformation of the electrode and sheath, axial heat conduction, heat absorption, and heat release of sheath pyrolysis are ignored. (4) The arc flow is in a state of local thermodynamic equilibrium, regardless of the chemical reactions involved in the arc. (5) The heat flux density of the cylindrical arc space in each circular cross section along the radius (r) distribution approximately fits the Gauss surface heat source model and is independent of the time of arc discharge and the direction of arc length. Additionally, the current range has little effect on the radius size of heating area formed by arc heat source. In this model, the externally wrapped polymer receives energy from the arc at the point of arc generation while receiving Joule heat from the current and heat conduction of the arc through the electrode away from

the arc. The equilibrium temperature of the carbon electrode and ignition delay time of the sheath can be expressed by Equation (10) and Equation (11), respectively.

$$T = T_\infty + C_1 e^{\sqrt{2h/krx}} + C_2 e^{-\sqrt{2h/krx}} + \frac{\rho_E}{2\pi^2 r^3}\frac{I^2}{h} \tag{10}$$

$$t_{ig} = \frac{\rho_s c_{p,s}\delta_s(d+\delta_s)L_s}{dL\dot{q}''_{arc-s} + d(L_s - L)\dot{q}''_{e-s}}(T_{ig} - T_\infty) \tag{11}$$

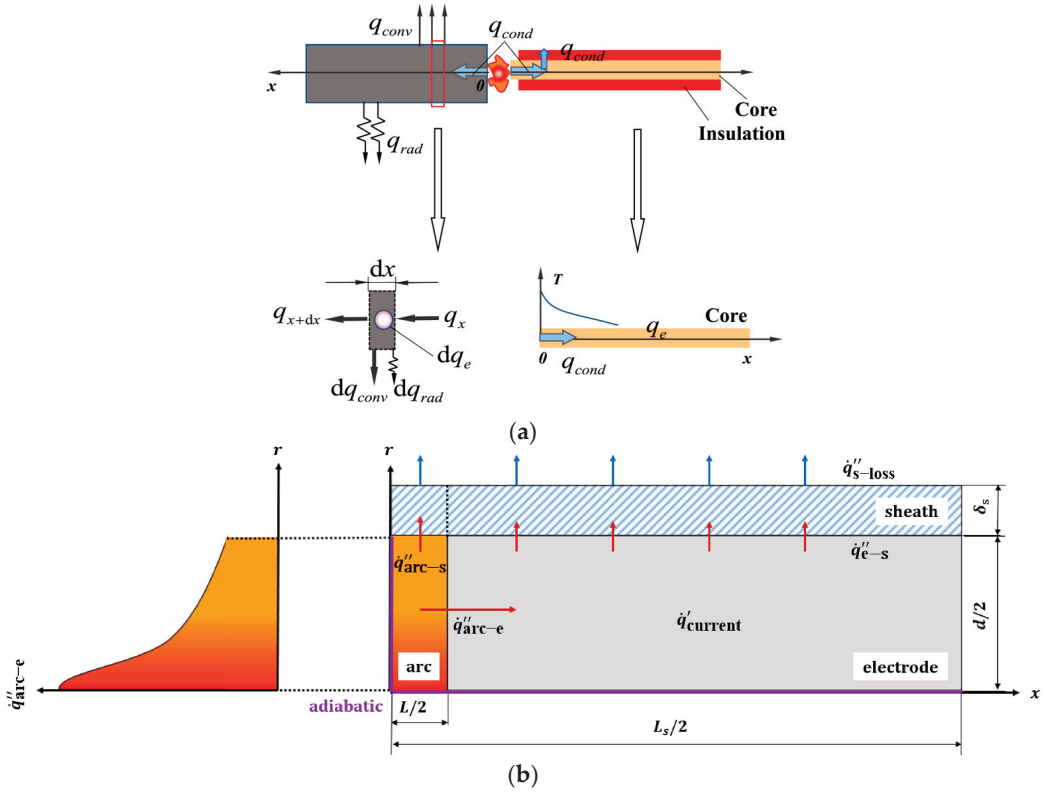

Figure 7. Heat transfer model. (**a**) Non-ignition (the red square represent control body). Reprinted from Ref. [114] with the permission of Elsevier; (**b**) ignition. Reprinted from Ref. [132] with the permission of Elsevier.

For overload-induced arc, the ignition process is very similar to the overcurrent ignition process. The difference is that the overcurrent ignition source is the spontaneous ignition of the pyrolysis mixture or high-temperature core-assisted ignition, but for the former, the pyrolysis mixture is ignited by the arc. Additionally, for multi-core wires, multiple arc breakdown will occur before the core fuses due to the high temperature [134,135], as shown in Figure 8. This means that there will be several ignition points and that the Joule heating effect will persist, which indicates that the actual cable and wire fire scenario may be much more dangerous than the single-core wire overcurrent or arc ignition.

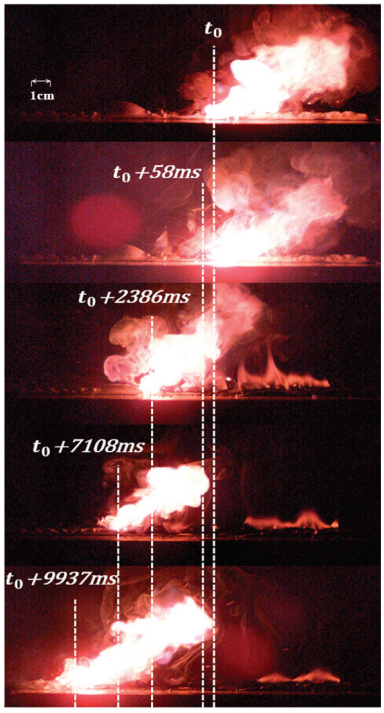

Figure 8. Multiple breakdown arc at 48A. Reprinted from Ref. [135] with the permission of Elsevier.

2.1.4. Ignition to Flame Propagation Transition

Regardless of the mode of ignition, it is not always possible to maintain combustion and spread after ignition. This may be due to heat sink of the high thermal conductance core, the inadequate heating energy, or the poor oxygen concentration leading to the reaction rate being too low. In this case, the combustion cannot be sustained [15,34]. Under external heating without an internal current, it is necessary for steady flame propagation that the preheating length by the igniter (L_{ig}), defined as the length from the center of heating region to the temperature point being $\theta = \frac{T-T_\infty}{T_{py}-T_\infty} = \frac{1}{e}$, should be larger than the preheating length of the steady flame ($L_s \sim \frac{\overline{\alpha}}{V_f}$) [34]. The transition under arc ignition or overcurrent ignition also needs to be studied because the flame spread distance varies with the overload current value after the core fusing under Joule heat and flame heating [134,135].

2.1.5. Pyrolysis Model

In all the kinds of ignition models discussed above, only the gas–solid phase heat transfer is usually considered, and the pyrolysis process of the material is ignored. In this year's research, more scholars began to consider the pyrolysis model within the ignition model, such as Guo's simulation of two ignition modes of continuous electric wires under microgravity conditions [120], L. Courty's simulation of the mass loss of wires and cables under the action of external heat sources [136], etc. In the fire community, the commonly used pyrolysis models are mainly the pyrolysis models of FDS, Thermakin, and GPYRO. A brief description of the governing equations of the simplified pyrolysis model will be given in the following paragraphs [137].

Condensed-phase mass conservation:

$$\frac{\partial \overline{\rho}}{\partial t} = -\dot{\omega}'''_{fg} \tag{12}$$

Condensed-phase species conservation:

$$\frac{\partial(\overline{\rho}Y_i)}{\partial t} = \dot{\omega}'''_{fi} - \dot{\omega}'''_{di} \tag{13}$$

Condensed-phase energy conservation:

$$\frac{\partial(\overline{\rho}\overline{h})}{\partial t} = -\frac{\partial \dot{q}''}{\partial z} + \sum_{k=1}^{K} \dot{Q}'''_{s,k} - \frac{\partial \dot{q}''_r}{\partial z} + \sum_{i=1}^{M} (\dot{\omega}'''_{fi} - \dot{\omega}'''_{di})h_i \tag{14}$$

where $\overline{h} = \sum_{i=1}^{M} Y_i h_i$, $\overline{k} = \sum_{i=1}^{M} X_i k_i$, $\overline{c} = \sum_{i=1}^{M} Y_i c_i$, $\dot{\omega}'''_{fi} = f(\alpha_i)\frac{(\overline{\rho}Y_i\Delta z)}{\Delta z} A_i \exp(-\frac{E_i}{RT})$.

The pyrolysis kinetic parameters such as A, E, n, and ΔH can be obtained from thermogravimetric analysis experiments. Scholars have conducted many studies on the pyrolysis characteristics of commonly used cable and wire materials such as PE [138–140], XLPE [141–143], EVA [144,145], PUR [146–148], and PVC [143,149–151], and the relevant literature can be consulted according to the specific material.

2.2. Fire Spread

After the insulation is ignited, the fire spread phenomenon can occur after meeting the conditions described in Section 2.1.4, the rate of which is another key to assessing the fire risk of wires. According to the interaction between air flow and fire spread, fire spread can be divided into opposed-flow fire spread and concurrent-flow fire spread [113]. The fire spread can also be divided into vertical fire spread, horizontal fire spread, and inclined fire spread according to the direction of fire spread. A schematic diagram is shown in Figure 9. The classical fire spread formula can be used to qualitatively express different fire spread behaviors.

In general, the process of flame propagation over the wire is generally considered as a series of steps that heat the polymer insulator to the characteristic temperature (i.e., the pyrolysis temperature T_p) at the pyrolysis front through inner core conduction and gas-phase flame feedback. As can be seen from Figure 8, regardless of the type of fire spread, the thermal effect affecting the flame spread in the control body comes from the following parts: the burnout zone, the combustion zone/pyrolysis zone, and the preheating zone [27,54,66,68]:

(1) the heat feedback of the flame to the preheating zone (including the convection component and the radiation component);
(2) the heat feedback from the core to the insulation in the preheating zone the heat feedback from the core to the insulation in the preheating zone (and joule heat generated by the energized core if the wire is energized);
(3) the molten insulation in the liquid phase and Marangoni convection (and the heat loss of dripping behavior if the molten insulation drips);
(4) the heat loss from the sample surface (convection and radiation).

One of the most important parameters to evaluate fire spread is the fire spread rate. According to the heat balance equation, the expression of the fire spread rate can be qualitatively given as follows:

$$V_f = \frac{\dot{q}''_f l_f + \dot{q}''_c l_c + \dot{q}''_m l_m - \dot{q}''_{p,loss} l_{p,loss}}{\sum(\rho c A)(T_{ig} - T_\infty)} \tag{15}$$

where the subscripts f, c, m, and p represent the flame, core, molten insulation, and insulation surface, respectively. l is the characteristic length of each heat transfer component.

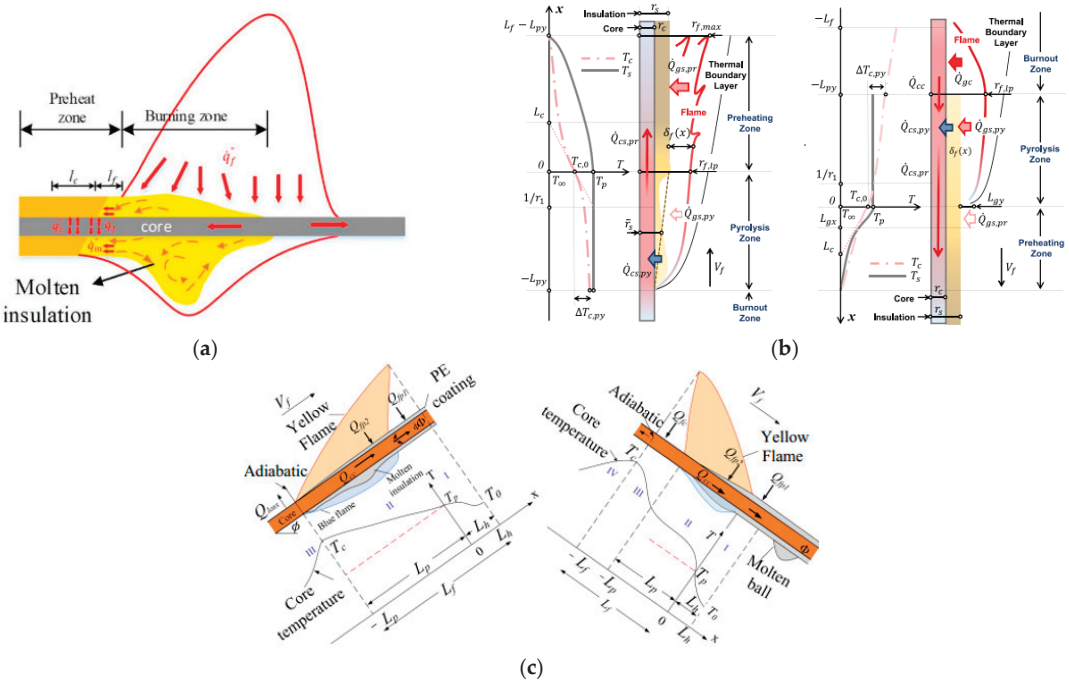

Figure 9. Schematic diagram of fire spread. (**a**) Horizontal fire spread. Reprinted from Ref. [71] with the permission of Elsevier. (**b**) Vertical fire spread: upward fire spread (left) and downward fire spread (right). Reprinted from Ref. [68] with the permission of Elsevier. (**c**) Inclined fire spread: upward fire spread (left) and downward fire spread (right). Reprinted from Ref. [32] with the permission of Elsevier.

Equation (15) is a simplified fire spread model that only considers the heat transfer effect. The phase transition, chemical reaction process, and unstable fire spread behavior in the actual wire fire spread process will affect the fire spread rate. Therefore, under different experimental designs, the results are difficult to uniformly analyze using Equation (15). In this case, only the research results of various scholars are summarized, and the influence mechanism of each factor will be analyzed based on a simple theoretical analysis based on previous studies.

2.2.1. The Metal Core

Different from other combustibles, wire fire has a unique phenomenon of core heat conduction. In the process of wire fire spreading, there are two states of heat sink under the burnout and burning zone and heat source under the preheat zone in different areas of wire fire [48,59], as shown in Figure 10. The competition mechanism of the heat sink and heat source is significantly different for different core materials and fire spread forms. The horizontal flame spread increases with wire conductance [76], while the vertical downward flame spread decreases with wire conductance [48], as shown in Figure 11b. This is mainly because the heat transfer from the wire core plays an important role in horizontal fire spread. With the increase in thermal conductivity, the preheating effect of the core is enhanced, and the fire spread rate increases. When the vertical fire spreads, the molten insulation will slide downward due to gravity, and the convection effect from Marangoni is enhanced, while the heat source effect of the wire core is weakened. At the same time, the heating of the burnout zone of the flame increases and the heat sink effect of the core with a high

thermal conductivity is enhanced, so the fire spread rate decreases with the increase in thermal inertia.

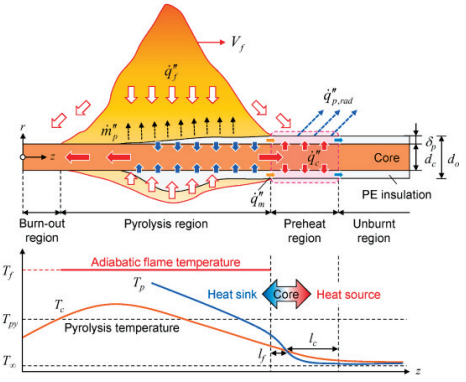

Figure 10. The heat sink and heat source of the core. Reprinted from Ref. [19] with the permission of Elsevier.

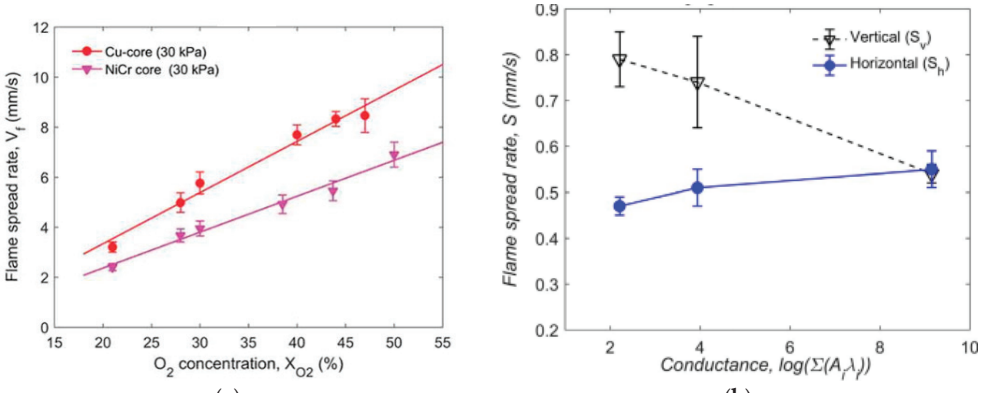

(**a**) (**b**)

Figure 11. Fire spread rate under different cores. (**a**) Horizontal fire spread rate over NiCr and Cu wires under different oxygen concentrations. Reprinted from Ref. [76] with the permission of Taylor & Francis. (**b**) Flame spread rate over LDPE wires as a function of the cross-section's thermal conductance. Reprinted from Ref. [48] with the permission of Elsevier.

2.2.2. Inclination Effect

As the angle changes, the position relationship between the flame and the wire will change, thus changing the heat transfer mechanism [49]. The research on the inclination effect was first carried out by Hu [54], according to which it was found that for a copper conductor with high thermal conductivity, the fire spread speed increased with the increase in the absolute angle. However, for a nickel–chromium conductor with a low thermal conductivity, it almost remained unchanged at −90 °C~+15 °C, and +15 °C~+75 °C increased with the increase in the angle, as shown in Figure 12. However, he did not propose an analysis of the inclination effect, but instead carried out theoretical calculations based on the flame characteristic lengths at different angles: the flame wrapping width W_f and pyrolysis length L_p, combined with a heat transfer analysis. Lu [152] proposed in his study on the interaction between inclination angle and horizontal wind that when the flame becomes longer and tilts toward the wire, the width of the combustion zone will also increase. The former enhances the convective heat flow of the flame to the preheating zone,

while the latter increases the core temperature, which also explains the inclination effect to a certain extent. Zhang [40] elaborated the inclination effect by considering the influence of inclination angle on net heat flow and expressed the positive heat flow of the negative angle and positive angle as shown in Equation (16) and Equation (17), respectively.

$$\dot{q}''_{downward} = \dot{q}''_c + \dot{q}''_f - \dot{q}''_{loss} \tag{16}$$

$$\dot{q}''_{upward} = \dot{q}''_c + \dot{q}''_g - \dot{q}''_{loss} \tag{17}$$

$$\dot{q}''_g \sim sin\theta \tag{18}$$

$$\dot{q}''_{loss} \sim 1 - \sin(\frac{90-\theta}{2}) \tag{19}$$

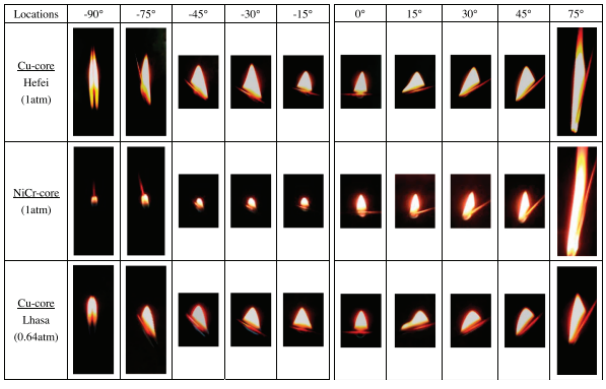

Figure 12. Fire spread over Cu and NiCr wires at different inclination angles. Reprinted from Ref. [54] with the permission of Elsevier.

Here, $\dot{q}''_g$ and $\dot{q}''_{loss}$ represent the heat flux induced by the gravity and the heat loss from the flame.

Other scholars such as Zhao [32] have considered the effects of the tilt angle on the Nussel number, the characteristic convection size, and the flame preheating length. The effects of the inclination angle on flame radiation were also considered in [31]. The above methods can reflect the inclination effects well, but it is still necessary to systematically summarize the inclination effects.

2.2.3. Oxygen Concentration

The effects of oxygen on combustion usually entail two aspects: (1) the pyrolysis rate of the polymer is accelerated, and the pyrolysis temperature is reduced [115,153]; (2) The gas-phase oxidation chemical reaction rate increases (explained by Equation (20)) and the flame temperature and the heat flux of the flame increase, as shown in Figure 12. Because of the enhancement in the heat flux of the flame and the decreased pyrolysis temperature, the limit of the ignition energy of the external heating source or Joule heat is smaller [14,15] and the fire spread rate increases, as shown in Figures 11a and 13b,c. However, for the vertical downward fire propagation of high-thermal-conductance core wire, the fire propagation rate shows a special non-monotonic change with the increase in oxygen concentration, as shown in Figure 13c. In this case, the fire spread rate presents three states with the change in oxygen concentration. The first state is a general monotone increase, which is called the "temperature-dependent regime". The second state is due to the increase in the flame heat flux to the limit, while the flame length decreases with the increase in

oxygen, resulting in a decrease in the thermal feedback from the flame received by the core. This leads to the weakening of the heat conduction of the wire core to the preheating zone, thus showing the phenomenon that the fire spread rate decreases with the increase oinoxygen concentration, which is called "negative oxygen dependence". However, for the NiCr core with a low thermal conductivity, the heat transfer in the preheating zone is not dominant. As a consequence, the decrease phenomenon does not exist. At a high oxygen concentration, because the flame is flame, more soot is generated. Therefore, the heat radiation from the flame is enhanced, and the fire spread rate increases [44].

$$\dot{q}''_{flame} = \dot{\omega}' \Delta H_f \delta_g = A e^{-\frac{E}{RT}} X_{O_2}^{n_{O_2}} X_f^{n_f} \Delta H_f \delta_g \quad (20)$$

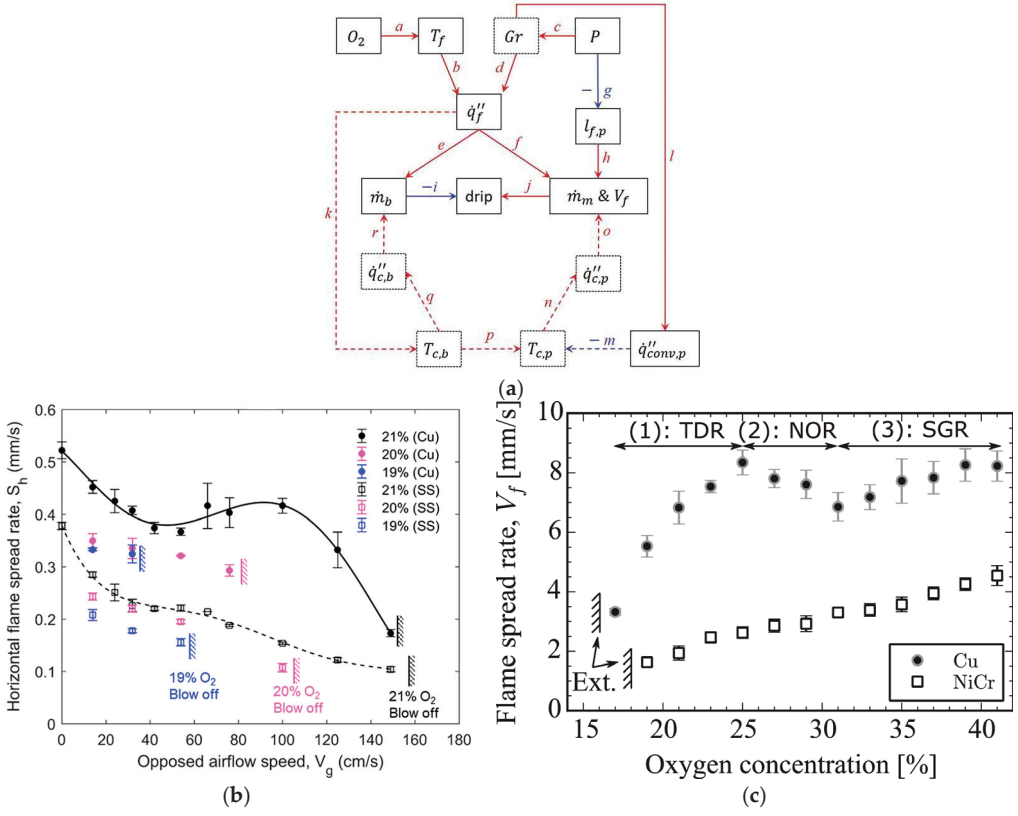

Figure 13. Fire spread rate varies with oxygen concentration. (**a**) The effects of oxygen concentration and pressure. Reprinted from Ref. [76] with the permission of Taylor & Francis. (**b**) Horizontal fire spread rate over SS (stainless steel) wire and Cu wire under different oxygen concentrations and opposed airflow speeds. Reprinted from Ref. [45] with the permission of Elsevier. (**c**) Vertical fire spread rate over Cu and NiCr wire under different oxygen concentrations. Reprinted from Ref. [44] with the permission of Elsevier.

Given the important role of oxygen in combustion, the minimum oxygen concentration at which ignition cannot occur or cannot maintain fire spread behavior after ignition—that is, the limiting oxygen concentration (LOC)—can be used as a parameter to evaluate the flammability of materials [154]. The LOC will change with different environments and other factors, and many studies have been carried out to study these aspects [34,49,116,155].

2.2.4. Ambient Pressure

Changes in pressure affect the process of mass transfer and convective heat transfer, and the specific performance is as follows [58–60,74]:

$$\alpha \propto \frac{1}{P},\ Gr \propto P^2,\ Re \propto P,\ Nu \propto P^{\frac{2}{15}},\ h \propto P^{\frac{1}{2}},\ L_f \propto P^{-\frac{2}{3}} \tag{21}$$

According to Equation (21), it can be inferred that with decreases in pressure, the convective heat loss decreases, making the fire spread rate increase, but the actual situation is different.

The effects of low and high pressure on the wire flame shape are shown in Figure 14. With increases in pressure, the fire spread rates are different for different cores and wire sizes, as shown in Figure 15. The increase in pressure has a negative effect on the fire spread rate of nickel–chromium alloy-core wire and has no obvious effects on the fire spread rate of iron-core wire. Meanwhile, for copper-core wire, there are different effects according to the different wire sizes. The main reason for this kind of wire core is that the wire core and the preheating effects of the flame show different behaviors under different pressures. Nakmura et al. [58] proposed a "flame-driven mode" and "wire-driven mode" to explain this phenomenon, illustrated in Figure 16. However, they only considered the change in the heating length of the gas phase and the solid phase with the pressure, and both of them decreased with the pressure, which could not explain the change in the fire spread of the copper core wire with the pressure. Based on this work, Hu [39] elaborated on the conversion mechanism and heat transfer mechanism of the two modes by considering the convective thermal feedback of the flame front supporting the flame-driven mode and the thermal feedback supporting the wire-driven mode and combined them with the core size. Zhao [31,47] also explained the effects of a high atmospheric pressure on the fire spread rate by analyzing the convection and radiant heat feedback of the flame. By considering the combustion efficiency and the characteristic scale of the wire core, Wang [72] gives the expression of the change of the fire spread rate with the pressure and the wire size ($V_f \propto \left(P^2 L^3\right)^a$).

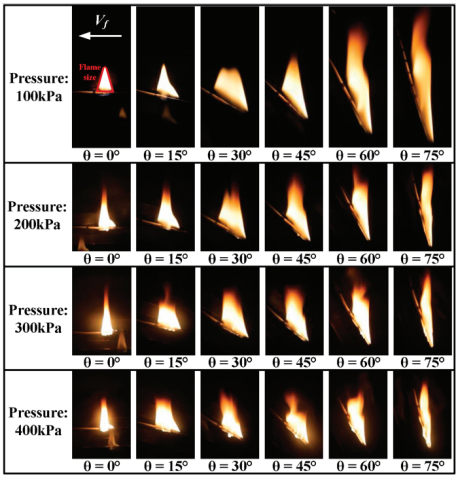

Figure 14. Flame shape under sub-atmospheric pressure. Reprinted from Ref. [31] with the permission of Elsevier.

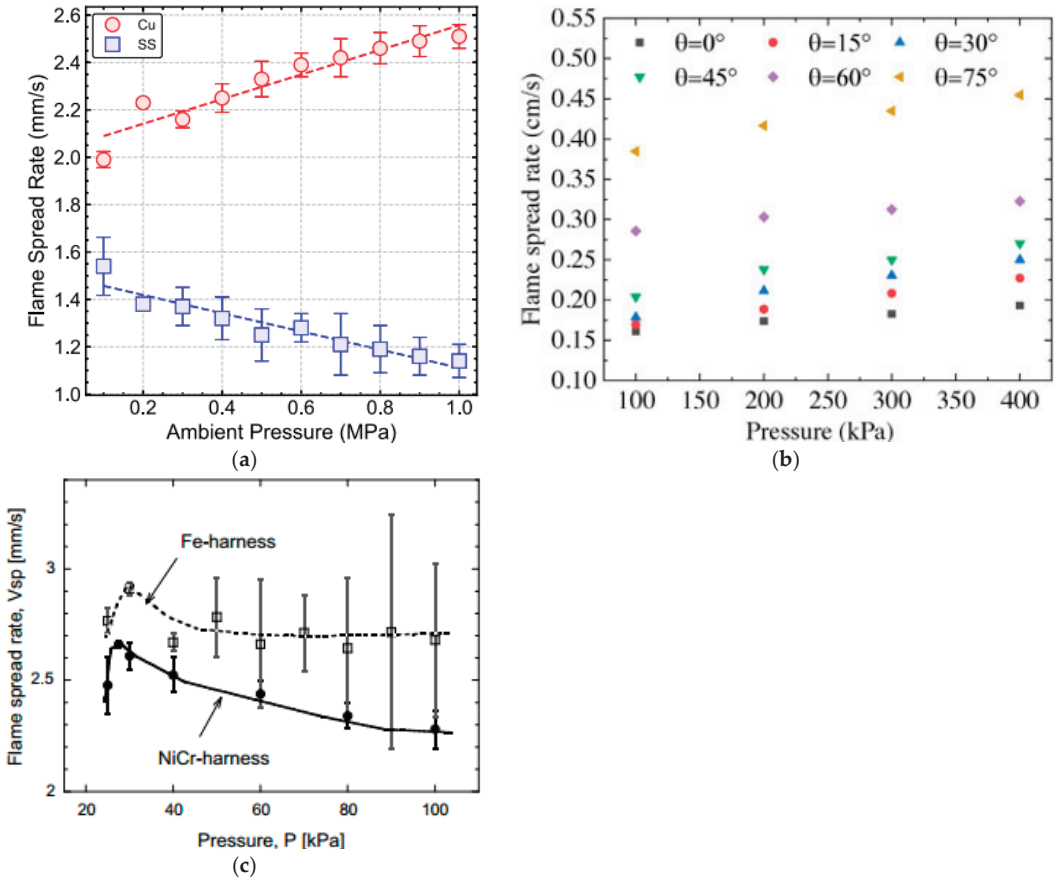

Figure 15. Flame spread rate under various pressures over different wires. (**a**) Cu and SS wires under sub-atmospheric pressure. Reprinted from Ref. [19] with the permission of Elsevier. (**b**) Cu wire versus inclination angle in high atmospheric pressure. Reprinted from Ref. [31] with the permission of Elsevier. (**c**) Fe and NiCr wire under sub-atmospheric pressure. Reprinted from Ref. [58] with the permission of Elsevier.

2.2.5. Gravity

Under normal gravity conditions, the flame spreading over the wire is usually a candle-like flame due to buoyancy, while in under microgravity conditions, it appears as a symmetrical spherical flame due to the disappearance of the buoyancy effect, as shown in Figure 17. The entire flame will be wrapped around the wire due to the curvature effect of the wire [64]. A spherical flame also appeared under a low pressure, but the color of the flame was different, as shown in Figure 18. This shows that the gas-phase transport process under low pressure and microgravity conditions is similar, but the chemical reaction rate is different [60]. In the absence of buoyancy, the thickness of the meteorological boundary layer increases, causing the characteristic time of the gas relative flow and diffusion to become longer. Additionally, the gas reaction may occur at low oxygen concentrations. Therefore, the LOC to maintain fire spread under microgravity conditions is smaller than that under gravity conditions [155,156].

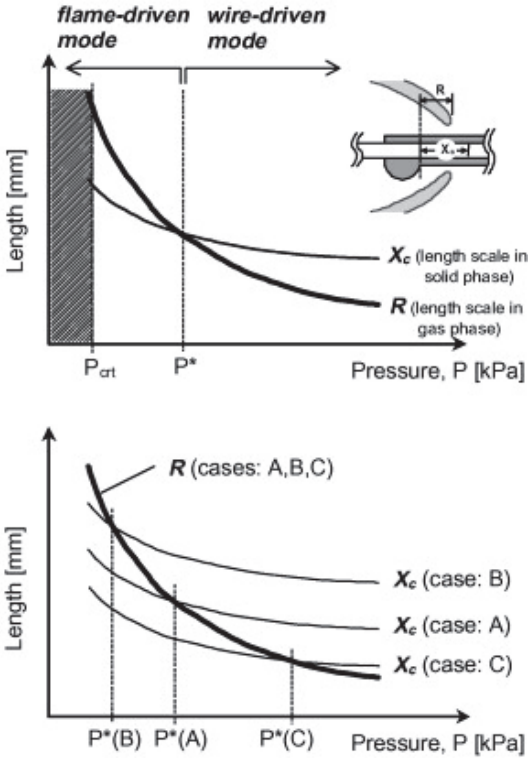

Figure 16. The heat transfer mechanisms of "wire-driven" and "flame-driven" modes. Reprinted from Ref. [58] with the permission of Elsevier.

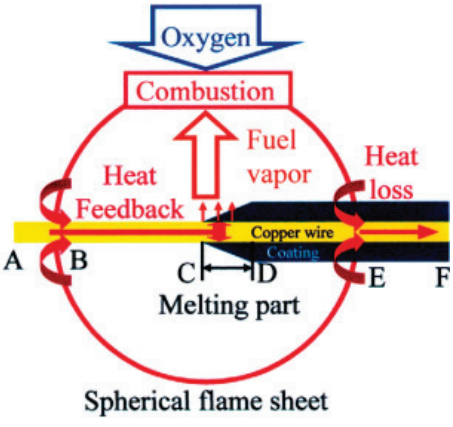

Figure 17. The mechanism for the formation of the spherical flame in wire insulation burning under microgravity conditions. Reprinted from Ref. [61] with the permission of Elsevier.

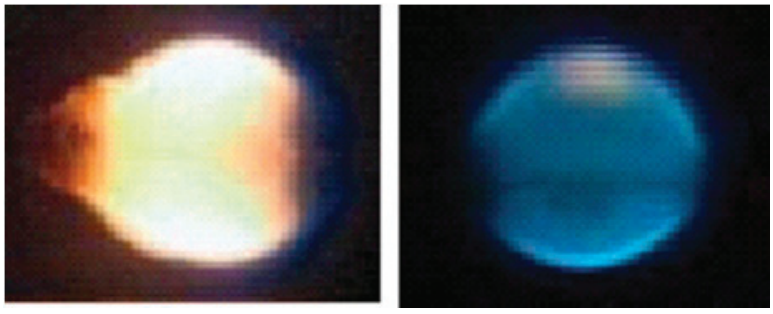

Figure 18. Flame shape under microgravity (**left**) and low pressure ($0.3P_0$) (**right**) conditions. Reprinted from Ref. [60] with the permission of Springer Nature.

As mentioned above, there are opposed-flow fire spread and concurrent-flow fire spread modes. Under normal gravity conditions, due to the induced effect of buoyancy, the upward spread of the flame in the vertical wire is also a special down-flow fire spread. However, this fire spread cannot reach a stable state due to the melting dripping caused by gravity, which causes the flame root to remain in the initial position until the flame wraps the entire sample. This fire-spreading behavior also changes under microgravity conditions [43]. Meanwhile, under microgravity conditions, according to the previous analysis, the flame will wrap around the online core, and in the case of the disappearance of natural convection, the preheating length will increase compared with that under normal gravity. This enhances the flame heat feedback under microgravity conditions, while the convective heat loss disappears. Therefore, the fire spread rate is greater than that under normal gravity conditions, as shown in Figure 19.

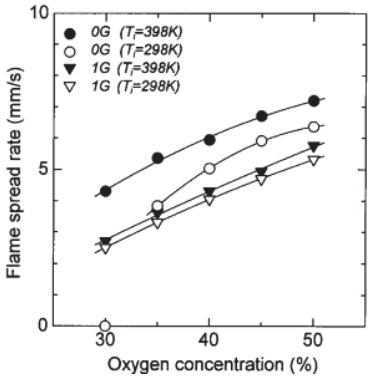

Figure 19. Flame spread rates in microgravity conditions and at normal gravity as a function of ambient oxygen concentration. Reprinted from Ref. [64] with the permission of Elsevier.

2.2.6. Airflow

According to the relationship between the direction of air flow and the direction of fire spread, it can be divided into opposed-flow, concurrent-flow, and transverse flow modes.

The influence of gas flow on the fire spread rate is mainly reflected in four aspects: preheating length, stand-off distance, flame temperature, and transport state of pyrolysis gas and oxygen. These produce four effects in the microgravity opposed-flow fire spread, resulting in three forms of change of the spread rate of opposed-flow fire spread with low-speed countercurrents, as shown in Figure 20 [62]. However, the flame behavior in normal gravity is different from that in microgravity due to the existence of the buoyancy effect, and the influence of opposed-flow velocity on the flame propagation rate seems

to be related to the heat conduction relationship of the core from the inclined flame heat feedback [20,59]. The fire spread rate varies with the air flow under normal gravity in three states: (I) at a low flow velocity, the fire spread rate decreases significantly; (II) the fire spread rate changes slightly at a medium flow velocity; (III) at a high flow velocity, the fire spread rate changes rapidly. Nakamura [59] explains the effects on the inbound flow and the effects of the core on the heat flow of the spreading flame. With increases in the opposed-wind velocity, the heat from the flame to the preheating zone decreases, and the heat transfer exposed to the wire core increases, thus increasing the heat transfer of the core to the preheating zone. For wire cores with a high thermal conductivity, this also means an increase in the heat loss caused by the heat sink. This explains the difference in the fire spread rate trend varying with the opposed-wind mode for different conductance cores.

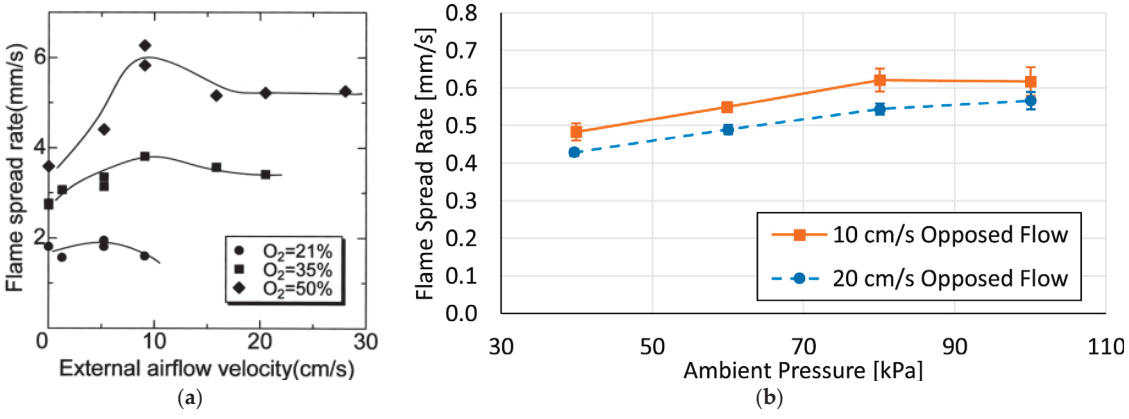

Figure 20. Opposed flow under (**a**) microgravity. Reprinted from Ref. [62] with the permission of Elsevier. (**b**) normal gravity. Reprinted from Ref. [20] with the permission of Elsevier.

However, with the opposed-wind mode, it does not always appear as the opposed-flow fire spread, such as the upward fire spread under different inclinations with opposed wind. This is because under normal gravity conditions, there will be buoyancy-induced air flow in the vertical upward direction, and the component of the wire direction can offset the opposed-wind velocity. This explains why there is the transition of concurrent fire spread induced by the buoyancy and opposed fire spread induced by the high-opposed wind velocity [49], as illustrated in Figure 21. At the transition of the concurrent fire spread and the opposed fire spread, the flame tends to be perpendicular to the wire, and there is a local maximum LOC because of the local minimum flame feedback and minimum heat conduction from the core.

The opposite of the opposed-flow effect is concurrent flow. Compared to the opposed flame spread, the concurrent fire spread is much faster, and with the velocity of the concurrent flow increasing, the fire spread rate (FSR) increases first in a nearly linear manner and then reaches its maximum value. When it is at the blow-off velocity, the FSR decreases slightly and is eventually blown off [42]. The trends of FSR under different concurrent-flow velocities and the heat transfer before reaching the maximum FSP are shown in Figure 22. As for the inclination wire, the change in the FSR is similar to that for horizontal wire. However, for the horizontal wire, the flame cannot be parallel to the wire due to the role of buoyancy, while for the inclined wire, there are three kinds of positions: the flame above the wire, the flame parallel to the wire, and the flame below the wire [152], as shown in Figure 23.

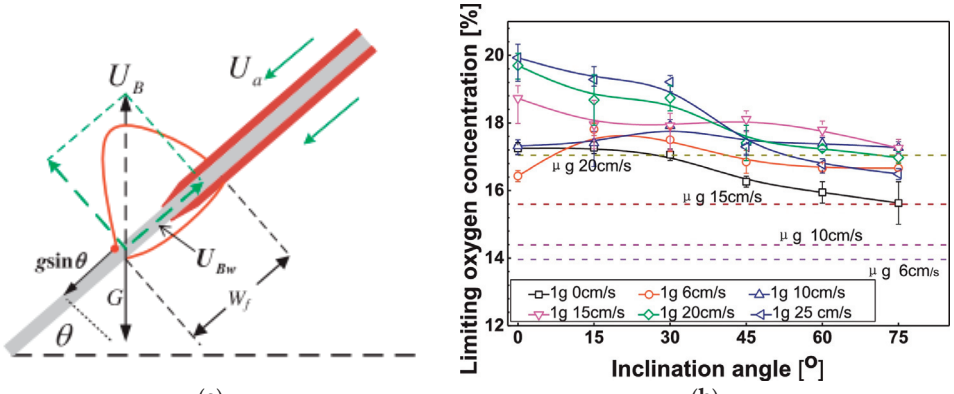

(**a**) (**b**)

Figure 21. Upward fire spread over inclined wires with opposed flow. Reprinted from Ref. [49] with the permission of Elsevier. (**a**) The physical interpretation of local maximum LOC based on the balance of buoyancy-induced flow in the wire's direction with opposed-flow speed. (**b**) The LOC varies with the opposed-flow velocity.

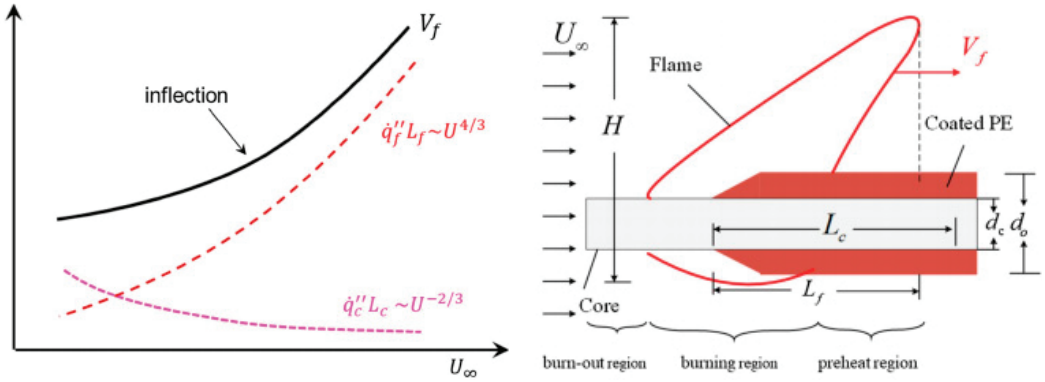

(**a**) (**b**)

Figure 22. The effect of the concurrent wind velocity. Reprinted from Ref. [42] with the permission of Springer Nature. (**a**) Trends of the flame heat feedback, heat conduction from the core, and FSR. (**b**) Diagram of the concurrent flame spread over a thin wire.

When the angle becomes 90 degrees, the opposed wind becomes the transverse wind, and the fire spread rate varies with the wind speed except periodically. Ma [23] proposes a theoretical model based on two characteristic lengths (flame-base width W_f and gas-phase length L_g), which explained the trends of FSR in the four regimes, as shown in Figure 24, from the point of view of heat transfer and chemical reactions:

(1) Regime A (as-phase convection-enhanced regime): The enhancement in the gas relative flow causes the enhancement of net heat flow in the low-velocity area.
(2) Regime B (cooling effect-enhanced regime): The heat loss because of the heat sink of the core results in the net heat flux increasing.
(3) Regime C (liquid-phase Marangoni convection effect regime): The heat flux from the molten material (liquid-phase Marangoni convection) and the solidified droplets formed downstream prevent the cooling of the naked core due to airflow, eventually causing an increase in the net heat flux.

(4) Regime D (limited chemical reaction regime): The high transverse flow velocity results in the limited chemical reaction rate.

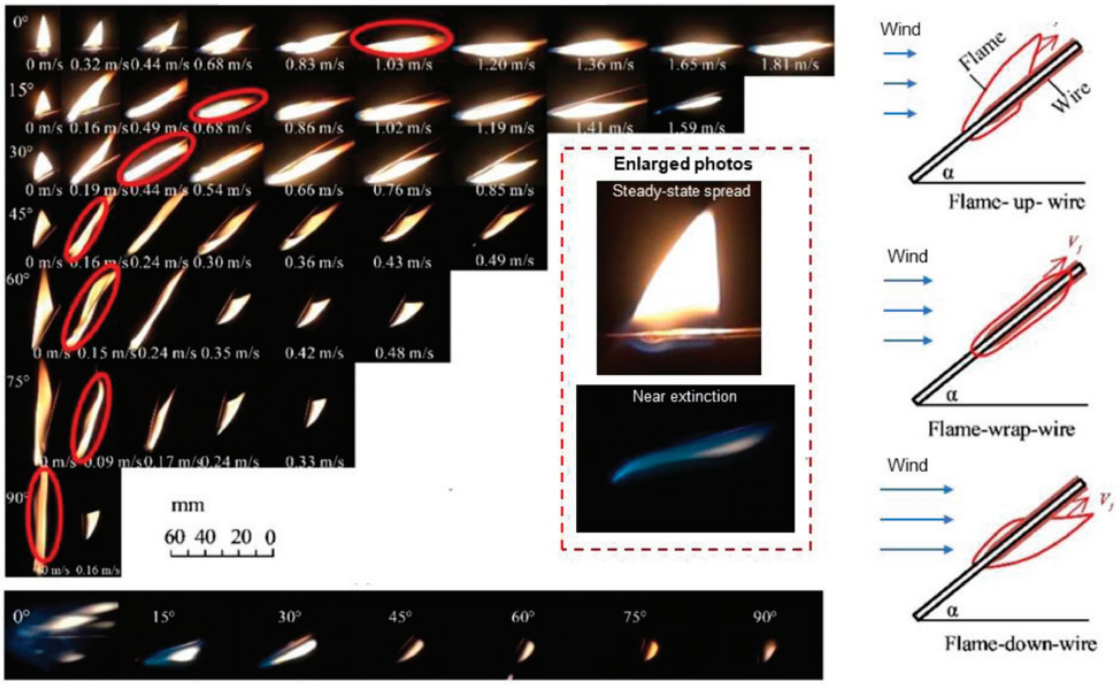

Figure 23. Flame behavior at different angles and parallel wind velocities. Reprinted from Ref. [152] with the permission of Elsevier.

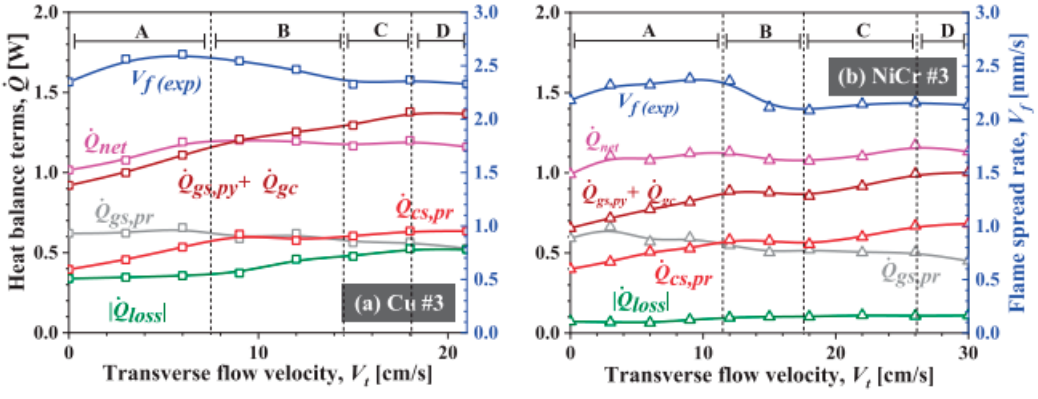

Figure 24. Heat balance terms and FSR as a function of transverse flow velocity for Cu wire and the NiCr wire. Reprinted from Ref. [23] with the permission of Elsevier.

2.2.7. Electric Current and Electric Field

The mechanism of conduction current and electric field on wire fire propagation is significantly different. The effect of current on fire spread is usually to weaken the heat sink of the core and promote its heat source. The presence of an electric field usually changes the charged particles in the reaction zone, affecting the flame shape and thus changing the heat transfer mode in the flame-spreading process. In addition, the chemical reaction rate related

to the charged particles will also be affected, and the specific forms of these effects include ionic wind effects, electrophoresis effects, electrospray effects, soot deposition effects, etc.

When the current is small, the fire spread rate and the size of flame are almost always increased with increases in the current because of the enhanced preheating from the core [29,74,75]. Additionally, because the core resistance and the convective heat loss indicated by the wire are related to the wire size (core radius and insulation layer thickness), there is usually a different trend for the fire spread rate with the increase in current, as shown in Figure 25. However, at the large currents, due to the large amount of heat production of the core, the softening of the insulation layer and the melting rate are enhanced, which promotes the generation of molten dripping. The flame height goes through three stages with the change in current: growth stage, steady stage, and drop stage, while the flame width is almost constant [157]. A comparison and the mechanism are shown in Figure 26c. Due to the enhanced dripping, the fire spread rate tends to remain constant at high currents, which has been explained by Tang [66] based on an analysis of heat transfer.

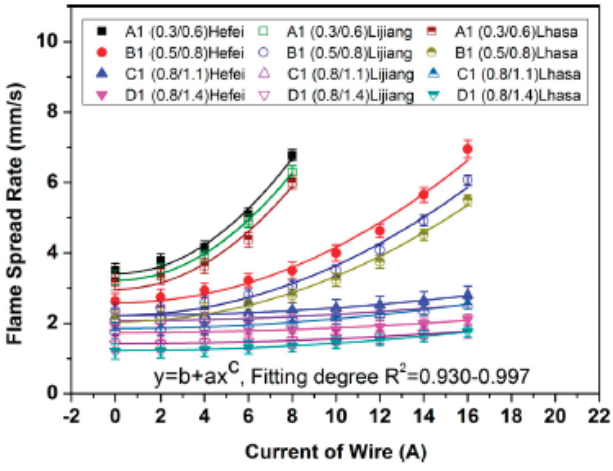

Figure 25. Flame spread rate as a function of currents for different-sized wires (the value in the label, such as 0.3/0.6, indicates the core diameter/wire diameter). Reprinted from Ref. [29] with the permission of John Wiley and Sons.

As mentioned above, the effect of the electric field on wire fire propagation mainly comes from ionic wind effects, electrophoresis effects, electrospray effects, soot deposition effects, etc. At low-frequency and high-frequency regimes of the electric field, the voltage has different effects on the wire fire propagation rate, which can be divided into three regimes, within which there are several distinct regimes depending on the frequency [52,57], as shown in Figure 27. Additionally, the inclination angle [46], core metal [24], and insulation thickness [41,69] also affect the effect of electric fields on fire spread. Figure 28 shows the specific fire behavior under the electric field. The above studies have explained the effects of electric fields on fire propagation to some extent. However, due to the complex mechanisms of the effects of electric fields on wire fire propagation behavior, the effect mechanism has not been explained by relevant theories, which deserves further research.

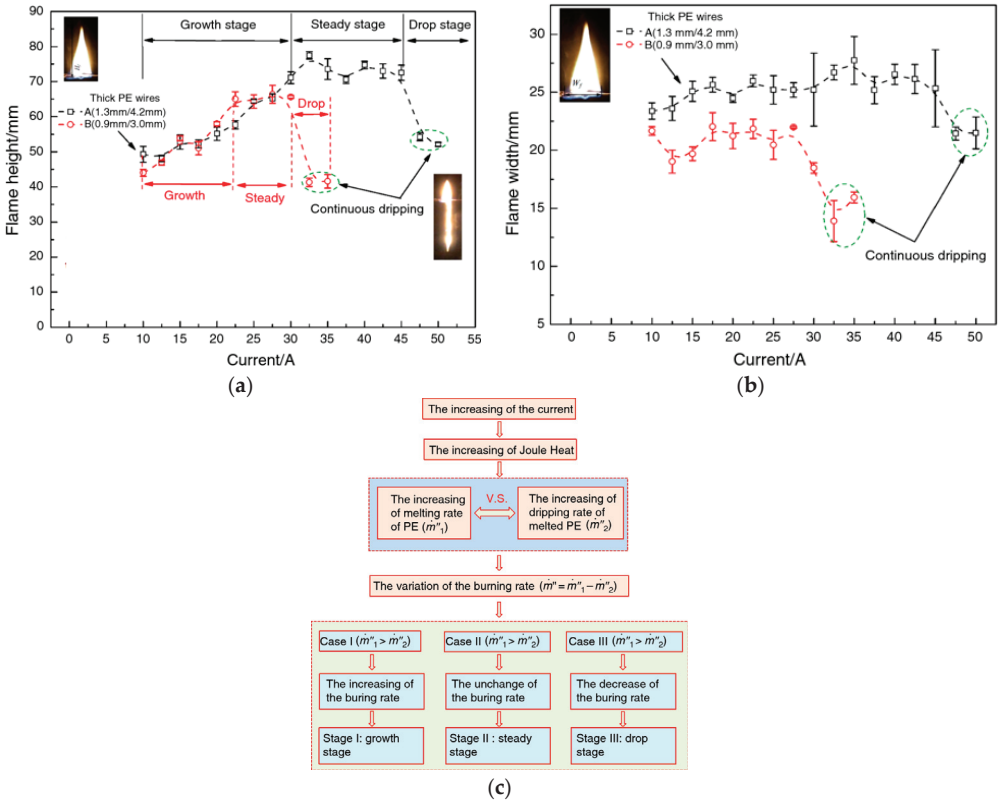

Figure 26. The size of the flame varies with the current and the mechanism. Reprinted from Ref. [157] with the permission of Springer Nature (**a**) Flame height; (**b**) flame width; (**c**) mechanism of flame variation with current.

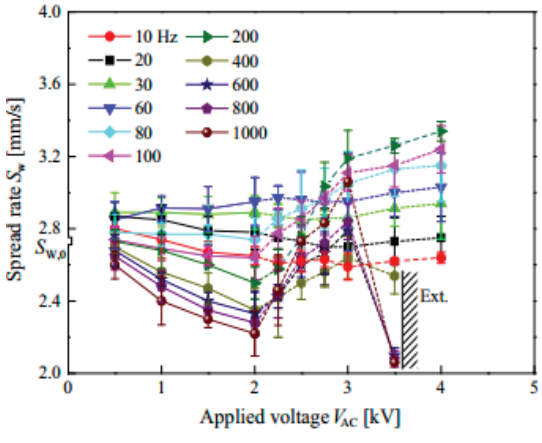

Figure 27. Variation in fire spread and flame shape at various frequencies and voltages. Reprinted from Ref. [52] with the permission of Elsevier.

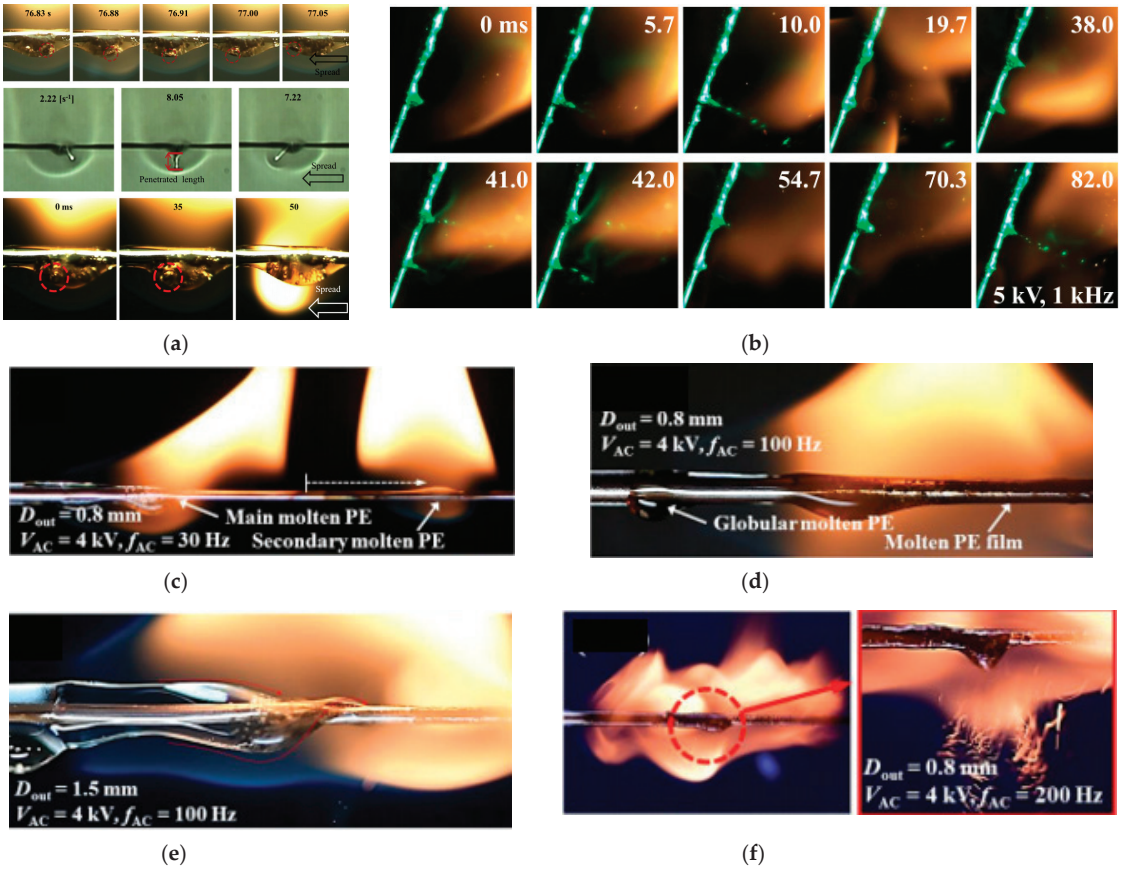

Figure 28. Specific fire behavior under an electric field. (**a**) Soot deposition. Reprinted from Ref. [52] with the permission of Elsevier. (**b**) electrospray. Reprinted from Ref. [46] with the permission of Elsevier. (**c**) dielectrophoresis phenomenon. (**d**) Globular molten PE near flame front along with formation of molten-PE film. (**e**) Globular molten PE near flame front and twisted molten PE related to rotating phenomenon of molten PE (**f**) Weak vortex flames at the front and rear flame edges. Reprinted from Ref. [69] with the permission of Elsevier.

2.3. Dripping

The melting rate of insulation can be represented as the sum of the burning loss and the dripping loss [19]:

$$\dot{m}_m = \dot{m}_b + \dot{m}_{dr} \tag{22}$$

The simple criterion for dripping is that the average melting rate is larger than the average burning rate, and the gravity of the accumulated molten ball exceeds its surface-tension [71,76,116]:

$$\dot{m}_m = \frac{\left(\dot{q}''_f l_f + \dot{q}''_c l_c\right)\pi d_0}{c_p A_p \left(T_p - T_\infty\right)} > \dot{m}_b = \frac{h_f}{c_g}\ln(1+\mathrm{B}) \tag{23}$$

$$B = \frac{Y_{O_2}\left(\frac{\Delta H_f}{\phi}\right)(1-\chi_f) - c_g\left(T_{py} - T_\infty\right)}{\Delta H_{py} + \left[\left(\dot{q}''_{s,r} + \dot{q}''_{c,loss}\right) + \dot{m}''_{dr} H_m\right]/\dot{m}''_b} \tag{24}$$

$$M_{dr}g = \rho_{dr}\left(\frac{\pi}{6}D^3\right)g \geq \sigma_{dr}(\pi D)\ or\ Bo = \frac{\rho_{dr}gD^2}{\sigma_{dr}} = 6 \tag{25}$$

where B is the mass transfer number, χ_f is the flame radiative loss fraction, ϕ is the equivalence ratio, $\dot{q}''_{s,r}$ is the surface re-reradiation, $\dot{q}''_{c,loss}$ is the heat loss of the core, H_m is the enthalpy of the molten PE dripping from the burning region, σ_{dr} is the surface tension of the molten ball, and Bo is the Bond number (or Eötvös number), the critical value of which for dripping is 6. As illustrated by the above equations, variations in the oxygen concentration and pressure will change the dripping behavior, which can be expressed by Figure 13a. Fang [76] finds the dripping limit and the fire spread limit under various oxygen concentrations and pressures, as shown in Figure 29.

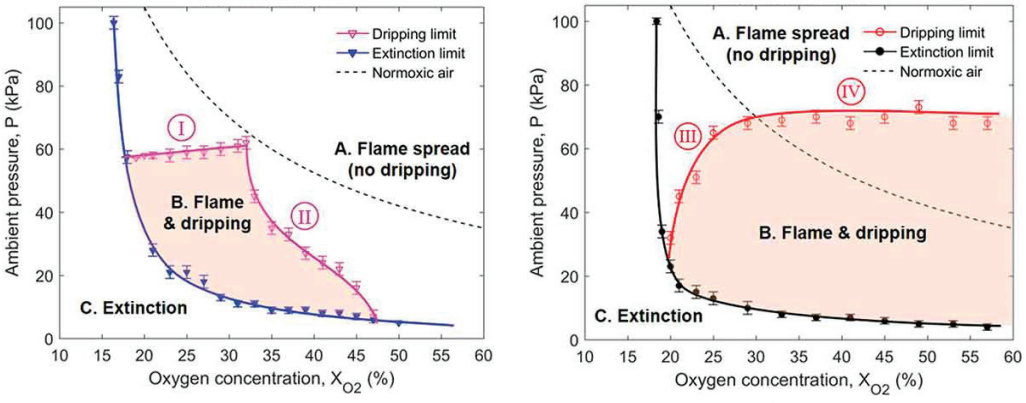

Figure 29. Dripping and fire spread limits of (**a**) Cu-core wire and (**b**) NiCr-core wire. Reprinted from Ref. [76] with the permission of Taylor & Francis.

Another important parameter is the dripping frequency f, which can be expressed as follows [71]:

$$f = \frac{3\dot{m}_{dr}\left[\dot{q}''_f l_f + \dot{q}''_c l_c + \dot{q}''_J l_p + \dot{q}''_m l_m\right]}{4\pi\rho_p^{\frac{1}{2}}\left(\frac{3\sigma_{dr}}{2g}\right)^{\frac{3}{2}}\delta_p c_p(T_P - T_b)} \tag{26}$$

As Equation (26) illustrates, the dripping frequency is affected by the current, except for the oxygen and pressure effects on the flame feedback, which are proportional to the square of the current. Studies by He [50] and Wang [33] also confirm this. In addition to the above effects, the droplet behavior is also affected by the inclination angels because of the sliding over the inclination wire. The specific sliding velocity U can be described as a dimensional version of Durbin's solution [158]:

$$U = \frac{\theta_0^2}{\mu ln\left[D(t)\tau_c\theta_0(1-\varepsilon^2)^{1/2}/3\mu U\right]}\left[\frac{1}{4}\rho_l g D^2(t)sin\alpha - 3\sigma\theta_0\varepsilon\right], \alpha \neq 0 \tag{27}$$

where τ_c is the critical shear stress; $\theta_0 = (\theta_A + \theta_R)/2$ and $\varepsilon = (\theta_A - \theta_R)/(\theta_A + \theta_R)$, and θ_A and θ_R are the advancing contact angle and the advancing contact angle of the droplet attached to the wire. It is obvious that dripping only occurs when the velocity is zero. Thus, there is a critical droplet size at $U = 0$ [18]:

$$D_{\text{crinkal}} = \left[\frac{6\sigma(\pi - 2\theta_R)}{\rho_l g \sin\alpha}\right]^{1/2}, \alpha \neq 0 \tag{28}$$

Although the formation conditions of the droplet behavior and related prediction models have been studied and proposed, the droplet behavior still cannot be accurately described because the relevant parameters of the material are temperature-dependent. More studies are required to understand the complex phase change process and formation process of droplets in wire fires.

2.4. Extinction

As with other fuels, the extinction of combustion comes from two aspects: the thin combustible component and a flame that is not strong enough to pyrolyze the fuel, which represent the blowoff and quenching, respectively. The Damkohler number (*Da*) [45,55], defined as the ratio of the gas-phase residence time (t_r) to the chemical reaction time (t_c), or the strain rate under mixed-flow (a_m), defined as the ratio of the mixed flow velocity to the radius of the wire [23,152], are used to explain the blow off:

$$Da^* = \frac{t_r}{t_c} = \frac{\alpha_g}{U_{mix}^2}\rho_g Y_F Y_{O_2} A exp\left(-\frac{E}{RT_f}\right) \tag{29}$$

$$a_m = \frac{U_{mix}}{R} \approx \frac{Usin\alpha}{R}, \begin{cases} r_0,\ 0^\circ < \alpha < 90^\circ \\ r_c = \frac{5}{8}r_0,\ \alpha = 90^\circ \end{cases} \tag{30}$$

For quenching, the characteristic parameters are the mass transfer number (*B*) or R_{loss} [22,55]:

$$B^* = \frac{Y_{O_2}\left(\Delta H_f/\phi\right)\left(1-\chi_f\right) - c_g\left(T_p - T_a\right)}{\Delta H_p + \left(\dot{q}''_{sr} + \dot{q}''_{c,loss} + \dot{m}''_{dr}H_m\right)/\dot{m}''^*_b} \tag{31}$$

$$R_{\text{loss}} = \left(\dot{Q}_{\text{rad}} + \dot{Q}_{c,loss}\right)/\dot{Q}_{gs} \tag{32}$$

where U_{mix} is the mixed flow velocity of the opposed flow and natural flow, Y_F and Y_{O_2} represent the volume fraction of fuel and oxygen, *R* represents the characteristic radius of the wire near extinction, α is the inclination angle of the wire, $\dot{Q}_{\text{rad}}$ is the radiation loss rate from the insulation surface to the ambient condition, and $\dot{Q}_{c,loss}$ is the heat loss rate of the wire.

As expressed as above, the extincition of the wire fire is determined by the oxygen, pressure, gravity, external flow, etc. Lower oxygen concentrations, pressures, and gravity can make the flame weaker or even extinct, as shown in Figure 17, because of the heat loss and burning rate, as illustrated in the preceding paragraph. Even if the flame is stronger, the external flow can bring the gas mixture away from the reaction region, which results in the extinction of the wire fire. Thicker insulation requires a higher flow velocity. In fact, blow-off and quenching could play simultaneous roles in flame extiction [23], which means that the boundary between combustion and extiction can be determined by the characteristic numbers of quenching and blow-off events, as shown in Figure 30. Morever, dripping, which removes significant amounts of heat and melt insulation, can also result in extinction, and a sudden weak flame can be observed at the time after dripping [71]. Due to the effects of electric fields on flame and heat transfer, extinction can also be observed with increases in voltage and frequency, but this mechanism has not been clarified [24,52].

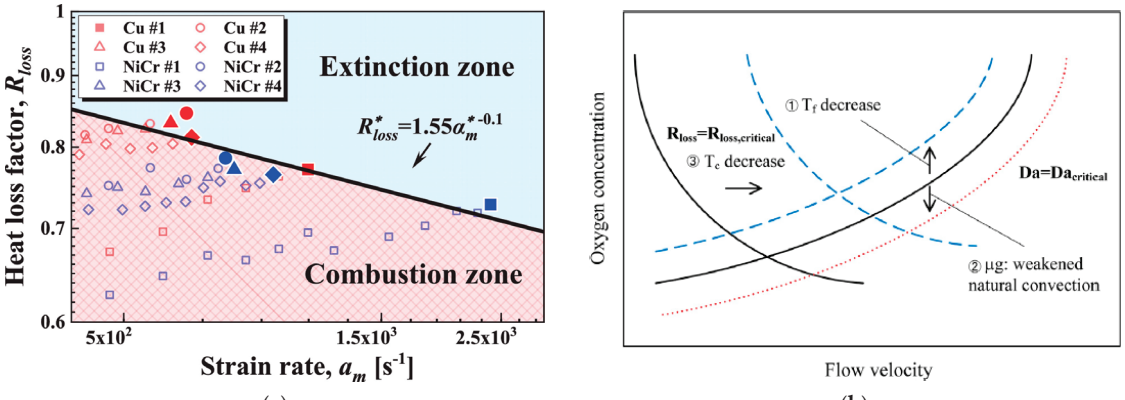

Figure 30. The boundary between extinction and combustion. (**a**) R_{loss} vs. a_m. Reprinted from Ref. [23] with the permission of Elsevier. (**b**) R_{loss} vs. Da. Reprinted from Ref. [55] with the permission of Elsevier.

3. Real Cable Fire Research

There are two aspects of cable fire studies: the combustion characteristics of cable materials and cable tray fire behavior.

3.1. Combustion Characteristics of Cable Materials

In terms of material combustion characteristics, studies generally use cone calorimeters, OSU calorimeters, and other equipment to study the ignition time, heat release rate, effective combustion heat, and flue gas generation of the cable.

Matheson et al. [159] and Barnes et al. [160,161] studied the combustion characteristics of halogenated and non-halogenated PVC cables and compared their fire resistance. They found that adding halogen elements improved the fire resistance of the cables, but the smoke production, toxicity, and corrosion were enhanced. Yang et al. [162] used a pyrolytic combustion flow calorimeter to test the flammability of eight cable materials, analyzing the heat release rate, ignition temperature, and total heat release. Romain et al. [163] also used CONE to study two kinds of halogen-free flame-retardant cables under different heat fluxes and cable spacing. The results showed that under the action of external radiation, the thermal thickness ignition model could better predict the ignition time, and the increase in cable spacing would slightly increase the ignition time. Gong [115] established a ring heating experiment platform and carried out cable ignition experiments under the heating condition of a t^2 heat source. He found five processes of thermal deformation of flame-retardant PVC cable before a fire: the inert stage, wave stage, expansion stage, contraction stage and stable stage. He also explained the special behavior of cable thermal expansion and ignition based on a thermogravimetric analysis.

In recent years, aging cable materials have attracted extensive attention from scholars, but the research conclusions are not the same or are even contradictory. Xie et al. [164] studied the fire protection characteristics of old and new cables using TGA-FTIR and a micro-calorimeter (MCC). The experimental results showed that when the temperature was higher than 277 °C, the mass loss of the aging cable jacket was significantly greater than that of the new cable jacket. The final residual mass of the old cable was much smaller than that of the new cable. In addition, in air or nitrogen atmospheres, the initial mass loss temperature of the new and old cables under various heating rates was generally the same, but the mass loss during the pyrolysis process of the old PVC sheath was larger than that of the new sheath, and the HCl release speed was slower than that of the new sheath. However, the initial release time was earlier than that of the new sheath. The results of the MCC showed that the old jacket burned more strongly and that the heat release per unit

mass was higher than the new jacket. However, in this experiment, there was no guarantee that the old and new jacket came from the same cable.

Li et al. [165] used a cone calorimeter to simulate the fire characteristics of crosslinked polyethylene cables under fire conditions. The experimental results showed that with increases in aging time, the ignition time first increased and then decreased, which may be due to the volatilization of combustible components such as plasticizers and lubricants in the initial insulation layer. In the later stage, due to the decrease in the thermal stability of the insulating material, the ignition time decreased, while the heat release rate was the opposite. Zhang et al. [166] used a cone calorimeter to study the effects of different aging times and types (thermal oxygen aging, hydrothermal aging, ozone aging, and xenon arc aging) on the fire resistance of two kinds of wires under a constant radiation intensity. The results showed that aging had different effects on the ignition time and heat release rate of different types of cables, but the ignition time was longer than that of non-aging cables. Among the four types of aging, the ignition time of thermal aging cables was longer than that of the other three types of aging, and the heat release rate was also higher than that of other aging modes. Kim et al. [167] analyzed the fire risk in the early, middle, and late stages of combustion of cables with different aging degrees based on the fire performance index (FPI) and fire growth index (FGI). The experimental results showed that in the early stage of combustion, with the extension of aging time, FPI showed an increasing trend due to the loss of volatile components in the cables. FGI showed a downward trend, and the fire risk was low, but in the middle and late periods, HRR, THR, and MLR were greater than those of non-aged cables. The fire risk increased, and the changes in CO_2, CO, and HCl with the degree of aging also varied. Fang et al. [168] conducted thermogravimetric analyses, differential scanning calorimetry tests, and fire spread tests on aging wires. The results of the thermogravimetric analyses and differential scanning calorimetry tests demonstrated that the aging wires showed different pyrolysis temperatures and crystallinities at different aging temperatures. However, different pyrolysis temperatures and crystallinities have different effects on the ignition delay time of chemical kinetics under different pressures. Chemical kinetics control the ignition delay in the low-pressure region, and heat transfer controls the ignition delay in the high-pressure region. The higher the pyrolysis temperature and crystallinity, the larger the chemical kinetic control area of the wire. Wang et al. [169–174], combined with previous studies, conducted a comprehensive study on aging cables from the aspects of pyrolysis, fire characteristics, and flame propagation behavior and determined the reaction models and pyrolysis kinetic parameters of LDPE and PVC with different degrees of aging based on thermogravimetric experiments. Combined with Fourier infrared (FTIR), micro-scale combustion calorimetry (MCC), and cone calorimetry, it was found that aging PVC sheath was easier to pyrolyze, the combustion of which was weaker and incomplete, and at a high heat flux, the TTI and pHRR of new and old cables are not significantly different. According to the results of XPS, after thermal aging, the metal in the wire core will diffuse into the insulation layer, which plays a catalytic role in the aging and pyrolysis of the insulation layer, and the fire spread rate generally shows a downward trend with the aging time.

3.2. Cable Fire Behavior

Studies on cable fire behavior are closely related to test standards related to cable combustion performance. The major European standards are shown in Table 1.

A cable tray is a common way of laying cables in nuclear power plants, the combustion of which is also one of the most common types, as shown in Figure 31.

The fire behavior of cable trays has been widely studied by scholars, and full-scale experimental studies are being led by several projects.

Table 1. Testing standards of cables.

Title	Content
EN 50200:2015 [175]	Method of test for resistance to fire of unprotected small cables for use in emergency circuits.
EN 50399 [176]	Methods of test for the assessment of vertical flame spread, heat release, smoke production, and the occurrence of flaming droplets/particles of vertically mounted electric cables under defined conditions.
IEC 60331 [177–179]	Tests for electric cables under fire conditions—circuit integrity—Part 1: Test method for fire with shock at a temperature of at least 830 °C for cables of rated voltage up to and including 0.6/1.0 kV and with an overall diameter exceeding 20 mm. Part 2: Test method for fire with shock at a temperature of at least 830 °C for cables of rated voltage up to and including 0.6/1.0 kV and with an overall diameter not exceeding 20 mm. Part 3: Test method for fire with shock at a temperature of at least 830 °C for cables of rated voltage up to and including 0.6/1.0 kV tested in a metal enclosure.
EN 60332-1-2 [180]	Test for vertical flame propagation for a single insulated wire or cable—Procedure for 1 kW pre-mixed flame.

Figure 31. Cable tray fire. Refs. [181,182].

From 1975 to 1987, Sandia National Laboratories conducted a series of studies on cable fire behavior [183], mainly including an electrical starting cable fire test in 1976, isolated cable tray fire test in 1978, cable fire test in exposed fire in 1977, cable tray fire corner effect test in 1979, flame-retardant sheathed cable test in 1978, and cable fire burning mode analysis in 1981. One of the findings was that the transverse cable bridge fire spreads upward in a "V" shape, and the "V" shape deviates from the center of gravity line at an angle of about 35°. The formation of this "V" shape spread mode is caused by the unequal horizontal spread rate of each layer of cable; that is, the spread rate of the upper layer cable is faster than that of the lower layer.

In 2000, several European national laboratories jointly carried out the FIPEC (Fire Performance of Electrical Cables) project [184], which carried out cable fire experiments of different sizes. Among them, according to the actual cable installation size, the real-size cable bridge fire experiment and small-size cable material cone calorimeter experiment were carried out. The real-size experiment was carried out in a relatively narrow corridor, involving the combustion characteristics of the transverse cable bridge and the vertical cable bridge. This established a relationship with the small-size experiment, which provided a basis for the measurement of the subsequent fire heat release rate.

A German study [109] carried out a vertical cable bridge fire experiment in open space to study the influence of preheating on the fire spread and burning rate of vertical cables and to simulate the different combustion characteristics of aging cables and new cables. The authors also studied the influence of natural ventilation on the fire characteristics of ordinary PVC cables and flame-retardant cables when laid vertically. The aim was to provide fire model support for nuclear power plant fire safety assessments.

In 2007, The Cable Response to Live Fire Project (CAROLEFIRE) [185], including a series of 78 small-scale tests and a second series of 18 intermediate-scale open burn tests, provided data supporting the resolution of a "risk-informed approach for post-fire safe shutdown circuit inspections" and improvements to fire modeling in the area of cable responses to fires.

At the same time, the Cable Heat Release, Ignition, and Spread in Tray Installations During Fire (CHRISTIFIRE) study [181,182] addressed the burning behavior of a fire beyond the point of electrical failure and developed the fire model FLASH-CAT to predict the HRR of horizontal cable tray fires, vertical cable tray fires, and the corridor fires. Then, Li et al. [105] and Huang et al. [103] improved the model and proposed improved prediction models for the fire release rate of vertical cable bridges and the fiery release rate of horizontal cable bridges, respectively, and they carried out experimental verification.

The OECD PRIME fire research program led by the France IRSN in collaboration with 12 countries was carried out to understand the mechanisms of smoke and heat transmission in multi-chamber fire scenarios and the impact of fires on targets, which included the following [88]:

(1) The effects of pressure induced by fires in forced ventilated enclosures;
(2) The effects of oxygen depletion on the fuel mass loss rate;
(3) The relative effects of heat and mass transfers from the fire compartment to an adjacent room;
(4) The effects of the ventilation flow rate on the velocity profiles from the fire room to neighboring compartments;
(5) Cable performance testing;
(6) The effects of damper closure on the fire scenario;
(7) The behavior of the activation of a sprinkler system in a fire scenario;
(8) The behavior of a cable fire in confined and ventilated fire scenarios;
(9) The behavior of an electrical cabinet fire in confined and ventilated fire scenarios.

In addition to the above large-scale projects on cable bridge fire research, there are also several studies on the fire characteristics of full-size cables.

Huang et al. [91,92,98,101,102] carried out a series of cable tray fire experiments including room fires with vertical cable tray fires in a confined compartment, the effects of cable arrangements and the sidewall effect on the HRR of horizon cable trays. They established several models for cable tray fire prediction.

Zhang et al. [96,100] proposed three new approaches (improved intra-variance, integral ratio, and N-percentage methods) in a three-layer zone model to predict the stratification interface of fire smoke. Then, they developed a modified HRR prediction model in the compartment by combining the carbon dioxide measurement of HRR and the three-zone model.

Tang et al. [89] studied the fire characteristic sand hazards of two typical cables used in nuclear power plants and considered the effects of the cable space, the results of which indicated that NPP flame-retardant cables have a low sustained damage, fire development rate, and overall fire risk. The distance has little effect on the burning time of the sheath, but it promotes the burning of the insulation layer. The time from the first peak to the second peak decreases with increases in the distance. Additionally, the effects of spacing on cable bridge fires are not monotonous. The combustion of cables with a spacing of 10 mm has a higher fire risk, and its quality loss rate is the largest.

The cable spacing effect with the interlayer distance was also studied by An [94]. The results illustrated that the larger the layer spacing, the higher the flame height and the

smaller the flame width. When the distance between layers is greater than 10 cm, the flame cannot spread to the upper layer of the cable. When the layer spacing is fixed, the flame width decreases with increases in cable spacing, and the flame height increases first and then decreases. When the cable spacing is 1.0 cm, the flame height is the largest.

Except for the spacing and interlayer distance, the effects of various fire loads and ventilation speeds on the cable fire spread speed and smoke temperature in a mine was also studied, which showed that the flame-retardant cable can be ignited and continuously burnt at a certain wind speed, but the combustion can be restrained at high wind speeds.

As summarized above, a large number of scholars and projects have systematically studied horizontal and vertical cable tray fires, as well as the effects of the ventilation status, spacing, fire load, and other factors. They have proposed a large number of heat release rate or ceiling temperature prediction models. For cable tray fires, in addition to experimental studies, CFD simulations are also an important branch. The studies in this area fall into two main categories.

On the one hand, some scholars use CFD simulation software, such as FDS, to simulate real cable tray fires. Tang et al. [186] simulated multi-layer cable fires using a fire dynamics simulator (FDS). The effects of the cable bridge spacing, ignition position, and tunnel ventilation speed on the fire characteristics were studied. Ferng et al. [187,188] used FDS to simulate cable burning and typical nuclear power plant fire scenarios and compared them with the experimental results. Qu et al. [189] established a multi-physics simulation model of a double-layer cable shaft based on the theories of electromagnetism fluid mechanics and thermodynamics. They also analyzed the temperature distribution of electromagnetic flow in the cable shaft and the influence of the fire-blocking material under rated working conditions.

On the other hand, based on the experimental data, inverse modeling can be carried out using simulation software. The most influential of these studies has been the output of the OECD PRIME Fire Research Project. Sophie et al. [83] used the CALIF3S/ISIS CFD software developed by IRSN and took the measured heat release rate in the experiments as the input data to simulate the fire of vertical and horizontal cable trays in the open atmosphere as well as the fire in confined and mechanically ventilated compartments. The differences between the pressure and gas temperature and the experimental results were analyzed. W. Hay et al. [190] used the same method to simulate a fire in PVC cables on a long cable tray in a large mechanical ventilation facility. Daniel et al. [191] and Verma et al. [192] combined FLASH-CAT and FDS to propose a method for determining the HRR of cable tray fires in a confined, ventilation-controlled environment. In addition to the studies mentioned above, some researchers also used small-scale test data (from cone calorimetry) to simulate full-scale cable tray fires [97,193,194].

3.3. The Release of Toxic Gases

As discussed in Chapter 1, toxic gases are a non-negligible potential threat to humans from cable fires. The vast majority of toxic gases in cable fires originate from the organic materials in insulation, sheathing, and other components. These toxic gases mainly include the following types [195–197]: nitrogen oxides (NO_x: nitrogen oxide (NO) and nitrogen dioxide (NO_2)); carbon oxide (CO) and carbon dioxide (CO_2); various saturated and unsaturated hydrocarbons; oxygen, hydrogen, fluorine, chlorine, sulfur, nitrogen, and bromine compounds; sulfur oxides (mainly SO_2), etc. For the toxicity testing of materials, many countries and organizations have put forward standard test codes with different focuses: DIN 53436 [198], NES713 [199], BS 7990:2003 [200], BS ISO 19703 [201], IEC/TS 60695-7-51 [202], etc.

The influences on the toxic gas composition in cable fires are mainly due to two aspects: the cable composition material and the type of combustion (flame-burning or smoldering). In recent years, some scholars have studied the release of toxic gases in cable fires for different cable materials and under different external conditions according to the above standard test codes or other test methods.

T. Richard et al. [203] tested the yield of toxic products from five commercial cables using the steady-state tube furnace method (IEC 60695-7-50 [204]) and compared them with the static tube furnace method (NF X 70-100 [205]) and the results of large-scale cable fire experiments. The results of the steady-state tube furnace method can be used to evaluate the toxicity of combustion cables to a certain extent.

Katarzyna et al. [206] studied a PVC-insulated copper electric wire with an unknown composition (PVC filled with chalk) using a steady tube furnace to examine the dependence of the amount of CO, CO_2, and HCl under ventilation-controlled conditions. They showed that the values of the CO_2 yields of the wire were three times and two times lower than the pure PVC and pure LDPE, respectively, while the values of the CO yield were four times higher than the pure polymers under different ventilation conditions. The value of the CO yield decreased with increasing ventilation, while the HCl yield was shown to be independent of the ventilation conditions.

Rafal et al. [207] studied the effects of cable insulation materials and the type of combustion on the generation of toxic gases and the response time of fire smoke detectors in cable fires.

Hyun et al. [208] conducted an experimental study of the toxicity index of non-aged to 40-year-old CR/EPR cables based on NES 713 [199], which showed that the evaluation toxicity index of the aged cables was higher than that of the non-aged cable.

Min Ho and Seok Hui et al. [209,210] studied the combustion, smoke emission, and toxic gas emission characteristics of four flame-retardant cables and two fiber optic cables based on ISO 5660-1 [211] and NES 713 [199]. Based on the research results, they simulated the cable laying room of a nuclear power plant and tested more advanced fire dynamics simulations in order to accurately assess the harm of toxic gases released by cable fires to humans.

In the above studies, the types and concentrations of toxic gases released by cable fires vary with different cables and environments, so it may be necessary to build a large database of toxic gases in cable fires under different conditions to achieve an accurate cable fire toxicity assessment method.

4. Conclusions

This work reviews the current research progress of laboratory wire and commercial cable fire research over the past decades. The influences of pressure, oxygen, gravity, external air flow, voltage, and current, as well as the effects of the wire placement mode on the ignition, fire spread, drip, and extinction of wires, are systematically discussed. Based on the basic research results of heat transfer and combustion, the fire behavior of wires under the above conditions was qualitative analyzed. Additionally, the ignition delay time model of three ignition modes, the flame propagation model and the critical criterion of dripping and extinction (blow off and quenching), were also discussed in detail. At the same time, for the studies of commercial cable fires, several large research projects and some researchers' works on real cable fire behaviors, numerical simulations, and the release of toxic gases were summarized.

Although the current studies on both wires and cables have been extensive and the consideration of various influencing factors is relatively comprehensive, there are still many aspects that are worthy of further study. First of all, in the study of wire combustion, the mixing and chemical processes of the gas phase, phase transition, and flow behavior of the solid phase are usually ignored in the study of the combustion behavior of the wire itself or the influence mechanism of environmental conditions on its combustion behavior. These complex behaviors are crucial to the burning and extinguishing of wires. The neglect of these components has led to the fact that the theoretical models and empirical or semi-empirical prediction models proposed so far can only be qualitatively analyzed and cannot simulate real wire combustion. Secondly, combustion under an electric field is essential for both wires and cables, and the current study has not revealed its true mechanisms. Instead, it has only explained the burning phenomenon of wires under electric fields. Finally, there is

a gap between the research of wire-burning behavior and the research of cable fire behavior, and the research conclusions of wire burning cannot be directly applied to real cable fires. Therefore, subsequent research should be gradually extended to cable fire on the basis of revealing the burning behavior of wires.

Finally, this paper only discusses the research progress on the fire and combustion characteristics of cables and wires. There are also other research fields worthy of attention, such as cable fire detection, especially with the application of artificial intelligence, which are also worthy of discussion and summary by scholars.

Author Contributions: Conceptualization, Y.Z. and S.W. (Shasha Wang); methodology, S.W. (Shijie Wang) and K.T.; investigation, Y.L.; resources, S.W. (Shijie Wang) and Y.Z.; writing—original draft preparation, F.Y.; writing—review and editing, Y.Z. and F.Y.; visualization, S.W. (Shasha Wang); supervision S.W. (Shijie Wang) and Y.Z; project administration, Y.Z and S.W. (Shasha Wang); funding acquisition, Y.Z. All authors have read and agreed to the published version of the manuscript.

Funding: This work was supported by the National Natural Science Foundation of China (52374225, 52074202).

Institutional Review Board Statement: Not applicable.

Informed Consent Statement: Not applicable.

Data Availability Statement: The original contributions presented in the study are included in the article, further inquiries can be directed to the corresponding authors.

Conflicts of Interest: The authors declare no conflicts of interest.

Nomenclature

Symbol	Implication	Symbol	Implication
A	Cross-section area (m^2)/ pre-exponential factor	Nu	Nusselt number
a	Strain rate (s^{-1})	$\dot{q}''/\dot{Q}''$	Heat flux (kW/m^2)
B	Mass transfer number	r	Radius (m)
Bo	Bond number	t	Time (s)
c	Specific heat (kJ/kg/K)/ proportionality constant	T	Temperature (K or °C)
D	Diffusion coefficient (m^2/s)/diameter (m)	U	Sliding velocity (m/s)
Da	Damkohler number	x	Wire axial direction
E	Gaseous reaction activation energy (kJ/mol)	δ	Thickness (m)
f	Frequency (s^{-1})	β	Coefficient
Gr	Grashoff number	$\dot{\omega}'$	Chemical reaction rate (mol/L/s)
ΔH	Reaction heat (kJ/mol)	X	Volume fraction (%)
h	Convective heat transfer coefficient ($W/(m^2 \cdot K)$)	ρ	Density (kg/m^2)
I	Electrical current (A)	σ	Surface tension (Pa)
k	Thermal conductivity (W/m/K)	ϕ	Equivalence ratio
L	Heating length (m)	τ	Critical shear stress (Pa)
Le	Lewis number	θ	Angle (°)
$\dot{m}$	Mass loss rate (kg/s)		

References

1. Residential Building Electrical Malfunction Fire Trends. Available online: https://www.usfa.fema.gov/statistics/residential-fires/electrical.html (accessed on 9 April 2024).
2. Eaton, T.E. Electric Services and Building Fires. *Fire Technol.* **1992**, *28*, 70–86. [CrossRef]
3. Andersson, P.; Rosell, L.; Simonson, M.; Emanuelsson, V. Small and Large Scale Fire Experiments with Electric Cables under Well-Ventilated and Vitiated Conditions. *Fire Technol.* **2004**, *40*, 247–262. [CrossRef]

4. Bakhman, N.N.; Aldabaev, L.I.; Kondrikov, B.N.; Filippov, V.A. Burning of Polymeric Coatings on Copper Wires and Glass Threads: II. Critical Conditions of Burning. *Combust. Flame* **1981**, *41*, 35–43. [CrossRef]
5. Bakhman, N.N.; Aldabaev, L.I.; Kondrikov, B.N.; Filippov, V.A. Burning of Polymeric Coatings on Copper Wires and Glass Threads: I. Flame Propagation Velocity. *Combust. Flame* **1981**, *41*, 17–34. [CrossRef]
6. Fernandez-Pello, A.; Hasegawa, H.; Staggs, K.; Lipska-quinn, A.; Alvares, N. A Study Of The Fire Performance Of Electrical Cables. *Fire Saf. Sci.* **1991**, *3*, 237–247. [CrossRef]
7. Tewarson, A.; Khan, M.M. Flame Propagation for Polymers in Cylindrical Configuration and Vertical Orientation. *Symp. Int. Combust.* **1989**, *22*, 1231–1240. [CrossRef]
8. Jia, S.; Ma, Y.; Guo, Z.; Hu, L. Experimental Study of Spontaneous Ignition of Overloaded Electrical Wires under Transverse Wind. *Proc. Combust. Inst.* **2023**, *39*, 4031–4039. [CrossRef]
9. Guo, F.; Kawaguchi, S.; Hashimoto, N.; Fujita, O. Effect of Pyrolysis Kinetic Parameters on the Overload Ignition of Polymer Insulated Wires in Microgravity. *Proc. Combust. Inst.* **2023**, *39*, 3939–3947. [CrossRef]
10. Kobayashi, Y.; Konno, Y.; Huang, X.; Nakaya, S.; Tsue, M.; Hashimoto, N.; Fujita, O.; Fernandez-Pello, C. Laser Piloted Ignition of Electrical Wire in Microgravity. *Proc. Combust. Inst.* **2019**, *37*, 4211–4219. [CrossRef]
11. Fang, J.; Zhao, S.; Wang, J.; Xue, Y.; He, X.; Zhang, Y. Sub-Atmospheric Bursting Ignition of Fluorinated Ethylene Propylene Wire Insulation. *Fire Saf. J.* **2018**, *100*, 45–50. [CrossRef]
12. He, H.; Zhang, Q.; Wang, X.; Wang, F.; Zhao, L.; Zhang, Y. The Influence of Currents on the Ignition and Correlative Smoke Productions for PVC-Insulated Electrical Wires. *Fire Technol.* **2017**, *53*, 1275–1289. [CrossRef]
13. Shimizu, K.; Kikuchi, M.; Hashimoto, N.; Fujita, O. A Numerical and Experimental Study of the Ignition of Insulated Electric Wire with Long-Term Excess Current Supply under Microgravity. *Proc. Combust. Inst.* **2017**, *36*, 3063–3071. [CrossRef]
14. Takano, Y.; Fujita, O.; Shigeta, N.; Nakamura, Y.; Ito, H. Ignition Limits of Short-Term Overloaded Electric Wires in Microgravity. *Proc. Combust. Inst.* **2013**, *34*, 2665–2673. [CrossRef]
15. Huang, X.; Nakamura, Y.; Williams, F.A. Ignition-to-Spread Transition of Externally Heated Electrical Wire. *Proc. Combust. Inst.* **2013**, *34*, 2505–2512. [CrossRef]
16. Fujita, O.; Kyono, T.; Kido, Y.; Ito, H.; Nakamura, Y. Ignition of Electrical Wire Insulation with Short-Term Excess Electric Current in Microgravity. *Proc. Combust. Inst.* **2011**, *33*, 2617–2623. [CrossRef]
17. Kong, W.; Wang, B.; Zhang, W.; Ai, Y.; Lao, S. Study on Prefire Phenomena of Wire Insulation at Microgravity. *Microgravity Sci. Technol.* **2008**, *20*, 107–113. [CrossRef]
18. Zhang, Y.; Fang, J.; Wang, J.; Zhang, Y.; Song, L. Lower Pressure Dripping Limits of Inclined Polyethylene-Insulated Wires during Flame Spreading under Different Oxygen Concentrations. *Fire Saf. J.* **2021**, *120*, 103108. [CrossRef]
19. Kobayashi, Y.; Nakaya, S.; Tsue, M.; Takahashi, S. Flame Spread over Polyethylene-Insulated Copper and Stainless-Steel Wires at High Pressure. *Fire Saf. J.* **2021**, *120*, 103062. [CrossRef]
20. Gagnon, L.; Fernandez-Pello, C.; Urban, J.L.; Carey, V.P.; Konno, Y.; Fujita, O. Effect of Reduced Ambient Pressures and Opposed Airflows on the Flame Spread and Dripping of LDPE Insulated Copper Wires. *Fire Saf. J.* **2021**, *120*, 103171. [CrossRef]
21. He, H.; Zhang, Q.; Shi, L.; Li, H.; Huang, D.; Zhang, Y. Experimental Study on the Thermoplastic Dripping and Flame Spread Behaviors of Energized Electrical Wire under Reduced Atmospheric Pressure. *Polymers* **2021**, *13*, 346. [CrossRef]
22. Nagachi, M.; Citerne, J.-M.; Dutilleul, H.; Guibaud, A.; Jomaas, G.; Legros, G.; Hashimoto, N.; Fujita, O. Effect of Ambient Pressure on the Extinction Limit for Opposed Flame Spread over an Electrical Wire in Microgravity. *Proc. Combust. Inst.* **2021**, *38*, 4767–4774. [CrossRef]
23. Ma, Y.; Zhang, X.; Lu, Y.; Lv, J.; Zhu, N.; Hu, L. Effect of Transverse Flow on Flame Spread and Extinction over Polyethylene-Insulated Wires. *Proc. Combust. Inst.* **2021**, *38*, 4727–4735. [CrossRef]
24. Kang, M.S.; Park, S.H.; Yoo, C.S.; Park, J.; Chung, S.H. Effect of Core Metal on Flame Spread and Extinction for Horizontal Electrical Wire with Applied AC Electric Fields. *Proc. Combust. Inst.* **2021**, *38*, 4747–4756. [CrossRef]
25. Guibaud, A.; Consalvi, J.-L.; Citerne, J.-M.; Legros, G. Pressure Effects on the Soot Production and Radiative Heat Transfer of Non-Buoyant Laminar Diffusion Flames Spreading in Opposed Flow over Insulated Wires. *Combust. Flame* **2020**, *222*, 383–391. [CrossRef]
26. An, W.; Tang, Y.; Liang, K.; Wang, T.; Zhou, Y.; Wen, Z. Experimental Study on Flammability and Flame Spread Characteristics of Polyvinyl Chloride (PVC) Cable. *Polymers* **2020**, *12*, 2789. [CrossRef]
27. Guibaud, A.; Citerne, J.-M.; Consalvi, J.-L.; Legros, G. On the Effects of Opposed Flow Conditions on Non-Buoyant Flames Spreading over Polyethylene-Coated Wires—Part II: Soot Oxidation Quenching and Smoke Release. *Combust. Flame* **2020**, *221*, 544–551. [CrossRef]
28. Guibaud, A.; Citerne, J.-M.; Consalvi, J.-L.; Legros, G. On the Effects of Opposed Flow Conditions on Non-Buoyant Flames Spreading over Polyethylene-Coated Wires—Part I: Spread Rate and Soot Production. *Combust. Flame* **2020**, *221*, 530–543. [CrossRef]
29. Wang, Z.; Zhou, T.; Wei, R.; Wang, J. Experimental Study of Flame Spread over PE-insulated Single Copper Core Wire under Varying Pressure and Electric Current. *Fire Mater.* **2020**, *44*, 835–843. [CrossRef]
30. Konno, Y.; Hashimoto, N.; Fujita, O. Role of Wire Core in Extinction of Opposed Flame Spread over Thin Electric Wires. *Combust. Flame* **2020**, *220*, 7–15. [CrossRef]

31. Zhao, Y.; Chen, J.; Chen, X.; Sheng, Y.; Lu, S.; Luo, S.; Deng, J. Influence of High Atmospheric Pressure on Flame Spread over Electric Wire at Different Inclinations. *Process Saf. Environ. Prot.* **2020**, *136*, 66–75. [CrossRef]
32. Zhao, L.; Zhang, Q.; Tu, R.; Fang, J.; Wang, J.; Zhang, Y. Effects of Electric Current and Sample Orientation on Flame Spread over Electrical Wires. *Fire Saf. J.* **2020**, *112*, 102967. [CrossRef]
33. Wang, Z.; Wei, R.; He, J.; Wang, J. Melt Dripping Behavior in the Process of Flame Spread over Energized Electrical Wire at Different Pressures. *Fire Mater.* **2020**, *44*, 58–64. [CrossRef]
34. Nagachi, M.; Mitsui, F.; Citerne, J.-M.; Dutilleul, H.; Guibaud, A.; Jomaas, G.; Legros, G.; Hashimoto, N.; Fujita, O. Effect of Ignition Condition on the Extinction Limit for Opposed Flame Spread over Electrical Wires in Microgravity. *Fire Technol.* **2020**, *56*, 149–168. [CrossRef]
35. Konno, Y.; Kobayashi, Y.; Fernandez-Pello, C.; Hashimoto, N.; Nakaya, S.; Tsue, M.; Fujita, O. Opposed-Flow Flame Spread and Extinction in Electric Wires: The Effects of Gravity, External Radiant Heat Flux, and Wire Characteristics on Wire Flammability. *Fire Technol.* **2020**, *56*, 131–148. [CrossRef]
36. Guibaud, A.; Citerne, J.-M.; Consalvi, J.-L.; Fujita, O.; Torero, J.; Legros, G. Experimental Evaluation of Flame Radiative Feedback: Methodology and Application to Opposed Flame Spread Over Coated Wires in Microgravity. *Fire Technol.* **2020**, *56*, 185–207. [CrossRef]
37. Guibaud, A.; Consalvi, J.L.; Orlac'h, J.M.; Citerne, J.M.; Legros, G. Soot Production and Radiative Heat Transfer in Opposed Flame Spread over a Polyethylene Insulated Wire in Microgravity. *Fire Technol.* **2020**, *56*, 287–314. [CrossRef]
38. Park, S.H.; Kang, M.S.; Cha, M.S.; Park, J.; Chung, S.H. Flame Spread over Twin Electrical Wires with Applied DC Electric Fields. *Combust. Flame* **2019**, *210*, 350–359. [CrossRef]
39. Hu, L.; Zhu, K.; Lu, Y.; Zhang, X. An Experimental Study on Flame Spread over Electrical Wire with High Conductivity Copper Core and Controlling Heat Transfer Mechanism under Sub-Atmospheric Pressures. *Int. J. Therm. Sci.* **2019**, *141*, 141–149. [CrossRef]
40. Zhang, Y.; Fang, J.; Wang, J.; Zhao, L.; Zhang, Y. The Effects of Angular Orientation and Ultraviolet Aging on ETFE Wire Flame Spread. *Fire Mater.* **2019**, *43*, 393–400. [CrossRef]
41. Park, S.H.; Lim, S.J.; Cha, M.S.; Park, J.; Chung, S.H. Effect of AC Electric Field on Flame Spread in Electrical Wire: Variation in Polyethylene Insulation Thickness and Di-Electrophoresis Phenomenon. *Combust. Flame* **2019**, *202*, 107–118. [CrossRef]
42. Lu, Y.; Huang, X.; Hu, L.; Fernandez-Pello, C. Concurrent Flame Spread and Blow-Off over Horizontal Thin Electrical Wires. *Fire Technol.* **2019**, *55*, 193–209. [CrossRef]
43. Nagachi, M.; Mitsui, F.; Citerne, J.-M.; Dutilleul, H.; Guibaud, A.; Jomaas, G.; Legros, G.; Hashimoto, N.; Fujita, O. Can a Spreading Flame over Electric Wire Insulation in Concurrent Flow Achieve Steady Propagation in Microgravity? *Proc. Combust. Inst.* **2019**, *37*, 4155–4162. [CrossRef]
44. Konno, Y.; Hashimoto, N.; Fujita, O. Downward Flame Spreading over Electric Wire under Various Oxygen Concentrations. *Proc. Combust. Inst.* **2019**, *37*, 3817–3824. [CrossRef]
45. Kobayashi, Y.; Konno, Y.; Huang, X.; Nakaya, S.; Tsue, M.; Hashimoto, N.; Fujita, O.; Fernandez-Pello, C. Effect of Insulation Melting and Dripping on Opposed Flame Spread over Laboratory Simulated Electrical Wires. *Fire Saf. J.* **2018**, *95*, 1–10. [CrossRef]
46. Lim, S.J.; Park, S.H.; Park, J.; Fujita, O.; Keel, S.I.; Chung, S.H. Flame Spread over Inclined Electrical Wires with AC Electric Fields. *Combust. Flame* **2017**, *185*, 82–92. [CrossRef]
47. Zhao, Y.; Chen, J.; Chen, X.; Lu, S. Pressure Effect on Flame Spread over Polyethylene-Insulated Copper Core Wire. *Appl. Therm. Eng.* **2017**, *123*, 1042–1049. [CrossRef]
48. Kobayashi, Y.; Huang, X.; Nakaya, S.; Tsue, M.; Fernandez-Pello, C. Flame Spread over Horizontal and Vertical Wires: The Role of Dripping and Core. *Fire Saf. J.* **2017**, *91*, 112–122. [CrossRef]
49. Hu, L.; Lu, Y.; Yoshioka, K.; Zhang, Y.; Fernandez-Pello, C.; Chung, S.H.; Fujita, O. Limiting Oxygen Concentration for Extinction of Upward Spreading Flames over Inclined Thin Polyethylene-Insulated NiCr Electrical Wires with Opposed-Flow under Normal- and Micro-Gravity. *Proc. Combust. Inst.* **2017**, *36*, 3045–3053. [CrossRef]
50. He, H.; Zhang, Q.; Tu, R.; Zhao, L.; Liu, J.; Zhang, Y. Molten Thermoplastic Dripping Behavior Induced by Flame Spread over Wire Insulation under Overload Currents. *J. Hazard. Mater.* **2016**, *320*, 628–634. [CrossRef]
51. Citerne, J.-M.; Dutilleul, H.; Kizawa, K.; Nagachi, M.; Fujita, O.; Kikuchi, M.; Jomaas, G.; Rouvreau, S.; Torero, J.L.; Legros, G. Fire Safety in Space—Investigating Flame Spread Interaction over Wires. *Acta Astronaut.* **2016**, *126*, 500–509. [CrossRef]
52. Lim, S.J.; Kim, M.; Park, J.; Fujita, O.; Chung, S. Flame Spread over Electrical Wire with AC Electric Fields: Internal Circulation, Fuel Vapor-Jet, Spread Rate Acceleration, and Molten Insulator Dripping. *Combust. Flame* **2015**, *162*, 1167–1175. [CrossRef]
53. Nakamura, Y.; Azumaya, K.; Iwakami, J.; Wakatsuki, K. Scale Modeling of Flame Spread Over PE-Coated Electric Wires. In *Progress in Scale Modeling*; Saito, K., Ito, A., Nakamura, Y., Kuwana, K., Eds.; Springer International Publishing: Cham, Switzerland, 2015; Volume II, pp. 275–292. ISBN 978-3-319-10307-5.
54. Hu, L.; Zhang, Y.; Yoshioka, K.; Izumo, H.; Fujita, O. Flame Spread over Electric Wire with High Thermal Conductivity Metal Core at Different Inclinations. *Proc. Combust. Inst.* **2015**, *35*, 2607–2614. [CrossRef]
55. Takahashi, S.; Ito, H.; Nakamura, Y.; Fujita, O. Extinction Limits of Spreading Flames over Wires in Microgravity. *Combust. Flame* **2013**, *160*, 1900–1902. [CrossRef]
56. Takahashi, S.; Takeuchi, H.; Ito, H.; Nakamura, Y.; Fujita, O. Study on Unsteady Molten Insulation Volume Change during Flame Spreading over Wire Insulation in Microgravity. *Proc. Combust. Inst.* **2013**, *34*, 2657–2664. [CrossRef]

57. Kim, M.K.; Chung, S.H.; Fujita, O. Effect of AC Electric Fields on Flame Spread over Electrical Wire. *Proc. Combust. Inst.* **2011**, *33*, 1145–1151. [CrossRef]
58. Nakamura, Y.; Yoshimura, N.; Ito, H.; Azumaya, K.; Fujita, O. Flame Spread over Electric Wire in Sub-Atmospheric Pressure. *Proc. Combust. Inst.* **2009**, *32*, 2559–2566. [CrossRef]
59. Nakamura, Y.; Yoshimura, N.; Matsumura, T.; Ito, H.; Fujita, O. Opposed-Wind Effect on Flame Spread of Electric Wire in Sub-Atmospheric Pressure. *J. Therm. Sci. Technol.* **2008**, *3*, 430–441. [CrossRef]
60. Nakamura, Y.; Yoshimura, N.; Matsumura, T.; Ito, H.; Fujita, O. Flame Spread over Polymer-Insulated Wire in Sub-Atmospheric Pressure: Similarity to Microgravity Phenomena. In *Progress in Scale Modeling*; Saito, K., Ed.; Springer: Dordrecht, The Netherlands, 2008; pp. 17–27. ISBN 978-1-4020-8681-6.
61. Umemura, A.; Uchida, M.; Hirata, T.; Sato, J. Physical Model Analysis of Flame Spreading along an Electrical Wire in Microgravity. *Proc. Combust. Inst.* **2002**, *29*, 2535–2543. [CrossRef]
62. Fujita, O.; Nishizawa, K.; Ito, K. Effect of Low External Flow on Flame Spread over Polyethylene-Insulated Wire in Microgravity. *Proc. Combust. Inst.* **2002**, *29*, 2545–2552. [CrossRef]
63. Fujita, O.; Kikuchi, M.; Ito, K.; Nishizawa, K. Effective Mechanisms to Determine Flame Spread Rate over Ethylene-Tetrafluoroethylene Wire Insulation: Discussion on Dilution Gas Effect Based on Temperature Measurements. *Proc. Combust. Inst.* **2000**, *28*, 2905–2911. [CrossRef]
64. Kikuchi, M.; Fujita, O.; Ito, K.; Sato, A.; Sakuraya, T. Experimental Study on Flame Spread over Wire Insulation in Microgravity. *Symp. Int. Combust.* **1998**, *27*, 2507–2514. [CrossRef]
65. Huang, X.; Zhou, Z.; Gao, J.; Hu, J.; Wang, C.; Zhang, X. Effect of Copper Core Diameter on Heat Transfer and Horizontal Flame Spread Behaviors over Electrical Wire. *Case Stud. Therm. Eng.* **2021**, *27*, 101296. [CrossRef]
66. Tang, K.; Wu, S.; Zhang, H.; Li, C.; Yuan, B.; Zhang, Y. Analysis of Heat Transfer during Flame Spread over Energized-Wire under High Currents. *Int. J. Therm. Sci.* **2022**, *171*, 107191. [CrossRef]
67. Huang, X.; Zhou, Z.; Hu, J.; Shao, Y.; Liu, Z.; Liu, Y. Experimental Study on Flame Spread Characteristics of Double PE-Insulated Wires with Different Spacing Distances. *Case Stud. Therm. Eng.* **2022**, *31*, 101822. [CrossRef]
68. Ma, Y.; Hu, L.; Jia, S.; Lv, J.; Xiong, S. Analysis of Upward- and Downward Flame Spread over Vertical Installed Polyethylene-Insulated Electrical Wires. *Combust. Flame* **2022**, *238*, 111896. [CrossRef]
69. Kang, M.S.; Park, J.; Chung, S.H.; Yoo, C.S. Effect of the Thickness of Polyethylene Insulation on Flame Spread over Electrical Wire with Cu-Core under AC Electric Fields. *Combust. Flame* **2022**, *240*, 112017. [CrossRef]
70. Li, C.; Chen, J.; Zhang, W.; Hu, L.; Cao, J.; Liu, J.; Zhu, Z.; Wu, S. Influence of Arc Size on the Ignition and Flame Propagation of Cable Fire. *Energies* **2021**, *14*, 5675. [CrossRef]
71. Zhang, Y.; Zhang, W.; Li, K.; Tang, K.; Liu, Z. Dripping Behavior Effects on Flame Propagation along Electrical Wires under High Currents. *Fire Saf. J.* **2021**, *123*, 103368. [CrossRef]
72. Wang, Z.; Wang, J. Experimental Study on Flame Propagation over Horizontal Electrical Wires under Varying Pressure. *Int. J. Therm. Sci.* **2020**, *156*, 106492. [CrossRef]
73. Wang, Z.; Wang, J. A Comprehensive Study on the Flame Propagation of the Horizontal Laboratory Wires and Flame-Retardant Cables at Different Thermal Circumstances. *Process Saf. Environ. Prot.* **2020**, *139*, 325–333. [CrossRef]
74. He, H.; Zhang, Q.X.; Zhao, L.Y.; Liu, J.; Wang, J.J.; Zhang, Y.M. Flame Propagation Over Energized PE-Insulated Wire Under Low Pressure. *Int. J. Comput. Methods Exp. Meas.* **2017**, *5*, 87–95. [CrossRef]
75. Wang, X.; He, H.; Zhao, L.; Fang, J.; Wang, J.; Zhang, Y. Ignition and Flame Propagation of Externally Heated Electrical Wires with Electric Currents. *Fire Technol.* **2016**, *52*, 533–546. [CrossRef]
76. Fang, J.; Zhang, Y.; Huang, X.; Xue, Y.; Wang, J.; Zhao, S.; He, X.; Zhao, L. Dripping and Fire Extinction Limits of Thin Wire: Effect of Pressure and Oxygen. *Combust. Sci. Technol.* **2021**, *193*, 437–452. [CrossRef]
77. Huang, X. Critical Drip Size and Blue Flame Shedding of Dripping Ignition in Fire. *Sci. Rep.* **2018**, *8*, 16528. [CrossRef] [PubMed]
78. Xie, Q.; Gong, T.; Huang, X. Fire Zone Diagram of Flame-Retardant Cables: Ignition and Upward Flame Spread. *Fire Technol.* **2021**, *57*, 2643–2659. [CrossRef]
79. Lee, J.; Kim, B.; Jung, Y.H.; Lee, S.; Shin, W.G. Numerical Study to Reproduce a Real Cable Tray Fire Event in a Nuclear Power Plant. *Nucl. Eng. Technol.* **2023**, *55*, 157–1584. [CrossRef]
80. Pretrel, H.; Zavaleta, P.; Suard, S. Experimental Investigation of the Effects of a Sidewall and Cable Arrangement on a Horizontal Cable Tray Fire in an Open Atmosphere. *Fire Mater.* **2022**, *47*, 718–732. [CrossRef]
81. Zavaleta, P.; Suard, S.; Audouin, L. Cable Tray Fire Tests with Halogenated Electric Cables in a Confined and Mechanically Ventilated Facility. *Fire Mater.* **2019**, *43*, 543–560. [CrossRef]
82. Suard, S.; Van Hees, P.; Roewekamp, M.; Tsuchino, S.; Gonzalez, R. Fire Development in Multi-Compartment Facilities: PRISME 2 Project. *Fire Mater.* **2019**, *43*, 433–435. [CrossRef]
83. Bascou, S.; Zavaleta, P.; Babik, F. Cable Tray FIRE Tests Simulations in Open Atmosphere and in Confined and Mechanically Ventilated Compartments with the CALIF3S/ISIS CFD Software. *Fire Mater.* **2019**, *43*, 448–465. [CrossRef]
84. Klein-Heßling, W. Validation of the Lumped Parameter Code COCOSYS against Large-scale OECD PRISME 2 Fire Experiments. *Fire Mater.* **2019**, *43*, 591–609. [CrossRef]
85. Plumecocq, W.; Audouin, L.; Zavaleta, P. Horizontal Cable Tray Fire in a Well-confined and Mechanically Ventilated Enclosure Using a Two-zone Model. *Fire Mater.* **2019**, *43*, 530–542. [CrossRef]

86. Zavaleta, P.; Hanouzet, R.; Beji, T. Improved Assessment of Fire Spread over Horizontal Cable Trays Supported by Video Fire Analysis. *Fire Technol.* **2019**, *55*, 233–255. [CrossRef]
87. Pelzer, M.; Klein-Heßling, W. Validation of COCOSYS Pyrolysis Models on OECD PRISME Fire Experiments. *Fire Saf. J.* **2013**, *62*, 174–191. [CrossRef]
88. Audouin, L.; Rigollet, L.; Prétrel, H.; Le Saux, W.; Röwekamp, M. OECD PRISME Project: Fires in Confined and Ventilated Nuclear-Type Multi-Compartments—Overview and Main Experimental Results. *Fire Saf. J.* **2013**, *62*, 80–101. [CrossRef]
89. Tang, K.; Zhang, Y.; Jiang, S.; Li, C.; Ma, C.; Liu, G.; Zhang, H.; Yuan, B. A Comparative Study on Fire Hazards of Cables Used in Nuclear Power Plants Based on Small- and Large-Scale Experiments. *J. Therm. Anal. Calorim.* **2022**, *147*, 14659–14671. [CrossRef]
90. Yang, H.; Zou, L.; Song, Z.; Wang, X.; Sun, Y.; Duan, Y. Identification of the Ignition Point of High Voltage Cable Trenches Based on Ceiling Temperature Distribution. *Symmetry* **2022**, *14*, 1417. [CrossRef]
91. Huang, P.; Ye, S.; Qin, L.; Huang, Y.; Yang, J.; Yu, L.; Wu, D. Experimental Study on the Maximum Excess Ceiling Gas Temperature Generated by Horizontal Cable Tray Fires in Urban Utility Tunnels. *Int. J. Therm. Sci.* **2022**, *172*, 107341. [CrossRef]
92. Huang, X.; Zhu, H.; He, L.; Peng, L.; Cheng, C.; Chow, W. Improved Model for Estimating Sidewall Effect on the Fire Heat Release Rate of Horizontal Cable Tray. *Process Saf. Environ. Prot.* **2021**, *149*, 831–838. [CrossRef]
93. Huang, X.; Wang, Y.; Ren, Z.; Li, Z.; Cheng, C.; Chow, W. Experimental Investigation on Maximum Ceiling Jet Temperature Generated by a Vertically Spreading Cable Fire. *Fire Saf. J.* **2021**, *120*, 103125. [CrossRef]
94. An, W.; Wang, T.; Liang, K.; Tang, Y.; Wang, Z. Effects of Interlayer Distance and Cable Spacing on Flame Characteristics and Fire Hazard of Multilayer Cables in Utility Tunnel. *Case Stud. Therm. Eng.* **2020**, *22*, 100784. [CrossRef]
95. Ke, G.; Zimeng, L.; Jinzhang, J.; Zeyi, L.; Yisimayili, A.; Zhipeng, Q.; Yaju, W.; Shengnan, L. Study on Flame Spread Characteristics of Flame-Retardant Cables in Mine. *Adv. Polym. Technol.* **2020**, *2020*, 1–7. [CrossRef]
96. Zhang, Y.; Liu, Z.; Lin, Y.; Fu, M.; Chen, Y. New Approaches to Determine the Interface Height of Fire Smoke Based on a Three-layer Zone Model and Its Verification in Large Confined Space. *Fire Mater.* **2020**, *44*, 130–138. [CrossRef]
97. Hehnen, T.; Arnold, L.; Mendola, S.L. Numerical Fire Spread Simulation Based on Material Pyrolysis—An Application to the CHRISTIFIRE Phase 1 Horizontal Cable Tray Tests. *Fire* **2020**, *3*, 33. [CrossRef]
98. Huang, X.; Zhu, H.; Peng, L.; Zheng, Z.; Zeng, W.; Bi, K.; Cheng, C.; Chow, W. Thermal Characteristics of Vertically Spreading Cable Fires in Confined Compartments. *Fire Technol.* **2019**, *55*, 1849–1875. [CrossRef]
99. Siemon, M.; Riese, O.; Forell, B.; Krönung, D.; Klein-Heßling, W. Experimental and Numerical Analysis of the Influence of Cable Tray Arrangements on the Resulting Mass Loss Rate and Fire Spreading. *Fire Mater.* **2019**, *43*, 497–513. [CrossRef]
100. Zhang, Y.; Tang, K.; Duan, H.; Niu, Y.; Huang, X.; Chen, B.; Liu, Z.; Chen, Y. Modified Carbon-Dioxide Measurement to Predict the Heat Release Rate of Fire Burning in a Compartment Based on the Three-Zone Model. *Fire Mater.* **2019**, *43*, 256–265. [CrossRef]
101. Huang, X.; Zhu, H.; Peng, L.; Zheng, Z.; Zeng, W.; Bi, K.; Cheng, C.; Chow, W. Burning Behavior of Cable Tray Located on a Wall with Different Cable Arrangements. *Fire Mater.* **2019**, *43*, 64–73. [CrossRef]
102. Huang, X.; Ren, Z.; Zhu, H.; Peng, L.; Cheng, C.; Chow, W. A Modified Zone Model on Vertical Cable Tray Fire in a Confined Compartment in the Nuclear Power Plant. *J. Fire Sci.* **2018**, *36*, 472–493. [CrossRef]
103. Huang, X.; Zhu, H.; Peng, L.; Zheng, Z.; Zeng, W.; Cheng, C.; Chow, W. An Improved Model for Estimating Heat Release Rate in Horizontal Cable Tray Fires in Open Space. *J. Fire Sci.* **2018**, *36*, 275–290. [CrossRef]
104. Zavaleta, P.; Audouin, L. Cable Tray Fire Tests in a Confined and Mechanically Ventilated Facility. *Fire Mater.* **2018**, *42*, 28–43. [CrossRef]
105. Li, L.; Huang, X.; Bi, K.; Liu, X. An Enhanced Fire Hazard Assessment Model and Validation Experiments for Vertical Cable Trays. *Nucl. Eng. Des.* **2016**, *301*, 32–38. [CrossRef]
106. Beji, T.; Verstockt, S.; Zavaleta, P.; Merci, B. Flame Spread Monitoring and Estimation of the Heat Release Rate from a Cable Tray Fire Using Video Fire Analysis (VFA). *Fire Technol.* **2016**, *52*, 611–621. [CrossRef]
107. Passalacqua, R.; Cortes, P.; Taylor, N.; Beltran, D.; Zavaleta, P.; Charbaut, S. Experimental Characterisation of ITER Electric Cables in Postulated Fire Scenarios. *Fusion Eng. Des.* **2013**, *88*, 2650–2654. [CrossRef]
108. McGrattan, K.; Lock, A.; Marsh, N.; Nyden, M.; Dreisbach, J.; Stroup, D. Understanding the hazards of grouped electrical cables. In Proceedings of the 2010 14th International Heat Transfer Conference, Washington, DC, USA, 8–13 August 2010.
109. McGrattan, K.B. *Evaluation of Fire Models for Nuclear Power Plant Applications: Benchmark Exercise #3: International Panel Report*; National Institute of Standards and Technology: Gaithersburg, MD, USA, 2007; p. NIST IR 7338.
110. Khan, M.M.; Bill, R.G.; Alpert, R.L. Screening of Plenum Cables Using a Small-Scale Fire Test Protocol. *Fire Mater.* **2006**, *30*, 65–76. [CrossRef]
111. Hees, P.V.; Axelsson, J.; Green, A.M.; Grayson, S.J. Mathematical Modelling of Fire Development in Cable Installations. *Fire Mater.* **2001**, *25*, 169–178. [CrossRef]
112. Alvares, N.; Fernandez-Pello, A.C. Fire Initiation and Spread in Overloaded Communication System Cable Trays. *Exp. Therm. Fluid Sci.* **2000**, *21*, 51–57. [CrossRef]
113. Quintiere, J. *Fundamentals of Fire Phenomena*; Wiley: Hoboken, NJ, USA, 2006; ISBN 978-0-470-09113-5.
114. Ge, F.; Qiu, T.; Zhang, M.; Ji, J. Experimental Research on the Thermal Characteristic of Low-Voltage Alternating Current (AC) Arc Faults. *Fire Saf. J.* **2023**, *136*, 103732. [CrossRef]
115. Gong, T.; Xie, Q.; Huang, X. Fire Behaviors of Flame-Retardant Cables Part I: Decomposition, Swelling and Spontaneous Ignition. *Fire Saf. J.* **2018**, *95*, 113–121. [CrossRef]

116. Miyamoto, K.; Huang, X.; Hashimoto, N.; Fujita, O.; Fernandez-Pello, C. Limiting Oxygen Concentration (LOC) of Burning Polyethylene Insulated Wires under External Radiation. *Fire Saf. J.* **2016**, *86*, 32–40. [CrossRef]
117. Huang, X.; Nakamura, Y. A Review of Fundamental Combustion Phenomena in Wire Fires. *Fire Technol.* **2020**, *56*, 315–360. [CrossRef]
118. Merzhanov, A.G.; Sirignano, W.A.; De Luca, L. *Advances in Combustion Science: In Honor of Ya. B. Zel'Dovich*; American Institute of Aeronautics and Astronautics: Reston, VA, USA, 1997.
119. Buckmaster, J. The Mathematical Theory of Combustion and Explosions. *Combust. Flame* **1987**, *67*, 185. [CrossRef]
120. Guo, F.; Kawaguchi, S.; Hashimoto, N.; Fujita, O. Identifying Two Ignition Modes of Polymer Insulated Wires with Continuous Excess Current in Microgravity. *Fire Saf. J.* **2023**, *141*, 103925. [CrossRef]
121. Kong, W.; Lao, S.-Q.; Zhang, P.-Y.; Zhang, X.-Q. Study on Wire Insulation Flammability at Microgravity by Functional Simulation Method. *Ranshao Kexue Yu Jishu J. Combust. Sci. Technol.* **2006**, *12*, 1–4.
122. Wang, K.; Wang, B.; Ai, Y.; Kong, W. Study on the Pre-Ignition Characteristics of Wire Insulation in the Narrow Channel Setup. *Sci. China Technol. Sci.* **2012**, *55*, 2132–2139. [CrossRef]
123. Wang, K.; Wang, B.; Kong, W.; Liu, F. Study on the Pre-Ignition Temperature Variations of Wire Insulation under Overload Conditions in Microgravity by the Functional Simulation Method. *J. Fire Sci.* **2014**, *32*, 257–280. [CrossRef]
124. Wang, K.; Xia, W.; Wang, B.; Ai, Y.; Kong, W. Study on Fire Initiation of Wire Insulation by a Narrow Channel at Low Pressure. *Microgravity Sci. Technol.* **2016**, *28*, 155–163. [CrossRef]
125. Wang, W.; Lu, C.; Ji, X.; Zhao, X.; Lyu, H. Research on Overcurrent Heating Characteristics of Copper Wires at Different Inclination Angles. *J. Therm. Anal. Calorim.* **2023**, *148*, 4833–4842. [CrossRef]
126. Incropera, F.P.; DeWitt, D.P.; Bergman, T.L.; Lavine, A.S. *Fundamentals of Heat and Mass Transfer*, 6th ed.; John Wiley & Sons: Hoboken, NJ, USA, 2006; ISBN 978-0-471-45728-2.
127. Fernandez-Pello, A.C. The Solid Phase. *Combust. Fundam. Fire* **1995**, *2*, 31–100.
128. Babrauskas, V. Research on Electrical Fires: The State of the Art. *Fire Saf. Sci.* **2009**, *9*, 3–18. [CrossRef]
129. Noto, F.; Kawamura, K. Tracking and Ignition Phenomena of Polyvinyl Chloride Resin under Wet Polluted Conditions. *IEEE Trans. Electr. Insul.* **1978**, *EI-13*, 418–425. [CrossRef]
130. Fisher, R.P.; Stoliarov, S.I.; Keller, M.R. A Criterion for Thermally-Induced Failure of Electrical Cable. *Fire Saf. J.* **2015**, *72*, 33–39. [CrossRef]
131. Babrauskas, V. *Ignition Handbook: Principles and Applications to Fire Safety Engineering, Fire Investigation, Risk Management and Forensic Science*; Fire Science Publishers: Issaquah, WA, USA, 2003; ISBN 978-0-9728111-3-2.
132. Kang, N.; Zhao, Z.; Lin, J.; Lu, S. Ignition of Silicone Rubber Sheaths by Series Arcs at Different Currents and Durations. *Fire Saf. J.* **2023**, *136*, 103753. [CrossRef]
133. Du, J.-H.; Tu, R.; Zeng, Y.; Pan, L.; Zhang, R.-C. An Experimental Study on the Thermal Characteristics and Heating Effect of Arc-Fault from Cu Core in Residential Electrical Wiring Fires. *PLoS ONE* **2017**, *12*, e0182811. [CrossRef] [PubMed]
134. Deng, J.; Lin, Q.-W.; Li, Y.; Wang, H.-B.; Wang, C.-P.; Zhao, Y.-H.; Lyu, H.-F.; Shu, C.-M. Ignition and Flame Spreading Features of Excessively Overloaded Polyvinyl Chloride Copper Wires. *Fire Technol.* **2023**, *59*, 3589–3607. [CrossRef]
135. Li, Y.; Sun, Y.; Gao, Y.; Sun, J.; Lyu, H.-F.; Yu, T.; Yang, S.; Wang, Y. Analysis of Overload Induced Arc Formation and Beads Characteristics in a Residential Electrical Cable. *Fire Saf. J.* **2022**, *131*, 103626. [CrossRef]
136. Courty, L.; Garo, J.P. External Heating of Electrical Cables and Auto-Ignition Investigation. *J. Hazard. Mater.* **2017**, *321*, 528–536. [CrossRef] [PubMed]
137. Kim, M.E. *Engineering Guide for Estimating Material Pyrolysis Properties for Fire Modeling*; Worcester Polytechnic Institute: Worcester, MA, USA, 2012.
138. Ogawa, S.; Mizukami, H.; Bando, Y.; Nakamura, M. The Pyrolysis Characteristics of Each Component in Municipal Solid Waste and Thermal Degradation of Its Gases. *J. Chem. Eng. Jpn.* **2005**, *38*, 373–384. [CrossRef]
139. Singh, A.; Kumar, R.; Soni, P.K.; Singh, V. Investigation of the Effect of Diisocyanate on the Thermal Degradation Behavior and Degradation Kinetics of Polyether-Based Polyurethanes. *J. Macromol. Sci. B Phys.* **2020**, *59*, 775–795. [CrossRef]
140. Balme, Q.; Rozaini, M.T.; Marias, F.; Lemont, F.; Charvin, P.; Sedan, J. Modeling the Rate of Batch-Mode Thermal Degradation of Polyethylene Suspended in an Oven. *Waste Biomass Valoriz.* **2021**, *12*, 4549–4566. [CrossRef]
141. Suraci, S.V.; Spinazzola, C.; Fabiani, D. Analysis on the Impact of Additives on Space Charge Behavior of Thermally Aged XLPE Plaques. In Proceedings of the 2022 IEEE Conference on Electrical Insulation and Dielectric Phenomena (IEEE CEIDP 2022), Auburn, AL, USA, 6–9 October 2022; IEEE: New York, NY, USA, 2022; pp. 41–44.
142. Boukezzi, L.; Rondot, S.; Jbara, O.; Boubakeur, A. Charging Kinetics of XLPE Insulation Cables Under E-Beam Irradiation in SEM: Effect of Thermal Aging. In Proceedings of the 2017 5th International Conference on Electrical Engineering—Boumerdes (ICEE-B), Boumerdes, Algeria, 29–31 August 2017; IEEE: New York, NY, USA, 2017.
143. Salivon, T.; Colin, X.; Salivon, T.; Comte, R. Degradation of XLPE and PVC Cable Insulators. In Proceedings of the 2015 IEEE Conference on Electrical Insulation and Dielectric Phenomena (CEIDP), Ann Arbor, MI, USA, 18–21 October 2015; IEEE: New York, NY, USA, 2015; pp. 656–659.
144. Zeng, D.W.; Born, M.; Wambach, K. Pyrolysis of EVA and Its Application in Recycling of Photovoltaic Modules. *J. Environ. Sci.* **2004**, *16*, 889–893.

145. Soudais, Y.; Moga, L.; Blazek, J.; Lemort, F. Comparative Study of Pyrolytic Decomposition of Polymers Alone or in EVA/PS, EVA/PVC and EVA/Cellulose Mixtures. *J. Anal. Appl. Pyrolysis* **2007**, *80*, 36–52. [CrossRef]
146. Coralli, I.; Gossmann, I.; Fabbri, D.; Scholz-Boettcher, B.M. Determination of Polyurethanes within Microplastics in Complex Environmental Samples by Analytical Pyrolysis. *Anal. Bioanal. Chem.* **2023**, *415*, 2891–2905. [CrossRef] [PubMed]
147. Yao, Z.; Yu, S.; Su, W.; Wu, D.; Liu, J.; Wu, W.; Tang, J. Probing the Combustion and Pyrolysis Behaviors of Polyurethane Foam from Waste Refrigerators. *J. Therm. Anal. Calorim.* **2020**, *141*, 1137–1148. [CrossRef]
148. Lapcikova, B.; Lapcik, L. TG and DTG Study of Decomposition of Commercial PUR Cellular Materials. *J. Polym. Mater.* **2011**, *28*, 353–366.
149. Jakic, M.; Vrandecic, N.S.; Klaric, I. Thermal Degradation of Poly(Vinyl Chloride)/Poly(Ethylene Oxide) Blends: Thermogravimetric Analysis. *Polym. Degrad. Stab.* **2013**, *98*, 1738–1743. [CrossRef]
150. Krongauz, V.V.V.; DePolo, W. Kinetics of Poly(Vinyl Chloride) Thermal and Thermo-Mechanical Degradation in the Presence of Epoxidized Plasticizer. Induction Effect. *J. Appl. Polym. Sci.* **2023**, *140*, e53482. [CrossRef]
151. Krongauz, V.V.; Lee, Y.-P.; Bourassa, A. Kinetics of Thermal Degradation of Poly(Vinyl Chloride). *J. Therm. Anal. Calorim.* **2011**, *106*, 139–149. [CrossRef]
152. Lu, Y.; Huang, X.; Hu, L.; Fernandez-Pello, C. The Interaction between Fuel Inclination and Horizontal Wind: Experimental Study Using Thin Wire. *Proc. Combust. Inst.* **2019**, *37*, 3809–3816. [CrossRef]
153. Kashiwagi, T.; Ohlemiller, T.J.; Werner, K. Effects of External Radiant Flux and Ambient Oxygen Concentration on Nonflaming Gasification Rates and Evolved Products of White Pine. *Combust. Flame* **1987**, *69*, 331–345. [CrossRef]
154. Fujita, O. Solid Combustion Research in Microgravity as a Basis of Fire Safety in Space. *Proc. Combust. Inst.* **2015**, *35*, 2487–2502. [CrossRef]
155. Osorio, A.F.; Mizutani, K.; Fernandez-Pello, C.; Fujita, O. Microgravity Flammability Limits of ETFE Insulated Wires Exposed to External Radiation. *Proc. Combust. Inst.* **2015**, *35*, 2683–2689. [CrossRef]
156. Olson, S.L. Piloted Ignition Delay Times of Opposed and Concurrent Flame Spread over a Thermally-Thin Fuel in a Forced Convective Microgravity Environment. *Proc. Combust. Inst.* **2011**, *33*, 2633–2639. [CrossRef]
157. Zhang, Y.; Tang, K.; Liu, Z.; Chen, Y. Experimental Study on Thermal and Fire Behaviors of Energized PE-Insulated Wires under Overload Currents. *J. Therm. Anal. Calorim.* **2021**, *145*, 345–351. [CrossRef]
158. Kim, H.-Y.; Lee, H.J.; Kang, B.H. Sliding of Liquid Drops Down an Inclined Solid Surface. *J. Colloid Interface Sci.* **2002**, *247*, 372–380. [CrossRef] [PubMed]
159. Matheson, A.F.; Charge, R.; Corneliussen, T. Properties of PVC Compounds with Improved Fire Performance for Electrical Cables. *Fire Saf. J.* **1992**, *19*, 55–72. [CrossRef]
160. Barnes, M.A.; Briggs, P.J.; Hirschler, M.M.; Matheson, A.F.; O'Neill, T.J. A Comparative Study of the Fire Performance of Halogenated and Non-Halogenated Materials for Cable Applications. Part II Tests on Cable. *Fire Mater.* **1996**, *20*, 17–37. [CrossRef]
161. Barnes, M.A.; Briggs, P.J.; Hirschler, M.M.; Matheson, A.F.; O'Neill, T.J. A Comparative Study of the Fire Performance of Halogenated and Non-Halogenated Materials for Cable Applications. Part I Tests on Materials and Insulated Wires. *Fire Mater.* **1996**, *20*, 1–16. [CrossRef]
162. Yang, H.; Fu, Q.; Cheng, X.; Yuen, R.K.K.; Zhang, H. Investigation of the Flammability of Different Cables Using Pyrolysis Combustion Flow Calorimeter. *Procedia Eng.* **2013**, *62*, 778–785. [CrossRef]
163. Meinier, R.; Sonnier, R.; Zavaleta, P.; Suard, S.; Ferry, L. Fire Behavior of Halogen-Free Flame Retardant Electrical Cables with the Cone Calorimeter. *J. Hazard. Mater.* **2018**, *342*, 306–316. [CrossRef] [PubMed]
164. Xie, Q.; Zhang, H.; Tong, L. Experimental Study on the Fire Protection Properties of PVC Sheath for Old and New Cables. *J. Hazard. Mater.* **2010**, *179*, 373–381. [CrossRef] [PubMed]
165. Li, J.M.; Zhang, J.Q.; Li, Q.; Guo, Z.D. Thermal Aging Effects on Fire Performance of the Cross-Linked Polyethylene Insulated Cable. *Mater. Sci. Forum* **2017**, *898*, 2399–2404. [CrossRef]
166. Zhang, B.; Zhang, J.; Li, Q.; Wang, L.; Xie, H.; Fan, M. Effects of Insulating Material Ageing on Ignition Time and Heat Release Rate of the Flame Retardant Cables. *Procedia Eng.* **2018**, *211*, 972–978. [CrossRef]
167. Kim, M.H.; Seo, H.J.; Lee, S.K.; Lee, M.C. Influence of Thermal Aging on the Combustion Characteristics of Cables in Nuclear Power Plants. *Energies* **2021**, *14*, 2003. [CrossRef]
168. Zhang, Y.; Fang, J.; Wang, J.; Zhao, L.; Zhang, Y. Ignition and Flame Spread over Thermal Aging Electrical Wires in Subatmospheric Pressure. *J. Thermoplast. Compos. Mater.* **2021**, *34*, 1428–1439. [CrossRef]
169. Wang, Z.; Wang, J. Comparative Thermal Decomposition Characteristics and Fire Behaviors of Commercial Cables. *J. Therm. Anal. Calorim.* **2021**, *144*, 1209–1218. [CrossRef]
170. Wang, Z.; Wang, J. An Experimental Study on the Fire Characteristics of New and Aged Building Wires Using a Cone Calorimeter. *J. Therm. Anal. Calorim.* **2019**, *135*, 3115–3122. [CrossRef]
171. Wang, Z.; Wei, R.; Ning, X.; Xie, T.; Wang, J. Thermal Degradation Properties of LDPE Insulation for New and Aged Fine Wires. *J. Therm. Anal. Calorim.* **2019**, *137*, 461–471. [CrossRef]
172. Wang, Z.; Wei, R.; Ouyang, D.; Wang, J. Investigation on Thermal Stability and Flame Spread Behavior of New and Aged Fine Electrical Wires. *J. Therm. Anal. Calorim.* **2020**, *140*, 157–165. [CrossRef]

173. Wang, Z.; Xie, T.; Ning, X.; Liu, Y.; Wang, J. Thermal Degradation Kinetics Study of Polyvinyl Chloride (PVC) Sheath for New and Aged Cables. *Waste Manag.* **2019**, *99*, 146–153. [CrossRef] [PubMed]
174. Wang, Z.; Wei, R.; Wang, X.; He, J.; Wang, J. Pyrolysis and Combustion of Polyvinyl Chloride (PVC) Sheath for New and Aged Cables via Thermogravimetric Analysis-Fourier Transform Infrared (TG-FTIR) and Calorimeter. *Materials* **2018**, *11*, 1997. [CrossRef]
175. *BS EN 50200:2015*; Method of Test for Resistance to Fire of Unprotected Small Cables for Use in Emergency Circuits. British Standards Institution: London, UK, 2015.
176. *EN 50399*; Common Test Methods for Cables under Fire Conditions—Heat Release and Smoke Production Measurement on Cables during Flame Spread Test—Test Apparatus, Procedures, Results. CENELEC: Brussels, Belgium, 2022.
177. *IEC 60331-1:2018*; Tests for Electric Cables under Fire Conditions—Circuit Integrity—Part 1: Test Method for Fire with Dhock at a Temperature of at least 830 °C for Cables of Rated Voltage up to and Including 0.6/1.0 kV and with an Overall Diameter Exceeding 20 mm. IEC: Geneva, Switzerland, 2018.
178. *IEC 60331-2:2018*; Tests for Electric Cables under Fire Conditions—Circuit Integrity—Part 2: Test Method for Fire with Shock at a Temperature of at least 830 °C for Cables of Rated Voltage up to and Including 0.6/1.0 kV and with an Overall Diameter not Exceeding 20 mm. IEC: Geneva, Switzerland, 2018.
179. *IEC 60331-3:2018*; Tests for Electric Cables under Fire Conditions—Circuit Integrity—Part 3: Test Method for Fire with Shock at a Temperature of at least 830 °C for Cables of Rated Voltage up to and Including 0.6/1.0 kV Tested in a Metal Enclosure. IEC: Geneva, Switzerland, 2018.
180. *IEC 60332-1-2:2004*; Tests on Electric and Optical Fibre Cables under Fire Conditions—Part 1–2: Test for Vertical Flame Propagation for a Single Insulated Wire or Cable—Procedure for 1 kW Pre-Mixed Flame. IEC: Geneva, Switzerland, 2018.
181. McGrattan, K.B.; Lock, A.J.; Marsh, N.D.; Nyden, M.R. *Cable Heat Release, Ignition, and Spread in Tray Installations during Fire (CHRISTIFIRE): Phase 1—Horizontal Trays*; NIST: Gaithersburg, MD, USA, 2012.
182. McGrattan, K.B.; Bareham, S.D. *Cable Heat Release, Ignition, and Spread in Tray Installations During Fire (CHRISTIFIRE) Phase 2: Vertical Shafts and Corridors*; NIST: Gaithersburg, MD, USA, 2013.
183. Nowlen, S.P. *A Summary of Nuclear Power Plant Fire Safety Research at Sandia National Laboratories 1975–1987*; US Nuclear Regulatory Commission (NRC): Washington, DC, USA; Div. of Engineering; Sandia National Lab. (SNL-NM): Albuquerque, NM, USA, 1989.
184. Grayson, S.J.; Van Hees, P.; Green, A.M.; Breulet, H.; Vercellotti, U. Assessing the Fire Performance of Electric Cables (FIPEC). *Fire Mater.* **2001**, *25*, 49–60. [CrossRef]
185. NUREG/CR-6931 Volume 1, "CAROLFIRE Test Report Volume 1: General Test Descriptions and the Analysis of Circuit Response Data, Draft for Public Comment," and NUREG/CR-6931 Volume 2, "CAROLFIRE Test Report Volume 2: Cable Fire Response Data for Fire Model Improvement, Draft for Public Comment-Revision 1", 30645 [E7-10611]. Available online: https://regulations.justia.com/regulations/fedreg/2007/06/01/E7-10611.html (accessed on 19 April 2024).
186. Tang, Z.; Gao, K.; Shan, Y.; Zhu, C.; Liu, Z.; Liu, Z. Study of the Fire Behavior of Multilayer Cables in a Mine Tunnel. *Energies* **2022**, *15*, 2059. [CrossRef]
187. Ferng, Y.M.; Liu, C.H. Investigating the Burning Characteristics of Electric Cables Used in the Nuclear Power Plant by Way of 3-D Transient FDS Code. *Nucl. Eng. Des.* **2011**, *241*, 88–94. [CrossRef]
188. Lin, C.-H.; Ferng, Y.-M.; Pei, B.-S. Development of CFD Fire Models for Deterministic Analyses of the Cable Issues in the Nuclear Power Plant. *Nucl. Eng. Des.* **2009**, *239*, 338–345. [CrossRef]
189. Qu, B.; Xiang, X.; Wu, S.; Li, K.; Li, X.; Zheng, Z. Simulation Analysis of Electromagnetic-Fluid-Temperature Field in Cable Shafts of High-Rise Buildings. *Math. Probl. Eng.* **2023**, *2023*, e7825964. [CrossRef]
190. Hay, W.; Seguillon, J.; Boyer, G. Numerical Simulations of a PVC Cable Fire on Long Cable-Trays in a Mechanically Ventilated Large Scale Facility. *Fire Saf. J.* **2023**, *138*, 103799. [CrossRef]
191. Tyas, D.; Bagshaw, D.; Plummer, J.; Nyogeri, L. Modelling the Heat Release Rate of PRISME Experimental Cable Fires in a Confined, Ventilation Controlled, Environment Using FLASH-CAT and FDS. *Fire Saf. J.* **2023**, *139*, 103828. [CrossRef]
192. Verma, N.; Hostikka, S.; Vaari, J.; Korhonen, T. Adapted FLASHCAT Methodology to Model Horizontal Cable Tray Fires Using Computational Fluid Dynamics. *Fire Saf. J.* **2023**, *138*, 103814. [CrossRef]
193. Beji, T.; Merci, B. Numerical Simulations of a Full-Scale Cable Tray Fire Using Small-Scale Test Data. *Fire Mater.* **2019**, *43*, 486–496. [CrossRef]
194. Alonso, A.; Lázaro, D.; Lázaro, M.; Alvear, D. Numerical Prediction of Cables Fire Behaviour Using Non-Metallic Components in Cone Calorimeter. *Combust. Sci. Technol.* **2023**, *195*, 1509–1525. [CrossRef]
195. Pitts, W.M. *Toxic Yield*; NIST: Gaithersburg, MD, USA, 2001.
196. Blomqvist, P.; Rosell, L.; Simonson, M. Emissions from Fires Part I: Fire Retarded and Non-Fire Retarded TV-Sets. *Fire Technol.* **2004**, *40*, 39–58. [CrossRef]
197. Blomqvist, P.; Rosell, L.; Simonson, M. Emissions from Fires Part II: Simulated Room Fires. *Fire Technol.* **2004**, *40*, 59–73. [CrossRef]
198. *DIN 53436*; Producing Thermal Decomposition Products from Materials in an Air Stream and Their Toxicological Testing. DIN: Berlin, Germany, 2015.
199. *NES713*; Determination of the Toxicity Index of the Products of Combustion from Small Specimens of Materials. NES: Washington, DC, USA, 1990.

200. *BS 7990:2003*; Tube Furnace Method for the Determination of Toxic Product Yields in Fire Effluents. British Standard: London, UK, 2003.
201. *BS ISO 19703:2018*; Generation and Analysis of Toxic Gases in Fire. Calculation of Species Yields, Equivalence Ratios and Combustion Efficiency in Experimental Fires. British Standard: London, UK, 2018.
202. *GSO IEC/TS 60695-7-51:2015*; Fire Hazard Testing—Part 7-51: Toxicity of Fire Effluent—Estimation of Toxic Potency: Calculation and Interpretation of Test Results. IEC: Geneva, Switzerland, 2015.
203. Hull, T.R.; Lebek, K.; Pezzani, M.; Messa, S. Comparison of Toxic Product Yields of Burning Cables in Bench and Large-Scale Experiments. *Fire Saf. J.* **2008**, *43*, 140–150. [CrossRef]
204. *IEC/TS 60695-7-50: 2002*; Fire Hazard Testing Part 7-50: Toxicity of Fire Effluent Estimation of Toxic Potency Apparatus and Test Method (Inactive). IEC: Geneva, Switzerland, 2002.
205. *NF X70-100*; Fire Behavior Tests—Analysis of Pyrolysis and Combustion Gases—Pipe Still Method. NF: La Plaine Saint-Denis, France, 2006.
206. Kaczorek-Chrobak, K.; Fangrat, J. PVC-Based Copper Electric Wires under Various Fire Conditions: Toxicity of Fire Effluents. *Materials* **2020**, *13*, 1111. [CrossRef] [PubMed]
207. Porowski, R.; Kowalik, R.; Ramiączek, P.; Bąk-Patyna, P.; Stępień, P.; Zielecka, M.; Popielarczyk, T.; Ludynia, A.; Chyb, A.; Gawdzik, J. Application Assessment of Electrical Cables during Smoldering and Flaming Combustion. *Appl. Sci.* **2023**, *13*, 3766. [CrossRef]
208. Seo, H.J.; Kim, N.K.; Lee, M.C.; Lee, S.K.; Moon, Y.S. Investigation into the Toxicity of Combustion Products for CR/EPR Cables Based on Aging Period. *J. Mech. Sci. Technol.* **2020**, *34*, 1785–1794. [CrossRef]
209. Kim, M.H.; Lee, S.H.; Jeong, S.Y.; Lee, S.K.; Lee, J.E.; Kwark, J.H.; Lee, M.C. Investigation of Combustion, Smoke, and Toxicity Characteristics of Flame-Retardant and Fiber-Optic Cables Used in Nuclear Power Plants. *J. Mech. Sci. Technol.* **2023**, *37*, 987–999. [CrossRef]
210. Lee, S.H.; Kim, M.H.; Jeong, S.Y.; Lee, S.K.; Lee, J.E.; Lee, M.C. Fire Dynamics Simulation in a Cable Spreading Room of a Nuclear Power Plant Using Fire Test Results of Heat Release and Toxic Gas Emission. *J. Mech. Sci. Technol.* **2024**, *38*, 1517–1532. [CrossRef]
211. *ISO 5660-1:2015*; Reaction-to-Fire Tests—Heat Release, Smoke Production and Mass Loss Rate. ISO: Geneva, Switzerland, 2015.

fire

MDPI

Review

A New Perspective on Hydrogen Chloride Scavenging at High Temperatures for Reducing the Smoke Acidity of PVC Cables in Fires. I: An Overview of the Theory, Test Methods, and the European Union Regulatory Status

Gianluca Sarti

Reagens S.p.A., Via Codronchi, 4, 40016 San Giorgio di Piano, BO, Italy; gianluca.sarti@reagens-group.com

Abstract: In the European Union, according to the second basic requirement for construction works of Regulation (EU) n. 305/2011, cables permanently installed in residential and public buildings must be classified in terms of reaction to fire, smoke production, flaming droplets, and acidity. The classification is harmonized; nevertheless, every European Union country decides what kind of classification a cable must have to be installed in a specific location, depending on its fire risk, following the assumption that the higher the fire risk of the area, the higher the fire performance of the cable. According to Regulation (EU) n. 305/2011, the acidity is indirectly assessed by performing EN 60754-2, giving an additional class based on pH and conductivity measurements. Hydrogen chloride (HCl) is one of the gases PVC cables release when they burn. In some applications out of the scope of the Regulation, acid scavengers are commonly used in special-grade PVC compounds to reduce the emission of acidic smoke. In this first part of the paper, the European rules on smoke acidity are presented, a review of the literature on HCl scavenging is performed, and an introduction on HCl scavenging at high temperatures is outlined. The paper shows how different experimental conditions and geometries of the test apparatuses used for assessing the smoke acidity can affect the emission of HCl in the gas phase and what critical issues affect the efficiency of acid scavengers at high temperatures in trapping HCl.

Keywords: acid scavengers; PVC; cables; smoke acidity

Citation: Sarti, G. A New Perspective on Hydrogen Chloride Scavenging at High Temperatures for Reducing the Smoke Acidity of PVC Cables in Fires. I: An Overview of the Theory, Test Methods, and the European Union Regulatory Status. *Fire* **2022**, *5*, 127. https://doi.org/10.3390/fire5050127

Academic Editors: Ying Zhang, Boyun Liu, Xiaoyu Ju and Xianjia Huang

Received: 11 August 2022
Accepted: 24 August 2022
Published: 27 August 2022

1. Introduction

HCl is released when a PVC cable burns, making the smoke acidic. Some fire scientists claim that its diffusion in a fire scenario can incapacitate and hinder a safe escape [1]. Nevertheless, many others highlight that its evaluation is not a critical measure in fire safety and that asphyxiant gases such as carbon monoxide (CO) drive the tenability and, after flashover, CO becomes the dominant intoxicant in fires [2–4]. However, the nature and quantity of toxic substances in smoke modestly depend on the kind of materials in fires. CO is released by all polymers, regardless of their chemical nature (approximately 20% of their weight after flashover) [3,5]. Additionally, CO reaches a high concentration before other intoxicants or irritant substances, such as HCl, can evolve to the gas phase, compromising the tenability conditions [6].

Furthermore, HCl decays quickly in real fire scenarios, and its content is much less than expected from the stoichiometric value in PVC-finished items. HCl is absorbed by "sorptive surfaces", trapped by fillers in PVC compounds, and washed away by water vapors, and its concentration in the gas phase rapidly goes down [2,3,7].

The heat released by the finished item, particularly the heat release rate, is crucial for assessing whether a small and controllable fire can turn into a large and deadly one, and therefore if the people can escape unharmed before the flashover is reached [8,9]. Furthermore, the smoke obscuration impedes people from escaping from the fire scenario

and being found by rescuers. Therefore, evaluation of the smoke production of the finished items is another strategic parameter, while the assessment of smoke acidity "has no general validity in fire hazard" [3]. Despite these considerations, since 2006 in the European Union (EU), an additional classification for acidity has been introduced in cables permanently installed in buildings, stopping the use of PVC cables in some locations. This paper explains the central principles for creating PVC compounds for cables with extremely low smoke acidity, aiming to get the best classification for acidity. The paper is divided into five parts. Part I is an introduction on the topic of acid scavenging at high temperatures and gives a review of the test methods for assessing smoke acidity, focusing on regulatory status in the EU and particularly on EN 60754-2. It also describes the basic concepts of acid scavenging at high temperatures in the condensed phase and its consequences on flame retardance, smoke production, and acidity.

The following parts show new data clarifying aspects presented in a series of conferences between 2017 and 2022, particularly AMI cables 2019, AMI cables 2020, and AMI formulation 2021: those conferences, regulatory context, and the research on low smoke acidity PVC compounds are described in this letter [10].

The parts are the followings:

- Part II: "Some examples of acid scavengers at high temperatures in the condensed phase";
- Part III: "EN 60754-2 and focus on the species in solution affecting pH and conductivity";
- Part IV: "The impact of acid scavengers on flame retardance and smoke emission";
- Part V: "Comparison between EN 60754-1 and EN 60754-2: what happens to acidity with the introduction of the thermal profile of EN 60754-1 in EN 60754-2".

2. Methods, Regulatory Status in the EU, the Pattern to Low Smoke Acidity PVC Compounds

2.1. List of Abbreviations and Acronyms

- HCl—hydrogen chloride;
- CO—carbon monoxide;
- PVC—poly(vinyl chloride);
- EU—European Union.

2.2. Smoke Acidity Test Methods

Several bench-scale tests can measure the concentration of acidic gases released during material combustion. They can measure the acid content statically or dynamically. The static test methods have a test apparatus based on a combustion chamber, a conveying system, and trapping devices, where the acidic substance is scavenged, analyzed, and quantified (titration, back titration, pH, conductivity, and ion chromatography). The test apparatus of the EN 60754 series and other "old" ones described in the past [11–14] are static methods. Methods with different sample quantities, heating regimes, and test apparatus geometries do not give comparable results.

The dynamic methods follow the concentration of the evolving gas during the combustion of the test specimen. TGA-FTIR, TGA-FTIR-GC-MS, and TGA-MS are the most common ones. FTIR sensors, capable of detecting the released gases and those responsible for making the smoke acidic, can be installed in a cone calorimetry test apparatus. In this way, acidic gases can be viewed "dynamically" during the combustion of the matrix.

The furnace tube is the most common test apparatus for assessing smoke acidity or corrosivity, particularly in some standards, such as the EN 60754 series. The sample, weighted in a combustion boat, is introduced into the quartz tube with a specific heating regime, according to the standard. A normalized air stream collects the fumes in some bubbling devices, where the ions are analyzed: directly by ion chromatography and titrimetric methods or indirectly by pH and conductivity measures. Methods based on the furnace test apparatus indirectly assess the smoke acidity generated by the burning sample. Measurements in tube furnaces are strongly affected by sample size. If the dimensions of the slices of the test specimen in the combustion boats are too big, char formation can

prevent the sample's total combustion, affecting the HCl concentration in the gas phase. The humidity should be carefully checked because moisture in the air flux can bring some chlorides to hydrolysis, freeing the trapped HCl in the gas phase. Even the geometry of the quartz tube and its connectors to the bubbling devices play a significant role. The terminal parts of the quartz tube, external to the furnace, are colder than the inner part. Here, the gas-phase substances can condensate and trap HCl, underestimating its concentration in bubbling devices. The release of trapped HCl can contaminate the successive runs, and therefore terminals should be introduced in the inner part of the furnace to evaporate all condensates before starting a new run.

For the same reason, the tubes, the connectors, the end connectors, and the bubbling devices must be washed carefully, recovering all dissolved HCl. All seals should be well-tightened to prevent the loss of HCl, and tubes must be sized as short as possible to recover all analytes easier during the washing procedures. Without those precautions, furnace tube measurements give poor repeatability and reproducibility.

The temperature and the heating rate strongly affect the emission of HCl of the sample in all kinds of bench-scale tests. If the test is performed at different temperatures and heating regimes, the concentration of HCl in the gas phase will differ [14–20].

2.3. Additional Classification for Acidity in the EU

Regulation (EU) n. 305/2011 (Construction Product Regulation, or CPR) lays down harmonized conditions for marketing construction products in the EU. One of the seven basic requirements of CPR is safety in case of fire; therefore, construction products must meet certain specific requirements in terms of reaction to fire. In the countries of the EU, tests, requirements, classifications, markings, and controls of construction products must be the same. They must have a harmonized classification according to EN 13501-1 and EN 13501-6.

In 2006, the Commission Decision of 27 October 2006, amending the Decision 2000/147/EC and implementing Council Directive 89/106/EEC (CPD), came into effect. It stated that cables permanently installed in the building had to be considered buildings and construction products, and additional classification for acidity had to be assessed. CPR, entered into force in 2017, has implemented the indications of CPD in terms of acidity without any modification in requirements or test methods. EN 13501-6 and EN 50575 lay down the test methods, requirements for getting the reaction to fire classification and the additional classifications for cables, CE marking, and declaration of performance (DoP).

The classes in terms of reaction to fire are the following: Aca, B1ca, B2ca, Cca, Dca, Eca, and Fca (A is more performant than F). The additional classifications for smoke (s1a, s1b, s2, and s3; s3 is less performant), flaming droplets (d0, d1, and d2; d2 is less performant), and acidity (a1, a2, and a3; a3 is less performant) complete the classification of the cable.

EN 13501-6 requires that acidity is indirectly assessed by performing EN 60754-2. The test apparatus of EN 60754-2 is a tube furnace where the sample is introduced and burnt for 30 min in isothermal conditions at temperatures between 935 °C and 965 °C. Two bubbling devices collect the smoke, and pH and conductivity are measured. Table 1 gives the pH and conductivity requirements for getting a specific additional class for acidity according to CPR.

Table 1. Additional classification for acidity and requirements according to EN 13501-6.

Class	Requirement Performing EN 60754-2
Class a_1	pH > 4.3, Conductivity < 2.5 (μS/mm)
Class a_2	pH > 4.3, Conductivity < 10 (μS/mm)
Class a_3	not a_1 or a_2

If the classification is harmonized at the European level, national codes and regulations of the countries in the EU define the classes the cables should have to be placed in locations depending on their specific fire risk. Thus, cables for medium and high-fire-risk locations

must have the best classes regarding reaction to fire, smoke production, flaming droplets, and acidity. Infrastructures, health and care facilities, educational facilities, commercials, industrials, and residentials have different fire risks. For example, in Italy, according to CEI UNEL 35016 and CEI 64-8 V4, cables in class B2ca s1a d1 a1 are needed for high-fire-risk locations. High-fire-risk locations are infrastructures such as air terminals, railway stations, marine stations, subways, road tunnels longer than 500 m, and railway tunnels over 1000 m long. In medium-fire-risk locations, such as health and care facilities such as hospitals, nursing homes, assisted residences, entertainment, educational facilities such as cinemas, theatres, discos, schools, museums, and residentials with more than 24 m height, cables Cca s1b d1 a1 are needed. Other locations, such as residential and commercial buildings less than 24 m in height (houses, bars, restaurants, shops, and medical offices) need bunched cables in class Cca s3 d1 a3 and single wires in class Eca. PVC compounds are suitable for manufacturing cables to match the class B2ca s1 d0 a3 [19,20], but nowadays there is no PVC compound for cables in class a1 or a2. Therefore, PVC cables are excluded in medium- and high-fire-risk locations. According to CPR, cables are the only buildings and construction products with an additional classification for acidity. The same is not required for other finished items such as flooring, linear insulation for pipes, and all finished items ruled by EN 13501-1.

In the EU, the market share of PVC compounds for wires and cables was 65% in 2000, which will be 35% in 2023, as forecasted in [21]. CPR has driven the growth of halogen-free cables [21], but other standard products, excluding a priori PVC compounds, do the same. The research in developing PVC compounds with a low smoke acidity lies in this regulatory context.

2.4. Definition of Acid Scavengers at High Temperatures

An acid scavenger is a "tool" for trapping acid substances through a reaction or a physical absorption, and it can even be designed to trap specific acidic substances. Acid scavengers discussed in this paper are specific to HCl. Acid scavengers acting as co-stabilizers for processing PVC compounds can be organic and inorganic substances. However, for working at high temperatures, the acid scavenger must be inorganic and stable during and after the combustion of the finished item. HCl scavengers have two main action mechanisms: scavenging in the gas phase and scavenging in the condensed phase.

An alkaline gas, neutralizing HCl, can reduce the smoke acidity in the gas phase, yielding products able to be transported by convention in the gas-phase stream. If EN 60754-2 is performed, these products can reach bubbling devices and dissolve electrolytes. In this kind of acid scavenging, the conductivity is therefore severely affected by the dissolved electrolytes. An example of this scavenging is when some precursors of NH_3 (such as melamine, urea derivatives, and ammonium octamolybdate) are used as flame retardants. In halogen-free systems, the TPU typically gives this kind of behavior, a high pH but extremely high conductivities, when EN 60754-2 is carried out due to specific flame retardants and charring agents releasing ammonia. For example, some TPU jackets for charging cables for electric vehicles must be flame retarded according to EN 50620 and IEC 62893 and cannot reach conductivities less than 10 μS/mm.

The action mechanism in the condensed phase is triggered by a solid acid scavenger trapping the gaseous HCl in a solid or liquid reaction product. This scavenging minimizes the contribution of other electrolytes in bubbling devices, except for non-scavenged HCl. Therefore, HCl is the driving force behind pH and conductivity.

This paper discusses scavenging in the condensed phase.

2.5. Acid Scavenger at High Temperatures in the Condensed Phase: Failures and Success

2.5.1. Where, When, and How

When a PVC compound is subjected to heat flux, the temperature increases, and three main zones can be identified: (a) pre-pyrolysis and combustion zone; (b) pyrolysis

and combustion zone; and (c) post-pyrolysis and combustion zone. Scheme 1 visually represents the three main zones.

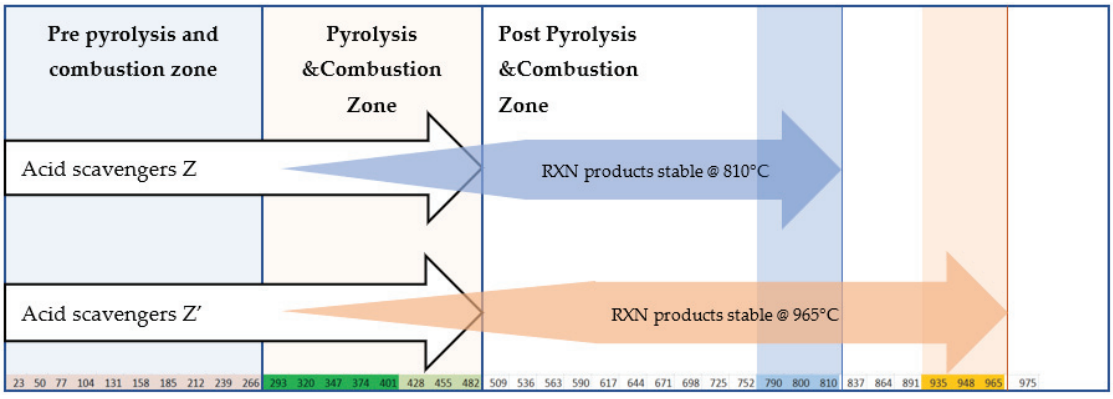

Scheme 1. Identification of the three main zones. The blue zone is the temperature range of EN 60754-1, and the orange one of EN 60754-2. Temperature in °C, "@" means "at".

The pre-pyrolysis and combustion zone is where thermal fluxes are low, and stabilizers play their fundamental role in preventing thermal degradation through HCl's well-known "zip elimination" [22]. In Scheme 1, the ranges of this zone are determined by all ingredients affecting the thermal stability of the compound, thus mainly stabilizers, but also the PVC resins, flame retardant fillers, plasticizers, and fillers. As the temperature increases over 270–300 °C, stabilizers end their action, the PVC compound starts the pyrolysis, and the evolving gases start their combustion. The PVC compound contains organic and inorganic additives. When the compound pyrolyzes, it makes free flammable and inflammable volatiles. Flammable volatiles burn, and the fire is supported by species such as ·H and ·OH, bringing energy to the flame. HCl is the primary, inflammable substance in the gas phase and plays a strategic role in trapping those radicals [23]. This phenomenon is common for all halogenated polymers and is called "flame poisoning". It is the reason for the inherent flame retardancy of PVC.

Wu and others have described the pyrolysis mechanism of PVC resin by a two-stage pyrolysis model [24]. However, the pyrolysis and combustion of PVC compounds for cables are made more complex by the presence of some additives. The kind and quantity of the volatiles released in the gas phase depend on the ingredients in the compound. The volatiles in the first stage of the degradation are mainly plasticizers, HCl, CO_2, CO, and benzene, while aliphatic hydrocarbons, CO_2, and CO are released in the second stage. If there is $CaCO_3$, another step centered at 750–850 °C is visible, related to its decarbonation. When all the organic substances are entirely burnt, the post-pyrolysis zone starts, where the stability of the reaction products coming from the reaction of the acid scavengers with HCl is crucial for getting low values of smoke acidity. Therefore, a substantial reduction of smoke acidity depends on the effectiveness of acid scavengers in holding and trapping HCl in solid ashes without any decomposition up to the maximum temperature required by the acidity test method. Performing EN 60754-1, the reaction product must be stable up to 810 °C and up to 965 °C if EN 60754-2 is carried out (Scheme 1).

2.5.2. Single-Step Reaction Versus Multiple-Step Reaction

References [16,17] claimed that acid scavengers could react through single- and multiple-step reactions. In their opinion, a single-step reaction involves just one acid scavenger following Scheme 1.

References [16,17] also claimed that, in PVC compounds, depending on the kind of ingredients, it is possible to also have multiple-step reactions involving more than a

single teammate, following the "relay race scheme" in Scheme 2. Here the performant acid scavenger A can react with HCl, creating A-Cl. If A-Cl is unstable, the second less-performant acid scavenger B gets HCl from A-Cl decomposition. If this HCl release is slower than that coming from PVC, and if B-Cl is stable, this "relay race scheme" brings a synergistic effect and increases the scavenging efficiency. Acid scavenger B can be added to the dry blend, or a precursor of B can yield B during the combustion. Multiple-step reactions can use more than two teammates. Part II of this paper will enter more into the details of multiple-step reactions, providing some examples.

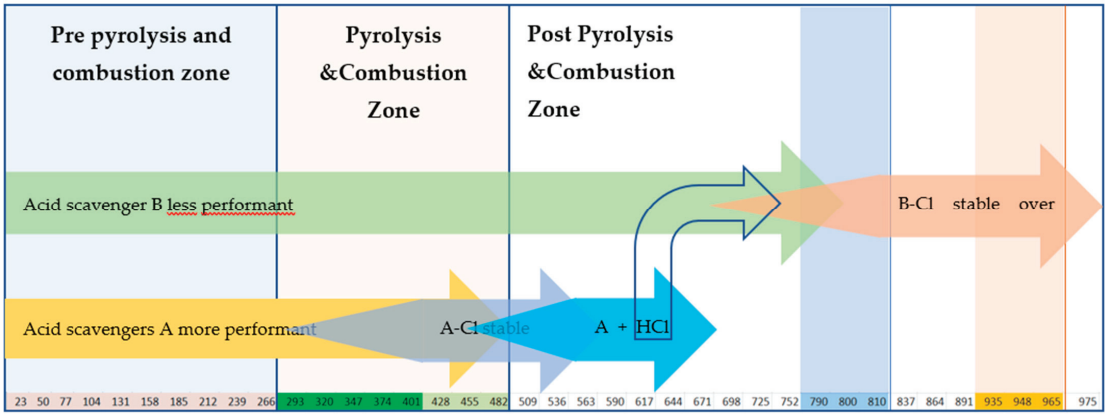

Scheme 2. Multiple-step reactions in HCl scavenging at high temperature. Temperature in °C, "@" means "at".

2.5.3. Main Failure Cases

Following the schemes mentioned above, the failure cases generating high smoke acidity should be mainly two: the kinetics of the scavenging action by an acid scavenger and the decomposition of the acid scavenger or its reaction products. If an acid scavenger has a slow kinetic in its reaction with HCl and the kinetic of the evolution of HCl is too fast, most of the HCl quickly reaches bubbling devices.

The Kinetics

Kinetics are strictly linked to the following:

- The chemical nature of the acid scavenger;
- Its particle size;
- Its dispersion properties;
- The test temperature and heating regimes.

1. Chemical nature

The higher reactivity of the acid scavenger, the quicker its reaction with HCl. So strong bases, such as hydroxides or oxides, are more efficient than weak scavengers, such as carbonates.

2. Particle size

The smaller the particle size, the more efficient the reaction is. Therefore, ground calcium carbonates (GCCs) are less efficient than ultrafine precipitated calcium carbonates (PCCs).

3. Dispersion

The better the acid scavenger dispersion, the more intimate contact with PVC, and the quicker the reaction with HCl. Furthermore, the zones in which acid scavenger misses emit massive amounts of HCl. It is worthy of mention that a finer particle size additive can bring about a worse dispersion of an acid scavenger in the matrix.

4. Temperature and heating regimes

The higher the temperature, the quicker the evolution of HCl from the burning matrix, and the more complex the chance for a solid acid scavenger to trap gaseous HCl. High temperatures give a severe drop in efficiency, and the presence of a heating regime and lower temperatures give more time to acid scavengers to trap HCl efficiently.

Decomposition of Acid Scavengers and Their Reaction Products

Suppose an unstable acid scavenger decomposes before the "pyrolysis and combustion zone", or its reaction product decomposes before reaching the test temperature. In that case, we will have an open door allowing HCl to get the bubbling devices. So many common organic acid scavengers used as long-term thermal stabilizers cannot be used as acid scavengers at high temperatures.

2.6. Definition of Efficiency of the Acid Scavenger

O'Mara proposed the Molar Absorption Efficiency (MAE) as a measure of the efficiency of an acid scavenger. MAE is the amount of HCl absorbed divided by the theoretical amount that could be absorbed by each filler [25]. Chandler and others defined efficiency based on the stoichiometry of reaction between $CaCO_3$ and HCl [14]. For calculating the efficiency of an acid scavenger through [25] or [14], we need to know precisely the reactions of all the involved actors. With multiple-step reactions, this cannot be feasible. It is better to propose a new definition of efficiency, considering not the moles of reactants and products but just the measure of the "effects" of the acid-scavenging reactions, whatever they are. The best candidate is an equation representing the efficiency E as a linear function of pH. Thus, performing EN 60754-2, we can propose Equation (1) as the definition of the efficiency of an acid scavenger at high temperature in the condensed phase:

$$E = 100 \times \frac{(\mathbf{pH} - \mathbf{pHs})}{(\mathbf{pHw} - \mathbf{pHs})} \quad (1)$$

where pH ∈ [**pHw**, **pHs**].

Equation (1) is a straight line, where the measured pH cannot stay outside its "existence region" (pHw–pHs). pHs is the minimum pH reachable when the stoichiometric quantity of HCl reaches the bubbling devices. It is a theoretical value and can be calculated directly from the sources of HCl in the formulation. pHw is the double deionized water (DDW) pH; i.e., the maximum reachable pH when HCl coming from the smoke is negligible. If the measured pH equals pHs, the efficiency is 0%, while if the measured pH equals pHw, the efficiency is 100%.

So, we can quickly get the efficiency of a specific acid scavenger in a single-step reaction or a "team" of acid scavengers in a multiple-step reaction by measuring the pH of the samples and DDW and calculating the pHs of the used formulations.

2.7. The Driving Force of pH and Conductivity in Solution

Reference [17] shows that, in aqueous solutions of HCl at different concentrations, conductivity and pH are linked by Equation (2):

$$\mathbf{c} = \mathrm{a} \times \mathrm{e}^{(-\mathrm{b} \times \mathbf{pH})} \quad (2)$$

where a and b are constants.

Suppose the scavenging of HCl is in the condensate phase and the contribution by the evaporation of reaction products is negligible. Performing EN 60754-2, the pH values and conductivities should fit Equation (2) very well. Therefore, ion chromatography (IC) should measure Cl- as the main species, being the concentration of other cations and anions insignificant. In this context, pH can be derived indirectly through IC measurements.

Part III of this paper enters more into the details of this topic, comparing the theoretical values coming from standard solutions of HCl, those calculated by Kohlrausch and Debye–Hückel–Onsager equations, and the experimental data coming from EN 60754-2.

2.8. Impact of Acid Scavengers on Flame Retardancy and Smoke Suppressant Properties

Acid scavengers interfere with the flame retardant mechanism in the gas and condensed phases, inhibiting flame retardancy. References [26–28] show the impact on the Limiting Oxygen Index (LOI) of several calcium carbonates with different particle sizes. In particular, the behavior of 0.1-micron calcium carbonate is better as acid scavengers compared to 14-micros and 1-micron ones. As expected by an inert filler, 14-micron calcium carbonate does not affect LOI, and LOI slightly increases as the filler concentration increases. However, 0.1-micron calcium carbonate is reactive. Getting in HCl with high efficiency, 0.1-micron calcium carbonate reduces LOI up to its stoichiometric value when the exact quantity of $CaCO_3$ is available for reacting completely with the potentially released HCl. After that, it increases again, behaving as an inert filler. The 1-micron calcium carbonate shows both characteristics; i.e., a constant trend up to stoichiometric value and a slight increase after. All these confirm that the higher the HCl scavenging, the lower the flame retardance. PVC with acid scavengers loses its inherent flame retardance. The scavenging of HCl also interferes with some conventional flame retardants used in PVC. Antimony trioxide (ATO) is a common flame retardant working only in the gas phase through the formation of $SbCl_3$, trapping the hot radicals feeding the flame [23]. Since $SbCl_3$ is less volatile than HCl or HBr, it stays longer in the flame, enhancing flame retardancy in PVC compounds. When a powerful acid scavenger at high temperatures is introduced into the compound, all HCl is trapped as chloride in the condensed phase, which prevents the formation of $SbCl_3$ and the reactions trapping the hot radicals. The consequence is a dramatic LOI drop, as reported in [16–18].

Furthermore, the scavenging of chlorine by acid scavengers interferes with the charring mechanism of some incipient Lewis acids used as flame retardants and smoke suppressants in PVC. Most of these precursors are metal oxides or salts reacting with HCl and yielding chlorides acting as potent Lewis acids. Starnes and co-workers [29,30], Jianqi Wang [31] and Li [32], and Rodolfo and Innocentini-Mei [33] studied some of them. Starnes and others [29,30] claimed the precursor of Lewis acid as an inhibitor of benzene formation from cis-trans polyene sequences to justify the smoke suppressant properties and the flame retardancy of some molybdenum compounds. In Starnes's theory in [29], Lewis acids seem to advantage parallel reactions, yielding to the production of crosslinked solid char through the following steps: the creation of preferential pathways bringing to all-trans sequences (Pathways 3 and 4 in Figure 1) and Diels–Alder reactions and Friedel–Crafts alkylations catalyzed by Lewis acid (Pathways 5 and 6 in Figure 1).

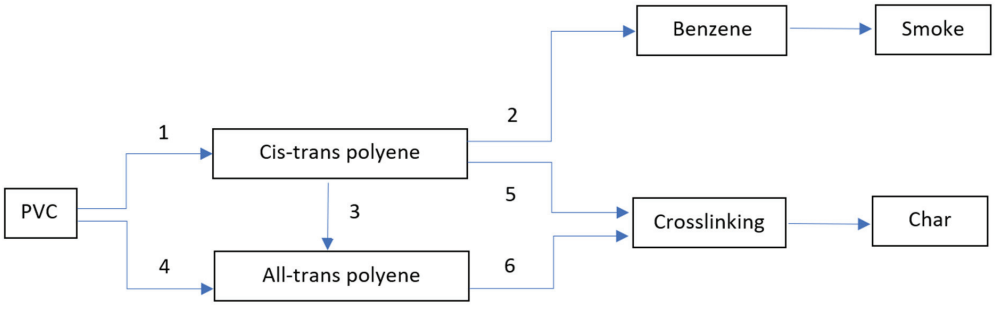

Figure 1. Pathways bringing to char and smoke in PVC combustion.

Without the Lewis acid, benzene is produced following Patterns 1 and 2 in Figure 1. The reaction is an intramolecular cyclization, as described by O' Mara [34]. Benzene is

formed during Stage 1 of the pyrolysis and combustion [24] and is a potent source of soot and smoke during PVC combustion.

Therefore, potent acid scavengers, inhibiting the reactions bringing about the formation of metal chlorides, switch off all pathways yielding the char, causing a substantial release of smoke, as reported in these proceedings [16,17]. All smoke suppressants involving chlorides, acting as Lewis acids promoting char, are, therefore, useless in low-smoke acidity compounds. Even the smoke suppressants avoiding cationic cracking at high temperatures in large fires [35,36] lay in that category. This topic will be discussed in detail in Part IV of the paper.

3. Conclusions

The acid scavenging of HCl at a high temperature can pass through a single-step or multiple-step reaction in which HCl is released and captured by different actors. Multiple-step reactions can be used to get the advantage of synergism capable of increasing the efficiency of the HCl scavenging. An acid scavenger at a high temperature in the condensed phase can fail or succeed, depending on how quickly it reacts with the HCl, the thermal stability of its reaction products, and how fast HCl evolves from PVC. Therefore, the acid scavenger's chemical nature, the particle size, how much disperses, the test temperature, and the heating regimes affect the efficiency of the scavenging. This topic will be discussed in detail in Part II of this paper.

Particularly, the temperature and heating regimes are critical parameters influencing the scavenging efficiency. Therefore, EN 60754-2 and EN 60754-2 with thermal profiles of EN 60754-1 have been compared in Part V of this paper.

Furthermore, EN 60754-2 is designed for collecting fumes in bubbling devices containing water, and it is strategic to know which species affect the pH and conductivity to "design" a good acid scavenger at high temperatures in the condensed phase. Suppose a mechanism of scavenging in the condensed phase is involved, and the volatility of the reaction products is low. In that case, the pH and conductivity are ruled only by the HCl reaching the bubbling device. IC should find Cl- as the predominant species, ICP and IC should determine the low concentration of all cations in the solution, and pH and conductivity should be linked by the mathematical formulation indicated in (2). This topic will be discussed in detail in Part III.

Lastly, HCl scavenging inhibits radical trapping and interferes with the char mechanisms of the PVC compound in case of fire. Therefore, the low smoke acidity compound can have less fire performance, with low flame retardance and more dense smoke. This drawback highlights the need to introduce a new generation of flame retardants and smoke suppressants if we want to keep the low smoke acidity, high flame retardancy, and minor smoke release together in a PVC compound. This topic will be discussed in detail in Part IV, where formulations containing potent acid scavengers giving low smoke acidity compounds reduce flame retardance and increase smoke release.

Funding: This research received no external funding.

Acknowledgments: The author wants to acknowledge Ing. Carlo Ciotti, Ing. Marco Piana, the PVC Forum Italia and the PVC4cables staff, and Emma Sarti for their help and support.

Conflicts of Interest: The authors declare no conflict of interest.

References

1. Hull, T.R.; Stec, A.A.; Paul, K.T. Hydrogen chloride in fires. *Fire Saf. Sci.* **2008**, *9*, 665–676. [CrossRef]
2. Obloj-Muzaj, M. Fire performance of PVC. *Int. Polym. Sci. Technol.* **2001**, *28*, 98–100. [CrossRef]
3. Hirschler, M. Fire safety, smoke toxicity, and acidity. In Proceedings of the Flame Retardants 2006, London, UK, 14–15 February 2006.
4. *ISO/TR 20118:2019*; Plastics—Guidance on Fire Characteristics and Fire Performance of PVC Materials Used in Building Applications 2019. ISO: Geneva, Switzerland. Available online: https://www.iso.org/standard/67071.html (accessed on 16 August 2022).
5. Babrauskas, V.; Gann, R.G.; Levin, B.C.; Paabo, M.; Harris, R.H.; Peacock, R.D.; Yusa, S. A methodology for obtaining and using toxic potency data for fire hazard analysis. *Fire Saf. J.* **1998**, *31*, 345–358. [CrossRef]

6. Guillaume, E.; Didieux, F.; Thiry, A.; Bellivier, A. Real-scale fire tests of one-bedroom apartments with regard to tenability assessment. *Fire Saf. J.* **2014**, *70*, 81–97. [CrossRef]
7. Beitel, J.J.; Bertelo, C.A.; Carroll, W.F.; Gardner, R.O.; Grand, A.F.; Hirschler, M.M.; Smith, G.F. Hydrogen chloride transport and decay in a large apparatus I. Decomposition of poly(vinyl chloride) wire insulation in a plenum by current overload. *J. Fire Sci.* **1986**, *4*, 15–41. [CrossRef]
8. Babrauskas, V.; Peacock, R.D. Heat release rate: The single most important variable in fire hazard. *Fire Saf. J.* **1992**, *18*, 255–272. [CrossRef]
9. Babrauskas, V.; Harris Jr, R.H.; Gann, R.G.; Levin, B.C.; Lee, B.T.; Peacock, R.D.; Paabo, M.; Twilley, W.; Yoklavich, M.F.; Clark, H.M. Fire hazard comparison of fire-retarded and non-fire-retarded products (NBS SP 749). In *Special Publication (NIST SP)*; National Institute of Standards and Technology: Gaithersburg, MD, USA, 1988. [CrossRef]
10. Sarti, G.; Piana, M. PVC in cables for building and construction. Can the "European approach" be considered a good example for other countries? *Acad. Lett.* **2022**, 5453. [CrossRef]
11. Greg, S. Quick method for determining the acid gas evolution from PVC formulations. *J. Vinyl Technol.* **1997**, *9*, 18–21. [CrossRef]
12. Sumi, K.; Morwick, D.W. *Acid Gas Evolution from PVC Using DBR/NRC Method*; Internal Report (National Research Council of Canada. Division of Building Research), no. DBR-IR-425; National Research Council of Canada: Ottawa, ON, Canada, 1976. [CrossRef]
13. Sze On Chan, H. Measurement of hydrochloric acid emission from burning PVC compounds. *J. Fire Sci.* **1984**, *2*, 106–122. [CrossRef]
14. Chandler, L.A.; Hirschler Smith, G.F. A heated tube furnace test for the emission of acid gas from PVC wire coating materials: Effects of experimental procedures and mechanistic considerations. *Eur. Polym. J.* **1987**, *23*, 51–61. [CrossRef]
15. Sarti, G. How formulations can influence the PVC cables fire behavior. In Proceedings of the 1st PVC4cables Conference, Lion, France, 26 October 2017. [CrossRef]
16. Sarti, G.; Piana, M. New formulations and test comparison for the classification of PVC cables under EU regulation n° 305/2011 for construction products. In Proceedings of the AMI Cables 2019, Duesseldorf, Germany, 5–7 March 2019. [CrossRef]
17. Sarti, G.; Piana, M. PVC cables and smoke acidity: A review comparing performances of old and new compounds. In Proceedings of the AMI Cables 2020, Duesseldorf, Germany, 3–5 March 2020. [CrossRef]
18. Bassi, I. Characterization of PVC Compounds and Evaluation of Their Fire Performance, Focusing on the Comparison between EN 60754-1 and EN 60754-2 in the Assessment of the Smoke Acidity. Master' Thesis, University of Bologna, Bologna, Italy, October 2021. Available online: https://www.pvc4cables.org/images/assessment_of_the_smoke_acidity.pdf (accessed on 16 August 2022).
19. Sarti, G.; Piana, M. Smoke acidity and a new generation of PVC formulations for cables. In Proceedings of the AMI Formulation 2021, Cologne, Germany, 16–18 September 2021.
20. Sarti, G. Developing and improving fire performance and safety in PVC. In Proceedings of the Future of PVC Compounding, Production & Recycling, online, 24–25 February 2022. [CrossRef]
21. Aupetit, A. Overview of the global cable industry–markets and materials. In *The Global Cable Industry: Materials, Markets*, 1st ed.; Beyer, G., Ed.; John Wiley & Sons Ltd: Chichester, UK, 2021; pp. 1–20. [CrossRef]
22. Starnes, W.; Xialong, G. Mechanism of autocatalysis in the thermal dehydrochlorination of poly(vinyl chloride). *Macromolecules* **2004**, *37*, 352–359. [CrossRef]
23. Laoutid, F.; Bonnaud, L.; Alexandre, M.; Lopez-Cuesta, J.M.; Dubois, P. New prospects in flame retardant polymer materials: From fundamentals to nanocomposites. *Mater. Sci. Eng. Rep.* **2009**, *63*, 100–125. [CrossRef]
24. Wu, C.H.; Wu, C.H.; Chang, C.Y.; Hor, J.L.; Shih, S.M.; Chen, L.W.; Chang, F.W. Two-stage pyrolysis model of PVC. *Can. J. Chem. Eng.* **1994**, *72*, 644–650. [CrossRef]
25. O'Mara, M.M. Pyrolysis–gas chromatographic analysis of poly(vinyl chloride). II. In situ absorption of HCl during pyrolysis and combustion of PVC. *J. Polym. Sci. Part A-1 Polym. Chem.* **1971**, *9*, 1387–1400. [CrossRef]
26. Brown, S.K.; Martin, K.G. Toxic gas and smoke measurement with the British Fire Propagation test. III: UPTV formulations with reduced HCl evolution. *Fire Mater.* **1985**, *9*, 95–102. [CrossRef]
27. Matthews, G.; Plumper, G.S. Effects of calcium carbonate fillers on the behaviour of PVC in fires. *Br. Polym. J.* **1981**, *13*, 17–21. [CrossRef]
28. Matthews, G.; Plumper, G.S. Effects of fillers on and the role of hydrogen chloride in the behaviour of PVC in fires. *Br. Polym. J.* **1984**, *16*, 34–38. [CrossRef]
29. Starnes, W.H.; Wescott, L.D.; Reents, W.D.; Cais, R.E.; Villacorta, G.M.; Plitz, I.M.; Anthony, L.J. Mechanism of poly(vinyl chloride) fire retardance by molybdenum(vi) oxide. Further evidence in favor of the lewis acid theory. In *Polymer Additives. Polymer Science and Technology*; Kresta, J.E., Ed.; Springer: Boston, MA, USA, 2007; Volume 26, pp. 237–248. [CrossRef]
30. Starnes, W.H., Jr.; Edelson, D. Mechanistic aspects of the behavior of molybdenum (VI) oxide as a fire-retardant additive for poly (vinyl chloride). An interpretive review. *Macromolecules* **1979**, *12*, 797–802. [CrossRef]
31. Li, B.; Wang, J. A cone calorimetric study of flame retardance and smoke emission of PVC. I. The effect of cuprous and molybdic oxides. *J. Fire Sci.* **1997**, *15*, 341–357. [CrossRef]
32. Li, B. A study of the thermal decomposition and smoke suppression of poly(vinyl chloride) treated with metal oxides using a cone calorimeter at a high incident heat flux. *Polym. Degrad. Stab.* **2002**, *78*, 349–356. [CrossRef]

33. Rodolfo, A.; Innocentini Mei, L.H. Metallic oxides as fire retardants and smoke suppressants in flexible poly(vinyl chloride). *J. Appl. Polym. Sci.* **2010**, *118*, 2613–2623. [CrossRef]
34. O' Mara, M.M. Combustion of PVC. *Pure Appl. Chem.* **1977**, *49*, 649–660. [CrossRef]
35. Zestos, A.G.; Grinnell, C.L.; Vinh, L.J.; Pike, R.D.; Starnes, W.H., Jr. Metal-exchanged clay and zeolite additives as smoke suppressants and fire retardants for poly(vinyl chloride). *J. Vinyl Addit. Technol.* **2009**, *15*, 87–91. [CrossRef]
36. Starnes, W.H., Jr.; Pike, R.D.; Cole, J.R.; Doyal, A.S.; Kimlin, E.J.; Lee, J.T.; Murray, P.J.; Quinlan, R.A.; Zhang, J. Cone calorimetric study of copper-promoted smoke suppression and fire retardance of poly(vinyl chloride). *Polym. Degrad. Stab.* **2003**, *82*, 15–24. [CrossRef]

fire

MDPI

Article

A New Perspective on Hydrogen Chloride Scavenging at High Temperatures for Reducing the Smoke Acidity of PVC Cables in Fires. II: Some Examples of Acid Scavengers at High Temperatures in the Condensed Phase

Gianluca Sarti

Reagens S.p.A., Via Codronchi, 4, 40016 San Giorgio di Piano, Italy; gianluca.sarti@fastwebnet.it

Abstract: In the European Union, according to Regulation (EU) n. 305/2011, cables permanently installed in residential and public buildings need additional classification for acidity. EN 60754-2 is the test method for assessing acidity, and three classes are provided: a1, a2, and a3 (less performant). The research on PVC compounds with low smoke acidity helps to produce cables in the best additional classes for acidity, giving the PVC cables the possibility to be used in medium and high fire risk locations. This paper shows the behavior of some acid scavengers at high temperatures performing EN 60754-2 in isothermal conditions at different temperatures between 400 °C and 950 °C. The test apparatus is a tube furnace where the test specimen is burnt, and the released gases are trapped in bubbling devices containing double deionized water. pH and conductivity are measured, the efficiency of the acid scavengers is assessed, and chemical analysis of the ashes is performed. That allows us to understand why some substances succeed and others fail in trapping hydrogen chloride (HCl). The most important conclusion in this paper is that the higher the temperature, the lower the performance of the acid scavenger, showing that HCl concentration in the gas phase depends strongly on the heating conditions of the test specimen.

Keywords: acid scavengers; PVC; cables; smoke acidity

Citation: Sarti, G. A New Perspective on Hydrogen Chloride Scavenging at High Temperatures for Reducing the Smoke Acidity of PVC Cables in Fires. II: Some Examples of Acid Scavengers at High Temperatures in the Condensed Phase. *Fire* **2022**, *5*, 142. https://doi.org/10.3390/fire5050142

Academic Editors: Ying Zhang, Boyun Liu, Xiaoyu Ju and Xianjia Huang

Received: 15 August 2022
Accepted: 15 September 2022
Published: 21 September 2022

1. Introduction

In the European Union (EU) in 2006, separate classes of reaction-to-fire performance were established for electric cables, including the additional classification for acidity, according to the Commission Decision of 27 October 2006, amending the Decision 2000/147/EC and implementing Council Directive 89/106/EEC, called Construction Product Directive or just CPD. At that time, the test method used to assess acidity was EN 50267-2-3 [1]. Since the Construction Product Regulation (Regulation (EU) n. 305/2011, or CPR) entered into force in 2017, EN 50267-2-3 became the test method for assessing smoke acidity, substituted later by EN 60754-2 [2]. EN 60754-2, EN 60754-1 [3] are similar to their siblings EN 50267-2-2 [4] and EN 50267-2-1 [5], used in EN 50525 series (see EN 50525-1 [6], annex B, table B2) to assess if a compound can be considered "halogen-free;" therefore, both are standards used by halogen-free producers. The paradox is that, while EN 60754-1 is a well-known and corroborated test method for PVC compound producers, EN 60754-2 is entirely unknown to them. The result is a historical lack of data on the pH and conductivities of PVC compounds for cables and difficulties in understanding how the classes a2 and a1 can be reached.

Some acid scavengers in the condensed phase at high temperatures are special calcium carbonates with fine particle sizes. In particular, precipitated calcium carbonate (PCC) was and still is the more suitable HCl scavenger for decreasing PVC compound smoke acidity. However, other extremely fine ground calcium carbonates (GCC) can be used [7,8]. In the past, the behavior of some HCl scavengers was evaluated, dynamically and statically, using different test apparatuses and conditions [9–12]. In particular, [12] shows how

different heating regimes can affect the evolution of HCl in the gas phase revealing how high temperatures and the absence of "gradual heating runs" hinder the action of the acid scavenger in trapping HCl.

This paper illustrates the behavior of 5 acid scavengers, alone and in combinations, performing EN 60754-2 in isothermal conditions for 30 min at 400 °C, 500 °C, 600 °C, 800 °C, and 950 °C. The performance has been evaluated through pH, conductivity, and efficiency. The efficiency has been calculated by the equation indicated in Part 1 of this paper [13]. This new way of evaluating the efficiency of acid scavengers has been proposed because simple and fast, involving a measure, the pH, directly quantified by EN 60754-2. The scientific community should test and evaluate it to establish its functionality and robustness.

Despite this, two main aspects can be highlighted when the potent acid scavengers have been evaluated in this research performing EN 60754-2 with isothermal profiles at different temperatures:

- the increase in the temperature severely affects their scavenging performance.
- at 950 °C, they go into crisis due to the too fast evolution of HCl in the gas phase.

This research has been developed in the regulatory context of smoke acidity in the EU, as explained in Part 1 of this paper [13].

2. Materials and Methods

2.1. Materials

Table 1 shows the first series of formulations. The amount of ingredients is expressed per hundred resin (phr). The formulation F50.0 represents the typical PVC jacket compound used in low voltage cables. The remaining formulations have been derived by F50.0, substituting $CaCO_3$ with different quantities of acid scavengers at high temperatures.

Table 1. First series of formulations: DINP means Di Iso Nonyl Phthalate. ESBO stands for Epoxidized Soy Oil Bean. The used antioxidant is Arenox A10, which is Pentaerythritol tetrakis(3-(3,5-di-tert-butyl-4-hydroxyphenyl)propionate), CAS number 6683-19-8. COS stands for Calcium Organic Stabilizer. PCC means Precipitated Calcium Carbonate. AS-1B and AS-6B are potent acid scavengers at high temperatures.

Raw Materials	Trade Name	F50.0 [phr]	F50.1 [phr]	F50.2 [phr]	F50.3 [phr]	F50.4 [phr]	F50.5 [phr]
PVC	Inovyn 271 PC	100	100	100	100	100	100
DINP	Diplast N	50	50	50	50	50	50
ESBO	Reaflex EP/6	2	2	2	2	2	2
Antioxidant	Arenox A10	0.1	0.1	0.1	0.1	0.1	0.1
COS	RPK B-CV/3037	3	3	3	3	3	3
$CaCO_3$	Riochim	90	0	0	0	0	0
$Al(OH)_3$	Apyral 40 CD	0	90	0	0	0	0
$Mg(OH)_2$	Ecopyren 3.5	0	0	90	0	0	0
PCC	Winnofil S	0	0	0	90	0	0
HTAS 1	AS-1B	0	0	0	0	90	0
HTAS 2	AS-6B	0	0	0	0	0	90

The formulations in Table 2 are designed to test the effect on the efficiency of PCC and $Mg(OH)_2$ at high loading levels. Here we focused on the synergism increasing the scavenging efficiency and the growth of smoke acidity due to dispersion phenomena.

Table 3 displays the third series of formulations focused on the $Mg(OH)_2$/PCC synergism.

The following materials have been used to perform EN 60754-2: Double Deionized Water (DDW) is internally produced by an ion exchange deionizer. The pH of DDW must be between 5.50 and 7.50, and the conductivity less than 0.5 μS/mm. Buffer and conductivity standard solutions come from VWR International (pH: 2.00, 4.01, 7.00, and 10.00, conductivity: 2.0, 8.4, 14.7, 141.3 μS/mm).

Table 2. Second series of formulations. pH and conductivity are measured according to EN 60754-2 at 950 °C. DINP means Di Iso Nonyl Phthalate. ESBO stands for Epoxidized Soy Oil Bean. The used antioxidant is Arenox A10, which is Pentaerythritol tetrakis(3-(3,5-di-tert-butyl-4-hydroxyphenyl)propionate), CAS number 6683-19-8. COS stands for Calcium Organic Stabilizer. PCC means Precipitated Calcium Carbonate.

Raw Materials	Trade Name	F50.6 [phr]	F50.7 [phr]	F50.8 [phr]	F50.9 [phr]	F50.10 [phr]
PVC	Inovyn 271 PC	100	100	100	100	100
DINP	Diplast N	50	50	50	50	50
ESBO	Reaflex EP/6	2	2	2	2	2
Antioxidant	Arenox A10	0.1	0.1	0.1	0.1	0.1
COS	RPK B-CV/3037	3	3	3	3	3
$CaCO_3$	Riochim	0	0	0	0	0
$Al(OH)_3$	Apyral 40 CD	0	0	0	0	0
$Mg(OH)_2$	Ecopyren 3.5	0	130	40	80	104
PCC	Winnofil S	130	0	90	180	234

Table 3. Synergism of PCC/$Mg(OH)_2$ couple. The measures are performed according to EN 60754-2 at 950 °C. DINP means Di Iso Nonyl Phthalate. ESBO stands for Epoxidized Soy Oil Bean. The used antioxidant is Arenox A10, which is Pentaerythritol tetrakis(3-(3,5-di-tert-butyl-4-hydroxyphenyl)propionate), CAS number 6683-19-8. COS stands for Calcium Organic Stabilizer. PCC means Precipitated Calcium Carbonate.

Raw Materials	Trade Name	50.6 [phr]	50.7 [phr]	50.18 [phr]	50.8 [phr]	50.19 [phr]	50.20 [phr]	50.21 [phr]	50.22 [phr]	50.23 [phr]
PVC	Inovyn 271 PC	100	100	100	100	100	100	100	100	100
DINP	Diplast N	50	50	50	50	50	50	50	50	50
ESBO	Reaflex EP6	2	2	2	2	2	2	2	2	2
Antioxidant	Arenox A10	0.1	0.1	0.1	0.1	0.1	0.1	0.1	0.1	0.1
COS	RPK B-CV/3037	3	3	3	3	3	3	3	3	3
$Mg(OH)_2$	Ecopyren 3.5	0	130	30	40	90	100	0	0	0
PCC	Winnofil S	130	0	100	90	40	30	100	90	40

2.2. Test Apparatus

Table 4 gives the list of utilized test apparatuses.

Table 4. Main test apparatuses utilized.

Test Apparatus	Producer	Model	Additional information
Plasticorder	Brabender	Palatograph EC	50 cm^3 chamber
Thermostat	Liebisch Labortechnik	LT-PVC-210-36-5	Test at 200 °C +/− 0.5 °C
Halogen Acid Gas test apparatus	SA Associates	Standard model	Porcelain combustion boats
Multimeter	Mettler Toledo	S213 standard kit	
Conductivity electrode	Mettler Toledo	S213 standard kit	
pH electrode	Mettler Toledo	S213 standard kit	
FTIR-ATR	Thermo Fisher Scientific	IS20	ATR correction to transmission
WD-XRF	Thermo Fisher Scientific	PERFORM'X	Borate Beads
Tensile testing machine	Hounsfield	H10KS	Specimen type 1A, 500 mm/min

2.3. Sample Preparation

PVC compound samples are prepared by weighing the stabilizers' ingredients in the 0.001 g balance. PVC, plasticizers, fillers, flame retardants, and acid scavengers are weighed in the 0.1 g balance. PVC and all the ingredients are mixed in a 20 L turbo-mixer up to 105 °C, producing 3 Kg dry-blend. The dry blend is processed in the plasticorder for 10 min at 160 °C, 30 rpm, getting 60 g kneaders. The kneaders are pressed at 160 °C for 4 min in 0.5 mm, 1 mm, and 6 mm sheets from which test specimens are obtained for the tests indicated in Tables 5 and 6.

Table 5. Tests for the main properties of the compound.

Standard	Measurement	Temperature	Note
ISO 527-1 [14]	Elongation at break	23 °C	Test specimens conditioned for 24 h at 23 °C
ISO 527-1 [14]	Tensile strength	23 °C	Test specimens conditioned for 24 h at 23 °C
ISO 1183 [15]	Specific Gravity	23 °C	After 24 h of conditioning at 23 °C
ISO 868 [16]	Hardness	23 °C	Shore A at 15, test specimens conditioned for 24 h at 23 °C
IEC 60811-405 [17]	Thermal Stability	200 °C	Test specimens conditioned for 24 h at 23 °C

Table 6. Tests for acidity assessment.

Technical Standard	Measurement	Temperature [°C]	Note
EN 60754-2	Smoke acidity	950	DDW, pH, and conductivity. The general method, according to the 2014 version.
Internal Method 2	Smoke acidity	400, 500, 600, 800	DDW, pH, and conductivity. The general method is according to the 2014 version.

2.4. Internal Tests and International Technical Standards Used

Tables 5 and 6 recall the used technical standards.

General method of EN 60754-2 is performed as follows: a calibrated reference thermocouple is used to control the temperature. The probe is introduced in the central part of the quartz glass tube, where an empty combustion boat is carried from the sample carrier. The temperature measured by the reference thermocouple is adjusted to 950 +/− 5 °C, maintaining it for at least one hour. The tube furnace is ready for the first run when the temperature is stable. Then, a sample of 1.000 +/− 0.001 g is weighed in a combustion boat. The porcelain combustion boat has dimensions according to the standard. It is quickly introduced into the quartz glass tube, moving the magnet along the sample carrier, while the countdown is activated when the combustion boat reaches the central part of the quartz glass tube. The smokes are purged in the bubbling devices containing DDW for 30 min by a normalized air flux (set according to the standard EN 60754-2 considering the geometry of the quartz glass tube). After 30 min, the connectors are disconnected, and the magnet extracts the combustion boat from the quartz glass tube. The water of the bubbling devices and from washing procedures is collected in a 1 L volumetric flask filled to the mark, and pH and conductivity are measured. The precautions indicated in Part I of this paper have been adopted to minimize the errors, which lead to poor repeatability and reproducibility [13].

Internal method 2 is performed as EN 60754-2 but applies different isothermal profiles. That procedure permits the evaluation of the performance of an acid scavenger at different temperatures, evaluating pH, conductivity, and efficiency. pH and conductivity measures are taken at 25 +/− 1 °C with the following procedure: the multimeter is calibrated with standard solutions before each measurement. The pH is calibrated at two points (4.01 and 7.00). Conductivity is calibrated at 1 point at 141.3 μS/mm. The solutions closer to the measured values are chosen as correction standards, and the measurements are corrected accordingly through a correction factor. pH and conductivity electrodes have a reference thermocouple that adjusts the fluctuation of temperature.

The smoke acidity measurements usually have low repeatability, especially if the temperature is high. This weakness is intrinsic to dynamics affecting the sample burning in a tube furnace. Samples do not burn the same way, and passivation can lead to some fluctuations in the results. Furthermore, as indicated in Part 1 of this paper [13], most procedures are done manually, which is the most significant source of errors. Therefore, a series of three measurements for each sample is performed, and this statistical method is used to calculate the mean value and outliers: from three test determinations, the mean value (μ), standard deviation (SD), and coefficient of variation (CV) are calculated for pH and conductivity using the following formulations:

$$\mu_x = \frac{1}{N}\sum_{i=1}^{N} x_i \tag{1}$$

$$SD_x = \sqrt[2]{\frac{1}{N}\sum_{i=1}^{N}(x_i - \mu_x)^2} \tag{2}$$

$$CV_x = \frac{SD_x}{|\mu_x|} \tag{3}$$

If the CV is higher than 5%, further three measurements are performed, and the mean value, standard deviation, and coefficient of variation are recalculated, including the previous values. That is the general method according to EN 60754-2:2014. EN 60754-2/A1:2020 [18] has introduced a new procedure for evaluating the data not considered in this paper.

Appendix B, Figures A12 and A13 give a schematic diagram of the sample preparation and testing process.

3. Results

3.1. First Series of Formulations

Table 7 shows the main properties of the first series of formulations. The main properties give a preliminary indication if the compound is suitable for manufacturing jackets according to EN 50525 series.

Internal method 2 has been performed at different temperatures, 400 °C, 500 °C, 600 °C, 800 °C, and EN 60754-2 at 950 °C. Table 8 shows the results of pH and conductivity for each formulation. Table 9 reports the elements found in ashes determined by XRF spectrometry. Figures A1–A6 show the FTIR spectra of the ashes of F50.0–F50.5 at different temperatures. Figures A7–A11 display the FTIR spectra of some standards compared to the FTIR spectra of F50.0–F50.5 ashes. Table 10 gives the principal FTIR bands of the substances found in the ashes.

Table 7. Focus on the main properties of the compounds. The mean values and the standard deviations are reported.

Formulation	F50.0	F50.1	F50.2	F50.3	F50.4	F50.5
Specific Gravity [g/cm^3]	1.542 +/− 0.012	1.505 +/− 0.021	1.503 +/− 0.004	1.542 +/− 0.007	1.445 +/− 0.014	1.446 +/− 0.009
Shore Hardness [type A, 15″]	88 +/− 1	89 +/− 1	89 +/− 1	88 +/− 1	90 +/− 1	90 +/− 1
Tensile strength [N/mm^2]	13.0 +/− 0.8	11.8 +/− 0.5	11.7 +/− 0.8	13.4 +/− 1.1	13.0 +/− 1.0	13.1 +/− 0.7
Elongation at break [%]	246.4 +/− 3.8	236.1 +/− 4.9	233.1 +/− 2.5	240.1 +/− 2.4	221.5 +/− 1.7	225.5 +/− 1.5
Thermal Stability [min]	104 +/− 3	79 +/− 2	73 +/− 4	76 +/− 5	291 +/− 11	299 +/− 12

Table 8. Mean values and SD of pH and conductivities at 400 °C, 500 °C, 600 °C, 800 °C, and 900 °C.

Method 2 at 400 °C	F50.0	F50.1	F50.2	F50.3	F50.4	F50.5
pH	2.48 +/− 0.06	2.37 +/− 0.06	2.81 +/− 0.07	3.71 +/− 0.03	4.03 +/− 0.19	3.88 +/− 0.12
Conductivity [µS/mm]	142.9 +/− 3.6	179.4 +/− 1.5	88.7 +/− 3.5	8.1 +/− 0.3	4.0 +/− 0.1	5.3 +/− 0.1
Method 2 at 500 °C	**F50.0**	**F50.1**	**F50.2**	**F50.3**	**F50.4**	**F50.5**
pH	2.48 +/− 0.04	2.41 +/− 0.03	2.41 +/− 0.09	3.73 +/− 0.10	3.70 +/− 0.15	3.69 +/− 0.13
Conductivity [µS/mm]	139.1 +/− 1.2	177.2 +/− 2.5	177.3 +/− 6.2	7.7 +/− 0.3	8.2 +/− 0.4	8.6 +/− 0.3
Method 2 at 600 °C	**F50.0**	**F50.1**	**F50.2**	**F50.3**	**F50.4**	**F50.5**
pH	2.51 +/− 0.02	2.30 +/− 0.01	2.31 +/− 0.03	3.69 +/− 0.07	3.70 +/− 0.10	3.65 +/− 0.05
Conductivity [µS/mm]	132.6 +/− 3.7	201.7 +/− 4.1	195.7 +/− 5.0	9.2 +/− 0.4	7.8 +/− 0.3	9.5 +/− 0.2
Method 2 at 800 °C	**F50.0**	**F50.1**	**F50.2**	**F50.3**	**F50.4**	**F50.5**
pH	2.63 +/− 0.13	2.30 +/− 0.09	2.29 +/− 0.09	3.26 +/− 0.11	3.52 +/− 0.02	3.20 +/− 0.03
Conductivity [µS/mm]	100.4 +/− 4.4	206.4 +/− 2.5	208.9 +/− 7.8	23.7 +/− 0.6	13.5 +/− 0.2	25.7 +/− 0.6
Method 2 at 950 °C	**F50.0**	**F50.1**	**F50.2**	**F50.3**	**F50.4**	**F50.5**
pH	2.62 +/− 0.03	2.27 +/− 0.10	2.27 +/− 0.02	2.74 +/− 0.06	2.89 +/− 0.08	2.79 +/− 0.02
Conductivity [µS/mm]	97.3 +/− 3.7	221.5 +/− 8.4	224.3 +/− 3.1	74.0 +/− 1.6	70.1 +/− 0.7	70.1 +/− 2.0

Table 9. Main elements in ashes detected by XRF.

Formulation	F50.0	F50.1	F50.2	F50.3	F50.4	F50.5
400 °C	Ca, Cl	Mg, Cl	Al, Cl	Ca, Cl	n.a.	n.a.
500 °C	Ca, Cl	Mg, Cl	Al, Cl	Ca, Cl	n.a.	n.a.
600 °C	Ca, Cl	Mg, Cl	Al, Cl	Ca, Cl	n.a.	n.a.
800 °C	Ca, Cl	Mg, Cl	Al, Cl	Ca, Cl	n.a.	n.a.
950 °C	n.a.	n.a.	n.a.	n.a.	n.a.	n.a.

n.a. = not available.

Table 10. Main FTIR bands in the ashes.

	1 [cm^{-1}]	2 [cm^{-1}]	3 [cm^{-1}]	4 [cm^{-1}]	5 [cm^{-1}]	6 [cm^{-1}]
$CaCO_3$	2509.64	1794.92	1417.26	873.10	846.70	710.66
$MgCl_2$	1616.43	1606.44				
$CaCl_2$	1628.43	1614.21				
MgO	Broadband centered at 548 cm^{-1}					
Al_2O_3	Broadband between 400 and 900 cm^{-1}					

The ashes are analyzed through the following procedure. After the combustion boat is extracted from the tube furnace, it is left to cool down and put in a PE zip lock bag.

Before the measurement, the combustion boat and standards are dried for 2 h in the oven at 105 °C. Metal oxides or chlorides are in the ash residue and are highly hygroscopic. During FTIR measurements, we cannot exclude the possibility that the samples can reabsorb some water. The measurement should be taken as fast as possible. XRF is conducted using borate-fused beads.

3.2. Second Series of Formulations

Table 11 shows the pH and conductivity of the second series of formulations used to evidence the $Mg(OH)_2$/PCC synergism.

Table 11. Synergism of PCC/$Mg(OH)_2$ couple. The measures are performed according to EN 60754-2 at 950 °C. The mean values and the SD are reported.

Formulation	F50.6	F50.7	F50.18	F50.9	F50.19	F50.20	F50.21	F50.22	F50.23
pH	2.93 +/− 0.06	2.34 +/− 0.04	3.19 +/− 0.11	3.75 +/− 0.08	2.65 +/− 0.02	2.51 +/− 0.04	2.90 +/− 0.01	2.89 +/− 0.00	2.33 +/− 0.02
Conductivity [µS/mm]	49.4 +/− 1.4	183.8 +/− 9.0	28.8 +/− 0.3	8.4 +/− 0.3	106.2 +/− 4.2	133.5 +/− 6.2	56.9 +/− 2.3	51.6 +/− 1.8	193.0 +/− 3.0

3.3. Third Series of Formulations

Table 12 shows the main properties of the formulations F50.6–F50.10 and pH and conductivities, focusing on the couple PCC/$Mg(OH)_2$ and the effect of its high loading level on acidity (the decrease of the smoke acidity performance due to the reduced dispersion of both additives). The smoke acidity has been measured using EN 60754-2 at 950 °C.

Table 12. Second series of formulations. Main properties of the compound. Mean values and SD are reported.

Formulation	F50.6	F50.7	F50.8	F50.9	F50.10
pH	2.93 +/− 0.06	2.34 +/− 0.02	3.32 +/− 0.06	3.75 +/− 0.08	3.75 +/− 0.09
Conductivity [µS/mm]	49.4 +/− 6.1	183.8 +/− 9.0	20.7 +/− 2.6	8.4 +/− 1.0	8.4 +/− 1.0
Specific Gravity [g/cm^3]	1.644 +/− 0.011	1.590 +/− 0.014	1.627 +/− 0.002	1.853 +/− 0.007	1.946 +/− 0.007
Hardness [SHA 15″]	91 +/− 1	92 +/− 1	91 +/− 1	97 +/− 1	98 +/− 1
Tensile strength [N/mm^2]	8.2 +/− 0.5	5.8 +/− 0.3	7.5 +/− 0.7	2.3 +/− 1.3	1.2 +/− 1.3
Elongation at break [%]	210.3 +/− 3.2	195.1 +/− 5.2	205.0 +/− 1.1	177.0 +/− 7.5	172.0 +/− 8.5
Thermal Stability [min]	76 +/− 5	71 +/− 3	61 +/− 2	57 +/− 4	38 +/− 3

3.4. The Efficiency of Scavenging

Tables 13–15 display the efficiency values, performing EN 60754-2 and the internal method 2 at the indicated temperatures.

Table 13. The mean efficiency and the SD of formulations F50.0–F50.5: EN60754-2 at different temperatures.

Temperature [°C]	F50.0	F50.1	F50.2	F50.3	F50.4	F50.5
400	8.0 +/− 1.5	5.1 +/− 1.6	16.9 +/− 1.9	40.0 +/− 0.8	50.8 +/− 5.1	45.1 +/− 3.1
500	8.1 +/− 1.0	6.3 +/− 0.7	6.3 +/− 2.4	40.6 +/− 2.6	41.8 +/− 4.1	40.2 +/− 3.4
600	8.6 +/− 0.4	3.1 +/− 0.3	3.4 +/− 0.7	39.7 +/− 1.8	40.9 +/− 2.7	38.9 +/− 1.2
800	12.0 +/− 3.5	3.3 +/− 2.5	3.1 +/− 2.3	28.2 +/− 2.8	36.9 +/− 0.7	27.1 +/− 0.9
950	12.2 +/− 0.7	2.4 +/− 2.6	2.3 +/− 0.4	14.7 +/− 1.5	18.7 +/− 2.2	16.0 +/− 0.4

Table 14. The mean efficiency and SD of formulations F50.6–F50.10: EN60754-2 at 950 °C.

	F50.6	F50.7	F50.8	F50.9	F50.10
950 °C	18.4 +/− 1.6	2.4 +/− 0.5	28.8 +/− 1.5	37.5 +/− 2.3	34.9 +/− 2.7

Table 15. The mean efficiency and SD of formulations F50.18–F50.23: EN60754-2 at 950 °C.

	F50.18	F50.19	F50.20	F50.21	F50.22	F50.23
950 °C	25.2 +/− 2.8	10.8 +/− 0.4	7.0 +/− 0.9	18.5 +/− 0.3	18.6 +/− 00	6.3 +/− 0.5

4. Discussion

4.1. Description of Used Acid Scavengers and Why They Have Been Selected

The acid scavengers have been chosen for different needs:

- GCC and PCC highlight the impacts of particle size on scavenging efficiency.
- AS-1B and AS-6B are mixtures of basic substances (different kinds and concentrations), comparing their performances with PCC, the standard acid scavenger for PVC.
- $Al(OH)_3$ shows the behavior of an inert and scarcely reactive acid scavenger.
- $Mg(OH)_2$ shows what happens when the reaction product with HCl decomposes.

4.2. Effect of Chemical Properties of a Substance on Efficiency

The chemical properties of acid scavengers greatly influence efficiency. For example, AS-6B (a mix of basic substances) shows higher efficiency than GCC or $Al(OH)_3$ (Tables 8 and 13). That confirms what was outlined by O'Mara in [19] and Brown and Martin in [20]. Thus, substances with high reactivity with HCl are always a good starting point for their evaluation as acid scavengers at high temperatures in the condensed phase. Figure 1 shows the efficiency of AS-6B, GCC, and $Al(OH)_3$ at different temperatures, performing internal method 2.

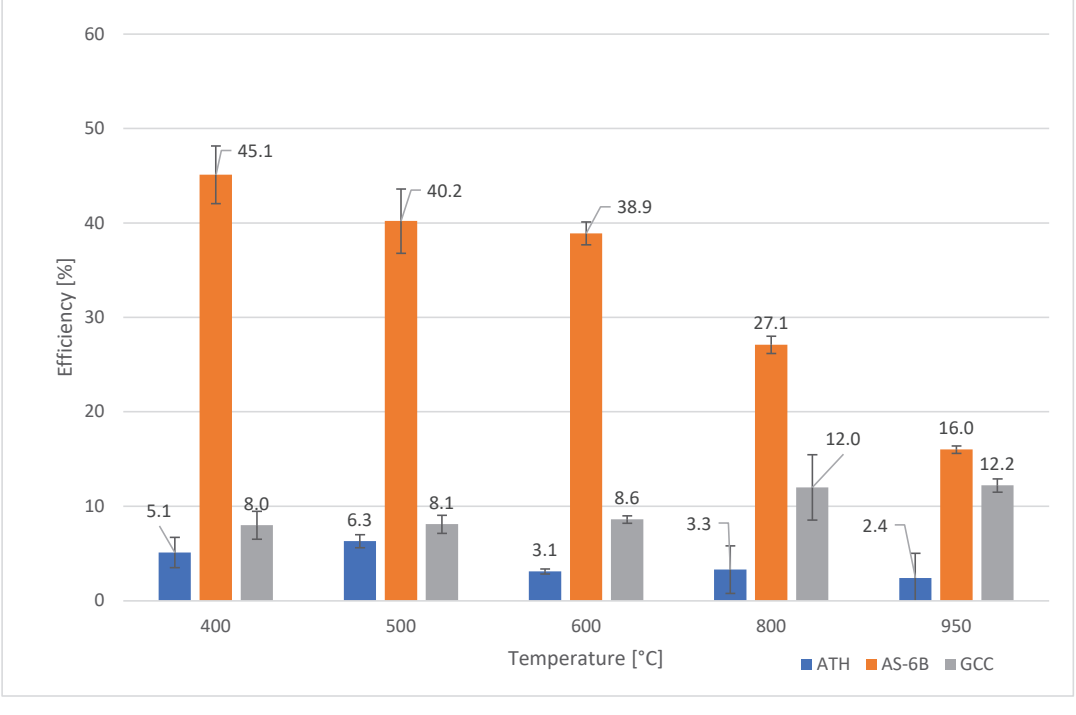

Figure 1. Efficiency % (T) of F50.5 (Orange), F50.0 (Gray), and F50.2 (Blue). Standard deviation ranges are reported. ATH stands for $Al(OH)_3$.

4.3. Effect of Particle Size on Efficiency

GCC has less efficiency than PCC (Tables 8 and 13), which is valid for all temperatures. F50.0 contains a GCC with a mean particle size of around 2 microns, while F50.3 has Winnofil S, a PCC having a particle size in the scale of nanometers and a BET between 15 m^2/g and 24 m^2/g [21]. O'Mara made the same assumption without any measurement in [19], claiming that the Molar Absorption Efficiency (MAE) depends on several variables, such as acid scavengers' dispersion efficiency and particle size. Matthews and Plemper in [7,8] have also shown how the reactivity of $CaCO_3$ is linked to particle size, and it can cause a substantial effect on flame retardancy. We will discuss this aspect in detail in Part IV of this paper.

In conclusion, substances with finer particle sizes show more reactivity with HCl because of a higher BET, which means more probability of intercepting gaseous HCl molecules. For this reason, PCC is more performant in scavenging than GCC.

One of the points to be highlighted is that the advantage of PCC is reduced as temperature increases, and at 950 °C, none of the acid scavengers at high temperatures can compete with the fast evolution of HCl (Table 13 and Figures 1 and 2).

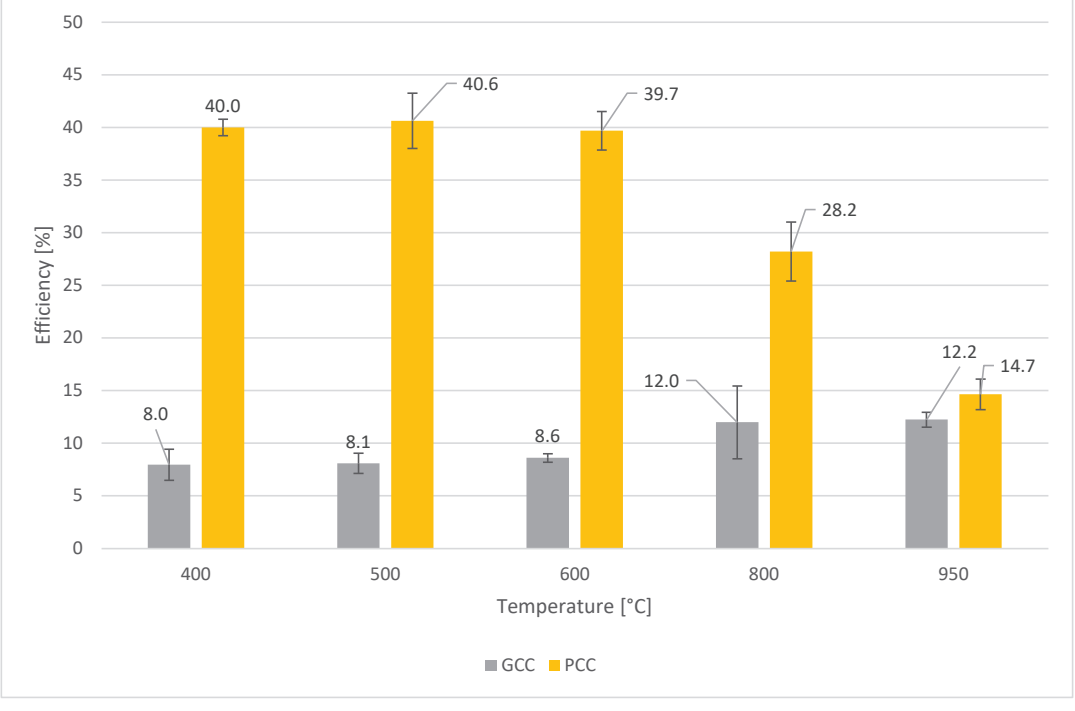

Figure 2. The efficiency % (T) of F50.0 containing 90 phr of GCC (gray), and F50.3, containing 90 phr of PCC (yellow). Standard deviation ranges are reported.

4.4. Effect of Dispersion on Efficiency

The formulation F50.8 contains PCC and $Mg(OH)_2$, 90 phr, and 40 phr, respectively, with a ratio of PCC/$Mg(OH)_2$ of 2.25. That is the best ratio found for the best efficiency. The efficiency of this acid scavenger couple is 28.8% (Table 14, Figure 3), with a pH of 3.32 (Table 12). By doubling the quantity of the couple with the same ratio, 37.5% of efficiency with a pH of 3.75 are reached (Tables 12 and 14). With a further improvement of the dosage, no further advantages are obtained (Table 14 and Figure 3). This behavior indicates poor dispersion as the dosage increases, impacting the scavenging performances. An inadequate

distribution weakens the intimate contact between PVC chains and acid scavengers. If this contact is missing in some zones, HCl is released, lowering the efficiency of acid scavengers. Sometimes, this can be compensated by increasing the shear during the process and using some tricks during the blending. Nevertheless, nanoscale fillers and substances prone to uptake water, such as $Mg(OH)_2$, are always inclined to give bad dispersion if we enhance their dosage. O' Mara in [19] claimed the impacts of the dispersion of acid scavengers on their efficiency.

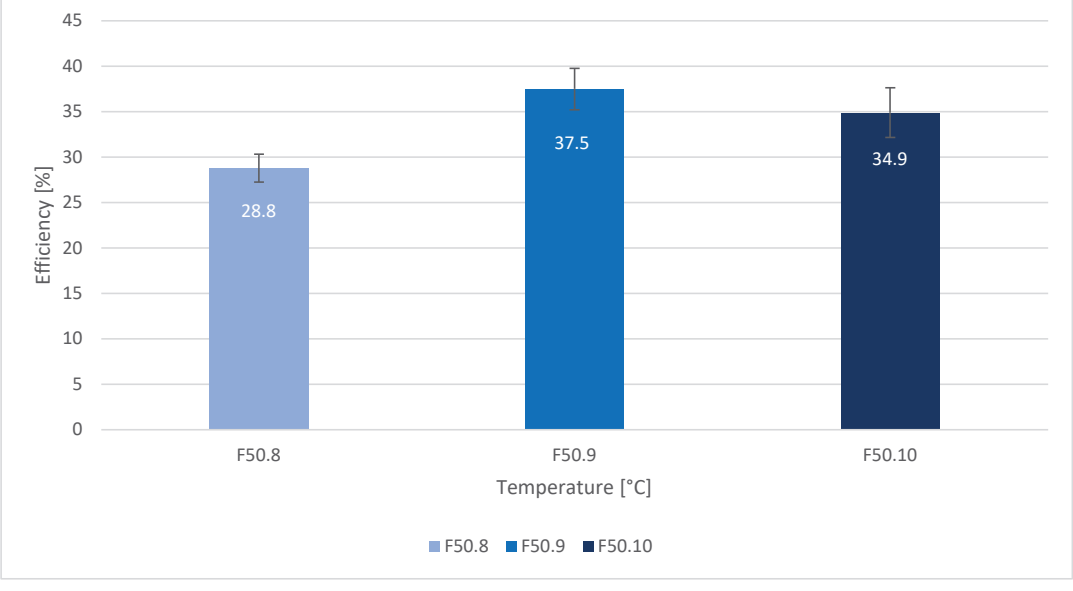

Figure 3. Efficiency % (T) of formulations containing PCC/$Mg(OH)_2$ at different dosages. Standard deviation ranges are reported.

4.5. Effect of Temperature on Efficiency

AS-6B gives stable reaction products with HCl, so the efficiency is only due to the kinetic of the reactions involved in trapping HCl. Its acid scavenger efficiency falls dramatically as temperature increases (Figure 4). The efficiency of other good acid scavengers, such as PCC, shows a similar trend (Figure 2). The explanation lies in the competition between two reactions. HCl evolves from the burning matrix, and acid scavengers try to fix it in ashes. The higher the temperature, the quicker the evolution of HCl. Over certain temperatures, the solid acid scavenger is too slow to trap HCl efficiently, and the system goes into crisis. Chandler and alt. in [12] and Bassi in [22] highlighted this phenomenon. Finally, a non-performant acid scavenger such as $Al(OH)_3$ fails at all tested temperatures.

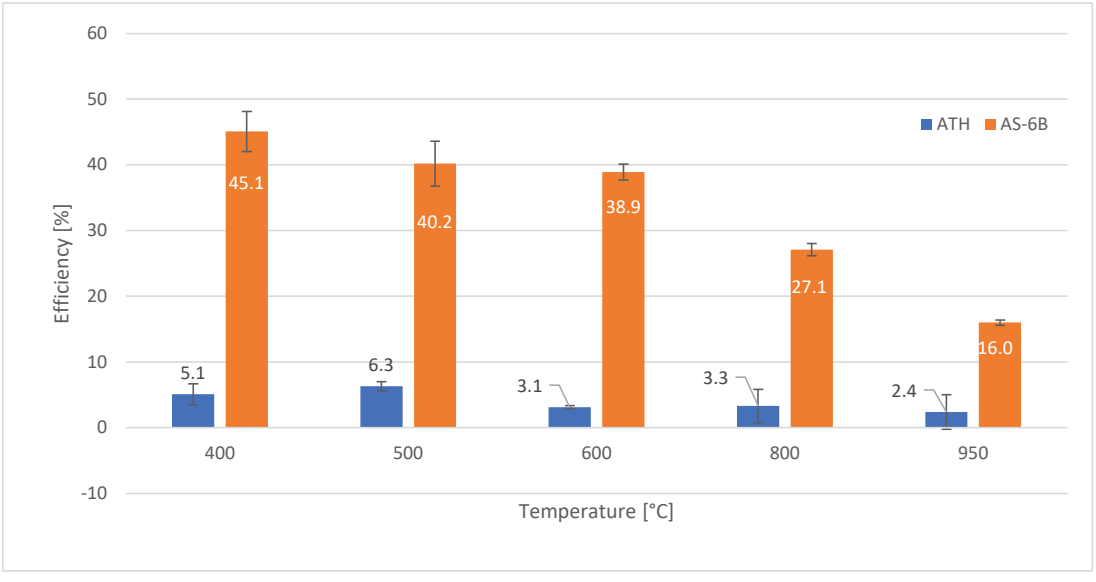

Figure 4. Efficiency % (T) of formulation F50.1 (blue) and F50.5 (orange) as a function of temperature. Standard deviation ranges are reported. ATH stands for $Al(OH)_3$.

4.6. Effect of Decomposition of Reaction Products on Efficiency

Kipouros and Sadoway claimed the $MgCl_2$ decomposition last step at 550 °C [23]. Galwey and Laverty between 350 °C and 550 °C [24]. The efficiencies reported in Figure 5 and FTIR spectra in Figure A3 confirm that over 400 °C, $MgCl_2$ decomposes. The ashes at 400 °C are black, and the FTIR spectrum at 400 °C shows the presence of an unknown substance, probably a mix of a variety of crosslinked organic compounds forming a black and solid char. Here, the second stage of pyrolysis and combustion zone starts, and the formation and rearrangement of the crosslinked matrix are expected. However, the FTIR spectrum shows the presence of weak $MgCl_2$ bands at 1616.4 cm^{-1} and 1606.1 cm^{-1}, confirming that $MgCl_2$ is diluted in the black char (Figure A3 at 400 °C). The signal of the organic crosslinked char entirely disappears at 500 °C, and therefore the $MgCl_2$ bands become evident. Nevertheless, at 500 °C, the principal band at 546.2 cm^{-1} confirms the presence of MgO (Figures A3, A9, and A11, Tables 9 and 10). $MgCl_2$ bands vanish completely at 600 °C, where MgO is the only source of Mg (Figures A3 and A11 and Tables 9 and 10). The decomposition of $MgCl_2$ is why the efficiency of $Mg(OH)_2$ decreases after 400 °C. Therefore, by performing internal method 2, $Mg(OH)_2$ shows the maximum efficiency at 400 °C (16.9%), and its efficiency drops to 2.3% at 950 °C.

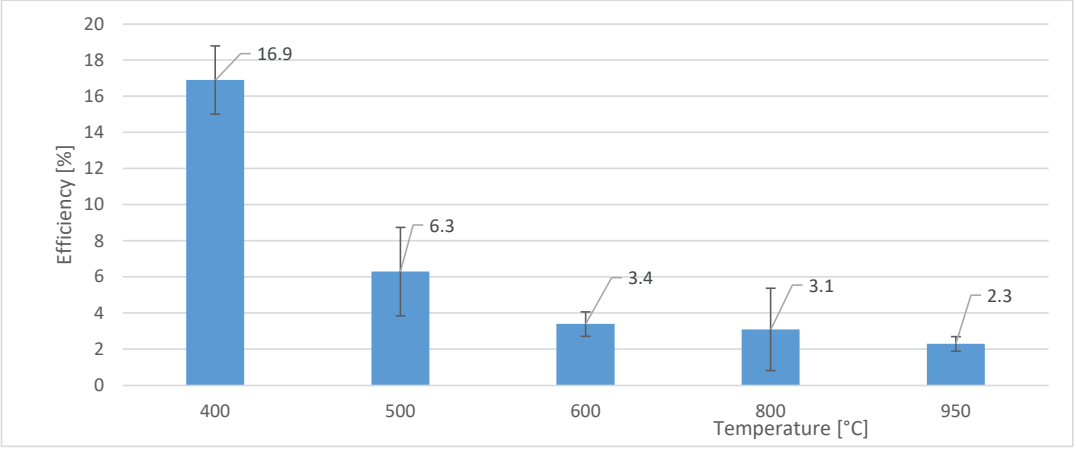

Figure 5. Efficiency % (T) of the formulation F50.2 containing $Mg(OH)_2$. Standard deviation ranges are reported.

4.7. Focus on the Single Acid Scavenger

4.7.1. Single-Step Reaction: GCC

GCC reacts with HCl in a single-step reaction, yielding $CaCl_2$, CO_2, and water. Its reaction product, $CaCl_2$, is stable up to 950 °C. The efficiency of GCC in F50.0 remains low, slightly increasing from 400 °C to 950 °C (Table 13), probably due to the formation of small quantities of CaO, which is more likely to happen at 800 °C and 950 °C, acting as a potent acid scavenger. This phenomenon gives a slight advantage to all kinds of $CaCO_3$ in the scavenging at temperatures over 800 °C. In PCC, this advantage is not visible (F50.3) because "covered" by PCC's high scavenging performances. FTIR (Figures A1 and A10, and Table 10) and XFR (Table 9) point to the involved reactions. At 400 °C, 500 °C, and 600 °C, $CaCO_3$ and $CaCl_2$ are in the ashes. At 800 °C, the decarbonation of $CaCO_3$ takes place when its bands disappear, leaving only $CaCl_2$ bands. Chandler and others highlight the tendency of $CaCl_2$ to be hydrolyzed over its fusion point by water vapor when water-saturated air fluxes are used [12]. Nevertheless, with dry air fluxes at 950 °C, $CaCl_2$ is a stable, transparent liquid, not showing any tendency to be hydrolyzed.

4.7.2. No Reaction: $Al(OH)_3$

$Al(OH)_3$ starts the decompositions between 180 °C and 200 °C, releasing water [25]. Therefore, during the combustion, the actual substance in the matrix is alumina (Al_2O_3). Al_2O_3 is an inert substance not capable of reacting with HCl. Figure A2 shows the FTIR spectra of the ashes of formulation F50.1 at different temperatures. Figure A8 indicates that all spectra of Figure A2 have an excellent match with Al_2O_3 (see also Table 10), and therefore alumina is in the ashes obtained at 400 °C, 500 °C, 600 °C, 800 °C, and 950 °C. The presence of Al is confirmed by XFR (Table 9), and chlorine is probably due to HCl trapped in the alumina surface. Additional measurements should clarify the presence of Cl in the F50.1 ashes. All these considerations explain why formulation F50.1 gives low and constant efficiency values at different temperatures (Figure 4 and Table 13). Hence, $Al(OH)_3$ is an extremely weak acid scavenger at high temperatures due to the chemical inertia of its reaction product, Al_2O_3.

4.7.3. Single-Step Reaction: $Mg(OH)_2$

$Mg(OH)_2$ reacts fast with HCl generating $MgCl_2$. $Mg(OH)_2$ starts the decompositions between 300 °C and 320 °C, releasing water [25]. Thus, it is a perfect flame retardant; nevertheless, it is an ineffective acid scavenger at temperatures over 500 °C. The for-

mulation F50.2 gives maximum efficiency at 400 °C, suddenly dropping down due to the instability of its reaction product, $MgCl_2$ (Table 13). Water vapor hydrolyzes $MgCl_2$ through the reactions reported in [23,24]. The result is the production of 2 moles of HCl and 1 mole of MgO per mole of decomposing $MgCl_2$. The ashes analysis (FTIR measures in Figures A3, A9 and A11, and Table 10) shows that the $MgCl_2$ hydrolysis is almost complete over 600 °C. Table 9 indicates that chlorine remains trapped in ashes (maybe passivation, preserving small quantities of $MgCl_2$, but further measurements should clarify this point).

All this puts in evidence a single-step reaction failing the scavenging at high temperature because $Mg(OH)_2$ yields an unstable product rereleasing HCl.

Table 8 shows how the formulations F50.1 and F50.2 reach almost the same pH and conductivities, indicating high acidity for different causes. As $Al(OH)_3$, $Mg(OH)_2$ is a very ineffective acid scavenger at high temperatures in the condensed phase, and therefore it does not show any effect in efficiency as temperature increases (Table 13). Again, a weak acid scavenger usually performs poorly at all temperatures.

4.7.4. Single-Step Reaction: PCC

Tables 8 and 13 show that PCC alone is a good acid scavenger. PCC is not a strong base, and due to its small particle size, it can scavenge HCl with good efficiency, yielding $CaCl_2$, CO_2, and water. $CaCl_2$ is stable at 950 °C. FTIR spectra confirm the formation of $CaCl_2$ and the disappearance of $CaCO_3$ bands (Figures A4 and A7, and Table 10) starting from 800 °C. The XRF measurements (Table 9) show the presence of chlorine and calcium. PCC shows good scavenging up to 800 °C.

4.7.5. Multiple-Step Reaction: PCC and $Mg(OH)_2$

Table 14 indicate that, if alone, $Mg(OH)_2$ shows a low impact on smoke acidity reduction. At 950 °C, the efficiency of F50.2 is extremely low, 2.3%. On the contrary, PCC performs better, and the efficiency reaches 14.7% in F50.3. Table 14 also shows that they have a strong synergism when used together. Figure 6 represents the efficiency at different ratios of loadings. $Mg(OH)_2$ and PCC reach maximum efficiency (28.8%) when PCC is 90 phr and $Mg(OH)_2$ 40 phr (F50.8). That efficiency is much more than the sum of the efficiency of $Mg(OH)_2$ and PCC alone (14.7% and 2.3%, respectively). The maximum is reached when the ratio PCC/$Mg(OH)_2$ is 2.25, as Figure 6 shows. Probably the ratio that gives the maximum efficiency depends on the quantity of the pair and particle size of PCC and $Mg(OH)_2$ because both substantially affect the scavenging performance. The synergism can be explained by a double-step reaction through which $Mg(OH)_2$ and PCC help each other. As a strong base, $Mg(OH)_2$ is the primary acid scavenger in the pyrolysis and combustion zone, and $MgCl_2$ is the main reaction product. The reactions during the matrix combustion are the following:

$$Mg(OH)_2 + 2HCl\ (g) \rightarrow MgCl_2\ (s) + 2H_2O\ (v) \quad (4)$$

$$MgO\ (s) + 2HCl\ (g) \rightarrow MgCl_2\ (s) + H_2O\ (v) \quad (5)$$

The second acid scavenger, PCC, reacts with HCl in less extent through reaction 6.

$$CaCO_3\ (s) + 2HCl\ (g) \rightarrow CaCl_2\ (s, l) + CO_2\ (g) + H_2O\ (v) \quad (6)$$

$MgCl_2$ is formed but decomposes between 350 °C and 550 °C [23,24] with a slow kinetic passing back its HCl to PCC. The synergism is explainable with a slow HCl release from $MgCl_2$ to PCC, enhancing the efficiency of PCC. All these aspects should be clarified deeper by FTIR-TGA measurements, pointing to the IR signals of HCl and CO_2 in the range 350 °C–550 °C. That will be discussed in a separate article. Schemes 1–3 represent the hypothesis on the synergism between PCC and $Mg(OH)_2$.

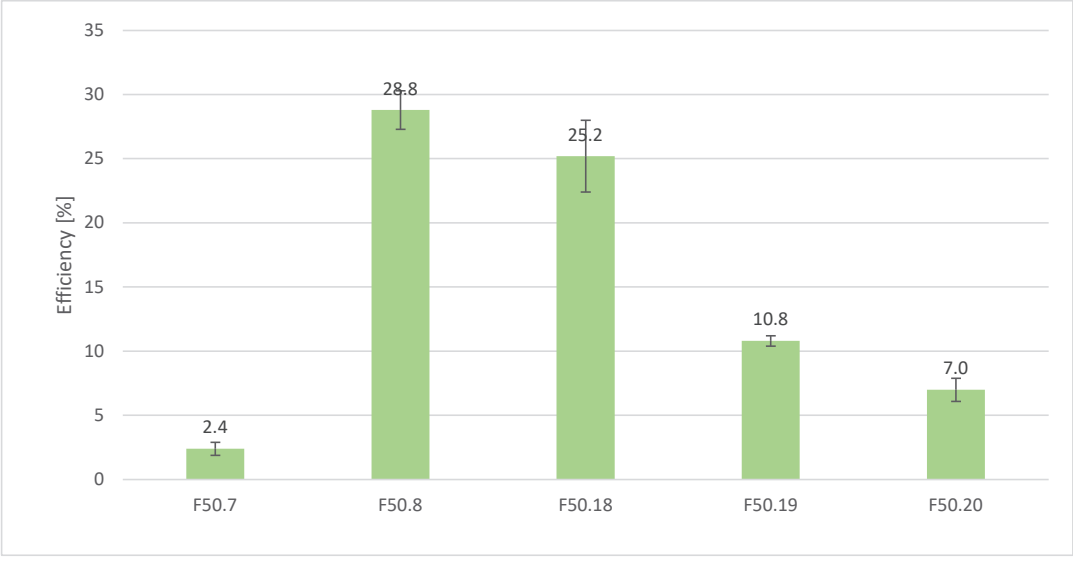

Figure 6. The efficiency of the formulations F50.7 ($Mg(OH)_2$ = 130; PCC = 0), F50.8 ($Mg(OH)_2$ = 40; PCC = 90), F50.18 ($Mg(OH)_2$ = 30; PCC = 100), F50.19 ($Mg(OH)_2$ = 90; PCC = 40), F50.20 ($Mg(OH)_2$ = 100; PCC = 30). Standard deviation ranges are reported.

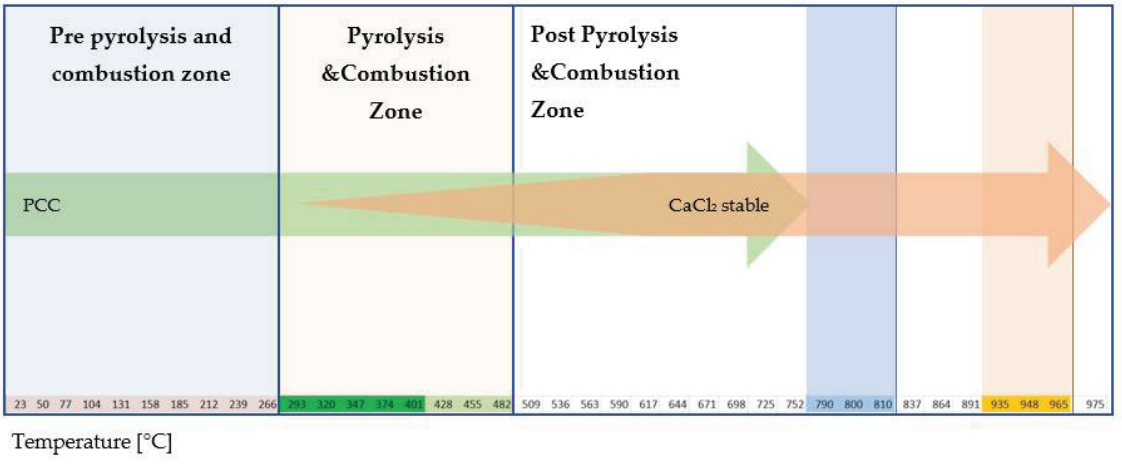

Scheme 1. The single-step reaction of PCC in HCl scavenging at high temperatures in the condensed phase.

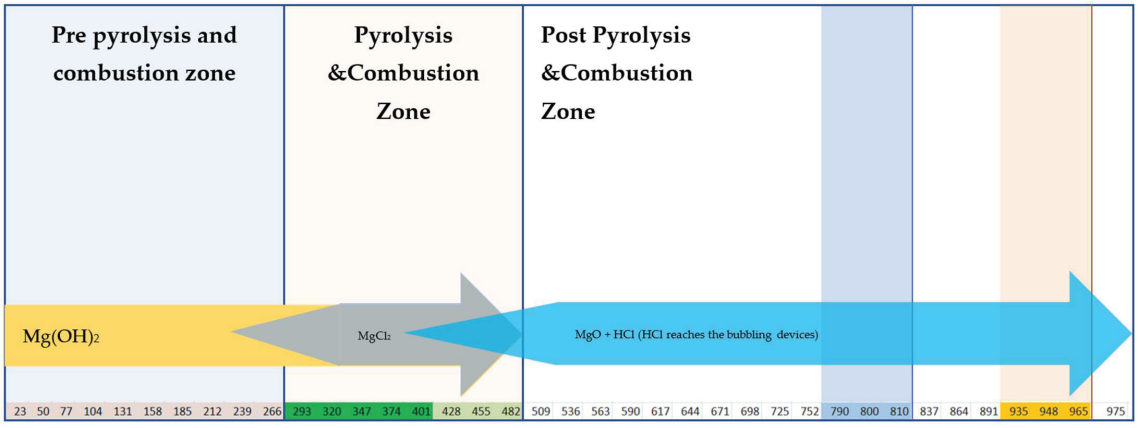

Scheme 2. The single-step reaction of $Mg(OH)_2$ in HCl scavenging at high temperatures in the condensed phase.

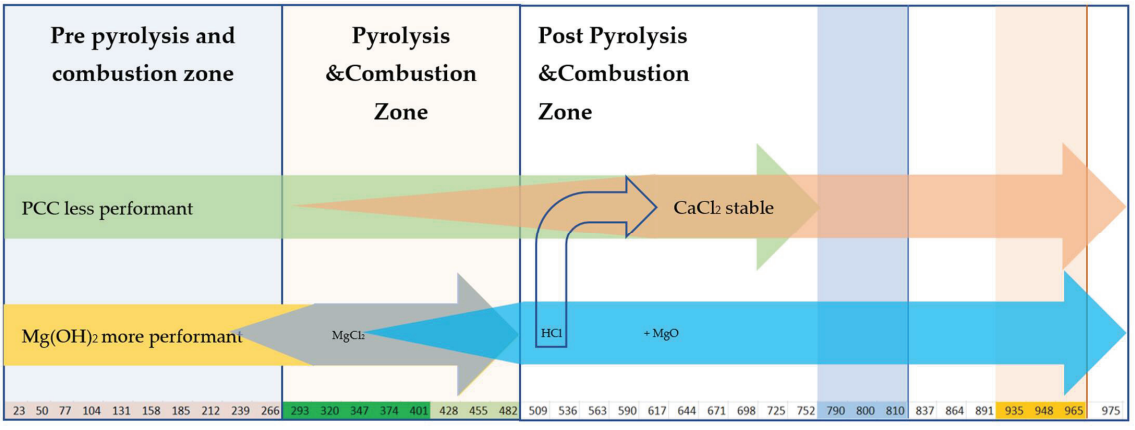

Scheme 3. Multiple-step reactions of PCC/$Mg(OH)_2$ in HCl scavenging at high temperatures in the condensed phase.

5. Conclusions

Acid scavengers at high temperatures in the condensed phase differ in chemical nature and particle size, and some of them have been tested with different thermal profiles, performing EN 60754-2. $Al(OH)_3$ and $Mg(OH)_2$ are not efficient acid scavengers. When the matrix burns, the former generates an inert substance, alumina, while the latter reacts with HCl, yielding $MgCl_2$, which decomposes over 500 °C, rereleasing HCl.

GCC is not a good acid scavenger, but its efficiency increases as its particle size decreases. PCC is, therefore, more efficient in scavenging HCl than GCC. It reacts well with HCl in a single-step reaction, yielding $CaCl_2$ stable up to 950 °C. When $Mg(OH)_2$ and PCC work together, PCC scavenges the HCl from $MgCl_2$ decomposition. Probably the synergism happens because $MgCl_2$ releases HCl slower than the PVC matrix, and PCC can scavenge it more efficiently. Poor dispersion eliminates all advantages of the synergism when the quantity of $Mg(OH)_2$ and PCC is too high.

Another aspect emerging from the data is the effect of temperature on the kinetic of HCl release. The higher the temperature, the lower the acid scavenger efficiency. This aspect confirms other researchers' past observations [12,22]. The rapid HCl evolution causes the collapse of the efficiencies of acid scavengers at high temperatures. Acid scavengers are solid substances, and while some advantages are obtained when a lower particle size grade is used, they are annihilated when temperatures are too high.

In conclusion, it must be highlighted that different heating regimes give different acidity results. This aspect confirms how difficult it is to estimate the HCl concentration in real fire scenarios from bench-scale tests because HCl concentration in the gas phase will depend not only on its decay [26–28] but also on temperatures reached in the fire.

Supplementary Materials: The supporting information can be downloaded at: https://www.mdpi.com/article/10.3390/fire5050142/s1.

Funding: This research received no external funding.

Institutional Review Board Statement: Not applicable.

Data Availability Statement: The data presented in this study are available in Supplementary Materials.

Acknowledgments: The author wants to acknowledge Ing. Carlo Ciotti, Ing. Marco Piana, all PVC Forum Italia and PVC4cables staff, and Emma Sarti for their help and support.

Conflicts of Interest: The authors declare that there is no conflict of interest regarding the publication of this paper.

Glossary/Nomenclature/Abbreviations

PVC	poly(vinyl chloride);
HCl	hydrogen chloride;
EU	European Union;
CPD	Construction Product Directive;
CPR	Construction Product Regulation;
PCC	Precipitated Calcium Carbonate;
CCC	Ground Calcium Carbonate;
Phr	Part per Hundred Resin;
DINP	Di Iso Nonyl Phthalate;
ESBO	Epoxidized Soy Bean Oil;
COS	Calcium Organic Stabilizer;
DDW	Double Deionized Water;
μ	Mean
SD	Standard Deviation;
CV	Coefficient of variation;
MAE	Molar Absorption Efficiency

Appendix A. FTIR Spectra of the Acid Scavengers at Different Temperatures and Some Substances Used to Confirm the Chemical Nature of the Substances in Ashes

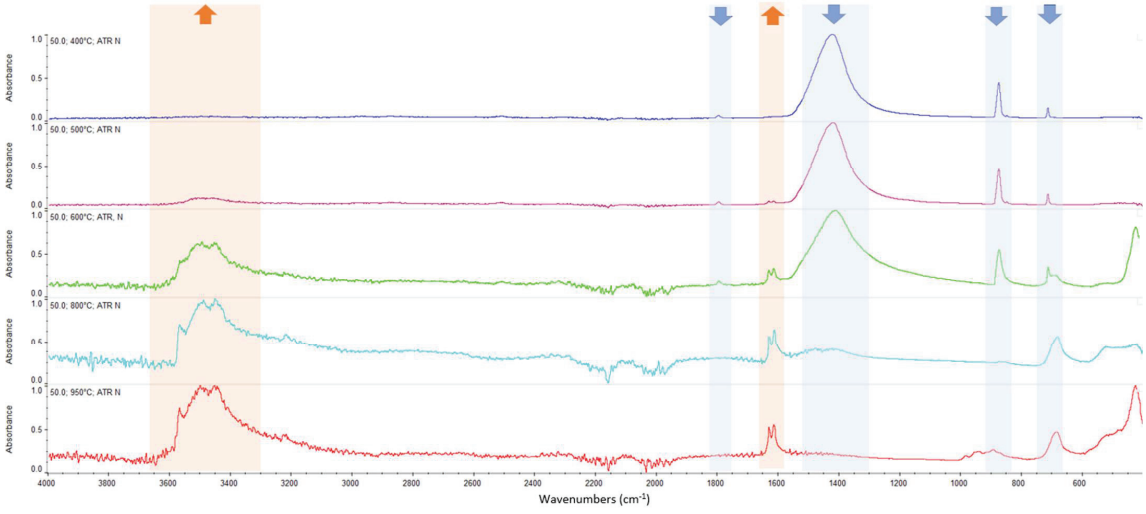

Figure A1. FTIR spectra of ashes of F50.0 at F950 °C (red), at 800 °C (light blue), at 600 °C (green), at 500 °C (purple), at 400 °C (blue).

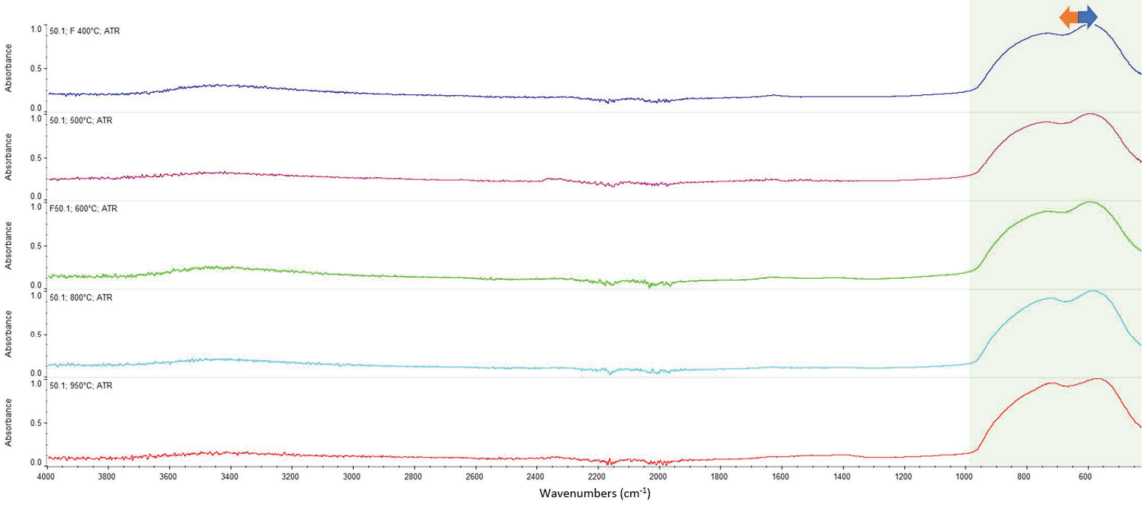

Figure A2. FTIR spectra of ashes of F50.1 at 950 °C (red), at 800 °C (light blue), at 600 °C (green), at 500 °C (purple), at 400 °C (blue).

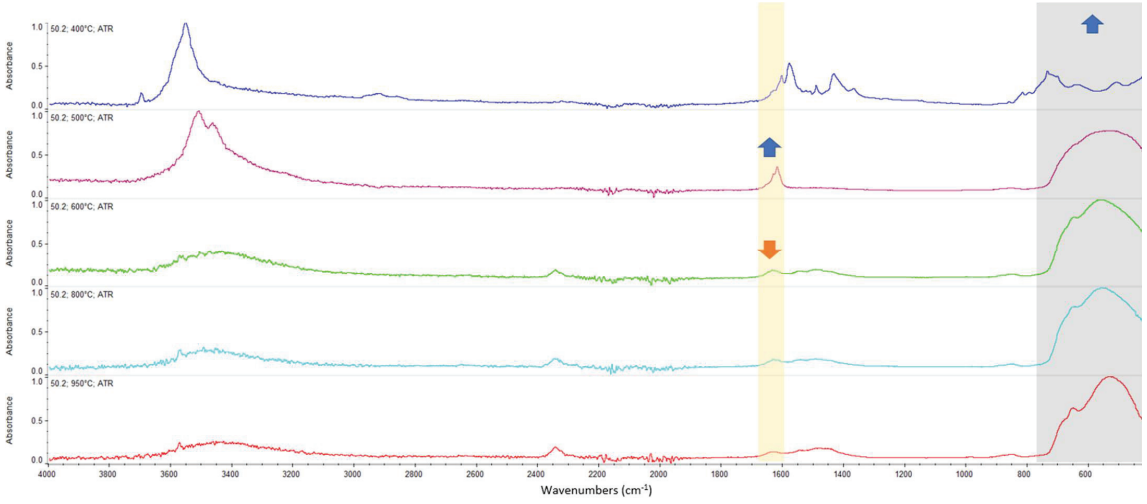

Figure A3. FTIR spectra of ashes of F50.2 at 950 °C (red), at 800 °C (light blue), at 600 °C (green), at 500 °C (purple), at 400 °C (blue).

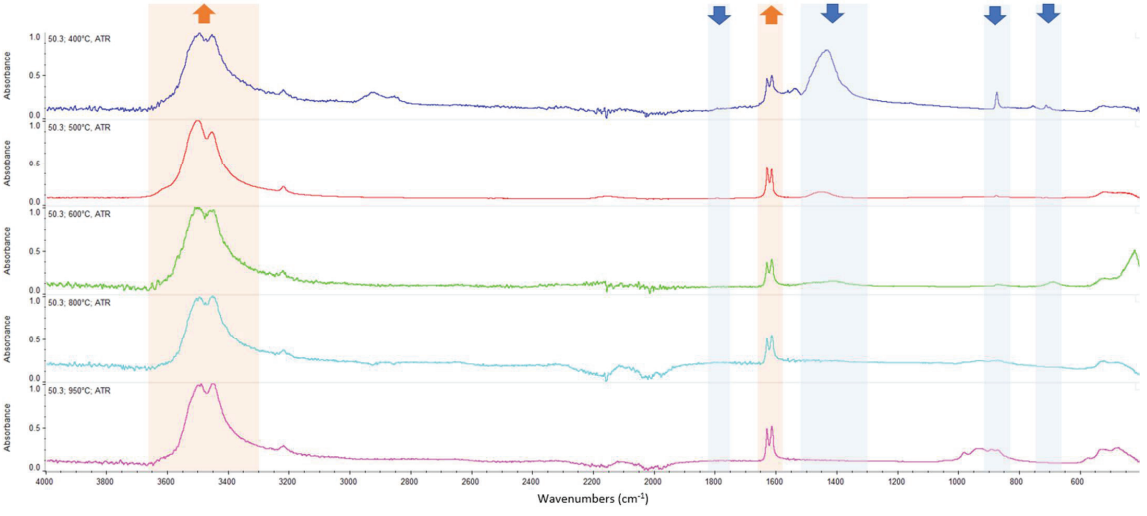

Figure A4. FTIR spectra of ashes of F50.3 at 950 °C (red), at 800 °C (light blue), at 600 °C (green), at 500 °C (purple), at 400 °C (blue).

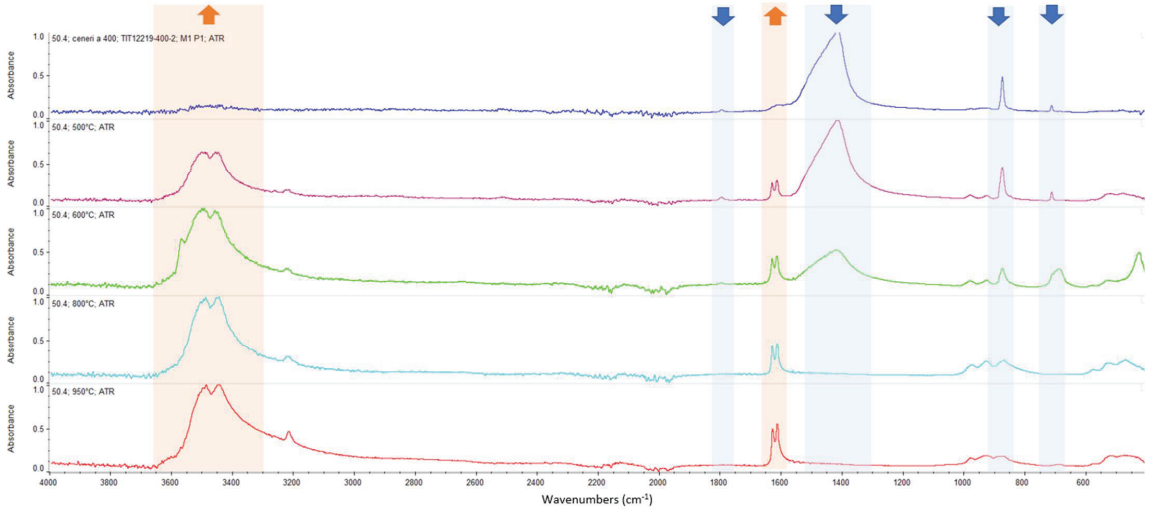

Figure A5. FTIR spectra of ashes of F50.4 at 950 °C (red), at 800 °C (light blue), at 600 °C (green), at 500 °C (purple), at 400 °C (blue).

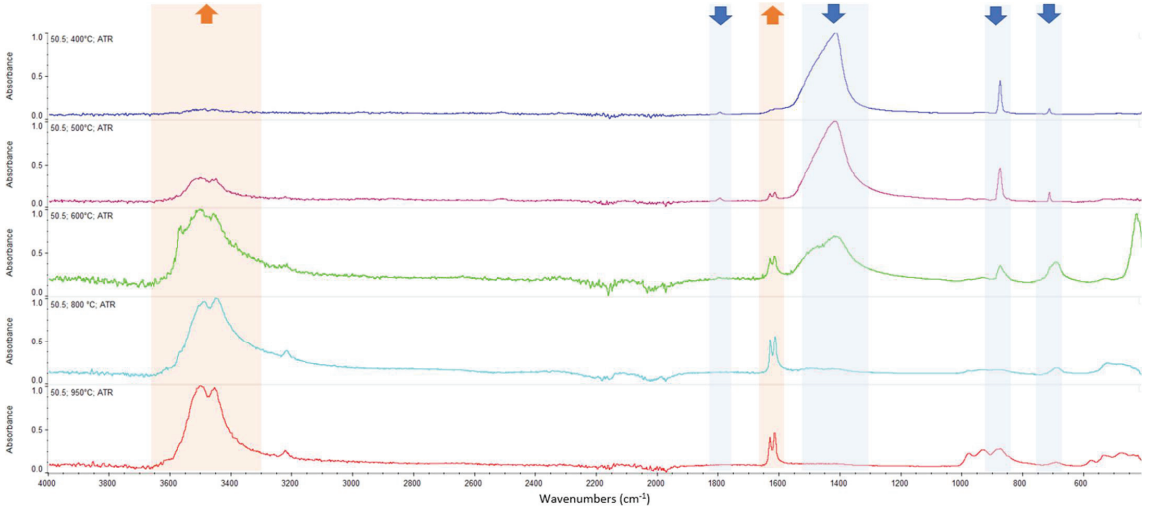

Figure A6. FTIR spectra of ashes of F50.5 at 950 °C (red), at 800 °C (light blue), at 600 °C (green), at 500 °C (purple), at 400 °C (blue).

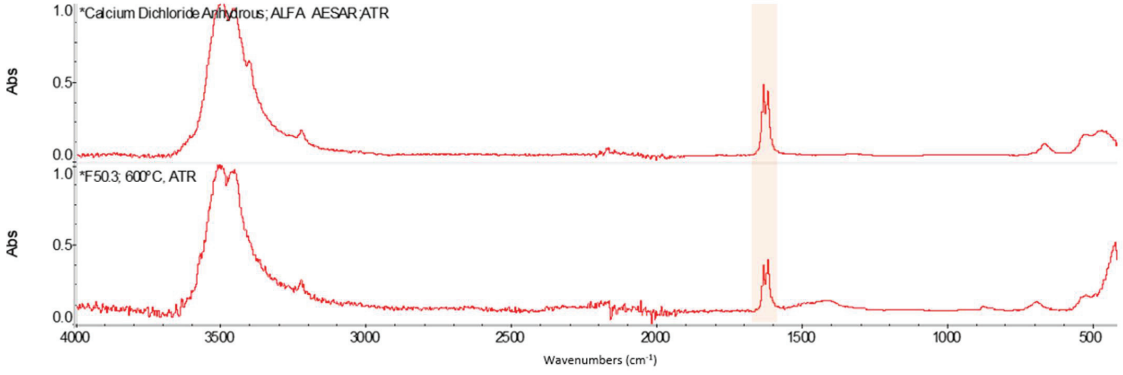

(**a**)

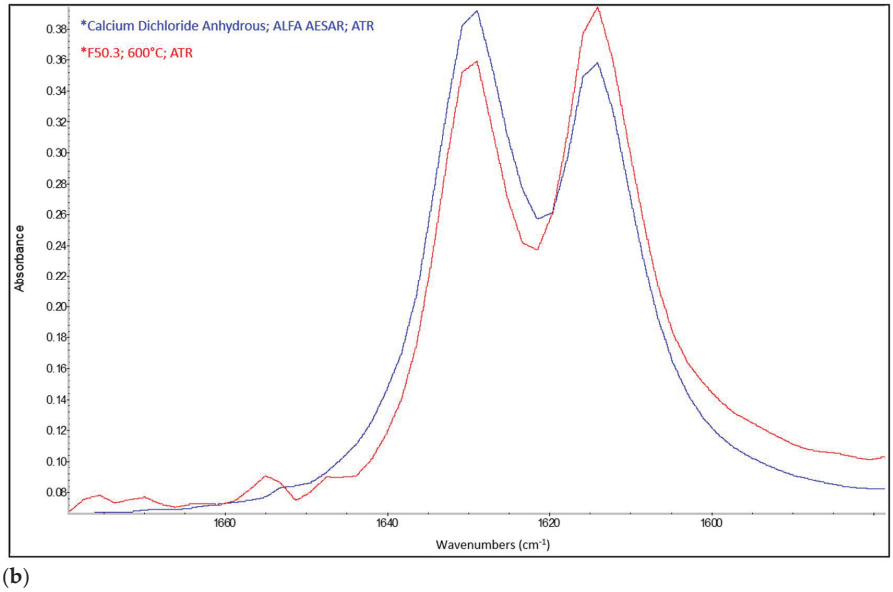

(**b**)

Figure A7. FTIR spectra: anhydrous $CaCl_2$ vs. ashes of F.50.3 at 600 °C: (**a**) scale 4000–400 cm^{-1} and (**b**) focus in the range 1660 cm^{-1}–1580 cm^{-1}, anhydrous $CaCl_2$ (blue) and ashes of F.50.3 (red). Anhydrous $CaCl_2$ shows two bands at 1628.43 cm^{-1} and 1614.21 cm^{-1}, and the sample spectrum matches them perfectly.

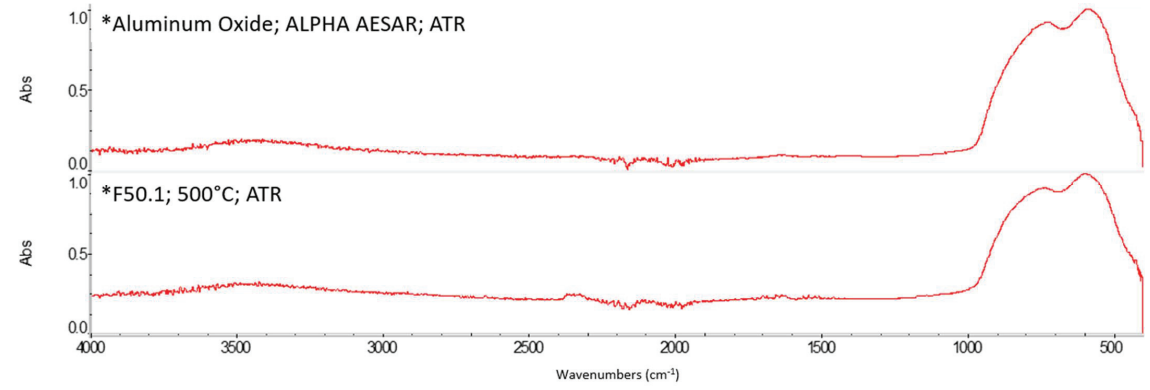

Figure A8. FTIR spectra. Al_2O_3 versus ashes of F50.1 at 500 °C.

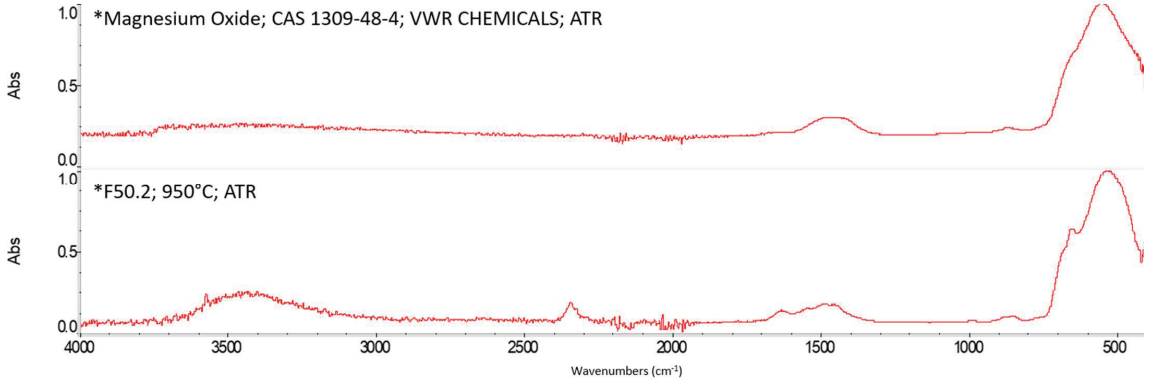

Figure A9. FTIR spectra: MgO versus ashes of F50.2 at 950 °C.

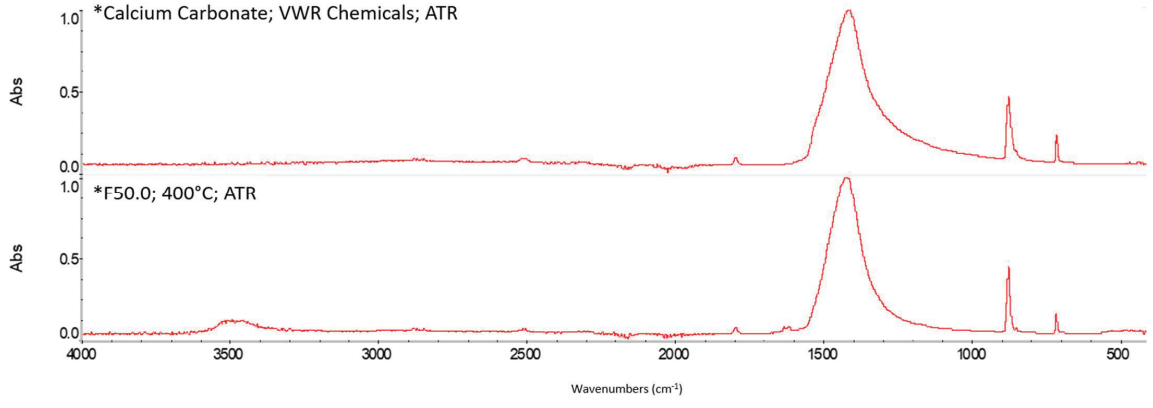

Figure A10. FTIR spectra: $CaCO_3$ versus ashes of F50.0 at 400 °C. F50.0 shows all the main $CaCO_3$ bands: 2509.64 cm^{-1}, 1794.92 cm^{-1}, 1417.26 cm^{-1}, 873.10 cm^{-1}, 846.70 cm^{-1} and 710.66 cm^{-1}.

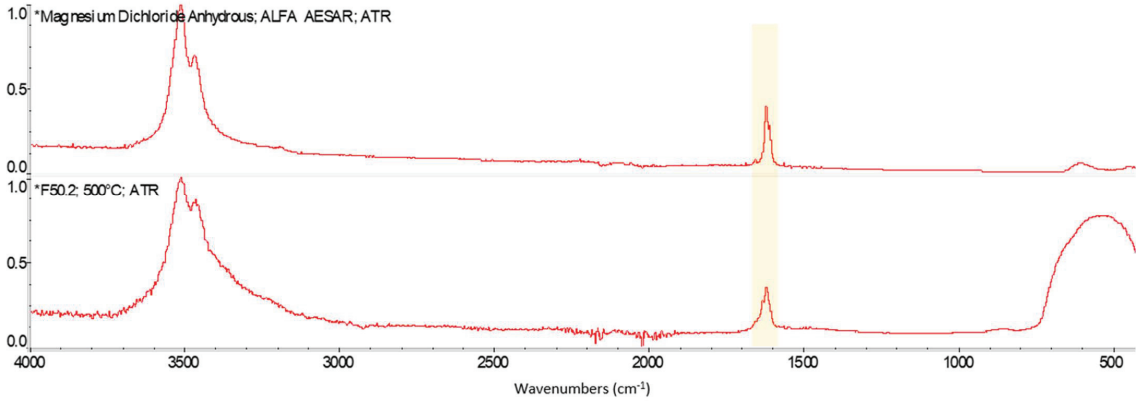

(**a**)

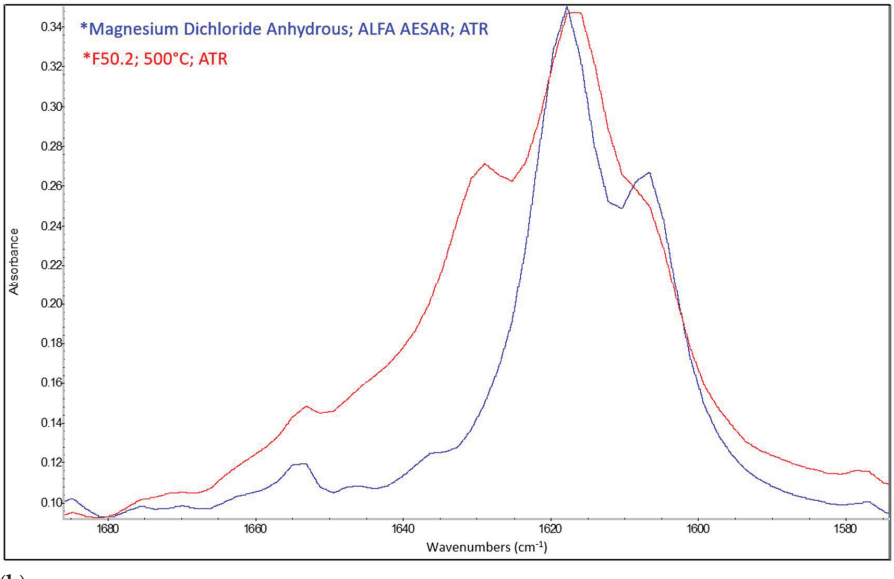

(**b**)

Figure A11. FTIR spectra: anhydrous $MgCl_2$ versus ashes of F50.2 at 500 °C. (**a**) scale 4000–400 cm^{-1} and (**b**) focus in the range 1660 cm^{-1}–1580 cm^{-1}, anhydrous $MgCl_2$ (red) and ashes of F50.2 (blue). The FTIR spectrum of the ashes matches the main bands of anhydrous $MgCl_2$ (1616.43 cm^{-1} and 1606.44 cm^{-1} and a minor band at 1653.26 cm^{-1}). Another band is present at 1629.91 cm^{-1}. The different structure of the spectrum of the ashes is probably due to different hydration states of $MgCl_2$.

Appendix B. A Schematic Diagram of the Sample Preparation and Testing Process

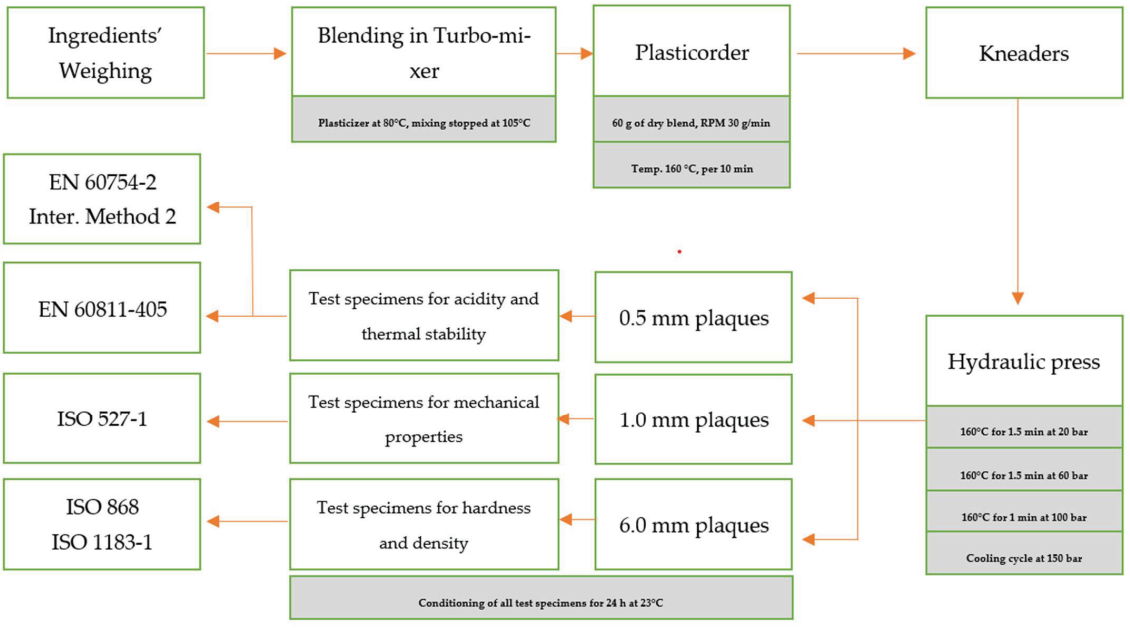

Figure A12. A schematic diagram of the sample preparation.

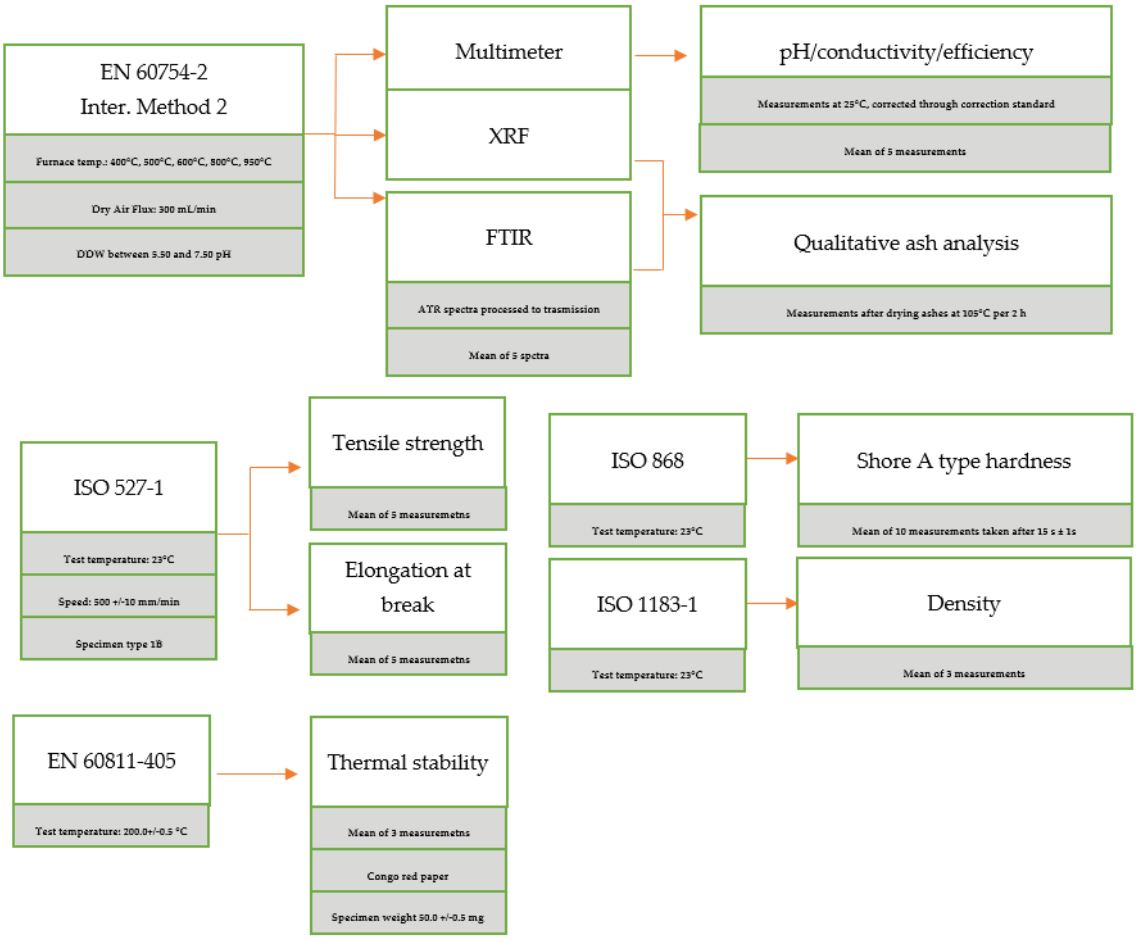

Figure A13. A schematic diagram of the testing process and main conditions.

References

1. *EN 50267-2-3*; Common Test Methods for Cables Under Fire Conditions—Tests on Gases Evolved during Combustion of Materials from Cables—Part 2–3: Procedures—Determination of Degree of Acidity of Gases for Cables by Determination of the Weighted Average of pH and Conductivity. CENELEC: Brussels, Belgium, 1998. Available online: https://my.ceinorme.it/home.html (accessed on 1 August 2022).
2. *EN 60754-2*; Test on Gases Evolved during Combustion of Materials From Cables—Part 2: Determination of Acidity (by pH Measurement) and Conductivity. CENELEC: Brussels, Belgium, 2014. Available online: https://my.ceinorme.it/home.html (accessed on 1 August 2022).
3. *EN 60754-1*; Test on Gases Evolved during Combustion of Materials from Cables—Part 1: Determination of the Halogen Acid Gas Content. CENELEC: Brussels, Belgium, 2014. Available online: https://my.ceinorme.it/home.html (accessed on 1 August 2022).
4. *EN 50267-2-2*; Common Test Methods for Cables under Fire Conditions—Tests on Gases Evolved during Combustion of Materials from Cables—Part 2-2: Procedures—Determination of Degree of Acidity of Gases for Materials by Measuring pH and Conductivity. CENELEC: Brussels, Belgium, 1998. Available online: https://my.ceinorme.it/home.html (accessed on 1 August 2022).
5. *EN 50267-2-1*; Common Test Methods for Cables under Fire Conditions—Tests on Gases Evolved during Combustion of Materials from Cables—Part 2-1: Procedures—Determination of the Amount of Halogen Acid Gas. CENELEC: Brussels, Belgium, 1998. Available online: https://my.ceinorme.it/home.html (accessed on 1 August 2022).
6. *EN 50525-1*; Electric Cables—Low Voltage Energy Cables of Rated Voltages up to and Including 450/750 V (U0/U)—Part 1: General Requirements. CENELEC: Brussels, Belgium, 2011. Available online: https://my.ceinorme.it/home.html (accessed on 1 August 2022).

7. Matthews, G.; Plumper, G.S. Effects of calcium carbonate fillers on the behaviour of PVC in fires. *Br. Polym. J.* **1981**, *13*, 17–21. [CrossRef]
8. Matthews, G.; Plumper, G.S. Effects of fillers on and the role of hydrogen chloride in the behaviour of PVC in fires. *Br. Polym. J.* **1984**, *16*, 34–38. [CrossRef]
9. Smith, G. Quick method for determining the acid gas evolution from PVC formulations. *J. Vinyl Technol.* **1997**, *9*, 18–21. [CrossRef]
10. Sze On Chan, H. Measurement of hydrochloric acid emission from burning PVC compounds. *J. Fire Sci.* **1984**, *2*, 106–122. [CrossRef]
11. Sumi, K.; Morwick, D.W. *Acid Gas Evolution from PVC Using DBR/NRC Method, Internal Report (National Research Council of Canada. Division of Building Research), No. DBR-IR-425*; National Research Council of Canada: Ottawa, ON, Canada, 1976. [CrossRef]
12. Chandler, L.A.; Hirschler, M.M.; Smith, G.F. A heated tube furnace test for the emission of acid gas from PVC wire coating materials: Effects of experimental procedures and mechanistic considerations. *Eur. Polym. J.* **1987**, *23*, 51–61. [CrossRef]
13. Sarti, G. A New Perspective on Hydrogen Chloride Scavenging at High Temperatures for Reducing the Smoke Acidity of PVC Cables in Fires. I: An Overview of the Theory, Test Methods, and the European Union Regulatory Status. *Fire* **2022**, *5*, 127. [CrossRef]
14. *ISO 527-1*; Plastics—Determination of Tensile Properties—Part 1: General Principles. ISO: Geneva, Switzerland, 2019. Available online: https://www.iso.org/standard/67071.html (accessed on 1 August 2022).
15. *ISO 1183-1*; Plastics—Methods for Determining the Density of Non-Cellular Plastics—Part 1: Immersion Method, Liquid Pycnometer Method and Titration Method. ISO: Geneva, Switzerland, 2019. Available online: https://www.iso.org/standard/34804.html (accessed on 1 August 2022).
16. *ISO 868*; Plastics and Ebonite—Determination of Indentation Hardness by Means of a Durometer (Shore Hardness). ISO: Geneva, Switzerland, 2003. Available online: https://www.iso.org/standard/34804.html (accessed on 1 August 2022).
17. *IEC 60811-405*; Electric and Optical Fiber Cables—Test Methods for Non-Metallic Materials—Part 405: Miscellaneous Tests—Thermal Stability Test for PVC Insulations and PVC Sheaths. IEC: Geneva, Switzerland, 2012. Available online: https://webstore.iec.ch/publication/3543 (accessed on 1 August 2022).
18. *EN 60754-2:2014/A1:2020*; Test on Gases Evolved during Combustion of Materials from Cables—Part 2: Determination of Acidity (by pH Measurement) and Conductivity. CENELEC: Brussels, Belgium, 2020. Available online: https://my.ceinorme.it/home.html (accessed on 1 August 2022).
19. O'Mara, M.M. Pyrolysis–gas chromatographic analysis of poly(vinyl chloride). II. In situ absorption of HCl during pyrolysis and combustion of PVC. *J. Polym. Sci. Part A-1 Polym. Chem.* **1971**, *9*, 1387–1400. [CrossRef]
20. Brown, S.K.; Martin, K.G. Toxic gas and smoke measurement with the British Fire Propagation test. III: UPTV formulations with reduced HCl evolution. *Fire Mater.* **1985**, *9*, 95–102. [CrossRef]
21. Commercial PCC Purchased by Imerys. Available online: https://www.imerys-performance-minerals.com/system/files/2021-02/DATPCC_Winnofil_S_LSK_EN_2019-07.pdf (accessed on 12 August 2022).
22. Bassi, I. Characterization of PVC Compounds and Evaluation of Their Fire Performance, Focusing on the Comparison between EN 60754-1 and EN 60754-2 in the Assessment of the Smoke Acidity. Master's Thesis, University of Bologna, Bologna, Italy, October 2021. Available online: https://www.pvc4cables.org/images/assessment_of_the_smoke_acidity.pdf (accessed on 1 September 2022).
23. Kipouros, G.J.; Sadoway, D.R. A thermochemical analysis of the production of anhydrous $MgCl_2$. *J. Light Met.* **2001**, *1*, 111–117. [CrossRef]
24. Galwey, A.K.; Laverty, G.M. The thermal decomposition of magnesium chloride dihydrate. *Thermochim. Acta* **1989**, *138*, 115–127. [CrossRef]
25. Laoutid, F.; Bonnaud, L.; Alexandre, M.; Lopez-Cuesta, J.-M.; Dubois, P. New prospects in flame retardant polymer materials: From fundamentals to nanocomposites. *Mater. Sci. Eng. Rep.* **2009**, *63*, 100–125. [CrossRef]
26. Hirschler, M. Fire Safety, Smoke Toxicity, and Acidity. In Proceedings of the Flame Retardants 2006, London, UK, 14–15 February 2006.
27. *ISO/TR 20118:2019*; Plastics—Guidance on Fire Characteristics and Fire Performance of PVC Materials Used in Building Applications. ISO: Geneva, Switzerland, 2019. Available online: https://www.iso.org/standard/67071.html (accessed on 1 August 2022).
28. Beitel, J.J.; Bertelo, C.A.; Carroll, W.F.; Gardner, R.O.; Grand, A.F.; Hirschler, M.M.; Smith, G.F. Hydrogen chloride transport and decay in a large apparatus I. Decomposition of poly(vinyl chloride) wire insulation in a plenum by current overload. *J. Fire Sci.* **1986**, *4*, 15–41. [CrossRef]

fire

MDPI

Article

Numerical Simulation of Ethanol Air Diffusion Flame Quenching under Transverse AC Electric Field

Shuai Zhao [1], Boyun Liu [1,*], Bo Zhao [1], Taiwei Li [2] and Qi Shu [1]

[1] School of Power Engineering, Naval University of Engineering, Wuhan 430033, China
[2] School of Weapons Engineering, Naval University of Engineering, Wuhan 430033, China
* Correspondence: boyunliu@163.com

Abstract: The electric field fire extinguishing technology is an efficient, clean, and new fire extinguishing technology that can be operated at a long distance. In order to study the synergistic mechanism of "electric-flow-heat" in the process of transverse AC electric field fire extinguishing, the ionic wind formed by the influence of electric field on each charged particle during the burning process of ethanol–air diffusion flame is simulated by the non-premixed combustion model, and the experimental phenomenon of flame quenching in the transverse AC electric field is reproduced by means of numerical simulation. The accuracy of the numerical model was verified by comparing the temperature and flow velocity in the region obtained from the simulation with the data measured in the experiment. According to both simulated and experimental phenomena, we present a hypothesis of how the flame is quenched under the influence of an electric field. The next research directions are: (1) improving the accuracy of numerical simulation by building fine models; (2) studying the dynamic mechanism of real flames by particle image velocimetry technology.

Keywords: computational fluid dynamics; chemical reactions; equilibrium; particles; dynamic simulation

Citation: Zhao, S.; Liu, B.; Zhao, B.; Li, T.; Shu, Q. Numerical Simulation of Ethanol Air Diffusion Flame Quenching under Transverse AC Electric Field. *Fire* **2022**, *5*, 196. https://doi.org/10.3390/fire5060196

Academic Editor: Alistair M. S. Smith

Received: 15 August 2022
Accepted: 8 November 2022
Published: 17 November 2022

1. Introduction

A flame is a weakly ionized plasma, in the role of the applied electric field its internal contains a large number of charged particles that will produce directional movement, and the formation of ionic wind, affecting the shape, stability, products, and other combustion characteristics of the flame [1–5]. The U.S. Defense Advanced Planning Agency (DARPA) has funded Harvard University's White Edge Research Group to carry out research on electric field fire extinguishing technology [6], the results of which show that electric field fire extinguishing technology in limited space for small and medium-sized flame extinguishing effect is good but cannot be applied to and open areas of large firefighting work. While most of the ships and ships at sea are metal structures, the cabin space is closed and narrow, electric field fire extinguishing technology is an auxiliary means of fire extinguishing and because of its repeated work and no residual harmful substances after extinguishing [7–9], has a greater prospect of application on surface ships [10]. The current research on electric field-driven flame dynamics is mostly focused on the influence of the electric field on the combustion characteristics of small flames, and less on the medium-sized flame combustion characteristics affected by the electric field and focus on the electric field on the flame of the direction of the promotion of combustion, stable combustion effect research, electric field fire extinguishing effect of research is scarce. The study of the flame quenching process caused by the application of a uniform transverse AC electric field can help to understand the mechanism of electric field fire extinguishing and has important significance for the design and development of marine electric field fire extinguishing devices.

Drews et al. in the research group of Whitesides found that time-oscillating electric fields applied to plasmas in flames can produce stable gas flow. AC electric fields can manipulate flames at certain distances without the need for proximal electrodes [11,12].

Belhi et al. [13–16] studied the effect of the AC electric field on three different values of ion mobility for the same flame and the effect of negative ions on ion wind. It was concluded that negative ions play a crucial role in the formation of the ion wind effect, especially when a negative potential or alternating potential is applied to the electrode. Belhi also demonstrated the role of the ion wind effect in influencing flame kinetics by means of a detailed computational model with three-dimensional simulations to reproduce laminarly premixed methane–air native flames subjected to a transverse DC electric field in the saturated state. Based on the response of the laminar premixed methane–air native flame under this condition, it also proposes a skeleton mechanism to predict the fundamental properties of combustion in methane–air flames and an ionization optimization mechanism, which contributes to the study of the charged particle mechanism of hydrocarbon fuels.

In China, Yunhua Gan and Yanlai Luo [17–20] explored the combustion characteristics and chemical reaction mechanism of ethanol–air non-premixed combustion flame under the action of the electric field and proposed a detailed chemical reaction mechanism of ethanol–air flame combustion containing charged particles based on the skeleton mechanism of the basic properties of combustion in methane–air flame proposed by Belhi, which contains 64 components and 423 reactions. Di Renzo et al. [21,22] combined Belhi's results to develop a spatial model of counter-current diffusion flame mixing fraction with a sub-breakdown electric field, and the computational results of this two-dimensional model agreed well with experimental data and significantly reduced computational costs. Research results [23,24], simulated the ethylene diffusion flame containing charged particles, and the flow of smoke particles in the flame under DC electric field.

Cui Wei carried out a theoretical simulation study on the effect of ions on the chemical kinetic properties of flames in methane–air premixed flames and the results further revealed that the effect of electric field on cyclonic flames is mainly caused by the ion wind effect which changes the position and shape of the flame surface [25]. Yan Limin conducted simulations and experiments on the interaction between electric field and small flame found that certain electric field conditions can strengthen the tiny-scale combustion, but too strong electric fields will blow out the small-scale flame [26].

In summary, the main research object of electric fields influencing flame is laminar small-scale flame, and the main research purpose is to enhance combustion stability of electric field. However, for the confined environments, such as naval ship cabins, the electric field fire extinguishing technology for large-scale flames has great application prospects.

In this study, the distribution of charged particles in ethanol flames is simulated by ANSYS FLUENT 2021R1 software; the electric field equations are integrated into the simulation to simulate the electric field force applied to the charged particles in the combustion region; the electric field extinguishing experiment is compared with the simulation of ethanol–air diffusion flames under the action of electric field to study the effect of electric field on the charged particles in ethanol–air diffusion flames and the flow field in the combustion region. The flame quenching phenomenon under the effect of transverse AC electric field was investigated.

2. Experimental Setup and Methods

The experimental setup consists of four main systems, namely the fuel supply system, the combustion system, the applied condition system, and the detection system. As shown in Figure 1 the fuel supply system used in this experiment is a micro-peristaltic pump with a flow error of less than 1%, maximum traffic rate is 8 L/h. The combustion system consists of atomized nozzles and an arc igniter. Pressure limit valve and filter screen in atomizer, starting pressure is 4.5 bar. The liquid fuel is ignited by an arc igniter at the outlet of the atomizer nozzle to form a diffusion flame, and the atomizer has an injection angle of 60. The influencing factor used in this paper is the transverse electric field. The transverse electric field is generated by a high-voltage AC power supply and two flat plate electrodes, the electric field strength of the AC power supply can be achieved by adjusting the voltage or changing the distance between the plates. The detection system consists of an

NPX-GS6500UM high-speed camera, an SG-313 wind speed probe, an S-sex thermocouple, and a computer. As shown in Figure 1, a sensor monitoring point is set at 0.05 m above each of the burner's present nozzles to detect the temperature and flow field velocity at that point.

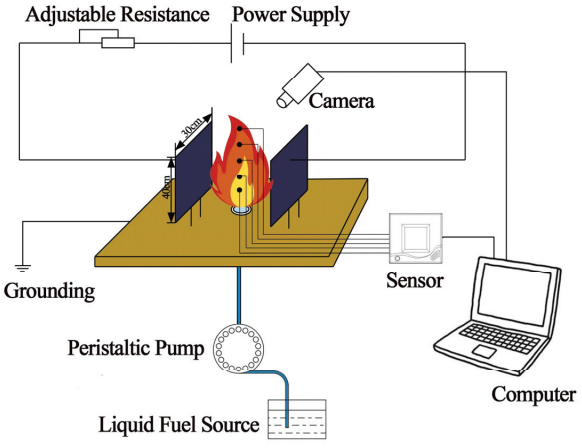

Figure 1. Experimental platform.

The fuel for this study was anhydrous ethanol and the thermophysical properties of 298 K anhydrous ethanol are shown in Table 1.

Table 1. Thermophysical properties of 298 K ethanol.

Purity	Density/g·cm^{-3}	Viscosity/mPa·s	Specific Heat Capacity/J·g^{-1}·K^{-1}	Electrical Conductivity/10^{-7} S·m^{-1}	Surface Tension/10^{-3} N·m
>99.7%	0.798	1.16	2.58	1.35	22.8

3. Numerical Simulation of Ethanol-Air Diffusion Flames under the Influence of Electric Fields

3.1. Chemodynamic Model

The formation of ions and electrons in hydrocarbon flames is the result of the interaction of CH and O radicals, so an accurate prediction of these two radicals is necessary to correctly determine the distribution of charged material. The literature [14] suggests that the CH and O radicals interact to produce positive ions and electrons during the combustion of hydrocarbon fuels:

$$CH + O \rightleftharpoons HCO^+ + e^- \quad (1)$$

To study the charged particles in ethanol–air diffusion flame affected by electric field forces, Luo [20] combined the mechanism proposed above for the charged particle skeleton reaction of methane containing 40 ionic reversible reactions and six charged substances (HCO^+, H_3O^+, e, O^{2-}, O^- and OH^-). In this study, a non-premixed model was used to predict the distribution of each component during ethanol combustion by compiling a custom function in Fluent software, selecting six charged substances (HCO^+, H_3O^+, e, O^{2-}, O^- and OH^-) in PDF (probability density function model) according to the literature [18], applying electric field forces to them, and simulating ethanol combustion in the directional movement of charged particles formed by the electric field force.

3.2. External Electric Field Model

In this study, the flow and combustion processes of the mixture follow conservation equations, including continuity, momentum, energy, and conservation of components as the controlling equations [27]. In this paper, a two-dimensional model simulation is used.

The continuity equation:

$$\frac{\partial(\rho u)}{\partial x} + \frac{1}{r}\frac{\partial(r\rho v)}{\partial r} = 0 \tag{2}$$

where ρ is the density of the fluid, u is the velocity of the fluid in the x direction and v is the velocity of the fluid in the r direction.

Conservation of momentum equation:

x Directions:

$$\begin{gathered}\frac{\partial(\rho uu)}{\partial x} + \frac{1}{r}\frac{\partial(r\rho uv)}{\partial r} = \\ -\frac{\partial p}{\partial x} + 2\frac{\partial}{\partial x}\left(\mu\frac{\partial u}{\partial x}\right) + \frac{1}{r}\frac{\partial}{\partial r}\left(r\mu\frac{\partial u}{\partial r}\right) + \frac{1}{r}\frac{\partial}{\partial r}\left(r\mu\frac{\partial v}{\partial x}\right) + F_x\end{gathered} \tag{3}$$

r Directions:

$$\begin{gathered}\frac{\partial(\rho uv)}{\partial x} + \frac{1}{r}\frac{\partial(r\rho vv)}{\partial r} = \\ -\frac{\partial p}{\partial r} + \frac{\partial}{\partial x}\left(\mu\frac{\partial v}{\partial x}\right) + \frac{\partial}{\partial x}\left(\mu\frac{\partial u}{\partial r}\right) + \frac{2}{r}\frac{\partial}{\partial r}\left(r\mu\frac{\partial v}{\partial r}\right) + \frac{2\mu v}{r^2} + F_r\end{gathered} \tag{4}$$

where μ is the dynamic viscosity of the fluid, p is the pressure on the fluid cell, F_x is the volume force in the x direction on the fluid cell and F_r is the volume force in the r direction on the fluid cell.

Conservation of energy equation:

$$\begin{gathered}\frac{\partial}{\partial x}(\rho uh_i) + \frac{1}{r}\frac{\partial}{\partial r}(r\rho vh_i) = \\ \frac{\partial}{\partial x}\left(\frac{k}{c_P}\frac{\partial h_i}{\partial x}\right) + \frac{1}{r}\frac{\partial}{\partial r}\left(r\frac{k}{c_P}\frac{\partial h_i}{\partial r}\right) - \frac{\partial(h_i\boldsymbol{J}_i)}{\partial x} - \frac{1}{r}\frac{\partial(h_i\boldsymbol{J}_i)}{\partial r} + \frac{\partial(zu)}{\partial x} + \frac{1}{r}\frac{\partial(rzv)}{\partial r} + S_h\end{gathered} \tag{5}$$

where k is the effective heat transfer coefficient, h_i is the enthalpy of component i, $\boldsymbol{J}_i$ is the diffusive flux of component i, c_P is the constant pressure specific heat capacity of the mixture, τ is the viscous dissipative stress and S_h is the volumetric heat source term.

An electric field can affect the movement of a particle through an electric force, which appears as a source term in the momentum equation [28]:

$$\begin{aligned}\mathbf{F}_r &= \sum_k^N q_k e\mathbf{E}_r n_k \\ \mathbf{F}_k &= \sum_k^N q_k e\mathbf{E}_k n_k\end{aligned} \tag{6}$$

where q_k and n_k are the number of charges of the charged substance, respectively, and k is the density. N is the number of species considered in the reaction mechanism, $e = 1.602 \times 10^{-19}$ C is the fundamental charge, and $\mathbf{E}$ is the electric field vector, defined by Gauss's law [15]:

$$\begin{aligned}\nabla\cdot\mathbf{E} &= -\nabla^2 V = \frac{\sum_k^{} q_k e n_k}{\epsilon_0} \\ \nabla\cdot\mathbf{E} &= \nabla\cdot\mathbf{E}_r + \nabla\cdot\mathbf{E}_k\end{aligned} \tag{7}$$

∇ is differential operator, V is the potential, ϵ_0 is the vacuum dielectric constant $\epsilon_0 = 8.854 \times 10^{-12}\mathrm{Fm}^{-1}$, n_k is the charge of the charged material and k is the density.

The particle diffusion velocity $\mathbf{V}_k$ is corrected to include the electric field effect

$$\rho Y_k\mathbf{V}_k = -\rho D_k\frac{W_k}{W}\nabla X_k + \frac{q_k}{|q_k|}\rho Y_k\mu_k\mathbf{E} \tag{8}$$

where X_k, Y_k, W_k and D_k are the molar fraction, mass fraction, molar mass and diffusion coefficient of component k, respectively. ρ and W are the mass-averaged density and molar mass, respectively. The first term to the right of the equal sign in Equation (8) is molecular diffusion as expressed by Fick's law of diffusion and the second term is the flux of charged particles drifting due to electromobility μ_k.

In this paper, we study the ethanol–air diffusion flame characteristics under the action of an applied transverse electric field. The supply voltage is connected to the left and right ends of the combustion system, and an electric field is formed between the electrode plates [20,24]:

$$\frac{\partial}{\partial x}\left(\frac{\partial V}{\partial x}\right) + \frac{1}{r}\frac{\partial}{\partial r}\left(r\frac{\partial V}{\partial r}\right) = -\frac{en_c}{\varepsilon_0} \tag{9}$$

where V is the potential, c is the charge density, n_c is the net charge density, and ε_0 is the vacuum dielectric constant.

The calculated electric field forces were added to the source term (DEFINE_SOURCE) of the momentum equation using the user-defined function (UDF) in Fluent software to solve the calculation and finally obtain the ethanol–air diffusion small flame combustion in the presence of an applied electric field.

The electric field strength between the electrode plates when the resulting applied AC electric field is not calculated, as shown in Figure 2. Where the applied electric field voltage U = 5 KV, the electrode distance is L = 150 mm, and the length of the electrode plate is 100 mm.

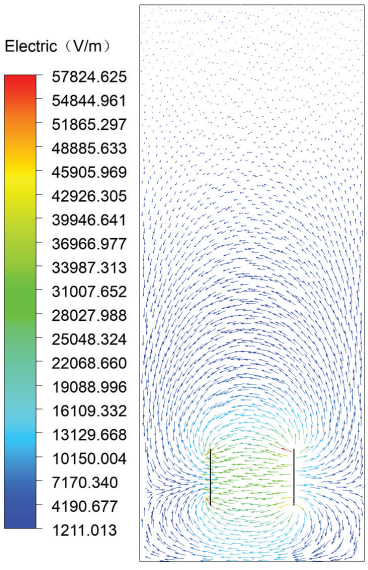

Figure 2. Electric field intensity of AC electric field.

3.3. Gridding and Boundary Conditions

In this paper, the ICEM meshing software is used to mesh the physical model created. Considering the difference between the solid and fluid zones, the calculation area is divided into the solid zone of the atomizer nozzle, the flow, and the combustion zone. The structure of the model is relatively regular in shape, so a map-type grid is used and the grid cell-type format is quad. As shown in Figure 3, the meshing and boundary condition settings for the numerical simulation in this paper are shown.

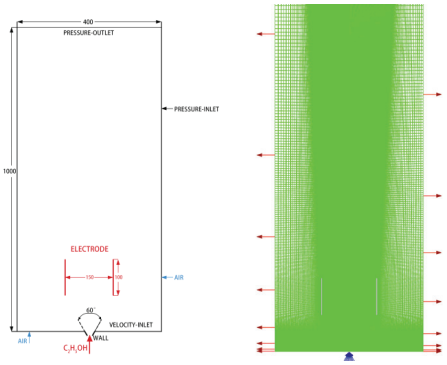

(**a**) (**b**)

Figure 3. Two-dimensional physical model of combustion system. (**a**) Schematic diagram of a two-dimensional physical model; (**b**) grid division.

In this study, three grid quantities, 54,021, 60,610, and 70,800, were set and the change in flame temperature was used to assess grid independence. When the grid number changed from 54,021 to 60,610, the flame temperature changed by 5.4%, and when the grid number changed from 60,610 to 70,800, the flame temperature changed by 1.1%. Therefore, the final choice of meshing with a mesh number of 60,610 gives a more accurate result. To facilitate the detection of changes in characteristic parameters during combustion, monitoring points are established at 0.05 m, 0.10 m, 0.15 m, 0.2 m, and 0.25 m above the burner sub-nozzle, and an isometric detection line is established at 0.2 m above the nozzle with the vertical center line of the jet as the axis of symmetry.

Before the simulation calculation, 15 sets of stable combustion experiments were carried out. The simulation calculation boundary conditions were measured by the experiment: the fuel flow rate is 0.0007 kg/s, and the fuel outlet speed is about 3 m/s, with the standard deviation less than 0.00001 and 0.1, respectively.

3.4. Solution Method

According to the chemical reaction process of ethanol–air diffusion flame, the non-premixed combustion model is selected for the study object, and the numerical simulation is based on the pressure solver with an implicit method to linearize the discrete control equations. The two-dimensional axial plane model is chosen, the absolute velocity is selected for the computational velocity, and the least squares cell is chosen for the gradient of the cell center variable. Pressure and velocity coupling is performed using the coupled algorithm. The finite volume method is used for discretization. The second-order upwind discretization format is used for momentum, energy, and components, and the standard discretization format is used for pressure. The energy residuals were set to 10–6 and the residuals of other parameters were set to 0.001. Based on the setup of the solution method described in this section, the results of the combustion process of the ethanol–air diffusion flame under the conditions of this study were calculated.

4. Numerical Simulation and Analysis of Experimental Results

4.1. Flame Temperature and Velocity

Figure 4 shows a comparison of the experimentally captured visible flame image with the calculated flame temperature profile when no electric field is applied. The results show that the temperature distribution obtained from the simulation is very similar to the flame profile given by the experimentally captured visible image of the flame, numerical simulated temperature distribution changes are close to the experimental measurements. A similar trend can be obtained by comparing the flame luminosity distribution measured

by Domenico et al. [29,30] with the temperature flame measured at a point above the equivalent burner.

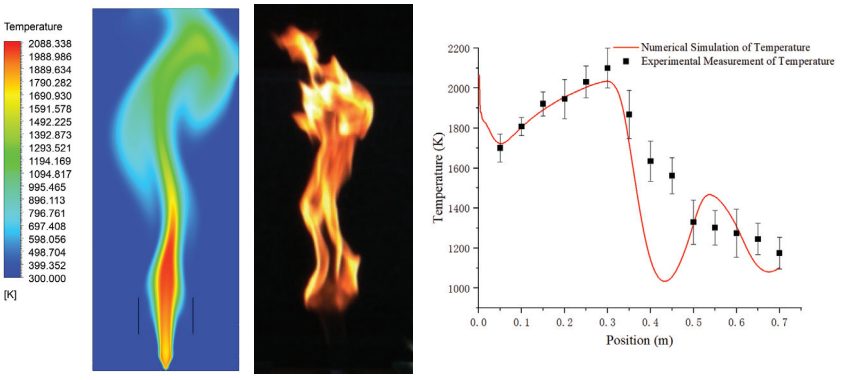

Figure 4. Contour of flame temperature and flame image in the experiment without electric field. (**a**) Flame temperature clouds; (**b**) experimental flame image; (**c**) comparison of simulated temperature distribution with experimentally measured temperature.

During the experiment, the fluid velocity was measured using an SG313 wind speed probe at 0.05 m intervals directly above the fuel nozzle. Figure 5 shows a cloud plot of the predicted flow field in the ethanol–air flame from this model and a comparison of the predicted fluid velocity in the combustion field with the experimental measurements. The results show that the velocity of the flow field above the burner obtained from the simulation is similar to the experimentally measured velocity and has a similar trend.

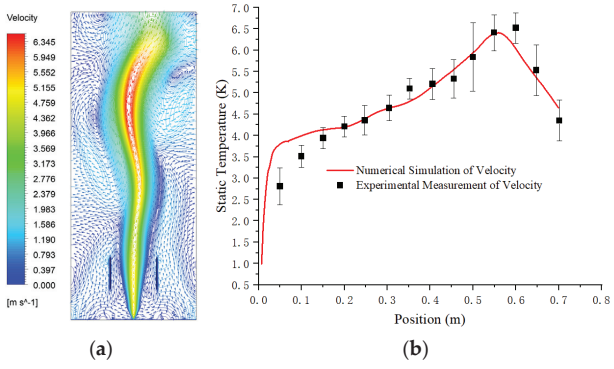

Figure 5. Prediction of flow velocity in combustion zone and experimental measurement data. (**a**) Flow field velocity vector diagram; (**b**) comparison of predicted flow rates with experimental measurement data.

4.2. The Electric Field Acts on the Flame to Produce Ionic Wind

The local magnification of the flow field between the pole plate is shown in Figure 6. Through the observation, it can be seen that between the pole plate, particles are charged by the action of the electric field force. From the original stable combustion state in the vertical upward motion direction, two strands change, respectively, to the nearest pole plate. Additionally, the formation of ion wind in this paper is called the electric field force–ion wind.

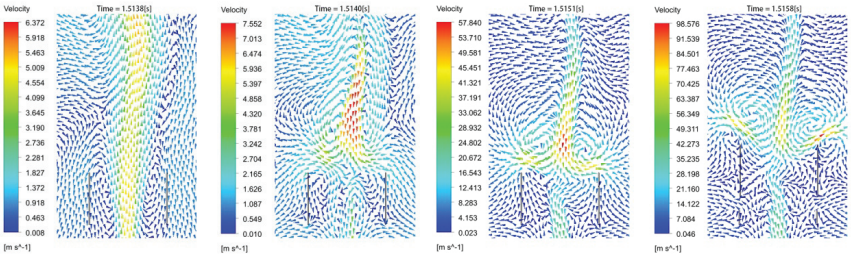

(**a**) (**b**) (**c**) (**d**)

Figure 6. Schematic diagram of flow field vector variation (**a**–**d**).

The electric field force–ionic wind affects the flow field between the pole plates. Figure 7a shows the variation of flow velocity with time at points 0.05 m, 0.10 m, 0.15 m, 0.2 m, and 0.25 m above the burner nozzle. It can be seen from the images that the flow velocity at the monitoring points of y = 0.15 and y = 0.20 points between the pole plates is growing under the influence of the transverse electric field force, i.e., the flow velocity between the pole plates is growing.

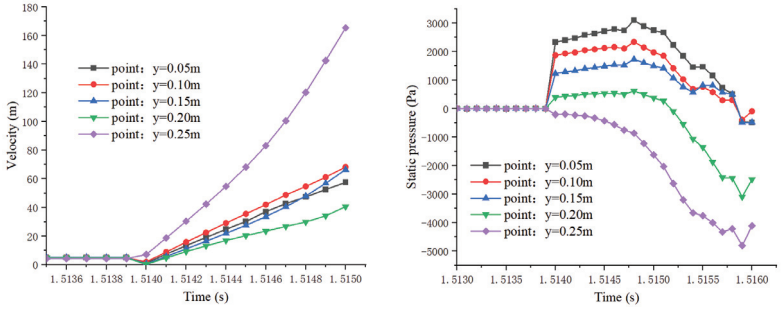

(**a**) (**b**)

Figure 7. (**a**) Initial application of electric field variation of static pressure with time at points 0.05 m, 0.10 m, 0.15 m, 0.2 m, 0.25 m above the burner nozzle; (**b**) initial application of electric field variation of flow velocity with time at points 0.05 m, 0.10 m, 0.15 m, 0.2 m, 0.25 m above the burner nozzle.

The Bernoulli integral according to the Euler equation has:

$$\frac{v^2}{2} + \int \frac{\mathrm{d}p}{\rho} = C \tag{10}$$

where v is the fluid velocity, p is the pressure per unit volume of fluid, ρ is the density per unit volume of fluid and C is a constant.

From Figure 6 b, it can be seen that as the flow velocity between the pole plates increases, the local low-pressure region rolls up the surrounding fluid and changes the fluid flow velocity and direction in the combustion field. By observation, it can be seen that the appearance of local low pressure further increases the flow velocity between the pole plates. From Figure 2, it can be seen that the electric field intensity between the pole plates is higher than the area outside the plates. The paraelectric effect is known according to the literature [28].

$$\begin{gathered} p_{\mathrm{e}} = \frac{1}{2}\rho v^2 = \frac{1}{2}\varepsilon E^2 \\ p_e + p_g = \left(\frac{1}{2}\varepsilon E^2\right) + \frac{nRT}{V} = Cons\tan t \end{gathered} \tag{11}$$

From the above equation, we can know that the electrostatic gradient between the poles is greater than the electrostatic gradient above the poles, then the pressure gradient between the poles is smaller as shown in Figure 8a, the surrounding gas at a higher pressure will flow to this part of the region, so the paraelectric effect. From Figure 8b it can be seen that the charged particles move to the part of high electric field strength, forming a high-speed gas flow.

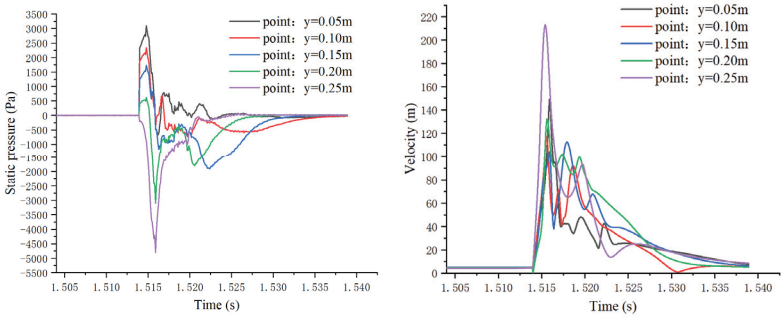

(**a**) (**b**)

Figure 8. (**a**) Variation of static pressure with time at points 0.05 m, 0.10 m, 0.15 m, 0.2 m, 0.25 m above the burner nozzle; (**b**) variation of velocity with time at points 0.05 m, 0.10 m, 0.15 m, 0.2 m, 0.25 m above the burner nozzle.

In summary, the flow field changes in the flame under the action of the transverse electric field can be divided into three stages.

(1) Electric field accelerated charged particles: In the initial stage of applying transverse AC electric field, charged particles in the combustion region between the pole plates are subjected to electric field force to form directional movement, forming electric field force–ion wind.

(2) Bernoulli effect to generate local low pressure: in this stage, the electric field force–ion wind increased the local flow velocity of the flow field, according to Bernoulli principle flow velocity increases dynamic pressure rises static pressure decreases, the formation of the local low-pressure region.

(3) Low-pressure suction formation paraelectric effect–ion wind: Bernoulli effect between the polar plates generated by the local low-pressure region will be formed on the surrounding fluid suction, that is, the air in the combustion region from low voltage gradient to high voltage gradient movement to form paraelectric effect–ion wind as shown in Figure 9, the flame impact.

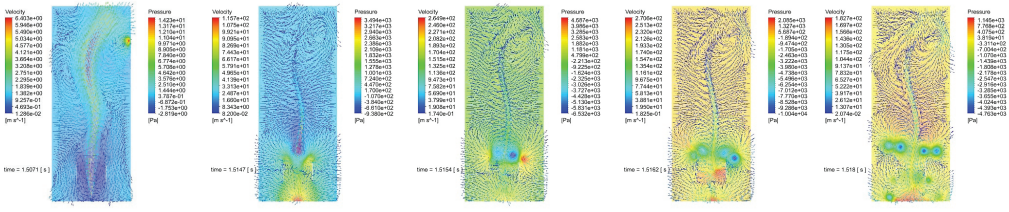

(**a**) (**b**) (**c**) (**d**) (**e**)

Figure 9. Flame by the lateral effect of the formation of paraelectric effect–ion wind (**a**–**e**).

4.3. Ionic Wind Fire Extinguishing

According to Equation (10), as C, ρ remains constant, the pressure per unit volume of fluid p decreases as the flow rate v within the combustion field increases. A local low-

pressure zone is formed at the 0.25 m detection point attachment above the nozzle as shown in Figure 9b. The appearance of the local low pressure resulted in the external fluid being sucked into the low-pressure area and forming a hedge with the rising fluid between the pole plates as shown in Figure 9c,d, the hedge of the fluid also resulted in, a reduction in the velocity of the flow field between the pole plates and a rise in static pressure at the remaining four detection points as shown in Figure 10a when the static pressure at the 0.25 m monitoring point above the burner nozzle continued to fall during the period 1.5139 s–1.5147 s.

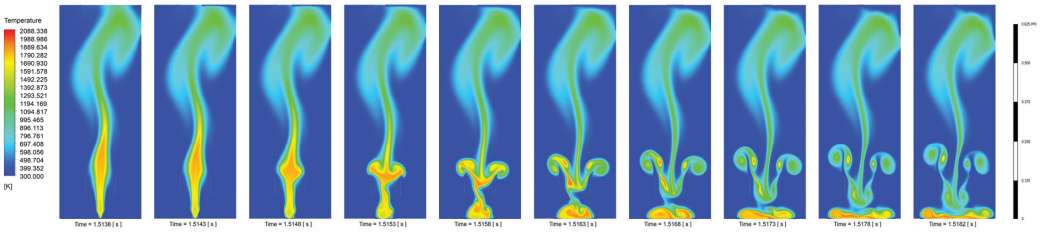

Figure 10. Numerical simulation of the change in temperature distribution of fire extinguishing by transverse AC electric field.

As the electric field continues to influence, as shown in Figure 11, by 1.5147 s all five monitoring points show a decreasing trend in static pressure, and by 1.5151 s all five monitoring points are at low pressure, the fluid outside the pole plate is sucked into the low-pressure region of the pole plate. As shown in Figure 11, a large amount of high-velocity fluid enters the combustion region in a short period of time resulting in a sudden drop in temperature between the plates, a decrease in reactant concentration, interruption of the combustion reaction, and flame extinction.

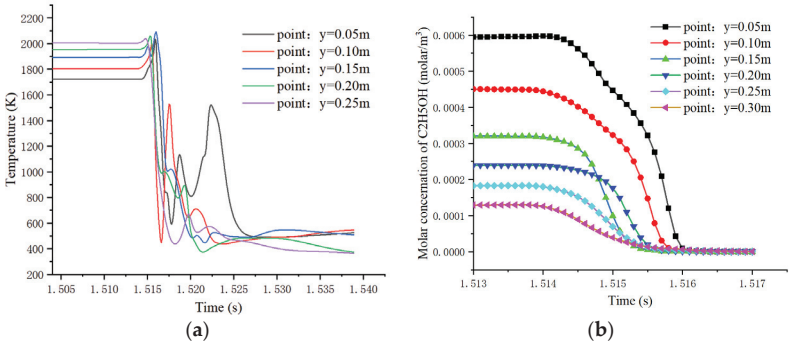

Figure 11. (**a**) Temperature change over time at each monitoring point; (**b**) ethanol concentration change over time at each monitoring point.

4.4. Experimental and Simulation Analysis

According to the literature [31,32], it is known that the hydrocarbon fuel flame air unaffected by the electric field enters the combustion area from the bottom of the flame or on both sides of the flame, and the charged particles are concentrated in the upper part of the combustion area and the movement area is vertically upward. Because the model uses a two-dimensional plane model for calculation and simulation, the air can only enter the plate into the combustion area from the gap above the plate and between the plate and the bottom of the grid, so the temperature decreases from the top down to below the ignition point in the numerical model.

When the flame is affected by the electric field, the large number of charged particles contained in the flame will produce a directional movement. The movement of the charged

particles causes the surrounding air to flow accordingly, and the flow rate in the combustion area is greater than the external flow rate. According to the Bernoulli phenomenon, the pressure between the plates is lower than the external standard atmospheric pressure, and the external air is pressed into the combustion area to form a strong air flow, that is, the isoelectric effect–ionic wind, which affects the material distribution and temperature in the combustion field, as shown in Figure 4, and eventually causes the flame extinguishing. However, during the experiment, the air can enter the flow field from the left and right sides of the plate and above the plate at the same time, so the strong air flow enters the negative pressure area between the plates from both sides of the plate, causing the flame to be extinguished from the bottom up, as shown in Figure 12.

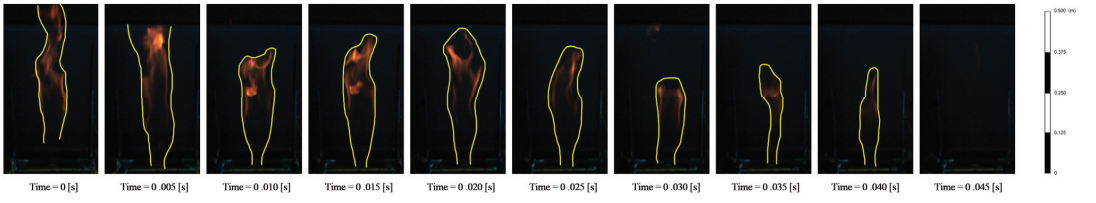

Figure 12. Flame luminosity changes in the transverse AC electric field experiment.

From the macro level, the basic elements of the combustion of ethanol and other liquid combustible materials are: combustible materials, oxide, ignition point, and chain reaction. Any combustion condition needs to meet the above four combustion factors, as long as any element of the four elements can be removed, it can prevent the occurrence of fire or extinguish the fire. The horizontal electric field causes the synergistic effect, ion wind, and low-pressure suction in the combustion area, which affects the temperature and combustible distribution in the combustion area, the temperature is reduced below the ethanol ignition point; ethanol is blown from the plate area, so the plate area does not meet the ethanol combustion conditions, ethanol diffusion flame is extinguished under the influence of the horizontal electric field.

At the micro-level, the time required for fuel combustion consists of two parts: the time (τ_s) when the fuel is mixed with the air, and the time (τ_c) when the fuel performs a chemical reaction. The laminar flame theory proposes that all the different flameout phenomena of the laminar flame can be explained by a single standard the number of Damköhler, which is defined as the ratio of the fuel oxidant mixture characteristic time to the chemical characteristic time, i.e.,

$$Da = \tau_s / \tau_c \tag{12}$$

In the diffusion flame, when $Da > 1$ the mixing process is slower than the chemical reaction process (the mixing characteristic time is greater than the chemical characteristic time), it is the combustion state; when $Da < 1$ the mixing process is faster than the chemical reaction process (the mixing holding time is less than the chemical characteristic time), it is the flameout state.

The mixing time of the fuel can be indicated by:

$$\tau_s = \delta_f / u_V \tag{13}$$

In this formula: δ_f for the flame thickness, u_V for the flow rate of ethanol steam.

Flame thickness can be obtained by the temperature distribution:

$$\delta_L = \frac{T_2 - T_1}{\max\left(\left|\frac{\partial T}{\partial x}\right|\right)} \tag{14}$$

T_1 for the initial fuel temperature, T_1 for the adiabatic flame temperature.

Generally, the reaction time of ethanol vapor oxidation is about 0.002 s [33], and the flame thickness in this study is 3.2 cm. Additionally, the substitution data can calculate a critical flow rate of 16 m/s when the Dunkel number is equal to 1. If the flow rate between the plates is more than 16 m/s, the mixing time of fuel and air during the combustion reaction is less than 0.002 s, $Da < 1$ is the flameout state, and the combustion reaction is extinguished by the interrupted ethanol diffusion flame.

5. Conclusions

In this paper, the distribution of charged particles in an ethanol–air diffusion flame is simulated using a non-premixed model combined with a previously proposed chemical reaction mechanism for the combustion of ethanol containing charged particles, and the quenching of the ethanol–air diffusion flame by a transverse electric field applied to the combustion region by a compiled UDS is reproduced. The experimental phenomena and simulation results lead to the following conclusions:

1. Using a non-premixed combustion model to simulate the quenching of ethanol–air diffusion flames by a transverse AC electric field between flat plate electrodes, the numerically simulated flame quenching process fits well with the experimental phenomenon and can be used as a basic model for the subsequent research and development of electric field fire extinguishing technology, which is of great significance for electric field driven flame research.
2. The "current-flow-heat" can be divided into three stages: (1) the electric field force; (2) the electric field force–ion wind increases the local flow velocity and the static pressure decreases; (3) the local low-pressure area, namely the air from low voltage gradient to high voltage gradient, which affects the combustion reaction.
3. Through the experimental and numerical simulation analysis, the transverse electric field fire extinguishing mechanism can be summarized as: macroscopic, the combustion area is affected by the paraelectric effect–ion transverse wind temperature reduced below the ethanol ignition point; ethanol is blown away from the plate area by the paraelectric effect–ion lateral wind blowing so that the area between the plates does not meet the combustion conditions of ethanol, and the ethanol diffusion flame is extinguished under the influence of the transverse electric field. Microscopically, the ethanol vapor particles move too fast in the paraelectric effect–ion wind hard combustion reaction, the mixing time of ethanol and air during the combustion reaction is less than 0.002 s, which is not enough to complete the combustion, and the ethanol diffusion flame is extinguished.

The next steps include the development of a 3D simulation model, the use of detailed charged particle chemistry models and laser-induced equipment to monitor component changes during electric fire suppression, and the use of particle image velocimetry to further investigate the mechanism of electric field-driven flame dynamics to support the development of electric field fire suppression technology.

Author Contributions: Conceptualization, B.L. and S.Z.; methodology, S.Z.; software, S.Z.; validation, S.Z., B.Z., T.L. and Q.S.; formal analysis, S.Z.; investigation, S.Z.; resources, S.Z.; data curation, S.Z. and T.L.; writing—original draft preparation, S.Z.; writing—review and editing, B.L.; visualization, B.Z.; supervision, B.L.; project administration, Q.S.; funding acquisition, B.L. and S.Z. All authors have read and agreed to the published version of the manuscript.

Funding: National Key R&D Program Project "Research on the Construction of the Fire Safety Protection System" (2021YFC3100202); National Natural Science Foundation of China Project Law of fire spreading behavior of energized cables and "electric-fluid-heat" Multi-field Synergy (52074202); Graduate Student Innovation Fund "Research on Clean and Efficient Fire Fighting Technology Based on Electric Field Interrupted Chain Reaction" (HGCXJJ2021013).

Institutional Review Board Statement: Not applicable.

Informed Consent Statement: Informed consent was obtained from all subjects involved in the study.

Data Availability Statement: Not applicable.

Conflicts of Interest: The authors declare no conflict of interest.

References

1. Kuhl, J.; Seeger, T.; Zigan, L.; Will, S.; Leipertz, A. On the effect of ionic wind on structure and temperature of laminar premixed flames influenced by electric fields. *Combust. Flame* **2017**, *176*, 391–399. [CrossRef]
2. Kuhl, J.; Jovicic, G.; Zigan, L.; Will, S.; Leipertz, A. Influence of electric fields on premixed laminar flames: Visualization of perturbations and potential for suppression of thermoacoustic oscillations. *Proc. Combust. Inst.* **2015**, *35*, 3521–3528. [CrossRef]
3. Kuhl, J.; Jovicic, G.; Zigan, L.; Leipertz, A. Transient electric field response of laminar premixed flames. *Proc. Combust. Inst.* **2013**, *34*, 3303–3310. [CrossRef]
4. Lacoste, D.A.; Xiong, Y.; Moeck, J.P.; Chung, S.H.; Roberts, W.L.; Cha, M.S. Transfer functions of laminar premixed flames subjected to forcing by acoustic waves, AC electric fields, and non-thermal plasma discharges. *Proc. Combust. Inst.* **2017**, *36*, 4183–4192. [CrossRef]
5. Tinajero, J.; Dunn-Rankin, D. Non-premixed axisymmetric flames driven by ion currentsNon-premixed axisymmetric flames driven by ion currents. *Combust. Flame* **2019**, *199*, 365–376. [CrossRef]
6. Cademartiri, L. Taming the flame: Electrical wave blaster could provide new way to extinguish fifires. In Proceedings of the 241st National Meeting and Exposition of the American Chemical Society (ACS), Anaheim, CA, USA, 27–31 March 2011.
7. Mu, S. Electric field cooling and electric field fire suppression. *Great Technol. (Sci. Myster.)* **2009**, *5*, 35.
8. Sher, E.; Pinhasi, G.; Pokryvailo, A.; Bar-On, R. Extinction of pool flames by means of a DC electric field. *Combust. Flame* **1993**, *94*, 244–252. [CrossRef]
9. Ata, A.; Cowart, J.S.; Vranos, A.; Getegen, B.M. Effects of direct current electric field on the blowoff characteristics of bluff-body stabilized conical premixed flames. *Combust. Sci. Technol.* **2005**, *177*, 1291–1304. [CrossRef]
10. Jia, L.; Jinhe, L. Research on the formation of a confined space emergency rescue fire fighting device based on the electric field model. *Saf. Sci. Technol.* **2018**, *13*, 54–55.
11. Drews, A.M.; Cademartiri, L.; Whitesides, G.M.; Bishop, K.J.M. Electric winds driven by time oscillating corona discharges. *J. Appl. Phys.* **2013**, *114*, 143302. [CrossRef]
12. Drews, A.M.; Cademartiri, L.; Chemama, M.L.; Brenner, M.P.; Whitesides, G.M.; Bishop, K.J.M. AC electric fields drive steady flows in flames. *Phys. Rev. E Stat. Nonlin. Soft Matter Phys.* **2012**, *86*, 036314. [CrossRef]
13. Belhi, M.; Domingo, P.; Vervisch, P. Modelling of the effect of DC and AC electric fields on the stability of a lifted diffusion methaneair flame. *Combust. Theory Model.* **2013**, *17*, 749–787. [CrossRef]
14. Belhi, M.; Lee, B.J.; Bisetti, F.; Im, H.G. A computational study of the effects of DC electric fields on non-premixed counterflow methane-air flames. *J. Phys. D Appl. Phys.* **2017**, *50*, 494005. [CrossRef]
15. Belhi, M.; Lee, B.J.; Cha, M.S.; Im, H.G. Three-dimensional simulation of ionic wind in a laminar premixed Bunsen flame subjected to a transverse DC electric field. *Combust. Flame* **2019**, *202*, 90–106. [CrossRef]
16. Lopez-Camara, C.F.; Belhi, M.; Im, H.G.; Dunn-Rankin, D. Numerical Simulations of Laminar Nonpremixed CH4-Air Jet Flames Influenced by Varying Electric Fields. In Proceedings of the 11th U.S. National Combustion Meeting, Pasadena, CA, CA, USA, 24–27 March 2019.
17. Gan, Y.; Wang, M.; Luo, Y.; Chen, X.; Xu, J. Effects of direct-current electric fields on flame shape and combustion characteristics of ethanol in small scale. *Adv. Mech. Eng.* **2016**, *8*, 1687814015624846. [CrossRef]
18. Luo, Y.; Gan, Y.; Jiang, Z. An improved reaction mechanism for predicting the charged species in ethanol-air flame. *Fuel* **2018**, *228*, 74–80. [CrossRef]
19. Luo, Y.; Jiang, Z.; Gan, Y.; Liang, J.; Ao, W. Evaporation and combustion characteristics of an ethanol fuel droplet in a DC electric field. *J. Energy Inst.* **2021**, *98*, 216–222. [CrossRef]
20. Luo, Y.; Gan, Y.; Xu, J.; Yan, Y.; Shi, Y. Effects of electric field intensity and frequency of AC electric field on the small-scale ethanol diffusion flame behaviors. *Appl. Therm. Eng.* **2017**, *115*, 1330–1336. [CrossRef]
21. Renzo, M.D.; Pascazio, G.; Urzay, J. The breakdown of self-similarity in electrified counterflow diffusion flames. *Combust. Flame* **2019**, *205*, 231–240. [CrossRef]
22. Renzo, M.D.; Palma, P.; Marco Donato, T.; Giuseppe, P.; Javier, U. The effects of incident electric fields on counterflow diffusion flames. In Proceedings of the 70th Annual Meeting of the APS Division of Fluid Dynamics, Denver, CO, USA, 19–21 November 2017.
23. Sayed-Kassem, A.; Gillon, P.; Idir, M.; Gilard, V. Numerical simulation of the effect of a DC electric field on a laminar ethylene diffusion flame. *Combust. Sci. Technol.* **2019**, 1–12.
24. Sayed-Kassem, A.; Elorf, A.; Gillon, P.; Idir, M.; Sarh, B.; Gilard, V. Numerical modelling to study the effect of DC electric field on a laminar ethylene diffusion flame. *Int. Commun. Heat Mass Transf.* **2021**, *122*, 105167. [CrossRef]
25. Wei, C.; Junyu, Y.; Yihua, R.; Li, S.-Q. Numerical Study About the Ions Effect to the Combustion Reaction Rate Under the Eclectic Field. *J. Eng. Thermophys.* **2018**, *39*, 1395–1400.
26. Limin, Y. *Experimental Study and Simulation Analysis of Electric Field and Small-Scale Flame Interaction*; Beijing Jiaotong University: Beijing, China, 2012.

27. Renzo, M.D.; Pascazio, G. A mixture fraction space model for counterflow diffusion flames with incident electric field. *Combust. Flame* **2020**, *218*, 260–275. [CrossRef]
28. Roth, J.R. Aerodynamic flow acceleration using paraelectric and peristaltic electrohydrodynamic effects of a One Atmosphere Uniform Glow Discharge Plasma. *Phys. Plasmas* **2003**, *10*, 2117–2126. [CrossRef]
29. De Domenico, F.; Guiberti, T.F.; Hochgreb, S.; Roberts, W.L.; Magnotti, G. Temperature and water measurements in flames using 1064 nm Laser-Induced Grating Spectroscopy (LIGS). *Combust. Flame* **2019**, *205*, 336–344. [CrossRef]
30. Yang, H.; Feng, Y.; Wang, X.; Jiang, L.; Zhao, D.; Hayashi, N.; Yamashita, H. OH-PLIF investigation of wall effects on the flame quenching in a slit burner. *Proc. Combust. Inst.* **2013**, *34*, 3379–3386. [CrossRef]
31. Yan, Y.; Huang, W.; Tang, W.; Zhang, L.; Li, L.; Ran, J.; Yang, Z. Numerical study on catalytic combustion and extinction characteristics of pre-mixed methane-air in micro flatbed channel under different parameters of operation and wall. *Fuel* **2016**, *180*, 659–667. [CrossRef]
32. Niu, J.; Ran, J.; Li, L.; Du, X.; Wang, R.; Ran, M. Effects of trapezoidal bluff bodies on blow out limit of methaneair combustion in a micro-channel. *Appl. Therm. Eng.* **2016**, *95*, 454–461. [CrossRef]
33. Gan, Y.; Wang, M.; Shi, Y. Combustion Temperature and Stability Characteristics of Ethanol Small-scale Jet Diffusion Flame. *Proc. CSEE* **2014**, *34*, 2802–2807.

fire

MDPI

Article

Enhanced Anti-Freezing Heating Cable Standard for Fire Prevention

Baek-Yong Jung [1,2,†], Seung-Mo Je [3,4,†], Hoon-Gi Lee [5,‡], Hong-Sik Kim [5,§], Jong-Young Park [5,§], Bu-Yeol Oh [5,‡], Jung-Woo Park [5,‡], Jun-Ho Huh [6,*] and Jae-Hun Lee [5,*]

1 Department of Electrical and Computer Engineering, University of Seoul, Seoul 02504, Republic of Korea
2 Senior Research of Electric and Electronic Center of Electrical, Energy Research Institute, Korea Testing & Research Institute (KTR), 98 Gyoyukwon-ro, Gwacheon-si 13810, Gyeonggi-do, Republic of Korea
3 Korea Midland Power Co., Ltd., 160 Boryeongbuk-ro, Boryeong 33439, Chungcheong, Republic of Korea
4 Department of Data Informatics, (National) Korea Maritime and Ocean University, Busan 49112, Republic of Korea
5 Fire Safety Research Division, National Fire Research Institute of Korea, Asan-si 31555, Chungcheongnam-do, Republic of Korea
6 Department of Data Science, (National) Korea Maritime and Ocean University, Busan 49112, Republic of Korea
* Correspondence: 72networks@kmou.ac.kr (J.-H.H.); jaehun19@korea.kr (J.-H.L.)
† These authors contributed equally to this work.
‡ Research Official.
§ Senior Research Official.

Abstract: Among the fire reports caused by seasonal devices registered with the Korea Fire Information Center in 2021, fires caused by heating cables accounted for the largest portion with 350 cases. As a result of analyzing the heating cable fires from 2015 to 2021, we have classified the heating cable fires into four types according to the method of winding the heating wire. First, we hypothesized that the temperature is high when the density is high due to the overlap of the hot wires or when there is a thermal insulating material. We predicted that the temperature would rise through a random game and established a reproducibility test plan. In order to check how heat generation changes depending on the winding method of antifreeze heating cables, we selected 10 manufacturers and checked the temperature characteristics according to the test conditions (Paragraph 11, Paragraph 19.101) of the Technical Regulations for Electrical and Telecommunication Products and Components of Korea (K 10013), tested the four methods mentioned in this thesis and compared and analyzed the results. The experiment results indicate that the temperature of the heater part in antifreeze heating cables was mostly higher than the conditions required by the existing standards in cases 1 to 4. In particular, in the case of No. 5 manufacturer's sample, the temperature of the heating cable of Case 1 was measured to be the highest at 119.0 °C. In addition, as a result of applying the data engineering reproducibility test results in the framework of the random game λ proposed in this thesis, we have derived the same results as the predicted hypothesis. Case 1 refers to the case where a fire occurs due to the heating cable being wrapped around the water pipe and insulation or taped outside; It is one of the methods that users actually use a lot in the field. Based on experiment, we have concluded that the fire risk is high under the Case 1 condition. Thus, the test conditions in the existing K 10013 Standard need to be strengthened according to the Case 1 condition.

Keywords: safety; fire; electric fire; fire prevention; deterioration of heater unit; data collection; anti-freezing heating cable; self regulating heating cable

Citation: Jung, B.-Y.; Je, S.-M.; Lee, H.-G.; Kim, H.-S.; Park, J.-Y.; Oh, B.-Y.; Park, J.-W.; Huh, J.-H.; Lee, J.-H. Enhanced Anti-Freezing Heating Cable Standard for Fire Prevention. *Fire* **2022**, *5*, 216. https://doi.org/10.3390/fire5060216

Academic Editor: Grant Williamson

Received: 8 November 2022
Accepted: 12 December 2022
Published: 16 December 2022

1. Introduction

Republic of Korea has four distinct seasonal climatic features, which result in a large annual range. The highest temperature in summer was 41.0 °C, and the lowest temperature in winter was −27.7 °C according to records by the Korea Meteorological Administration over the last 10 years (2011–2021). This climate characteristic has many advantages, but

there are also many disadvantages [1,2]. In particular, the disadvantage can be fatal in the water and water grid, which is indispensable in human life. The volume increases when water freezes, and the increase in volume tends to destroy the water transport path, leading to a limited supply of water, which is essential to human life [2]. It can even affect individual happiness and cause great social and economic losses. Therefore, preventive measures are necessary. Prevention requires maintaining the temperature of the water transport path above a certain value. There are various approaches to it, but using anti-freezing heating cables can be considered a method that is easy to implement and cost-effective. However, the anti-freezing heating cables that convert electric energy into thermal energy can increase the risk of fire due to aging and faulty installation by the users. As shown in Figure 1, fires caused by heating cables were the most frequent among the fires caused by seasonal devices reported to the National Fire Information Center last year, followed by fires due to wood-fired boilers.

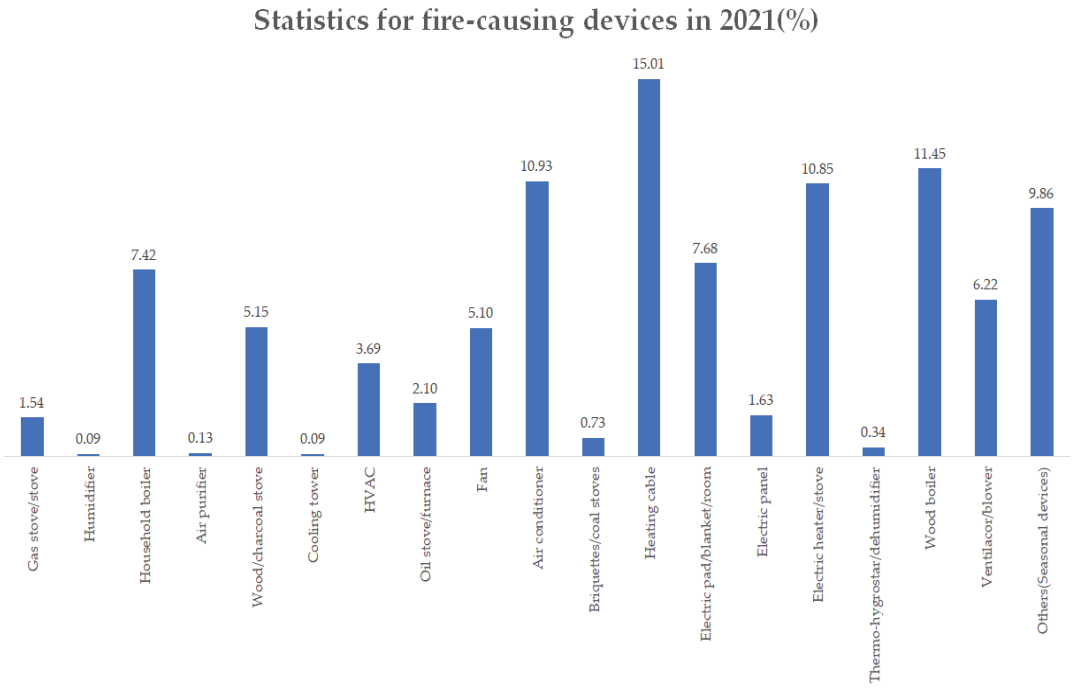

Figure 1. Statistics of fire-causing devices reported to National Fire Information Center.

These cables are easily installed, and the installation cost is low, hence their increasing use. However, the number of fires occurring in general households or farms is proportionally higher compared to other appliances according to the device classification of fires by electrical factors.

As such, although heating cables are seasonal devices that can be efficiently suitable for the geographical characteristics of the Republic of Korea with its large annual range, it is necessary to prepare measures to prevent fires caused by electrical factors as they account for the highest percentage.

In the paper, we analyze the cause of fire due to heating cables and conduct a reproducibility test to determine the data engineering approach to prevent fires. In other words, fires caused by anti-freezing heating cables are increasing every year, and they can lead to large fires. As a result, there is an urgent need to analyze the cause of fires in anti-freezing heating cables and provide a fire prevention measure. Thus, this study sought to classify

fire cases through the fire survey reports and analyze comparatively the test conditions in the safety evaluation standards of anti-freezing heating cables and conditions by fire cases, thereby deriving a basis for strengthening reasonable test standards (drafts) when operating a system of electrical appliance safety standards.

2. Related Research

The study on the fire hazards of short-circuiting of the anti-freezing heating cable by Lim Jung-Ho, Bang Seon-Bae, and Park Kwang-Mook [3] studied the risk of short-circuit fire by comparing the serial heating cables and self-regulating cables. According to the paper, in the case of serial heating cables, the current was three times higher during a short circuit, but the measured temperature of the sheath was lower than the rated temperature.

However, the risk of fire due to heat storage increased over time. In the case of self-regulating cables, the risk of fire due to the arc was high due to the current flow of 30 amps or more during a short circuit [3,4]. The study on natural convection thermal flow characteristics in closed circular piping with anti-freezing heating cables by Seo Gyu-Weon, Park Hyeong-Seon, and Yun Joon-Kyu [4] analyzed the thermal flow characteristics in closed circular piping according to the location of the heating cable. It showed that the heat transfer was best when $\theta = 135^{\circ}$ with one heat source, and that the heat transfer efficiency can be increased when $\theta = 135^{\circ}$ and $\theta = 180^{\circ}$ with two heat sources. The study on the potential fire due to anti-freezing heating cables by Lee Jeong-Hoon and Park Jeong-Yeol [5] identified four sources of fire by anti-freezing heating cables (fire due to short circuit, heat storage, defective contact, and electric leak) and analyzed the fire potential from them.

The headline analysis on natural convection for nanofluids [6–9] confined within square cavities with various thermal boundary conditions by Basak, T., and Chamkha, A.J. reported [7] that the average Nusselt number showed greater enhancement of heat transfer rates for all nanofluids for Ra = 105, and that alumina-water and copper-water exhibited greater enhancement of heat transfer rates. The paper "A Comparative Study on Arrhenius Equations and BP Neural Network Models to Predict the Hot Deformity Behaviors of Hypereutectoid Steel" developed [10] a BP neural network model using the data obtained from heat-to-heat compression tests at a specific temperature range to predict the high-temperature deformation state of hyper eutectoid steel. The paper "Fatigue life prediction of tire sidewall using modified Arrhenius Equation" proposed [11] a method of assessing tire fatigue life using the Arrhenius Equation.

2.1. Anti-Freezing Heating Cable (Self-Regulating Heating Cable)

Anti-freezing Heating Cables (Self Regulating Heating Cables) are mainly used as freeze protection for various types of pipes or tanks such as water pipes, water meters, and tanks during the winter season [12]. Although the use of these cables is increasing due to their simple installation method and low cost, the number of fire incidents caused by them in general homes or farms is continuously rising proportionally. The heating cables that are being used for the anti-freezing purpose include self-regulating cables, belt heaters, and constant wattage heating cables [13].

Among these three cables, self-regulating heating cables are being used widely to protect water pipes and tanks from freezing and bursting as they are easy to install with a low cost and maintenance. The user can cut the cable to any required length.

C Erickson [14] published Reliable and Cost-Effective Electrical Heating of Pipelines with Self-Regulating Heating Cable, proposing a method that utilizes the cable resistance when controlling the pipeline temperatures feedback.

Additionally, L Lardear [15] published Control of Self-Regulating Heating Cable for Use in Pipeline Heating Applications, focusing on the method of controlling temperatures without using existing sensors.

In the study Extreme Overheating in Self-Regulating Heating Cables by Hansen, Walter [16], it was found that the saltwater intrusion caused by the mechanical damage of cable or its leaking end resulted in cable damage.

The study Structure and Applications of CB/Crystal Fluoride Resin Alloy in Self-Regulated Heating Cables was published by J Wang et al. [17].

Meanwhile, a research work Application Self-Regulating Heating Cable Curing of Concrete in Winter was presented by Jin Bao Guo et al. [18], where he proposed a specific method that uses self-regulating heating cable for curing concrete in the winter season.

Additionally, N Khrenkov [19] published The Influence of Environmental Conditions on the Characteristics of Self-Regulating Cables. Meanwhile, Li-Chun Wang et al. [20] studied the charring effect and flame retardant properties of thermoplastic elastomer composites applied for cable. Yanyan Zou et al. [21] researched the determination of the solid-phase reaction mechanism and chlorine migration behavior of co-pyrolyzing PVC-$CaCO_3$-based polymer using temperature-dependent FTIR and XRD analysis. Zhi Wang [22] conducted a comprehensive study on the flame propagation of horizontal laboratory wires and flame-retardant cables under different thermal circumstances.

2.2. Related Domestic and International Regulations

Electrical appliances that require safety management by the product certification system as prescribed by the Electrical Appliances and Consumer Products Safety Control Act should meet the minimum safety requirements before they are released to the market. Even for certified products and products that are not subject to prior certification, those that pose or are likely to pose a threat to consumers' safety are recalled from the market or consumers through safety investigations based on the Framework Act on the Safety of Products as shown in Figure 2.

Figure 2. Product Safety Management System.

The anti-freezing heating cable is controlled by the product safety management system and is classified as a "product subject to safety confirmation" based on the safety standards of electrical appliances subject to the safety certification in attached 25 of Article 63 of the Operation Guidelines for Electrical Appliances and Consumer Products Safety Control, Public Notice No. 2021-0177 by the Korean Agency for Technology and Standards [2].

Based on the regulation, any party that manufactures or imports anti-freezing heating cables are allowed to sell only those products that have been reported to the Minister of Trade, Industry, and Energy (delegated to the certifying body) after undergoing product

test from the safety certifying body and receiving confirmation that they meet the safety standard, as shown in Figure 3 (no factory examination and regular inspection).

Figure 3. Safety Verification and Certification Procedure.

2.3. Anti-Freezing Heating Cables According to the Electrical Appliances and Consumer Products Safety Control Republic of Korea Act

Since 1974, the Republic of Korea has designated relatively high-risk items among the electrical appliances using AC power of no more than 1000 volts or DC power as electrical appliances subject to safety certification as prescribed by the Electrical Appliances and Consumer Products Safety Control Act to protect the people from the risk of electric shock/fire and other hazards caused by electrical appliances [1]. The electrical appliance safety certification scheme allows sales of only electrical appliances certified for safety by the safety certification bodies (Korea Testing Certification, Korea Testing Laboratory, and Korea Testing and Research Institute).

Since 2009 [2], only 66 low-risk products have been classified as products subject to safety verification to be sold after being tested by a government-designated safety verification testing body and reported to the safety verifying agency. However, the existing Safety Certification Scheme is still in place for parts like wires and products with relatively high risk due to the built-in heater and others.

Figure 4 shows comparison of procedures for electrical appliances subject to safety certification and those subject to safety verification.

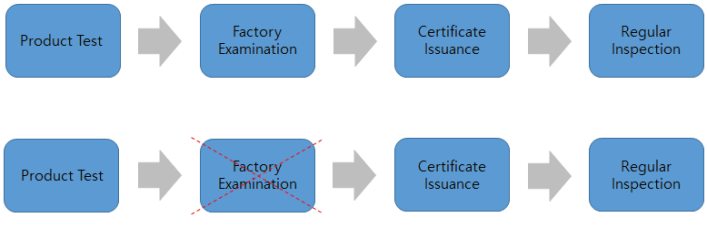

Type		Safety Certification	Safety Verification
Product test		○	○
Factory confirmation	Manufacturing and inspection equipment	○	X
	Raw material and process equipment	○	X
	Product inspection	○	X
Certification and report issuance		Certificate	Report
Regular inspection (Product test + factory confirmation)		○	X
No. of items		37 types	66 types

Figure 4. Comparison of procedures for electrical appliances subject to safety certification and those subject to safety verification.

Figure 5 shows fire statistics related to heating per year. The anti-freezing heating cables (classified as Water service anti-freezing device under the electrical appliance safety standard) are currently classified as subject to safety verification. The reports on fire accidents in the past 7 years show that heating cables have caused an average of 315 fire accidents in the past 7 years.

Although their use is increasing due to their advantages such as simple installation and low cost, self-regulating heating cables account for a large proportion of seasonal appliance fire accidents that occur in homes and farms.

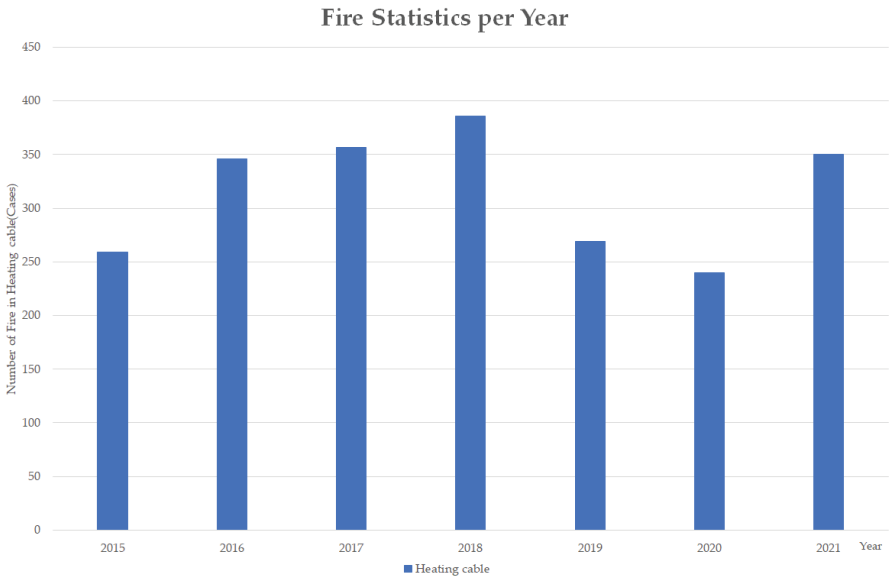

Figure 5. Fire statistics related to heating per year.

3. Anti-Freezing Heating Cables

Anti-freezing heating cables refer to equipment that prevents the water inside the water service pipe from freezing as the temperature sensor in the anti-freezing machine is run automatically when the water temperature inside the exposed pipe drops due to the cold wave in winter and reaches the freezing point.

They are defined in the K 10013 Standards by the Korea Agency for Technology and Standards, which are applied to the safety of anti-freezing appliances or flexible heating appliances that deliver heat to things for household and similar purposes under rated voltage of 250 V.

3.1. Work with Anti-Freezing Heating Cables

The survey on the ways users work with anti-freezing heating cables shows four main types. They can be classified into ① heating cables wrapped around water service pipes and thermal insulation or taping on the outside, ② insulations around water service pipes and heating cables wrapped around them, ③ heating cables irregularly wrapped in multiple layers around a water service pipe, and ④ heat cables wrapped around water pipes at regular intervals. Among them, case ① accounted for the highest proportion, followed by ④, ②, and ③.

3.2. Four Cases of Sites of Fire Caused by Anti-Freezing Heating Cables during the Period

3.2.1. Case 1: Fire Caused by Heating Cables Wrapped around Water Service Pipes and Thermal Insulation or Taping on the Outside

The case is a fire from anti-freezing heating cables wrapped around water service piping installed outside a house, resulting in the loss of some pipes and wires before the fire was self-extinguished (October 2019).

The investigation indicated that the anti-freezing heating cables themselves caused the fire as there was a statement from an official that there were sparks and flame from the water service pipes, and an electrical arc (short circuit) trace was found in the heater part of the heated wire as shown in Figure 6.

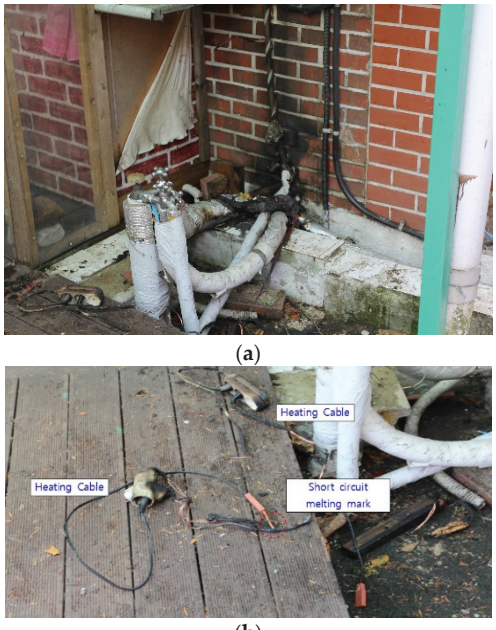

(**a**)

(**b**)

Figure 6. Case of fire caused by heating cables wrapped around water service pipes and thermal insulation or taping on the outside. (**a**) Case 1—Fire site ①. (**b**) Case 1—Fire site ②.

Figure 6 shows the fire that occurred in the heating cables wrapped around the water service pipes and thermal insulation or taping on the outside. As a brief summary, a fire occurred in the anti-freezing heating cables in the water service pipes installed outside the house in an anonymous area in South Korea in October 2019, burning the water service pipes and some wires before it was extinguished.

The fire investigation results revealed that sparks and flames were seen in the water service pipes as stated by the person concerned, and there were no negligent factors such as cigarette butts around or fire source neglect. In addition, electrical arc (short circuit) traces were found in the heating cables. Based on this evidence, the fire seemed to have been caused by the anti-freezing heating cables themselves. Figure 6a shows the photo of the actual fire site, and Figure 6b is the photo of the collected and spread heating cables as the cause of the fire in Figure 6a for fire investigation.

3.2.2. Case 2: Fire Caused by Insulations around Water Service Pipes and Heating Cables Wrapped around Them

The case is a fire that started from heating cables installed on the water pipes connected to an outside boiler room on the first floor but was extinguished with a fire extinguisher after some loss of insulation and others (July 2020).

The investigation indicated that the anti-freezing heating cables themselves caused the fire as there was a statement from a witness that the fire started on the floor of the boiler room. No parts other than the heating cables were lost as shown in Figure 7, and the heating cables have been there for a long time.

(**a**)

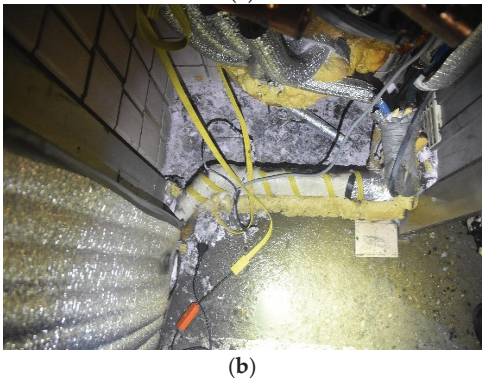

(**b**)

Figure 7. Fire caused by insulations around water service pipes and heating cables wrapped around them. (**a**) Case 2—Fire site ①. (**b**) Case 2—Fire site ②.

Figure 7 shows a case of fire caused by insulations around the water service pipes and the heating cables wrapped around them. As a brief summary, a fire was ignited from the heating cables installed in the water service pipes, which were connected to the external boiler room on the first floor in an anonymous region in Korea in July 2020, and the insulations, etc. were partially burned before the fire was extinguished by an extinguisher.

The fire investigation results revealed that the person concerned witnessed the fire from the floor in the boiler room and that parts other than the surrounding areas of the heating cables were not burned and were attached for a long time. Based on these circumstances, the anti-freezing heating cables themselves seemed to have been the cause of the fire. Figure 7a shows the photo of the actual fire site, and Figure 7b is the photo of the spread heating cables as the cause of the fire in Figure 7a.

3.2.3. Case 3: Fire Caused by Heating Cables Irregularly Wrapped in Multiple Layers around a Water Service Pipe

The case is a fire caused by heat accumulated by anti-freezing heating cables installed in the drainpipe in the ceiling of the entrance to the parking lot (ground level 1) of a five-story building (March 2015). The investigation revealed that the anti-freezing heating cables themselves caused the fire as there was a statement from a witness who saw the first smoke inside the parking lot, and there were no flammable materials other than the anti-freezing heating cables around the drainpipe in the ceiling of the parking lot as shown in Figure 8.

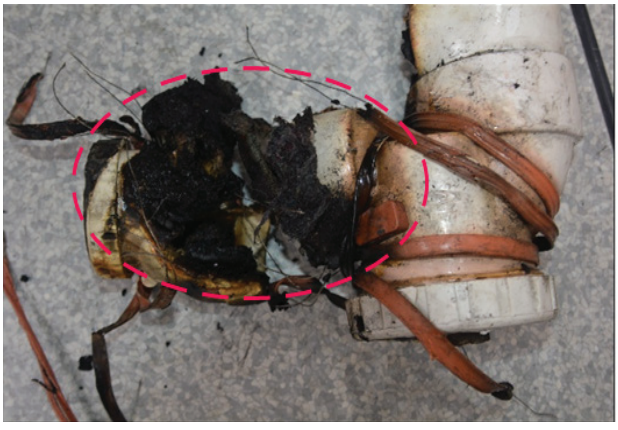

(**a**)

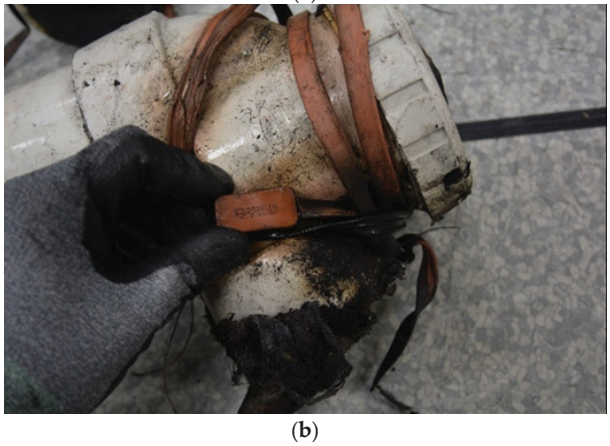

(**b**)

Figure 8. Fire caused by heating cables irregularly wrapped in multiple layers around a water service pipe. (**a**) Case 3—Fire site ①. (**b**) Case 3—Fire site ②.

Figure 8 shows the heating cables irregularly wrapped in multiple layers around a water service pipe.

As a brief summary, the fire was due to heat accumulation in the anti-freezing electrical heating cables installed on the ceiling drain pipes at the entry of the parking place (ground floor) in a five-story building in an anonymous area in Korea in March 2015.

The fire inspection results revealed that the first smoke occurred inside the parking place as witnessed and stated by the person concerned and that there were no materials that could be ignited other than the anti-freezing heating cables around the ceiling drain pipe at the upper part of the parking place. Based on this evidence, the fire seemed to have been caused by the accumulated heat in the anti-freezing heating cables.

Figure 8a shows the photo of the actual fire site, and Figure 8b is the photo enlarging the heating cable product to confirm the cause of the fire shown in Figure 8a.

3.2.4. Case 4: Fire Caused by Heat Cables Wrapped around Water Pipes at Regular Intervals

The case is a fire caused by heating cables installed to prevent the freezing of boiler pipes of the sewage drain pipes on top of the terrace in a row house (March 2015). The investigation found no fire factors such as arson, gas leak, or flammable material. Considering the fact that the anti-freezing heating cables have always been powered on for three

years since installation, and the combustion was centered on the sewage pipe as shown in Figure 9, it is estimated to be a fire caused by the anti-freezing heating wire itself.

(**a**)

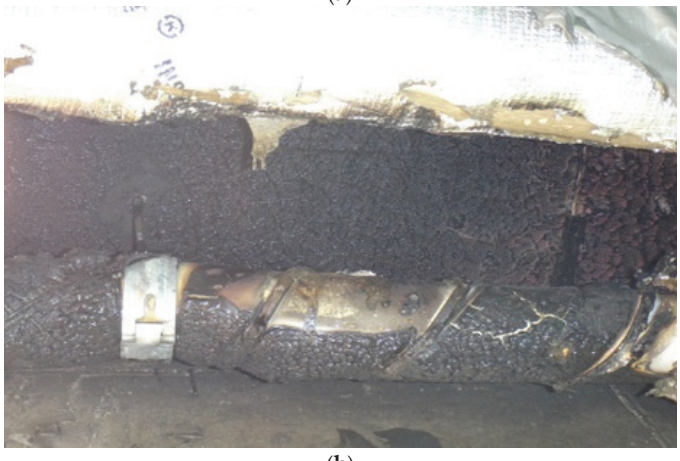

(**b**)

Figure 9. Fire caused by heat cables wrapped around water pipes at regular intervals. (**a**) Case 4—Fire site ①. (**b**) Case 4—Fire site ②.

Figure 9 shows the heating cables wrapped around water pipes at regular intervals. As a brief summary, it was a fire caused by the heating cables installed to prevent freezing at the boiler drain pipes in the wastewater drain pipe at the upper part of the veranda in an anonymous area in Korea in March 2015.

The fire investigation results revealed that the ignition was not caused by arson or gas leaks and ignitable substances. Power was supplied constantly for about 3 years after the installation of the anti-freeze heating cables, and burning occurred around the waste drain pipe. Comprehensively considering these circumstances, the fire seemed to have been caused by the anti-freezing heating cables.

Figure 9a shows the photo of the actual fire site. Figure 9b shows the photo that enlarges the heating cables to confirm the cause of the fire shown in Figure 9a.

4. Design and Experiment with Reproducibility Tests from a Data Engineering Perspective

A correlation is a relationship between cause and effect. It is possible to express a cause-and-effect relationship between an act and a subsequent occurrence of facts.

Demand decreases as the price rises. The price rise is the cause, and the decrease in demand is the effect. Price increases as market demand increases. The increase in market demand is the cause, and the price rise is the effect. As the price increases, the supply increases. (The Law of Supply) When the supply in the market increases, the price goes down.

So, what are the causes of the fire? The answers vary depending on the situation. In the case of autumn forest fires, dry environments or hikers' cigarette butts can cause fires. In the case of electric vehicles, a defective battery can cause a fire. However, as opposed to its results, it is not easy to clearly prove fire causes. Because a fire alters potential evidence of fire causes, it is hard to infer the causes from damaged evidence (burned ash, generated thermal energy, etc.). As such, we have designed a random game λ as a data engineering reproducibility test design and applied it to identify the factors that cause a high-temperature situation through the information given in the fire situation.

The following is a setup to check the cause and effect of the fire case due to the heating cable: Consider the situation in three dimensions according to the density of heating cables, presence of insulation material, and sequence of insulation material and heating cables. Assume the presence and absence of insulation material in each case of the high- and low-density heating cables as shown in Table 1. The situation of the insulation material being present can be divided into the situation of the insulation material or heating cables being wound first. Suppose a program returns either 1 or 0 depending on whether the increase or decrease in asset A matches the results of asset B's rise or fall.

Table 1. A program that returns a value according to the density of heating cables.

-	High-Density of Heating Cables	The Low Density of Heating Cables
Presence of insulation material	1	0
Absence of insulation material	0	−1

On the other hand, assume program R that adds the points shown in the table if there is a fire in the presence or absence of insulation material while the heating cable density is high or low, as shown in Table 2. The program returns 1 in the event of fire when the insulation material is present, and the heating cables are densely wound first. It returns 0 in the case of a fire with the insulation material having low heating cable density or if the density of the heating cables is high but there is no insulation material. It returns -1 when there is no insulation material and the density of the heating cables is low and returns Σ return value/n when the test count is n. The average program result value varies according to the correlation between the density of the heating cables, the presence/absence of the insulation material, and fire. Let us assume that many fires occur if the insulation material is present and the density of heating cables is high. Assuming each case occurs with the same probability, the program's return value for the situation converges at 0.25.

Table 2. Program 2 returns a value according to the density of the heating cables.

Assuming That Insulation Material Is Present	High-Density of Heating Cables	The Low Density of Heating Cables
Insulation material later	1	0
Insulation material first	0	−1

However, it would not be accurate to assume that the fire occurs more often as the return value deviates more from 0.25, the insulation material is present, and the density of heating cables is high.

In Tables 1 and 2, three state values are classified according to the presence or absence of each insulation and the density of the cable. In Table 1, the density of heating cables is high. It can be defined as returning a value of 1 in case of fire when insulation is present. Similarly, it can be defined as returning a value of -1 when a fire occurs in a hot wire with no insulation and low density.

In addition, this program can be defined to return 0 when the density is low when there is insulation or when the density is high when there is no insulation. Let's consider a situation in which insulation is present and a high density of heat rays is repeatedly provided. At this time, as the average value returned by the corresponding program is closer to 1, it can be seen that the frequency of occurrence of fire will be high when the insulation material is present and the density of the heating cable is high. It can be assumed that as the average of the returned values is farther from 1, the fire, the presence of insulation, and the denseness of the heating wire will be less related to the fire.

In Table 2, three state values were assigned according to whether or not the insulation was first installed and the three state values were according to the density of the cable. If a hot wire is first constructed and a fire occurs when the density of the installed hot wire is high, a program that returns a value of 1 can be defined. This program constructs the insulation material first and returns a value of 01 if a fire occurs when the heating wire is low. In the case of the heat wire not being dense, the heat wire constructed first, and if the heat wire is dense, a value of 0 is returned.

If the heating cable is first constructed, let's assume that the average of the returned values of 1 is repeatedly given a situation in which the density of the installed hot wire is high. The closer the value is to 1, the greater the correlation between the variable and fire, while the farther the value is from 1, the lower the correlation between the variable and fire.

Assume program R to examine the relationship between the density of heating cables and the sequence in which the insulation material and heating cables are installed. The program returns 1 in the event of fire when the insulation material is installed later and the heating cables are densely wound first. It returns 0 in the case of fire when the insulation material is installed later with low heating cable density, or the density of the heating cables is high but the insulation material is installed first. It returns -1 when the insulation material is installed first and the density of heating cables is low and returns Σ return value/n when the test count is n. The program's output differs depending on the correlation between the installation sequence of the insulation material and heating cables and the density of the heating cables. Assume that the heating cables are wound first followed by the insulation material while the density of heating cables is high. Moreover, if each case occurs with the same probability, the output value is likely to converge at 0.25 when the correlation with the fire is high.

4.1. Design of Reproducibility Test

We purchased anti-freezing heating cables (10 units) from an online market and compared and analyzed the test results according to the Electrical Appliance Safety Standard (K 10013) and the results of the reproducibility test applied to fire accident cases. The analysis is then tested with the random game λ mentioned above.

The test conditions are as follows. Anti-freezing heating cables are subject to conformity assessment according to safety standards KC 60335-1 (Household and similar electrical appliances—Safety Part 1: General requirements) and K 10013 (Individual requirements of heating devices having the safety of household and similar electrical devices and the flexibility of water service anti-freezing devices and similar) for conformity assessment. The product test items related to fire are "11. Additionally, temperature rise and "19. Abnormal operation." Therefore, the conditions for comparing the results of the conformity assessment test and the reproducibility test for the anti-freezing electric heating

cables should be the same as the "General conditions for the test" stated in K 60335-1 and K 10013. Meanwhile, Table 3. below shows the abovementioned Bell test modified for the reproducibility test.

Table 3. Modification of the bell test for the reproducibility test.

Modified Random Game λ	The Low Density of Heating Cables	High-Density of Heating Cables
Insulation material later	1	-
Insulation material first	0	-
No insulation material	-	2

Rule 1: +1 point in the case of heating cables wrapped around water service pipes and thermal insulation or taping on the outside.

Rule 2: 0 points in the case of the insulation around water service pipes and heating cables wrapped around them.

Rule 3: +2 points in the case of heating cables irregularly wrapped in multiple layers around a water service pipe.

Since program R in this random game λ is a reproducibility test, assume that it returns the average by adding the points presented in cases of the highest temperature. Use the anti-freezing heating cables (10 types) purchased online. Program R's output values are between 0 and 2. A value closer to 1 means that case 1 is more likely to record a higher temperature. A value closer to 0 means that case 2 is more likely to record a higher temperature. A value closer to 2 means that case 3 is more likely to record a higher temperature.

Each value in the table is the score obtained in the corresponding state. Lambda Game is a program that proves a causal relationship exists when the average of random values approaches a specific value as the number of trials increases. The unit for the game is not separately marked because the purpose of the game is to show cause and effect more objectively, and the value output as a result of the game is a kind of score that shows how likely it is to be the cause of a fire according to the closeness of the value.

The case temperatures in Table 4. are the averages of the three measures for the product. The result of assigning the score of the case of the highest average value is the output value of 1.3. Therefore, the temperature value of the anti-freezing heating cables is highest in case 1, meaning the risk of fire increases when heating cables are wrapped around water service pipes and thermal insulation or taping on the outside. Table 5 shows the results of the reproducibility test and the score for the random game λ.

We have chosen six samples from 10 local manufacturers, respectively. The materials of the selected products were Polyethylene, Poly Vinyl Chloride, Polyolefin, and Silicone. Table 4 shows the temperature rise (11.) and abnormal operation (19.101) tests along with the test results of cases 1 to 4 according to the conditions of the K 10013 standard.

The tests of clauses 11 and 19.101 and cases 1 to 3 of Table 4 were carried out in a test environment condition of −10 °C to 5.0 °C while the test of case 4 was conducted in a test environment condition of 20 °C. As for the test methods, 1.15 times the rated input (W) is applied in the case of clause 11, and 1.24 times the rated input (W) is applied in the case of clause 19.101 and cases 1–4 [23–25] (1.15 times was referenced from the condition in Paragraph 11 in the IEC 60335-1 Standard.)

The abnormal operation test method involved applying 1.24 times the rated power input (W) for each product [23–25].

(1.24 times was referenced from the condition in Paragraph 19.3 in the IEC 60335-1 Standard.)

Table 4. Comparison of the results of the K 10013 test and reproducibility test.

No.	Photo	Sheath Material	Paragraph 11	Paragraph 19.101	Reproducibility Test (Case 1)	Reproducibility Test (Case 2)	Reproducibility Test (Case 3)	Reproducibility Test (Case 4)
			Temperature (°C)	Temperature (°C)	Temperature (°C)	Temperature (°C)	Temperature (°C)	Temperature (°C)
1		Polyethylene	49.1 68.4 59.8	53.8 54.8 55.3	60.4 62.7 65.2	51.2 53.6 56.5	62.0 64.3 62.9	60.5 61.8 62.0
2		Poly Vinyl Chloride	30.4 23.2 18.1	44.6 45.9 47.5	46.5 49.5 52.2	27.1 25.8 23.2	37.4 33.8 36.7	42.1 43.6 44.0
3		Polyolefin	28.7 35.9 27.4	39.5 37.5 38.2	40.2 38.4 39.2	25.5 25.6 28.9	33.0 31.9 32.1	34.9 34.3 34.4
4		Poly Vinyl	57.2 51.8 21.8	53.6 50.9 21.8	68.7 71.5 78.3	34.4 34.5 33.2	41.8 15.1 45.4	47.0 47.5 45.7
5		Chloride	41.5 79.0 63.4	42.9 78.8 66.1	95.8 110.9 119.0	46.0 45.7 52.3	58.1 54.9 55.5	30.7 30.4 29.7
6		Poly Vinyl	19.2 20.1 26.2	19.6 19.9 28.0	53.2 58.0 60.8	22.8 23.2 21.1	26.4 30.1 27.5	26.0 36.5 27.0
7		Silicone	24.7 26.2 25.4	24.6 24.4 25.2	57.6 57.6 57.9	27.9 27.2 27.6	42.4 47.6 44.9	46.9 48.0 47.5
8		Poly Vinyl	7.9 29.6 29.8	24.0 27.2 27.0	27.8 27.5 28.4	27.8 29.9 33.0	25.8 26.8 25.5	55.9 56.7 55.8
9		Chloride	17.8 18.6 21.5	18.5 19.3 20.5	25.7 38.0 32.6	16.0 16.4 15.6	25.0 37.2 32.2	39.2 38.3 39.2
10	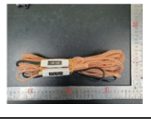	Silicone	44.1 15.6 42.1	45.5 46.4 41.8	63.9 69.4 77.3	36.1 36.9 40.9	45.1 45.6 46.5	43.5 47.0 43.6

Table 5. Results of the reproducibility test and score value of random game λ.

No.	Case 1 (°C)	Case 2 (°C)	Case 3 (°C)	Max. Value (°C)	A Score of Random Game λ
1	62.7	53.7	63.0	63.0	2
2	49.4	25.3	35.9	49.4	1
3	39.2	26.6	32.3	39.2	1
4	72.8	34.0	46.7	72.8	1
5	108.5	48.0	30.2	108.5	1
6	57.3	22.3	29.8	57.3	1
7	57.6	27.5	47.4	57.6	1
8	27.9	30.2	56.1	56.1	2
9	32.1	16.0	38.9	38.9	2
10	70.2	37.9	44.7	70.2	1

Case 1: 4.2.1. Case 1: Fire caused by heating cables wrapped around water service pipes and thermal insulation or taping on the outside.

Case 2: 4.2.2. Case 2: Fire caused by insulations around water service pipes and heating cables wrapped around them.

Case 3: 4.2.3. Case 3: Fire caused by heating cables irregularly wrapped in multiple layers around a water service pipe.

Case 4: 4.2.4. Case 4: Fire caused by heat cables wrapped around water pipes at regular intervals (20.0 °C).

Cases 1 to 4 show the results of the test conducted equally after dividing the test in 19.101 into four detailed methods.

The theory was designed to show a correlation between the fire and heating cables/thermal insulation. For Cases 1, 2, and 3, a score was given. When a certain score was close to that score, it was considered to be related to fire. Each case was a circumstance that was likely to induce fire. We will see the correlation with fire for cases wherein an average of the sum of all scores converged when the number of trials was large. This was designed to explain the data engineering of the fire scenarios.

Based on these results, if we conduct an experiment under the same temperature condition, we can conclude that the Case 1 condition has a relatively high temperature (with thermal insulation) and a high risk of fire due to the electrical factor.

Most of the fires on the anti-freeze heating wire lead to fires due to the factors of the heating wire itself, as mentioned above and as shown in this fire case analysis. The fundamental cause is the rupture of the coating of the heating wire (deterioration phenomenon and overcurrent due to moisture infiltration, etc.). As indicated in the experimental results, the temperature difference by manufacturer and installation condition was about 91 °C (28.4–119.0 °C).

Thermal deterioration varies depending on the composition of covering materials, which are made of cross-linked polyethylene (XLPE), polyethylene (PE), vinyl chloride (PVC), ethylene propylene rubber (EPR), etc. The continuous rated temperature is 90 °C for XLPE, 75 °C for PE, 60 °C for PVS, and 80 °C for EPR. When the rated temperature is continuously exceeded, the covering material hardens and weakens (embrittlement) due to thermal deterioration, and cracks occur when bending or impact is applied.

The score of the random game λ in Table 5 is a simple score, so it is not indicated in a separate unit. The cable was investigated for the fire correlation of the following three variables such as "the density of heating cables," "the presence or absence of insulating materials," and "the presence or absence of the priority of heating cables and insulating materials." We have ignored other variables. That is to reproduce the danger of fire to

which civilians are exposed. To this end, we purchased heating cables and insulation materials that could be easily purchased on the market and conducted tests without any adjustments made to the products.

4.2. Data Engineering Perspective of Reproducibility Test

As Investigated earlier, there were four types of fire incidents involving anti-freezing electric heating wires (Four types fire incidents involving anti-freezing electric wires during the period from 2015 to 2021). Although these wires are being tested with a conformity assessment system (KC Certification) according to Electrical Appliances Safety Standards (K 10013), they are not clear enough.

Section 11.7 of K 10013 states that the submersibles should be submerged and those to be used by attaching themselves with the testing sample should be attached to their normal state of use. For the others, the testing samples having an automatic temperature regulator should be placed on a surface-flat wooden platform (10 mm), setting the temperature at maximum. For those without any temperature regulators, operate the sample as it is.

However, it was possible to find four different cases of use and in order to investigate which of them had the worst conditions, the conformity test was performed for each case with the same assessment standards (K 10013), among which Section 11 (heating) and 19 (abnormal operation) directly associated with the possibility of fire were applied. A comparative test was conducted for Section 19 to check the maximum temperature for each type.

Meanwhile, the three measuring points include internal and external temperatures of each heating wire coiling around the sample (i.e., between the pipe and heating wire and the wire itself: two points) and one point for the insulator.

The temperature measurement method was measured using a calibrated digital thermometer (FW1012, YOKOGAWA). In addition, the accuracy of this equipment is verified by calibration once a year at the domestic KOLAS calibration institute. The calibration date is 10 February 2022.

- Setup conditions: Four types.
- Test environment: −10 °C~5 °C, 20 °C (only case4).
- Testing voltage: 1.24 X Rated Input of each appliance (Section 19 Abnormal Operation).
- Temperature channel information:

CH004: Measured between the thermal insulation and heating cable (if there is no thermal insulation, measure between the heating cables).
CH005: Measurement of the heating cable.
CH006: Measured between the water service pipe and heating cable.

The results of the temperature rise (Paragraph) and abnormal operation (Paragraph) tests according to the K 10013 test specification showed a temperature deviation of 58.0 °C in the heater parts (Paragraph 11: 21.5–79.0 °C and Paragraph 19: 20.5–78.8 °C) as shown in Figure 10 Moreover, the reproducibility test showed that case 1 (heating cables wrapped around water service pipes and thermal insulation or taping on the outside) was the highest temperature condition and that the difference in temperature at heater parts by-product was about 91.0 °C (28.4 °C to 119.0 °C).

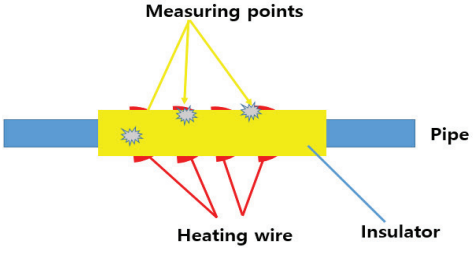

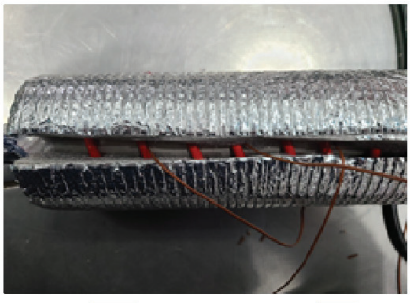

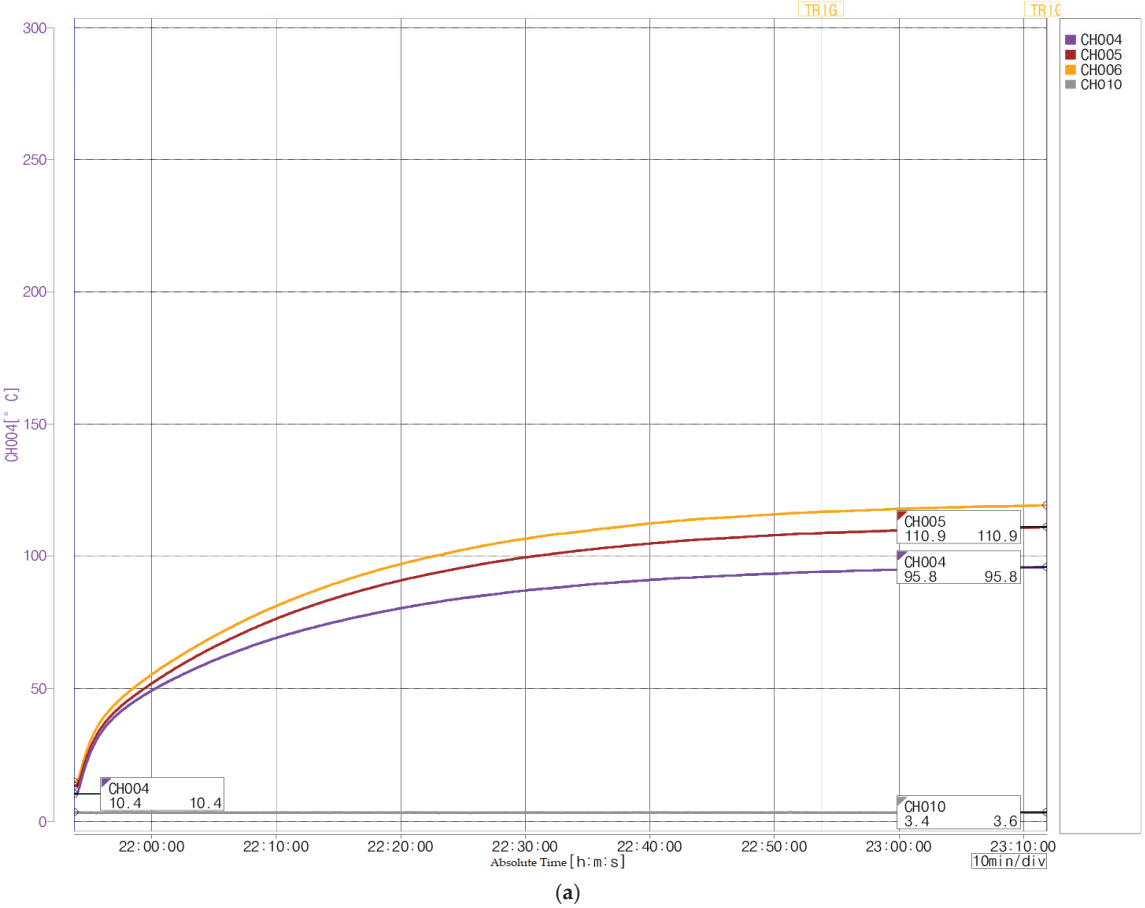

(**a**)

Figure 10. *Cont.*

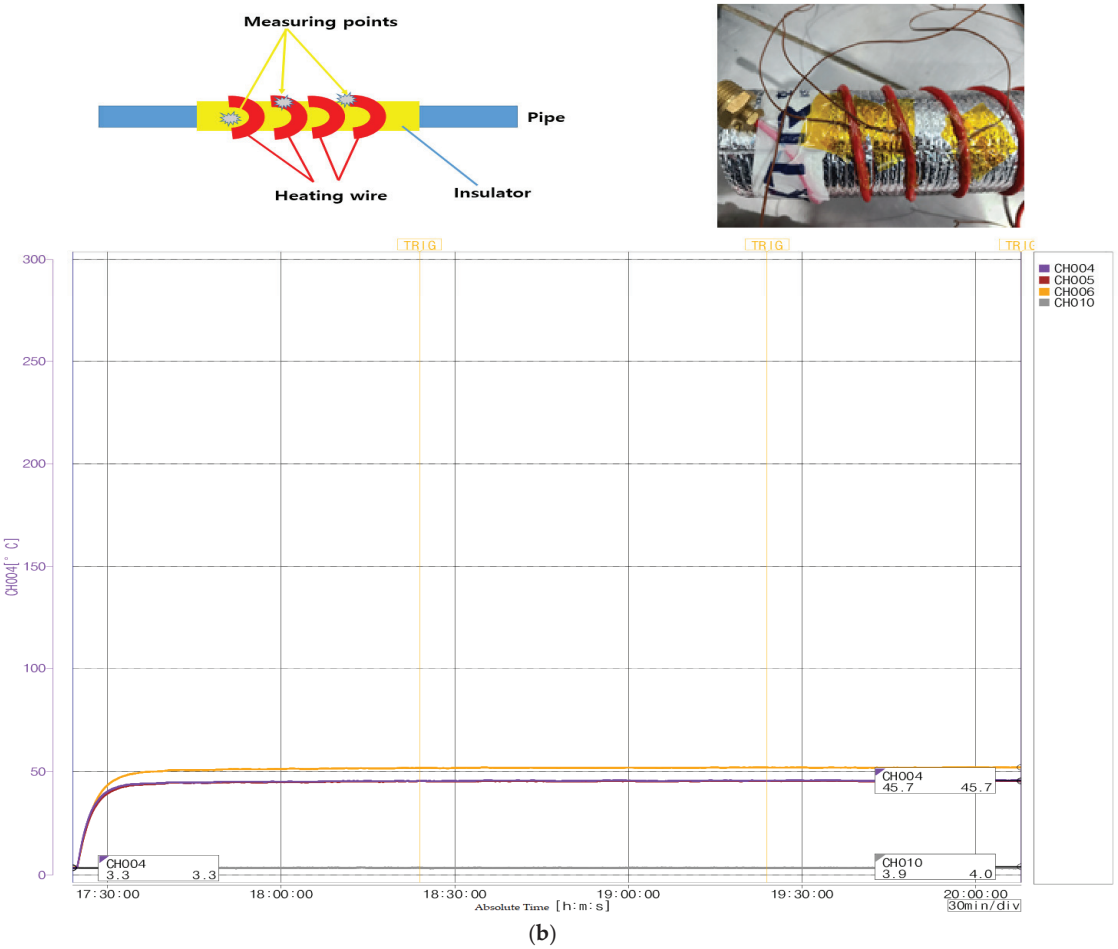

(**b**)

Figure 10. *Cont.*

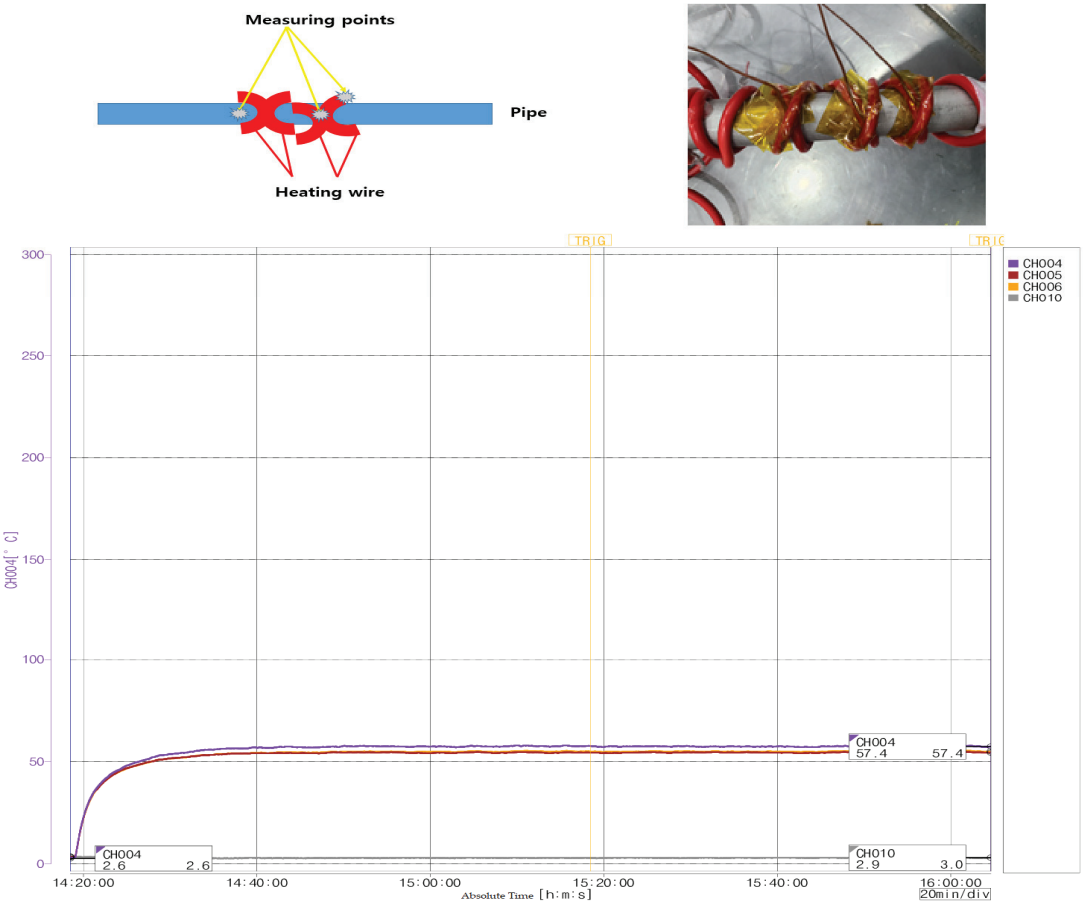

(**c**)

Figure 10. *Cont.*

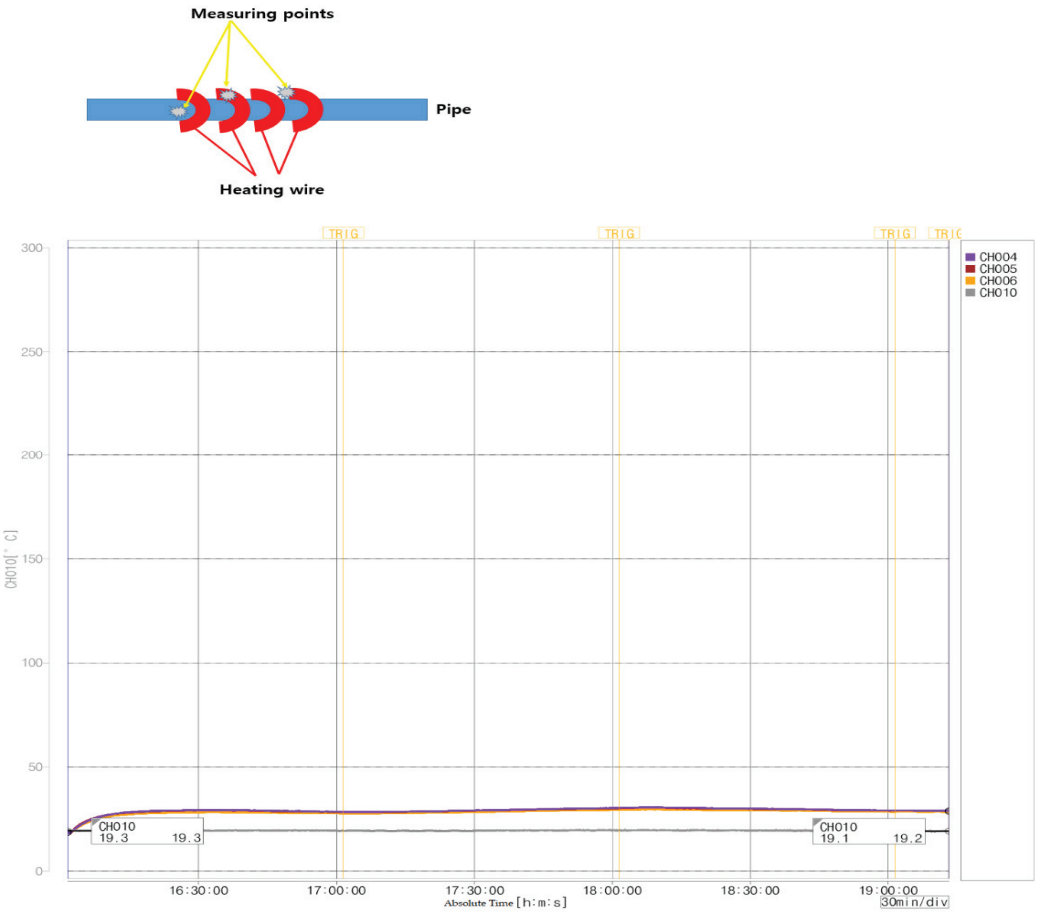

(**d**)

Figure 10. (**a**) Sample reproducibility test Case 1: Heating cables wrapped around water service pipes and thermal insulation or taping on the outside. (**b**) Sample reproduction test Case 2: Insulation around water service pipes and heating cables wrapped around them. (**c**) Sample reproduction test Case 3: Heating cables irregularly wrapped in multiple layers around a water service pipe. (**d**) Sample reproduction test Case 4: Sample reproducibility test: Undetectable temperature (20.0 °C).

Figure 10a shows the test results of Case 1 for the No. 5 product in Table 4. The experiment in Figure 10a showed the No. 5 sample data wherein the anti-freezing heating cables were wrapped around the water service pipe, and then thermal insulation was taped on the outside. Here, three different temperature points were designated to observe the highest temperature rise (Case 1). The result verified that the temperature at CH006 (measurement point between the water service pipe and heating cable) was the highest at 119.0 °C.

Figure 10b shows the test results of Case 2 for No. 5 product in Table 4. In the experiment in Figure 10b, thermal insulation was wrapped around the water service pipe, and anti-freezing heating cable was taped on the outside. Afterward, three different temperature points were designated to observe the highest temperature rise. The results verified that the temperature of CH006 (measurement point between the water service pipe and heating cable) was the highest at 52.3 °C.

Figure 10c shows the test results of Case 3 for No. 5 product in Table 4. In the experiment in Figure 10c, the anti-freezing heating cable was wrapped around the water service pipe without thermal insulation. However, the heating cable's interval was irregular, and the cables were overlapped. Afterward, three different temperature points were designated to observe the highest temperature rise. The results verified that the temperature of CH004 (measurement point between the water service pipe and heating cable) was the highest at 58.1 °C.

Figure 10d shows the test results of Case 4 for No. 5 product in Table 4. In the experiment in Figure 10d, the anti-freezing heating cable was wrapped around the water service pipe without thermal insulation. However, the heating cable's interval was irregular, and cables were overlapped. Afterward, three different temperature points were designated to observe the highest temperature rise. The results verified that the temperature of CH004 (between the heating cables) was the highest at 30.7 °C.

Figure 11a shows the test results of Case 1 for No. 8 product in Table 4. The experiment in Figure 11a exhibited the No. 8 sample data, wherein anti-freezing heating cables were wrapped around the water service pipe and then thermal insulation was taped on the outside. Here, three different temperature points were designated to observe the highest temperature rise (Case 1). The result verified that the temperature at CH006 (measurement point between the water service pipe and heating cable) was the highest at 28.4 °C.

Figure 11b shows the test results of Case 2 for No. 8 product in Table 4. In the experiment in Figure 11b, thermal insulation was wrapped around the water service pipe, and then an anti-freezing heating cable was taped on the outside. Afterward, three different temperature points were designated to observe the highest temperature rise. The results verified that the temperature of CH006 (measurement point between the water service pipe and heating cable) was the highest at 33.0 °C.

Figure 11c shows the test results of Case 3 for No. 8 product in Table 4. In the experiment in Figure 11c, the anti-freezing heating cable was wrapped around the water service pipe without thermal insulation. In the experiment in Figure 11c, thermal insulation was wrapped around the water service pipe, and anti-freezing heating cable was taped on the outside. However, the heating cable's interval was irregular, and the cables were overlapped. Then, three different temperature points were designated to observe the highest temperature rise. The results verified that the temperature of CH005 (measurement point at the heating cable) was the highest at 26.8 °C.

Figure 11d shows the test results of Case 4 for No. 8 product in Table 4. In the experiment in Figure 11d, the anti-freezing heating cable was wrapped around the water service pipe without thermal insulation. However, the heating cable's interval was irregular, and the cables were overlapped. Afterward, three different temperature points were designated to observe the highest temperature rise. The results verified that the temperature of CH005 (at the heating cable) was the highest at 56.7 °C.

Figures 10 and 11 Results of the reproducibility test. As shown in Figure 10a,d with No. 5 products and Figure 11a,d with No. 8 products, tests were conducted under the conditions of Cases 1, 2, 3, and 4, which are summarized as follows:

Overall, for Product Nos. 1 to 7 and 10, the temperature of most products was the highest under the Case 1 condition; for Product Nos. 8 and 9, the temperature was the highest under the Case 4 condition.

These results were attributed to the effect of internal heat storage as the test progressed under the condition of the thermal insulation installed. As shown in Case 1, the temperature was high. Note that, for Product Nos. 8 and 9, the temperature was assumed to be high under the Case 4 condition because of the structural characteristics according to the product operation mechanism.

(For Cases 1 and 2, experiments were conducted with thermal insulation; for Cases 3 and 4, however, experiments were conducted without thermal insulation.)

In addition, for Case 4, tests were conducted at 20.0 °C unlike Cases 1 to 3. For Cases 1 to 3, experiments were conducted at a range of -10 °C to 0 °C according to the K 10013 standard.

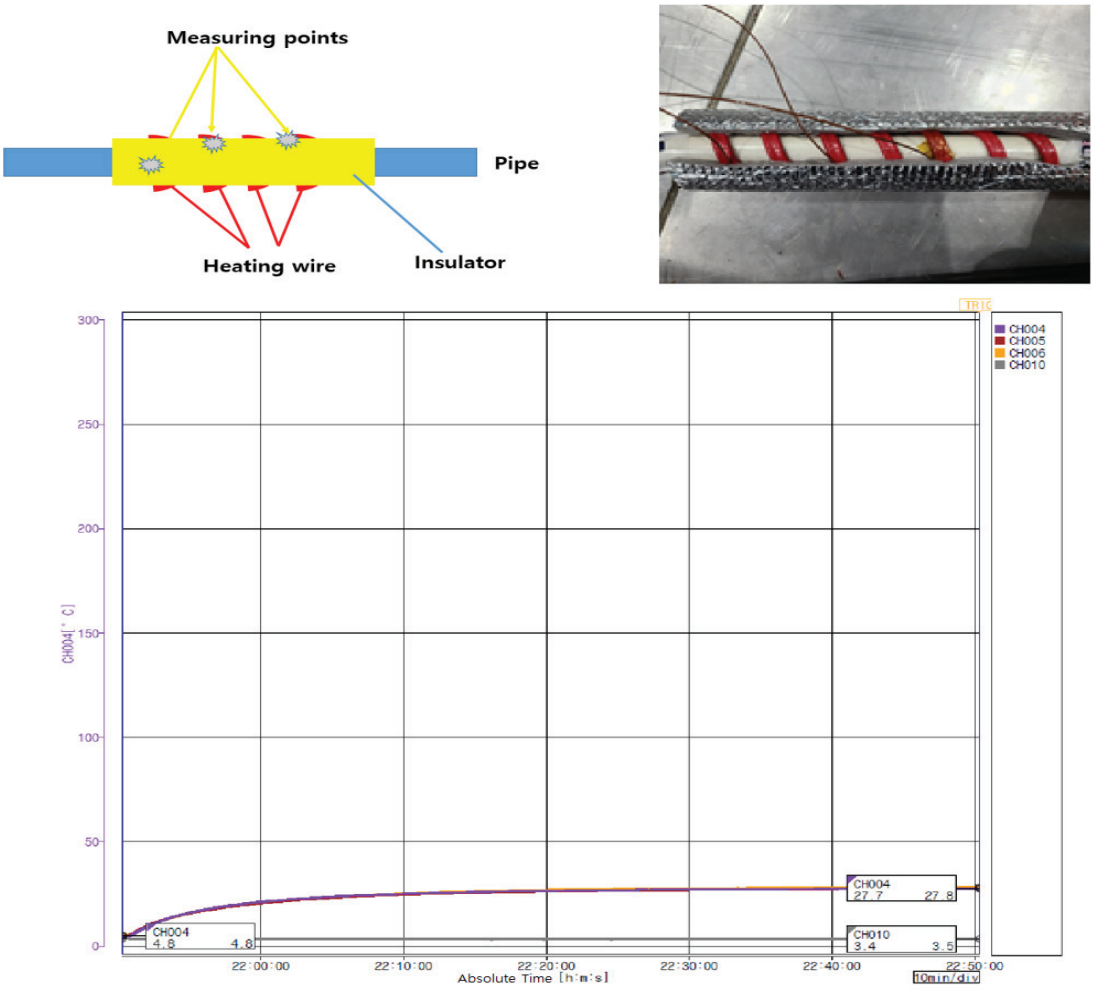

(**a**)

Figure 11. *Cont.*

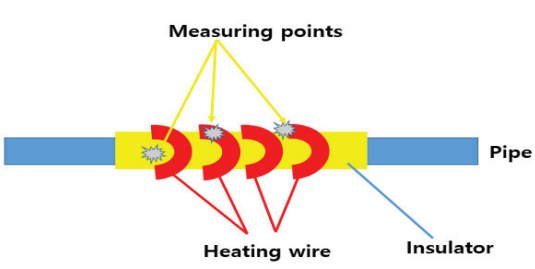

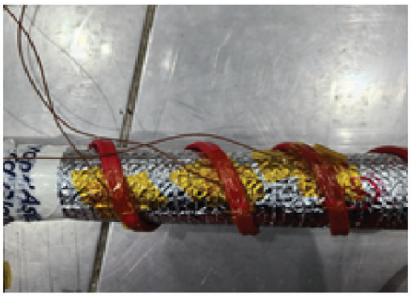

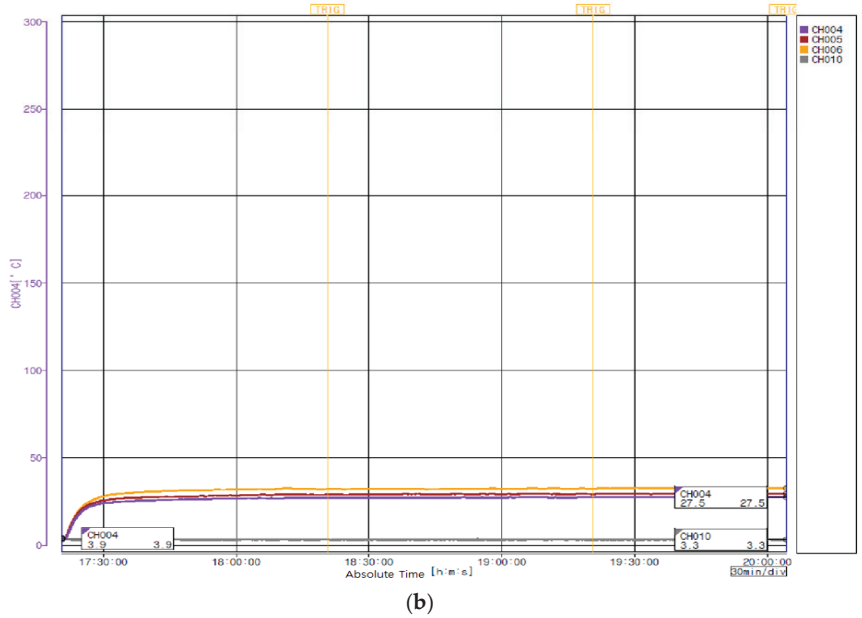

(**b**)

Figure 11. *Cont.*

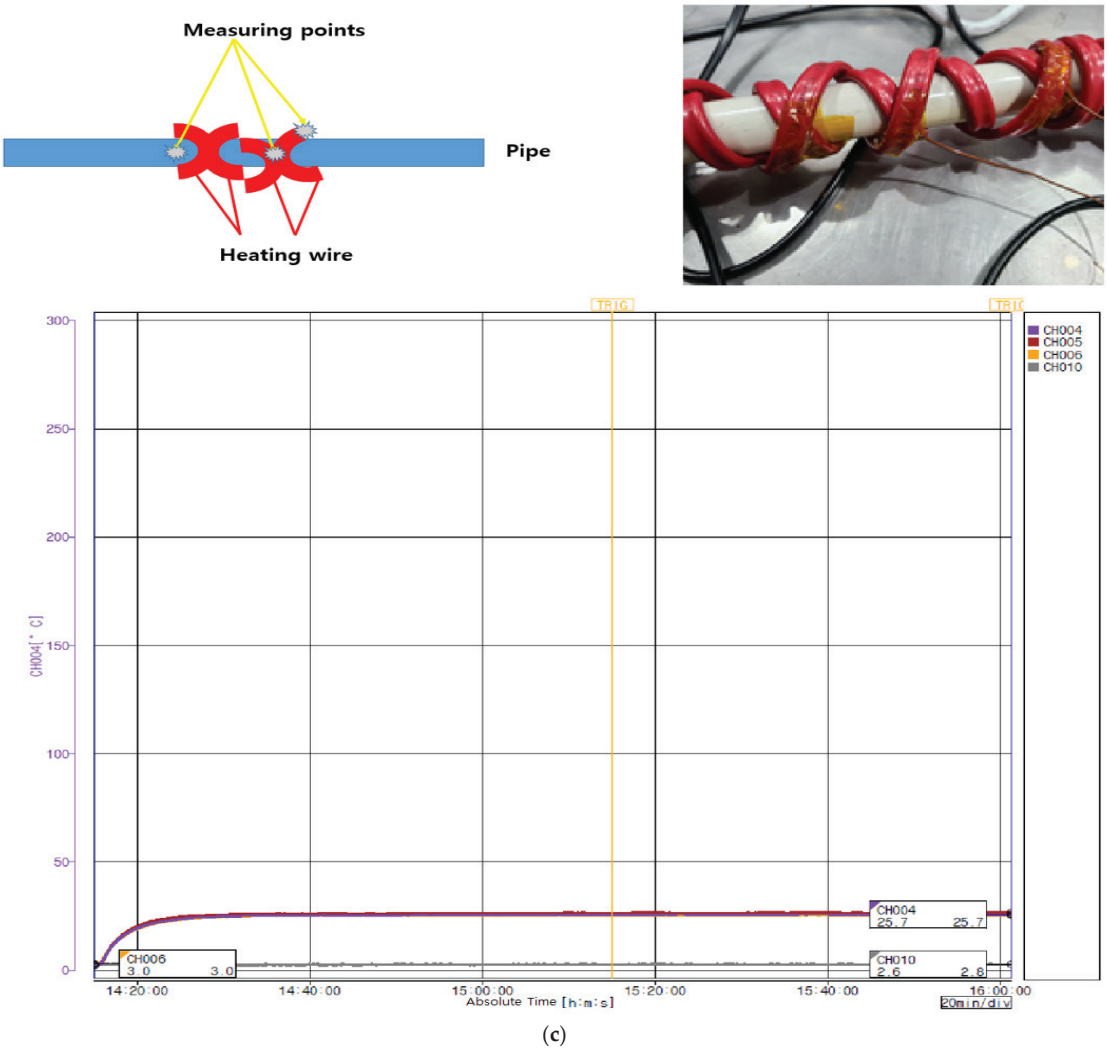

(**c**)

Figure 11. *Cont.*

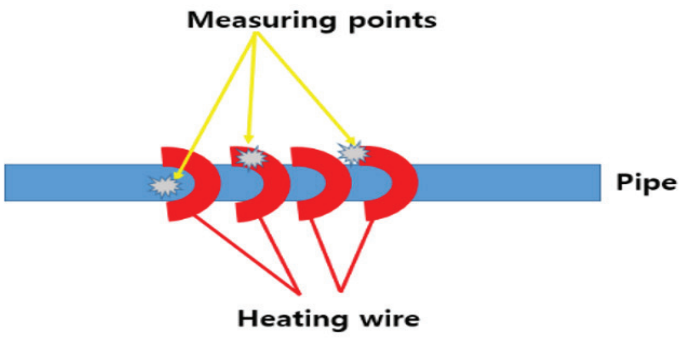

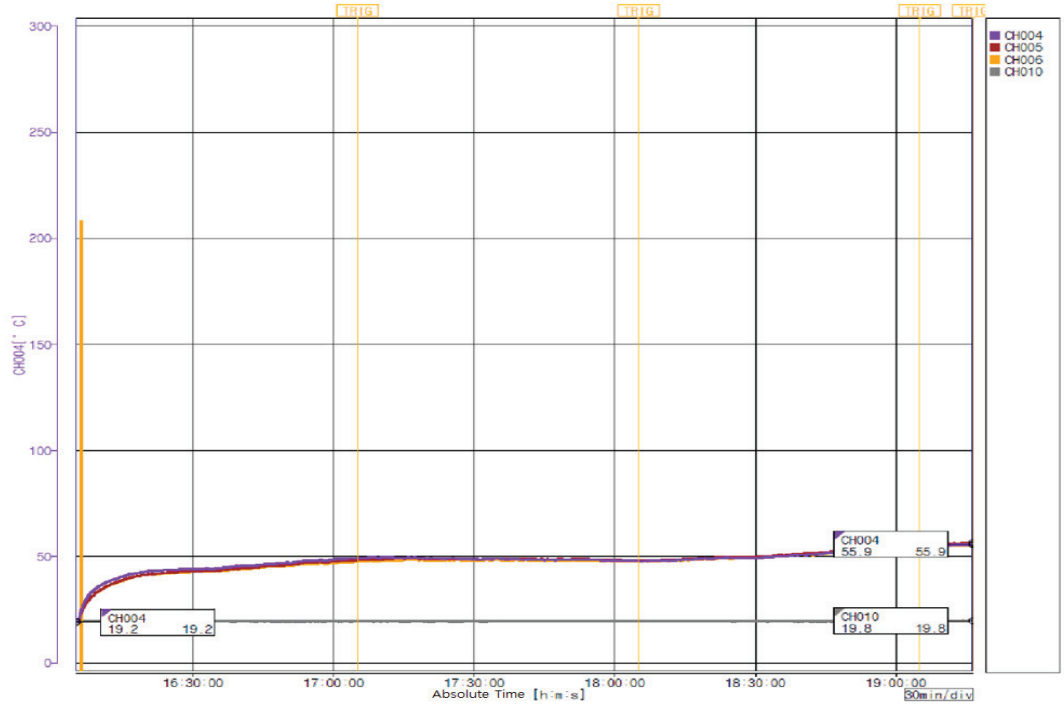

(**d**)

Figure 11. (**a**) Sample reproducibility test: Case 1: Heating cables wrapped around water service pipes and thermal insulation or taping on the outside. (**b**) Sample reproducibility test Case 2: Insulation around water service pipes and heating cables wrapped around them. (**c**) Sample reproduction test: Case 3: Heating cables irregularly wrapped in multiple layers around a water service pipe. (**d**) Sample reproduction test: Undetectable temperature (20 °C).

5. Conclusions

The occurrence of a fire can be inferred from the winding method of the antifreeze heating cables. In order to figure out how the heat differs depending on the winding method of heating cables, we have selected 10 manufacturers, checked the temperature characteristics under the test conditions (Paragraph 11, Paragraph 19.101) of the Technical Regulations for Electrical and Telecommunication Products and Components of Korea

(K 10013), tested the four methods mentioned in this thesis and compared and analyzed the results.

This paper aims to clearly present the cause of fire on heating cables exposed to the general public by using the experimental design framework of Lambda Game while creating a policy and utilization environment that can reduce the risk for users.

To this end, this paper uses products that can be easily purchased on the market and examines the variables such as "the density of heating cables," "the presence or absence of insulating materials," and "the presence or absence of the priority of heating cables and insulating materials" from the perspective of actual users, in order to suggest in which cases the risk of fire is high.

To meet the goal, it would be better to use and test a large number of products, but we thought that doing so would rather hinder the purpose of this paper, as there were limits to the types of products that users actually purchased frequently among the products available in Korea at that time. Therefore, we purchased heating cables that could be easily purchased on the market and conducted experiments."

The experiment results indicate that the temperature of the heater part in antifreeze heating cables was mostly higher than the conditions required by the existing standards in cases 1 to 4. In particular, in the case of the No. 5 manufacturer's sample, the temperature of the heating cable of Case 1 was measured to be the highest at 119.0 °C. In the process of comparative analysis of the results, we have applied the data engineering reproducibility test results in the frame of the random game λ and derived the same results as the predicted hypothesis.

In future work, we will analyze the thermosetting life expectancy prediction experiment and durability according to the chemical material (component ratio) of the water freeze prevention device (hereinafter "heating wire") heating wire coating, and come up with the most reasonable method for fire prevention.

Author Contributions: Conceptualization, B.-Y.J., S.-M.J., H.-G.L., H.-S.K., J.-Y.P., B.-Y.O., J.-W.P., J.-H.H. and J.-H.L.; Data curation, S.-M.J., H.-S.K., J.-Y.P., B.-Y.O., J.-W.P. and J.-H.L.; Formal analysis, B.-Y.J., H.-S.K., J.-Y.P., B.-Y.O., J.-W.P. and J.-H.L.; Funding acquisition, B.-Y.J. and J.-H.L.; Investigation, B.-Y.J., S.-M.J., H.-G.L., J.-H.H. and J.-H.L.; Methodology, B.-Y.J., S.-M.J., H.-G.L., H.-S.K., J.-Y.P., B.-Y.O., J.-W.P. and J.-H.L.; Project administration, J.-H.H. and J.-H.L.; Resources, B.-Y.J., S.-M.J., H.-G.L., H.-S.K., J.-Y.P., B.-Y.O., J.-W.P. and J.-H.L.; Software, S.-M.J., H.-S.K., J.-Y.P., B.-Y.O., J.-W.P. and J.-H.H.; Supervision, J.-H.H. and J.-H.L.; Validation, S.-M.J., H.-G.L. and J.-H.L.; Visualization, B.-Y.J., S.-M.J. and J.-H.H.; Writing—original draft, B.-Y.J., S.-M.J., H.-G.L., H.-S.K., J.-Y.P., B.-Y.O., J.-W.P., J.-H.H. and J.-H.L.; Writing—review and editing, J.-H.H. and J.-H.L. All authors will be informed about each step of manuscript processing including submission, revision, revision reminder, etc. via emails from our system or assigned Assistant Editor. All authors have read and agreed to the published version of the manuscript.

Funding: This research received no external funding.

Institutional Review Board Statement: Not applicable.

Informed Consent Statement: Not applicable.

Data Availability Statement: Not applicable.

Conflicts of Interest: The authors declare no conflict of interest.

Abbreviations

Anti-freezing Heating Cable	Self Regulating Heating Cable
Electrical arc	Short Circuit
KC 60335-1	Household and similar electrical appliances—Safety Part 1: General requirements
K 10013	Individual requirements of heating devices having the safety of household and similar electrical devices and the flexibility of water service anti-freezing devices and similar.
CH004	Measured between the thermal insulation and heating cable (if there is no thermal insulation, measure between the heating cables).
CH005	Measurement of the heating cable.
CH006	Measured between the water service pipe and heating cable.

References

1. National Fire Data System. Available online: https://nfds.go.kr/stat/general.do (accessed on 8 August 2022).
2. Jae-Hun, L.; Jong-Young, P.; Bu-Yeol, O.; Jung-Woo, P. National Fire Research Institute of Korea: Fire Safety Research Division. A Study on Strengthening Standards for Fire Prevention of Anti-freeze Electric Heating Cable. In *2020 Research Report of National Fire Research Institute of Korea*; The Government of the Republic of Korea: Seoul, Republic of Korea, 2020; pp. 1–100. (In Korean)
3. Lim, J.-H.; Bang, S.-B.; Park, K.-M. A Study on the Fire Risk of Anti-Freezing Heating Wire. In Proceedings of the 35th Spring Conference of the Korean Institute of Fire Investigation and the 14th Arson & Fire Poster Contest, Seoul, Republic of Korea, 17 April 2018; pp. 140–146.
4. Seo, K.-W.; Park, H.-S.; Yoon, J.-K. A Study on the Heat Flow Characteristics of Natural Convection in an Enclosed Circular Tube with Anti-freezing Heat Trace. *J. Korean Soc. Mech. Technol.* **2015**, *17*, 1143–1151.
5. Lee, J.H.; Park, J.E. Research for the Igniting Possibility of Preventing Freeze and Burst Heat Rays. In Proceedings of the 22nd Fall Conference of the Korean Institute of Fire Investigation, Seoul, Republic of Korea, 2011; pp. 213–252.
6. Sheikholeslami, M.; Gorji-Bandpy, M.; Soleimani, S. Two phase simulation of nanofluid flow and heat transfer using heatline analysis. *Int. Commun. Heat Mass Transf.* **2013**, *47*, 73–81. [CrossRef]
7. Basak, T.; Aravind, G.; Roy, S.J. Visualization of heat flow due to natural convection within triangular cavities using Bejan's heatline concept. *Int. J. Heat Mass Transf.* **2009**, *52*, 2824–2833. [CrossRef]
8. Basak, T.; Chamkha, A.J. Heatline analysis on natural convection for nanofluids confined within square cavities with various thermal boundary conditions. *Int. J. Heat Mass Transf.* **2012**, *55*, 5526–5543. [CrossRef]
9. Wakeman, R. *Practicing Utopia: An Intellectual History of New Town Movement*; University of Chicago Press: Chicago, IL, USA, 2016; pp. 1–308.
10. Qiao, L.; Deng, Y.; Wang, Y.; Zhu, J. A Comparative Study on Arrhenius Equations and BP Neural Network Models to Predict Hot Deformation Behaviors of a Hypereutectoid Steel. *IEEE Access* **2020**, *8*, 68083–68090. [CrossRef]
11. Moon, B.; Kim, K.; Park, K.; Park, S.; Seok, C.-S. Fatigue life prediction of tire sidewall using modified Arrhenius equation. *Mech. Mater.* **2020**, *147*, 103405. [CrossRef]
12. Yun, S.-R. A Study on the Risk for Self-regulating heating cable. *Fire Prot. Technol.* **2013**, *54*, 10–13. (In Korean)
13. Yu, Y.-C.; Jee, S.-W. Investigation on the Ignition of Self-Regulating Heating Cables due to Overheating. *Fire Sci. Eng.* **2021**, *35*, 100–104. [CrossRef]
14. Erickson, C. Reliable and cost-effective electrical heating of pipelines with self-regulating heating cables. *IEEE Trans. Ind. Appl.* **1988**, *24*, 1089–1095. [CrossRef]
15. Lardear, J. Control of self-regulating heating cable for use in pipeline heating applications. *IEEE Trans. Ind. Appl.* **1991**, *27*, 1156–1161. [CrossRef]
16. Hansen, W. *Extreme Overheating in Self-Regulating Heating Cables, Technical Report*; U.S. Department of Energy Office of Scientific and Technical Information: Washington, DC, USA, 2004; pp. 1–31.
17. Wang, J.; Guo, W.; Cheng, S.; Zhang, Z. Structure and applications of CB/crystal fluoride resin alloy in self-regulated heating cables. *J. Appl. Polym. Sci.* **2003**, *88*, 2664–2669. [CrossRef]
18. Guo, J.B.; Liu, L.; Wang, Q. Application Self-Regulating Heating Cable Curing of Concrete in Winter. *Appl. Mech. Mater.* **2014**, *638–640*, 1531–1535. [CrossRef]
19. Khrenkov, N.; Strupinskiy, M. The influence of environmental conditions on the characteristics of self-regulating cables. *Int. J. Appl. Electromagn. Mech.* **2020**, *63*, S3–S12. [CrossRef]
20. Wang, L.-C.; Sun, Q.; Zhang, C.-C. The Charring Effect and Flame Retardant Properties of Thermoplastic Elastomers Composites Applied for Cable. *Fibers Polym.* **2020**, *21*, 2599–2606. [CrossRef]
21. Zou, Y.; Li, Y.; Bourbigot, S.; Zhang, J.; Guo, Y.; Li, K.; Baolati, J. *Determination of Solid-Phase Reaction Mechanism and Chlorine Migration Behavior of Co-Pyrolyzing PVCCaCO$_3$ Based Polymer Using Temperature-Dependent FTIR and XRD Analysis*; Polymer Degradation and Stability; Elsevier: Amsterdam, The Netherlands, 2021; Volume 193, p. 109741.

22. Wang, Z.; Wang, J. A comprehensive study on the flame propagation of the horizontal laboratory wires and flame-retardant cables at different thermal circumstances. *Proc. Saf. Environ. Prot.* **2020**, *139*, 325–333. [CrossRef]
23. International Standards (IEC). *Household and Similar Electrical Appliances-Safety-Part 1: General Requirements*; International Standards (IEC): Geneva, Switzerland, 2004.
24. Korea Certification (KC). In *Safety of Household and Similar Electrical Appliances Part 2: Particular Requirements for Anti-Freezing Appliances of a Waterworks*; Korea Certification (KC): Seoul, Republic of Korea, 2008.
25. Lee, J.-H.; Park, J.-Y.; Oh, B.-Y.; Park, J.-W. A Study on Strengthening Standards for Fire Prevention of Anti-freeze Electric Heating Cable. *Fire Sci. Eng.* **2021**, *35*, 94–99. (In Korean) [CrossRef]

fire

MDPI

Article

Evaluation of Fire Hazard in Electrical Installations Due to Unfavorable Ambient Thermal Conditions

Seweryn Szultka [1], Stanislaw Czapp [1,*], Adam Tomaszewski [2] and Hayat Ullah [1]

[1] Faculty of Electrical and Control Engineering, Gdansk University of Technology, Narutowicza 11/12, 80-233 Gdansk, Poland
[2] Institute of Fluid-Flow Machinery, Polish Academy of Sciences, Fiszera 14, 80-231 Gdansk, Poland
* Correspondence: stanislaw.czapp@pg.edu.pl

Abstract: Evaluation of fire hazard caused by electrical installations is a difficult and important topic, and it limits the possibility of loss of life or health of people, as well as the occurrence of significant property damage. In particular, this hazard was caused by power cables and especially photovoltaic (PV) installations. The authors proved that power cables directly exposed to strong solar radiation are likely to exceed maximum permissible temperature in unfavorable ambient conditions. Overheated and damaged cable insulation can be a source of electric shock and a strong leakage current causing fire. In the case of typical PV connectors (MC4 connectors), the main problem is poor contact at the connections of the PV cables. A poor connection can even cause the connector to melt, as shown in this study. In the paper, the authors present a computer simulation regarding critical thermal points of electrical installations, in particular, of the PV type. It may be an indication of what should be paid attention to when designing and implementing such installations. This is important for the safety of people and buildings.

Keywords: fire hazard; numerical simulations; overheating; power cables; photovoltaics

Citation: Szultka, S.; Czapp, S.; Tomaszewski, A.; Ullah, H. Evaluation of Fire Hazard in Electrical Installations Due to Unfavorable Ambient Thermal Conditions. *Fire* **2023**, *6*, 41. https://doi.org/10.3390/fire6020041

Academic Editor: Xiaoyu Ju

Received: 27 December 2022
Revised: 13 January 2023
Accepted: 18 January 2023
Published: 20 January 2023

1. Introduction

The current-carrying capacity of power cables is an important operational parameter of both transmission and distribution networks. The current-carrying capacity is a measure of the power transmission of power lines, including low-voltage cable lines directly connected to electricity consumers. This capacity informs about the maximum value of the electric current flowing through the power cables, which will not cause thermal damage to the insulation as a result of exceeding the permissible temperature for a long time. The continuous increase in the demand for electricity and the increasing number of generation sources integrated with the power system, as part of renewable energy sources, result in the growing interest in the possibilities of increasing the load of power cable lines. The current-carrying capacity of power cables depends mainly on: the construction of the power cables and their arrangement and environmental conditions. The influence of each of these factors on the current-carrying capacity of conductors is defined in the IEC [1–4] and IEEE [5] standards. These standards take into account individual factors selectively and do not refer to all phenomena actually occurring in power installations. The indicated standards do not take into account, among others, the influence of: variable wind speed and direction, variable insolation, dry zones around underground power cables, as well as many other factors affecting the current-carrying capacity of conductors. The indicated standards are based on the Neher–McGrath calculation method from 1957 [6]. However, this method is not very precise [7]. Therefore, reliable knowledge of the current-carrying capacity can be obtained through experimental tests and numerical analysis. As reported in [8–10], numerical calculations of thermal states of power cables with the use of dedicated software are becoming more and more important, and the provisions of the above-mentioned standards are only used to confirm the results of simplified numerical modeling.

Knowledge of the actual operating conditions of power cables allows to avoid design errors and, as a result, will increase the reliability and safety of power installations [11,12].

The temperature of the wiring elements has a significant impact on their durability, especially their thermal endurance [13]. The authors of the referred article pointed out that there is a real risk of the wires overheating in the air, especially in the presence of direct sunlight. The authors of the paper [12] indicated the important role of the color of the roofing and the distance of the electrical installation from the roof surface. However, the impact of the indicated factors in the context of photovoltaic (PV) installations was not analyzed. The paper [14] pointed to a significant problem related to the destruction of electrical equipment (including power cables and connectors). The described destructive phenomena did not refer to the contact resistance of materials. In the article [15], it is indicated that, based on operational experience, 70% of power line failures occur in places where they are connected. This is the effect of the contact resistance and its increasing value as a result of the phenomena occurring in the contact structure, as well as the influence of external forces. In addition, a damaged electrical contact point most often causes overheating of the connector, as well as short circuits and fire. In addition, temperature is a reliable and important indicator in assessing the condition of a cable joint. In turn, the article [16] proposed a real-time temperature monitoring system for power cable joint. The proposed solution to the problem of heating the joints is suitable only for special applications. To emphasize the importance of the problem of heating up the cable connection points, GPRS wireless communication technology was also proposed [17].

Problems with the DC joints/connectors are the main cause of failure as well as fire risk in PV systems [18,19]. It is estimated that nearly 70% of all fires in PV installations are the result of improper connections in DC circuits [18]. From a scientific point of view, a potential cause of fire in PV systems due to the DC connector is the increase in its contact resistance. An equally important issue related to the fire protection of PV installations is the occurrence of possible arc faults, very often caused by bad connections. The authors of the paper [20] indicate the types and characteristics of arc faults in PV installations but do not indicate the methods of detecting such hazards. The paper [21] indicates the types of short circuits occurring in PV installations based on practical events in PV farms. The authors of the paper point out the special role of protections integrated with inverters (protection against arc faults). The article [22] provides information on the occurrence and characteristics of earth fault currents on the DC side and the related possible fire hazard of PV installations.

This article presents the influence of unfavourable environmental conditions (insolation, low wind speed) on the temperature distribution of power cables and cable connectors used in typical PV installations. The effect of contact resistance of the connections on their temperature is also investigated. The above-mentioned issues are not deeply analysed in the literature. Results of the authors' investigation show the points of electrical installations which may be a cause of the possible fire hazard as well as electric shock. Indicating these points is a key issue to prevent fires in new installations.

The rest of the paper is organized as follows. Section 2 presents an analysis of the influence of solar radiation on the current-carrying capacity and temperature of AC power cables. In Section 3, an analysis of the heating of DC connectors in theoretical and practical terms is provided. Section 4 summarizes the obtained results.

2. The Impact of Solar Radiation on the Temperature Distribution and Current-Carrying Capacity of AC Power Cables

In order to present the impact of unfavorable ambient conditions on the long-term current-carrying capacity (and thus on the temperature distribution) of power cables, a low-voltage power cable line was tested by computer simulations. The simplified model presented in Figure 1 was implemented in a 3-D numerical model in the ANSYS Fluent software.

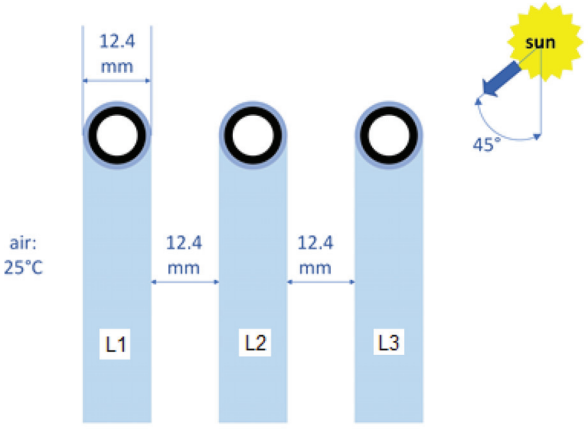

Figure 1. The analyzed power cable line composed of three single-core cables.

Figure 1 shows a power cable line laid vertically in air at a temperature of 25 °C. The given air temperature corresponds to Polish climatic conditions in accordance with the standard [3]. Three power cables (three-phase alternating current line of nominal frequency 50 Hz) with a cross-sectional area of 35 mm^2 with a conductor made of copper and insulation and a sheath made of PVC are arranged with a spacing equal to the diameter of the power cable.

In the numerical model, all heat exchange mechanisms involved in the real system were introduced:

- Joule's heat—generated by the flow of electric current,
- solar radiation heat,
- convection heat,
- dissipated radiation heat.

In order to investigate the effect of the real conditions of cables heating, the heat of solar radiation falling at an angle of 45° on the cable surface (conditions typical for Europe), convective air movement and a radiation model according to the discrete ordinates theory were modeled. An example of a computational mesh in a cross section is shown in Figure 2.

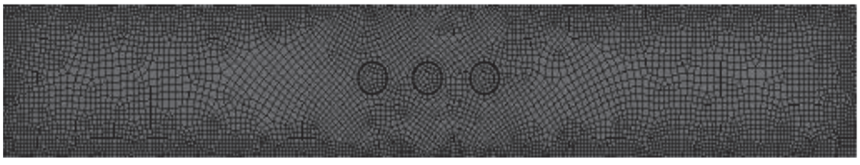

Figure 2. A view showing the numerical grid for power cable temperature estimation.

The total number of mesh elements was approximately 9 million finite volumes. The results of particular calculation variants are presented in the further part of the article. A steady-state simulation was performed and turbulence model k-epsilon was chosen. The proper materials were set in the model in certain cell zones and the boundary conditions were as follows:

- mass flow inlet (bottom side of domain),
- pressure outlet (upper side of domain),
- mesh interfaces between different cell zones,
- heatflux (the inner side of power cables),
- heatflux (external side of power cables, which is exposed to solar radiation).

In the case of heating the cable line in accordance with the presented assumptions and in the absence of electric current flow, the temperature distribution around the cables was obtained as shown in Figure 3.

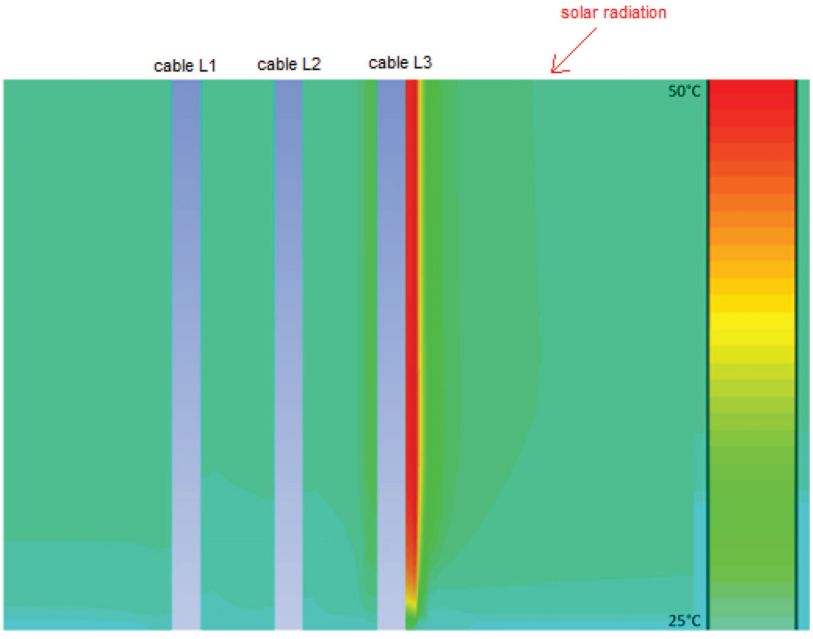

Figure 3. Temperature distribution around unloaded power cables (I_Z = 0 A) taking into account solar radiation (close-up view of the cables).

In the analyzed model, Figure 3 shows the effect of solar radiation alone (without current load) on the temperature of the power cable especially in the L3 phase (cable on the right). Taking into account the solar radiation and the lack of current load on the cables, the cable insulation temperature in the L3 phase reaches 50 °C. Thus, the solar radiation increased the temperature of the power cable insulation by 25 °C (from ambient temperature equal to 25 °C).

Figure 4 shows the temperature distribution around power cables which are symmetrically loaded and unaffected by solar radiation. The current-carrying capacity of the cable system is equal to 152 A. The current value was achieved by iteratively increasing the Joule's heat in the conductor until the permissible temperature (70 °C for PVC insulation) was reached.

Figure 5 shows the temperature distribution around power cables which are symmetrically loaded and under the influence of solar radiation. The current-carrying capacity of each power cable is 96 A. The current value was determined on the basis of computer calculations—in the assumed conditions it obtains the max temperature of the cable insulation equal to 70 °C (max permissible).

Comparing the simulation results presented in Figures 4 and 5, one can notice a significant decrease in the current-carrying capacity of power cables due to the impact of solar radiation. As a result of the influence of the heat of solar radiation, the current-carrying capacity of power cables decreased by nearly 37%. If the need to reduce the load of the power cables is not taken into account (the cables would be loaded with 152 A instead of 96 A), the permissible temperature could be locally exceeded, which results in a reduction in insulation durability [13]. Significant overheating of the cables and damage to the insulation may also cause significant leakage current and, consequently, risk of electric shock or fire.

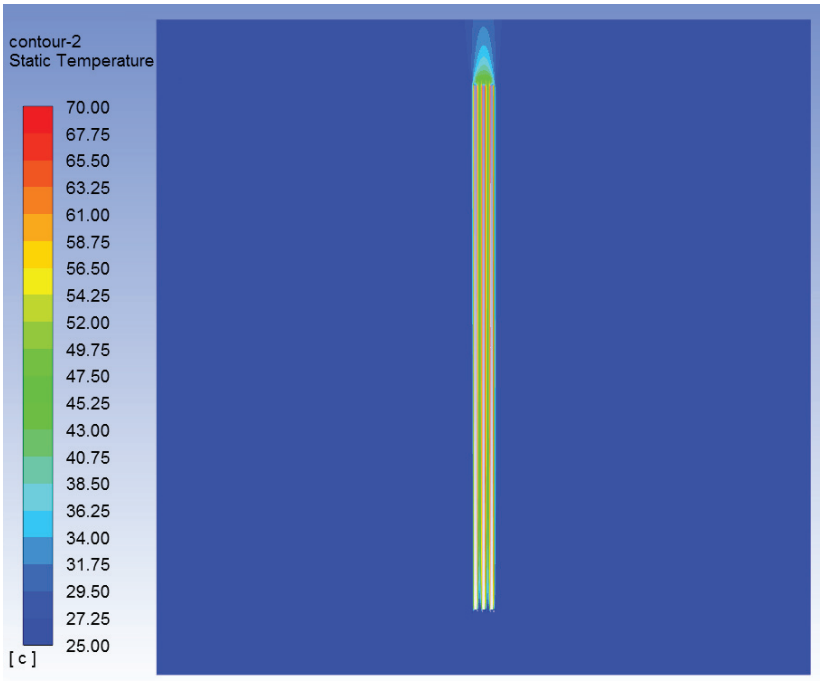

Figure 4. Temperature distribution around power cables (max permissible load: $I_{ZL1} = I_{ZL2} = I_{ZL3} = 152$ A) without solar radiation.

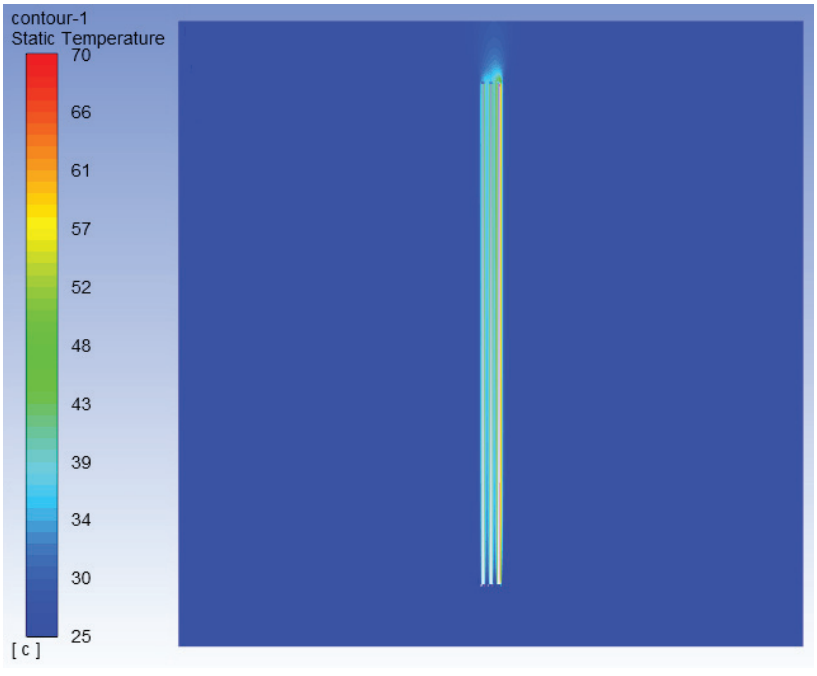

Figure 5. Temperature distribution around power cables (max permissible load: $I_{ZL1} = I_{ZL2} = I_{ZL3} = 96$ A) taking into account solar radiation.

3. The Impact of Solar Radiation and Quality of Connections on Temperature Distribution in DC Connectors

Several simulations were carried out to assess the effect of insolation and contact resistance on the temperature of DC connectors used in PV systems. For this purpose, the DC connector, commonly known as the MC4 connector, was the subject of the analysis. The connector model shown in Figure 6 has been performed in accordance with the manufacturer's catalog card [23]. The numerical approach was very similar to the one presented for the power cables in previous section. The only significant difference is that the "Solar calculator" option was set in the model instead of implementing the additional heatflux zone to simulate solar radiation. Moreover, we only consider DC flow. The computational model includes a constant value of solar radiation intensity (1200 W/m^2), an ambient temperature of 30 °C (assumed by the authors' free air temperature during a hot day in Polish climatic conditions), and low convection air movement (0.4 m/s). The parameters of the model are to reflect unfavorable heat exchange conditions in the summer months on the roof [24]. Other important simulation parameters are: connector material (polyamide), absorptivity material (0.9), and DC wire resistance (6.1 mΩ/m). It was assumed that the contact resistance between the connectors and the connected wires (resulting from the quality of cable assembly) is neglected.

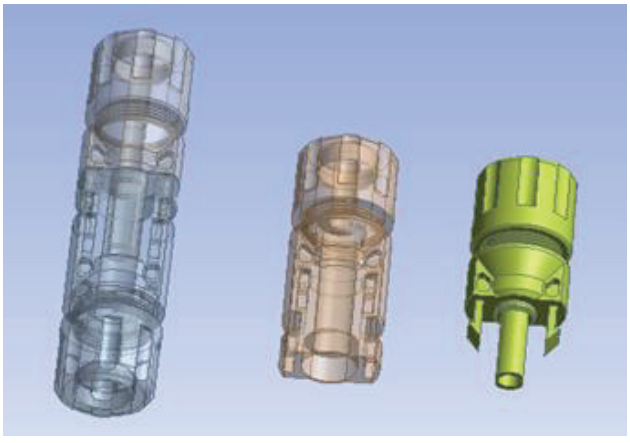

Figure 6. Analyzed MC4 connectors (simulation with ANSYS).

In the first stage of the investigation, the effect of solar radiation on the heating of the MC4 connector, without the flow of electric direct current, was examined. Figure 7 shows the heating effect of the DC connector only under the influence of solar radiation. According to the obtained simulations, the DC connector reaches a maximum temperature of 55 °C.

Then, the conditions of heat exchange with the environment with the participation of solar radiation and nominal operating conditions were examined (Figure 8).

The distribution of temperature presented in Figure 8 shows relatively good conditions for heat dissipation to the environment. Despite the flow of electric current with an assumed typical value for the connector (15 A), the increase in the temperature of the connector is recorded in the range of 6 degrees Celsius compared with no load (Figure 7). It is worth noting that the result of the temperature distribution in Figure 8 was obtained for the contact resistance respected by the manufacturer (max. 0.25 mΩ) and the rated contact force of 50 N.

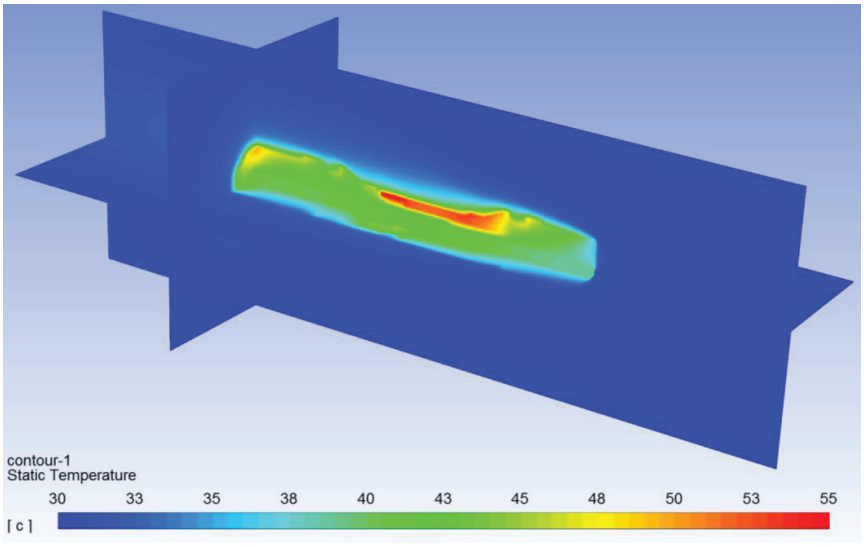

Figure 7. Temperature distribution around DC connector without current flow (I = 0 A) and with solar radiation. Max temperature: 55 °C.

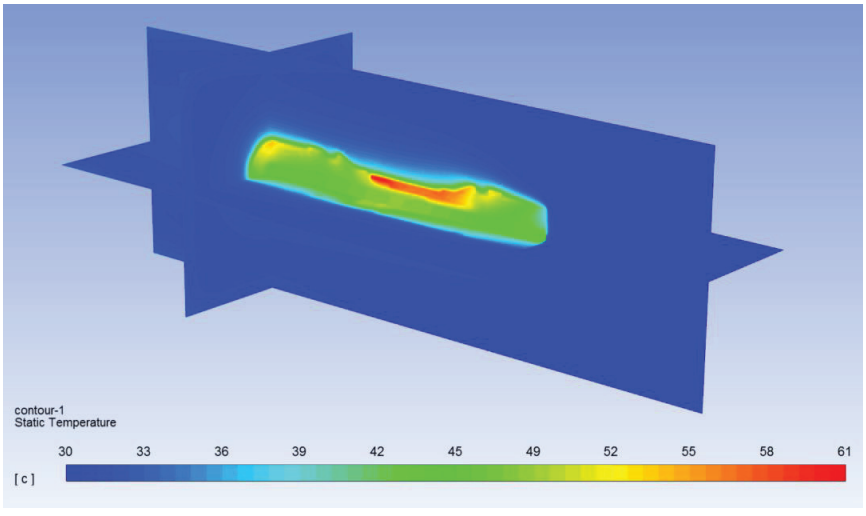

Figure 8. Temperature distribution around DC connector with current flow (I = 15 A) and solar radiation. Max temperature: 61 °C.

As mentioned in the first part of the article, a significant fire hazard from a DC connector can be caused by an increase in its contact resistance above the values allowed by the manufacturer. To investigate this effect, possible contact resistance values were determined depending on the contact force, based on the following equation:

$$R_{\mathrm{p}} = \frac{c \cdot \rho}{(0,1F_{\mathrm{k}})^{m}} \quad (1)$$

where:

R_{p}—contact resistance, mΩ,

C— constant dependent on the contact area, -,

ρ—contact material resistivity, Ωm,
F_k—contact force, N,
m—constant depending on the type of contact, -.

According to the information contained in [25], for the contact material of which the DC connector is made (tin-plated copper), the value of the $c \cdot \rho$ coefficient (the product of constant dependent on the contact area and contact material resistivity) is equal to 1. The value of the constant m is equal to 1 (the contact of the planes). The list of calculated contact resistance values R_p depending on the contact force F_k is provided in Table 1.

Table 1. Calculated contact resistance values R_p depending on the contact force F_k.

No./Case	F_k, N	R_p, mΩ	I, A
1	50	0.2	15
2	40	0.25	14.98
3	30	0.33	14.97
4	20	0.5	14.94
5	10	1	14.85
6	1	10	13.22
7	0.5	20	11.4
8	0.3	33.33	9

The results contained in Table 1 show the value of the calculated contact resistance depending on the decreasing value of the contact force (values lower than the nominal contact force).

In the analyzed DC circuit, the current value decreases with increasing resistance—this phenomenon is taken into account for values included in Table 1. Importantly, the results presented in the first and second cases of Table 1 are consistent with the manufacturer's data. The reduced contact forces shown in Table 1 are the forces that actually occur in PV installations due to poor wiring. The presented Equation (1) assumes the averaged values of the contact coating resistance. It should be emphasized that in the case of favorable corrosion conditions of the connectors (especially moisture ingress), the coating resistance value is significantly increased.

Figures 9–11 show the temperature distribution around the DC connector, for various values of the contact resistance and the flowing electric current (cases 6, 7, and 8 from Table 1).

As the contact resistance increases, the maximum DC connector temperature also increases. It is worth emphasizing that, according to the manufacturer's card, the upper temperature limit of the connector is equal to 105 °C. Therefore, in the cases shown in Figures 9–11, this temperature has been exceeded, which results in a reduction in the durability of the connector, its possible change in structure, and possible loss of insulating properties. A summary of the calculation results of the connector heating, depending on the contact resistance, is shown in Figure 12.

The graph presented in Figure 12 refers to the data provided in Table 1. The temperature of the DC connector increases with the increase in contact resistance R_p. A significant increase in temperature is observed, in particular, for the initial increases in contact resistance (up to 1 Ω). The presented effects of excessive heating of the DC connector constitute a real fire hazard due to the possible generation of minimal ignition energy for the dust–air mixture or other diffusing mixtures present in the vicinity of the PV installation [26]. In a typical PV system, there are many DC connection points made by a set of connectors (plug-socket). If one of these connections is poorly made, it will deteriorate during operation as a result of increased contact resistance: this place heats up when current flows and a "hot spot" occurs. Due to the appearance of heat, the contact material may diffuse or even melt until, at some point, the connection will be completely broken. In this case, an arc can form over a very small air gap, resulting in a fire hazard [27]. The described occurrence of hot

spots of connectors is not only a theoretical problem—it occurred in practice, as shown in Figure 13.

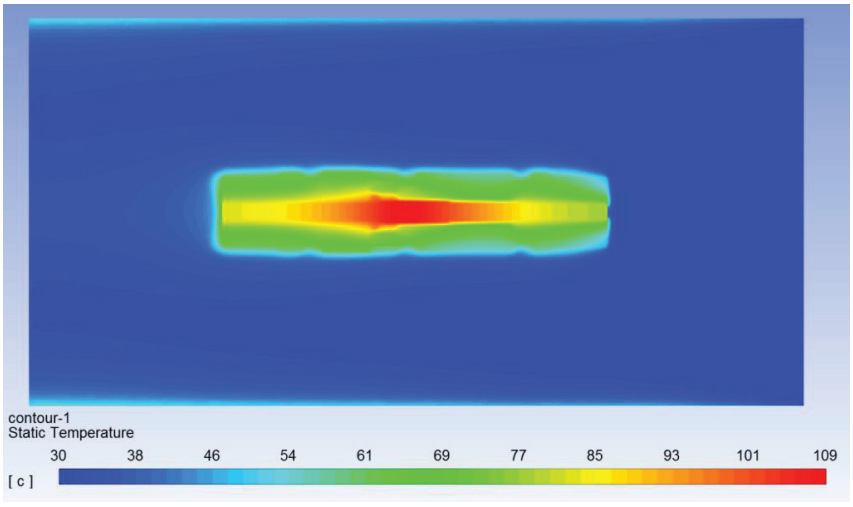

Figure 9. Temperature distribution around DC connector with current flow (I = 13.22 A)—case 6 in Table 1. Max temperature: 109 °C.

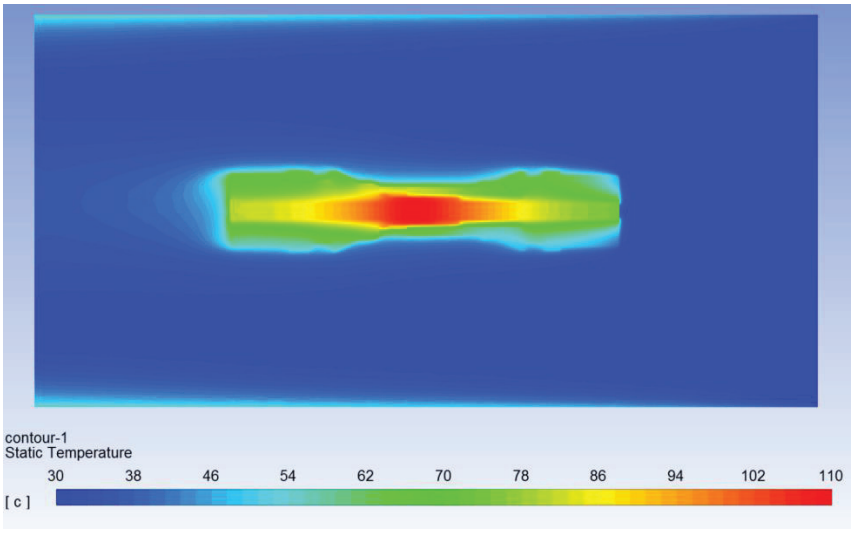

Figure 10. Temperature distribution around DC connector with current flow (I = 11.4 A)—case 7 in Table 1. Max temperature: 110 °C.

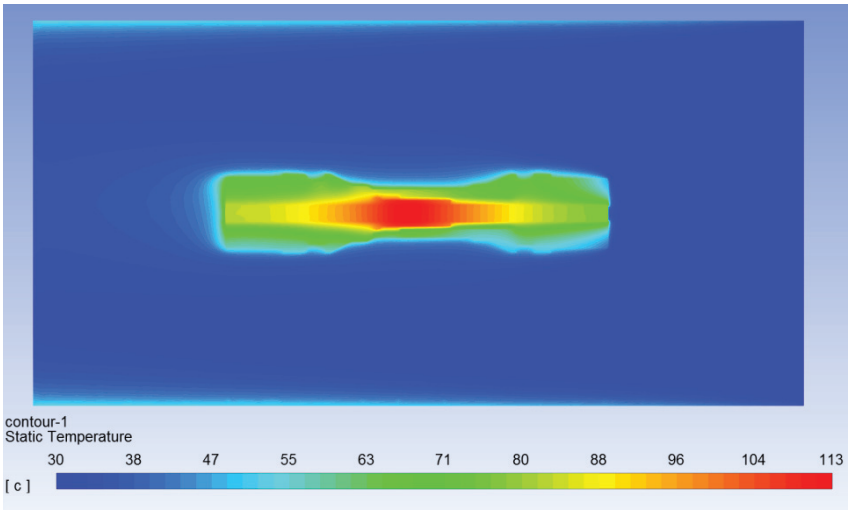

Figure 11. Temperature distribution around DC connector with current flow (I = 9 A)—case 8 in Table 1. Max temperature: 113 °C.

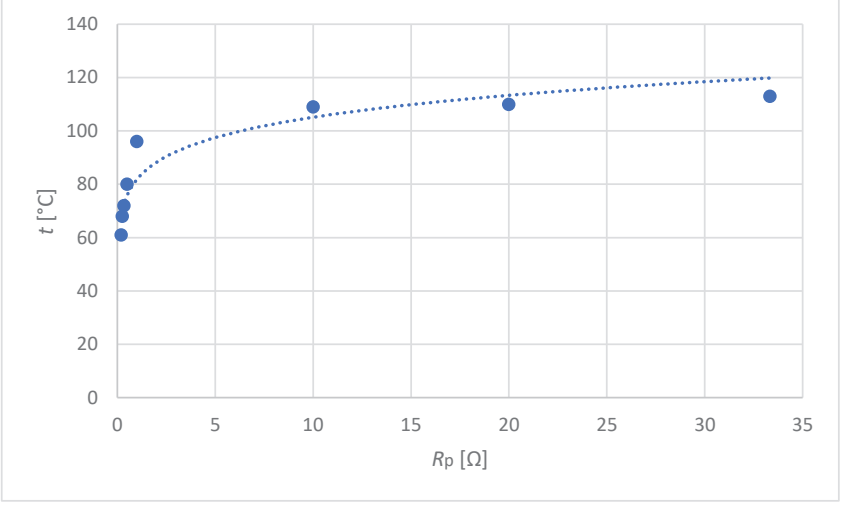

Figure 12. The dependence of the temperature of the DC connector on the value of its contact resistance.

The DC connector on the left in the photo (Figure 13) is new and unused. The connector on the right in the photo comes from a real PV installation, where the contact resistance increased above the nominal value as a result of the power cables being stretched during power generation. Finally, part of the insulation of the connector melted, which can be seen in Figure 13. This effect can also cause a fire hazard.

Figure 13. Comparison of the shape of MC4 connectors—the connector on the left is fully functional and the connector on the right is damaged due to overheating.

4. Conclusions

Currently, PV installations are very common, both as big power plants and micro-installations. Micro-installations coupled with residential buildings are a potential fire hazard, especially due to the careless mounting of these installations. As it results from the simulation tests contained in this article, both strong insolation of the wires and their poor connections may cause a significant increase in the temperature of the elements of the electrical installation. The temperature of PV DC connectors can reach 113 °C—it exceeds the value allowed by the manufacturer, which is indicated at 105 °C. A significant increase in the temperature of the PV connector occurs in the range of small contact resistance values (initial increases, up to 1 Ω)—see Figure 12.

A significant increase in temperature may lead to damage to the insulation of wires/connectors, and thus increase the risk of fire and the risk of electric shock for those in contact with these elements. Cable insulation exposed to solar radiation can heat up to 50 °C (without current load), and designers usually assume it is only 25 °C. A current load can therefore lead to the overheating of this insulation.

The results of simulation tests indicate critical points of installations, in particular PV ones, and may be a recommendation of what should be paid attention to when de-

signing and implementing such installations. This is important for the safety of people and buildings.

Author Contributions: Conceptualization, S.C. and S.S.; methodology, A.T. and S.S.; validation, S.C., A.T. and S.S.; formal analysis, S.C. and S.S.; investigation, A.T. and S.S.; resources, S.C. and S.S.; data curation, S.C., A.T. and S.S.; writing—original draft preparation, A.T. and S.S.; writing—review and editing, H.U., S.C., and A.T.; visualization, A.T. and S.S.; supervision, S.C.; project administration, S.C. and S.S. All authors have read and agreed to the published version of the manuscript.

Funding: This research received no external funding.

Institutional Review Board Statement: Not applicable.

Informed Consent Statement: Not applicable.

Data Availability Statement: Data is contained within the article.

Conflicts of Interest: The authors declare no conflict of interest.

References

1. *IEC 60287-1-1:2001*; Electric Cables–Calculation of the Current Rating–Part 1-1: Current Rating Equations (100% load factor) and Calculation of Losses–General. International Electrotechnical Commission: Geneva, Switzerland, 2001.
2. *IEC 60287-2-1:2001*; Electric Cables–Calculation of the Current Rating–Part 2-1: Thermal Resistance–Calculation of the Thermal Resistance. International Electrotechnical Commission: Geneva, Switzerland, 2001.
3. *IEC 60287-3-1:1999*; Electric Cables–Calculation of the Current Rating–Part 3-1: Sections on Operating Conditions–Reference Operating Conditions and Selection of Cable Type. International Electrotechnical Commission: Geneva, Switzerland, 1999.
4. *IEC 60364-5-52:2009*; Low-Voltage Electrical Installations–Part 5-52: Selection and Erection of Electrical Equipment–Wiring Systems. International Electrotechnical Commission: Geneva, Switzerland, 2009.
5. IEEE 835: POWER CABLE AMPACITY TABLES, 1994. Publisher: Institute of Electrical & Electronics Engineers.
6. Neher, J.H.; McGrath, M.H. The calculation of the temperature rise and load capability of cable systems. *AIEE Trans.* **1957**, *76*, 752–772. [CrossRef]
7. Boron, S. Current-carrying capacity of mining flexible cables at intermittent and short-time duty. *Syst. Support. Prod. Eng.* **2017**, *6*, 21–30.
8. Holyk, C.; Anders, G.J. Power cable rating calculations—A historical perspective. *IEEE Ind. Appl. Mag.* **2015**, *21*, 6–64. [CrossRef]
9. Plesca, A.; Scintee, A. Thermal Aspects Related to Power Assemblies. *Adv. Electr. Comput. Eng.* **2010**, *10*, 23–27. [CrossRef]
10. Czapp, S.; Czapp, M.; Szultka, S.; Tomaszewski, A. Ampacity of power cables exposed to solar radiation–recommendations of standards vs. CFD simulations. *E3S Web Conf.* **2018**, *70*, 111–112. [CrossRef]
11. Spyra, F. External factors influence on current-carrying capacity in an electric power cable line. *Energetyka* **2007**, *6–7*, 451–454.
12. Brender, D.; Lindsey, T. Effect of rooftop exposure in direct sunlight on conduit ambient temperatures. In Proceedings of the IEEE Industry Applications Conference Forty-First IAS Annual Meeting, Tampa, FL, USA, 8–12 October 2006; pp. 705–711. [CrossRef]
13. Czapp, S.; Szultka, S.; Ratkowski, F.; Tomaszewski, A. Risk of power cables insulation failure due to the thermal effect of solar radiation. *Eksploat. Niezawodn. Maint. Reliab.* **2020**, *22*, 232–240. [CrossRef]
14. Paul, S.; Costea, A. Independent thermal protection for electrical circuit breaker panels, electrical power cables and lines. A practical solution proposal. In Proceedings of the 9th International Conference on Electronics, Computers and Artificial Intelligence (ECAI), Targoviste, Romania, 29 June–1 July 2017; pp. 1–5. [CrossRef]
15. Luo, H.; Cheng, P.; Liu, H.; Kang, K.; Yang, F.; Yang, Q. Investigation of contact resistance influence on power cable joint temperature based on 3-D coupling model. In Proceedings of the IEEE 11th Conference on Industrial Electronics and Applications (ICIEA), Hefei, China, 5–7 June 2016; pp. 2265–2268. [CrossRef]
16. Wenzhi, C.; Xiaohui, H.; Zhendong, G.; Chengrong, L. The design of temperature monitoring system for power cable joint. In Proceedings of the IEEE International Conference on Condition Monitoring and Diagnosis, Bali, Indonesia, 23–27 September 2012; pp. 671–676. [CrossRef]
17. Wang, W.; Wang, L.A. temperature remote monitoring system of cable joint. In Proceedings of the 2nd International Conference on Signal Processing Systems, Dalian, China, 5–7 July 2010; pp. 690–694. [CrossRef]
18. Czaja, P. Bezpieczeństwo pożarowe instalacji fotowoltaicznych. *Przeglad Elektrot.* **2021**, *97*, 105–108. [CrossRef]
19. SOLWIS Home Page. Available online: https://uzgodnienia-ppoz.online/nie-ma-kompatybilnych-zlaczek-solarnych (accessed on 5 December 2022).
20. Strobl, C.; Meckler, P. Arc Faults in Photovoltaic Systems. In Proceedings of the 2010 Proceedings of the 56th IEEE Holm Conference on Electrical Contacts, Charleston, SC, USA, 4–7 October 2010; pp. 1–7. [CrossRef]
21. Khorshed Alam, M.; Khan, F.; Johnson, J.; Flicker, J. A Comprehensive Review of Catastrophic Faults in PV Arrays: Types, Detection, and Mitigation Techniques. *IEEE J. Photovolt.* **2015**, *5*, 982–997. [CrossRef]

22. Falvo, M.C.; Capparella, S. Safety issues in PV systems: Design choices for a secure fault detection and for preventing fire risk. *Case Stud. Fire Saf.* **2015**, *3*, 1–16. [CrossRef]
23. Stäubli Web Site. Available online: https://www.staubli.com/content/dam/spot/SOL-Main-11014092-en.pdf (accessed on 15 December 2022).
24. Nominal Operating Cell Temperature. Available online: https://www.pveducation.org/pvcdrom/modules-and-arrays/nominal-operating-cell-temperature (accessed on 17 December 2022).
25. Książkiewicz, A. Electrode Processes in Low Voltage Alternating Current Relays. Ph.D. Thesis, Poznan University of Technology, Poznan, Poland, 2016.
26. Jaskółowski, W. Threats connected with combustion of cable insulation. *Elektroinfo* **2015**, *5*. Available online: https://www.elektro.info.pl/artykul/ochrona-ppoz/59537,zagrozenia-powstajace-przy-spalaniu-izolacji-kabli-lub-przewodow-elektrycznych (accessed on 18 December 2022).
27. Fronius Home Page. Available online: https://www.forum-fronius.pl/ograniczenie-ryzyka-wystapienia-pozaru-w-instalacjach-pv/ (accessed on 20 December 2022).

fire

MDPI

Article

A New Perspective on Hydrogen Chloride Scavenging at High Temperatures for Reducing the Smoke Acidity of PVC Cables in Fires, IV: The Impact of Acid Scavengers at High Temperatures on Flame Retardance and Smoke Emission

Iacopo Bassi [1], Francesca Delchiaro [1], Claudia Bandinelli [1], Laura Mazzocchetti [2], Elisabetta Salatelli [2] and Gianluca Sarti [1,*]

[1] Reagens S.p.A., Via Codronchi, 4, 40016 San Giorgio di Piano, Italy; iacopo.bassi@reagens-group.com (I.B.); francesca.delchiaro@reagens-group.com (F.D.); claudia.bandinelli@reagens-group.com (C.B.)
[2] Department of Industrial Chemistry "Toso Montanari", University of Bologna, Viale Risorgimento 4, 40136 Bologna, Italy; laura.mazzocchetti@unibo.it (L.M.); elisabetta.salatelli@unibo.it (E.S.)
* Correspondence: gianluca.sarti@fastwebnet.it

Abstract: In PVC compounds, hydrogen chloride plays a fundamental role in ·H and ·OH radical trapping, lowering the flame energy during combustion. Furthermore, it yields actual Lewis acids promoting the cross-linking of the polyene sequences from PVC degradation and bringing a char layer, protecting PVC items from flames. Therefore, PVC is inherently flame-retarded. However, plasticized PVC requires flame retardants and smoke suppressants to enhance fire performance. Low-smoke acidity PVC compounds have been developed to reduce the HCl emission during combustion and, therefore, the acidity of the smoke. They contain potent acid scavengers capable of acting at high temperatures. They react with hydrogen chloride in the condensed phase, making it unavailable in the gas and even in the condensed phase, compromising the reaction to fire and enhancing the smoke produced during the combustion. The effect of the sequestration of hydrogen chloride in PVC compounds for cables by potent acid scavengers is studied in this paper through measurements of oxygen index, heat release, and smoke production. It is noteworthy that the potent acid scavengers strongly affect parameters such as the oxygen index, the fire growth rate in cone calorimetry, the specific (total) heat capacity, and the specific heat of combustion of fuel gases in micro combustion calorimetry. In some formulations, acid scavengers reduce the oxygen index below the values of the formulations without flame retardants and double their fire growth rate. In fact, they neutralize the action of antimony trioxide and Lewis acid precursors commonly used as flame retardants and smoke suppressants in PVC items, making them prone to ignite, release smoke, and spread flame. A new generation of flame retardants and smoke suppressants is needed to keep together the low-smoke acidity and the fire performance in PVC items.

Keywords: acid scavengers; PVC; cables; smoke acidity

Citation: Bassi, I.; Delchiaro, F.; Bandinelli, C.; Mazzocchetti, L.; Salatelli, E.; Sarti, G. A New Perspective on Hydrogen Chloride Scavenging at High Temperatures for Reducing the Smoke Acidity of PVC Cables in Fires, IV: The Impact of Acid Scavengers at High Temperatures on Flame Retardance and Smoke Emission. *Fire* **2023**, *6*, 259. https://doi.org/10.3390/fire6070259

Academic Editors: Ying Zhang, Xiaoyu Ju, Xianjia Huang and Fuchao Tian

Received: 6 June 2023
Revised: 24 June 2023
Accepted: 27 June 2023
Published: 30 June 2023

1. Introduction

1.1. Thermal Degradation, Thermal Decomposition, Pyrolysis, and Combustion: The Basic Concepts

The thermal degradation of unstabilized PVC starts at 100 °C [1] through zip elimination bringing polyene sequences and emitting hydrogen chloride (HCl). Most scientists consider the mechanism of PVC degradation ionic, and the resin defects and radicals play a fundamental role in lowering its thermal stability [2–6]. PVC cannot be processed in articles without additives preventing its thermal degradation. Moreover, additives must also give the final items the characteristics they need for the specific application, such as, among others, good weathering performances, aging resistance, and flame retardance.

Additive-containing PVC formulations are called PVC compounds. Due to PVC's low thermal stability, the main additives are thermal stabilizers. They delay the degradation processes induced by temperature and shear and shift them to higher temperatures, allowing the processing of PVC compounds at 150–220 °C. Primary stabilizers substitute the weakest moiety of the chain, the allylic chloride, forming a stronger bond with carbon than chlorine itself. They also contain co-stabilizers, helping the primary stabilizers in the chlorine displacement, blocking the action of byproducts or radicals speeding the zip elimination, and/or shortening the polyene sequences from the zip elimination of HCl. Co-stabilizers can have a preventive action, inhibiting the behavior of those substances, which increases the speed of the HCl elimination or curative activity when a repairing action of polyene sequences is involved.

Fires and their consequences differ depending on their heat flow, temperatures reached, ventilation, and mass of burning materials. After the ignition, i.e., the initial stage where temperatures are around 300–400 °C, if not inhibited, fire enters a stage where temperatures easily reach 600 °C and further its fully developed stage, easily overcoming 600 °C [7].

The heat released in fires brings physical and chemical changes to PVC items, causing thermal decomposition and combustion. PVC, stabilizers, co-stabilizers, plasticizers, lubricants, impact modifiers, processing aids, pigments, fillers, flame retardant fillers, flame retardants, and light stabilizers start all to decompose in the condensed phase or evaporate, releasing gaseous byproducts directly in the gas phase, where combustible fuels burn. Without the protection of stabilizers, PVC resin rapidly changes its chemical nature, forming polyene sequences, developing smoke, creating a char from cross-linked polyene sequences, and releasing massive amounts of HCl. Thermal decomposition and the involved species play a fundamental role in the combustion of PVC items, and knowing the underlying chemistry of such processes is crucial to address the reduction of heat, smoke, and gases such as HCl.

Several authors carried out different techniques to study PVC decomposition. Flash pyrolysis coupled with gas chromatography (GC), direct pyrolysis in the mass spectrometer (MS), and thermal gravimetric analysis (TGA) in different atmospheres and with different detection methods of the gases brought different interpretations of the reactions involved in the thermal decomposition of PVC [8–12]. TGA measures the weight loss, and if coupled with Fourier transform infrared (FTIR), MS, or GC-MS, the gases released during the decomposition can even be identified and quantified. Most scientists agree that PVC has two main stages during its decomposition. The first one refers to the zip elimination of HCl, the formation of the polyene sequences, their cross-linking, and the competitive reaction yielding benzene. The second relates to the decomposition of the cross-linked matrix to char residue and combustible fuels. Several additives commonly used in PVC compounds for processing or conferring specific properties further complicate the decomposition pattern and the involved reactions.

1.2. The First Stage of the Thermal Decomposition/Combustion

Performing a TGA of PVC in N_2, depending on heating regimes, highlights that the decomposition's first stage occurs between 220 °C and 350 °C. Here, HCl is released from the polymer's backbone, and polyene sequences are formed. Intramolecular reactions can bring the benzene formation [8,9,13], while intermolecular reactions lead to the cross-linking of the matrix [9,10,12,14]. At the end of the first stage, between 330 °C and 350 °C, when HCl is almost totally released, only the condensation products of the polyene sequences remain, and a plateau between 350 °C and 450 °C follows, with no volatile release.

However, PVC compounds contain additives such as stabilizers, plasticizers, flame retardants, and flame retardant fillers, and the types and their quantity can affect TGA shapes.

TGA and TGA-GC-MS or TGA-FTIR can highlight much about the decomposition of PVC compounds. Nevertheless, temperatures and physical and chemical properties are not the only parameters influencing fire behavior. Combustion is a complex phenomenon influenced by item shape and surrounding conditions such as oxygen concentration and

kind of ignition [15]. In any case, the combustion process implies two distinct categories of chemical reactions. The first happens in the condensed phase, where the oxygen concentration is low, and the thermal decomposition passes through a pyrolysis process, releasing volatile fuels. The second is the oxidation of the volatiles in the gas phase, producing the energy supporting the pyrolysis process.

In the first stage of thermal decomposition, PVC and the organic and inorganic additives in PVC items decompose thermally in a pyrolysis process where oxygen is starving. Depending on the ingredients in PVC compounds, different gases can be released at different rates. Some gases reaching the air burn, releasing energy and smoke. Others do not burn and dilute the fuels or cool the flame down. Organic substances and their byproducts can evaporate and burn in the flame: plasticizers [16], primary stabilizers and organic co-stabilizers, lubricants, processing aids, and many others can increase the heat release rate and the smoke production. Others, such as the water vapor from the thermal decomposition of flame retardant fillers such as magnesium dihydroxide (MDH) or aluminum trihydroxide (ATH), lower the flame's energy by acting as a heat sink diluting the fuels. Even side reactions between HCl and fillers such as calcium and magnesium carbonate can produce gases such as CO_2, weakening the flame. However, the main gas in the flame in this stage is HCl, released by the thermal decomposition of PVC. Here, the common acid scavengers used in the stabilizer one pack can no longer compete with the fast evolution of HCl in the gas phase.

HCl is not an inert gas such as water vapor or CO_2. Within the flame, it initiates a series of catalytic reactions capable of scavenging the radicals ·H and ·OH, lowering the flame's energy [17,18]. This phenomenon is called "the poisoning of the flame" and is the reason why all halogenated polymers are inherently flame-retardant. If Sb_2O_3 (ATO) is used, HCl also plays a central role in yielding $SbCl_3$. When it evaporates in the flame, it scavenges the hot radicals feeding the flame more efficiently than HCl alone, reducing its energy further [17,18].

The combustion in the flame can be seen as a competition between two reactions: the first brings the complete oxidation of the fuel when oxygen is rich and the flame is high in energy. The second happens when the flame's energy is low and oxygen starves. It causes a dehydrogenation of the organic substances in the fuel, releasing airborne water and carbon agglomerates we perceive as smoke. This last condition is reached when ATO is used, and items release massive smoke.

In the condensed phase, the polyene sequences formed during the zip elimination process can react intramolecularly (cis-olefinic structures), generating benzene, soot, and smoke, or intermolecularly (trans-olefinic structures) yielding cross-linked structures [9,10,12,13,18]. This last condition prevents smoke production. HCl is also crucial in the condensed phase, reacting with incipient Lewis acids commonly present in PVC smoke suppressants and forming actual Lewis acid, catalyzing the formation of trans-olefinic structures and promoting the intermolecular reaction yielding a cross-linked matrix and char. Therefore, HCl scavengers interfere with the smoke suppressant mechanism inhibiting smoke production.

1.3. The Second Stage of the Thermal Decomposition/Combustion

Performing a TGA of PVC in N_2, the second stage of the decomposition is over 450 °C. Here, the cross-linked matrix starts releasing volatiles (aliphatic hydrocarbons and alkylated aromatic) [12], leaving at the end carbonaceous char.

In a real fire scenario, the condensation products formed over 450 °C in PVC items release volatile fuels in the gas phase, and a carbonaceous char is formed in the condensed phase. The fuels burn, increasing the flame energy, and on the contrary, the formed carbonaceous char hampers the spread of the flame, creating a protective and insulating barrier. The char can be formed if oxygen is low in concentration in the gas phase, when temperatures are not so high as to bring it to complete combustion, or its thickness is so high that it hinders oxygen from permeating it entirely. However, the fuels released in this stage are mainly aliphatic moieties. They burn, releasing less smoke but more energy in the flame

than the aromatics in stage 1. The presence of Lewis acids coming from the typical smoke suppressants used in PVC items can even increase the quantity of those fuels in the gas phase because they promote the cationic crack of the char, and other strategies for avoiding this problem can be used [18–21]. When temperature increases over 600 °C and if oxygen is enough in the gas phase, the final step of the decomposition/combustion stage leads to the post-pyrolysis/combustion stage, where only ashes of oxides and chlorides remain.

Therefore, the thermal decomposition, released gases, and the gas- and condensed-phase reactions differ depending on the temperature, oxygen concentration, and the PVC compound's ingredients. Knowing the type of reactions in the flame and in the condensed phase is crucial to actively act to reduce the flame's energy, directly or indirectly, or to suppress smoke: that will have consequences on the fire performances of PVC items in terms of ignitability, flammability, flame spread, heat release, and smoke production.

For this aim, flame retardants and smoke suppressants are developed and utilized in PVC compounds. They can work in the gas or condensed phases and act physically or chemically. Refs. [17,22] give a detailed overview of mechanisms, types, and dosages.

1.4. Low-Smoke Acidity Compounds and Acid Scavengers at High Temperatures in the Condensed Phase

Low-smoke acidity PVC compounds have been developed to reduce the release of HCl in case of fire. In the low-smoke acidity compounds for cables, acid scavengers at high temperatures acting in the condensed phase are added to capture HCl [23,24]. The consequent reduction of HCl in the gas phase and metal chlorides in the condensed phase inhibits the fire performances of PVC compounds for cables: the consequence is the emission of more heat and smoke despite flame retardants and smoke suppressants added to the compounds.

The paper shows the impact of some acid scavengers at high temperatures on flame retardance and smoke emission of some PVC compounds for cables. Refs. [23,24] detail the main characteristics of the acid scavengers used in this paper, including dispersion properties and mechanism of action. This article compares the formulations with and without acid scavengers acting in the condensed phase. Ease of extinction has been measured according to ASTM D 2863 [25] (Limiting Oxygen Index, or LOI). Cone calorimetry has been used for determining heat release and smoke production according to ISO 5660-1 [26]. Micro combustion calorimetry (MCC) has been carried out according to ASTM D 7309 [27] to focus on the dynamic of the pyrolysis and combustion in the range of 250–750 °C. The presence of ATO in the PVC compound is entirely obliterated by the activity of potent acid scavengers that act by trapping HCl; that reflects in a lower LOI, higher fire growth rate (FIGRA), higher total heat release (THR), higher specific heat release (h_c), and higher specific heat of combustion of fuels gases ($h_{c\ gas}$). If a smoke suppressant is used in the presence of HCl scavengers, its action will be inhibited, causing a higher unexpected total smoke production (TSP).

The data indicate that low-smoke acidity PVC compounds will have fewer fire performances, and, therefore, finding other routes to get back the reaction to fire and smoke reduction becomes a task of extreme importance.

2. Materials and Methods

2.1. Materials

Table 1 shows the first set of formulations intending to show the interaction between acid scavengers at high temperatures in the condensed phase with a flame retardant acting in the gas phase, such as ATO. REA1 is the reference formulation without fillers, flame retardants, and smoke suppressants and represents the lower edge of performances in flame retardance and smoke production. REA2 comes from REA1 by adding 3 phr of ATO. It considers the effect of ATO without the impact of fillers capable of absorbing HCl interfering with the flame poisoning of ATO. REA3–5 focus on the effect of particle size of different grades of $CaCO_3$ on HCl absorption and its impact on flame retardancy

and smoke production. REA3 and REA4 contain ground milled calcium carbonate (GCC) with different particle sizes (Table 1), while REA5 contains ultrafine precipitated calcium carbonate (UPCC). REA6-8 focus on the different impacts on flame retardance by HCl scavengers having a different efficiency due to a different chemical nature: REA6 contains AS-6B, a potent acid scavenger at high temperatures in the condensed phase, REA7 contains an ineffective acid scavenger as MDH, and REA8 contains an inert acid scavenger such as ATH (see Section 4.1). The characteristics of those flame retardant fillers are well explained in Ref. [23]. REA9 shows the synergism between MDH and UPCC, described in the second part of this article [24]. That aims to highlight how they impact the HCl poisoning mechanism in the gas phase differently.

Table 2 formulations aim to show the impact of HCl scavengers on the performance of a potent flame retardant acting in the condensed phase. Reaguard B-FR/9211 is a commercial flame retardant and smoke suppressant produced by Reagens S.p.A. REAC0 contains exclusively 10 phr of Reaguard B-FR/9211, without flame retardant fillers. REAC1 contains ATH, not scavenging HCl, representing high flame retardancy and low smoke production levels. REAC2 contains MDH. It scavenges HCl, but it re-releases HCl again at 350–550 °C [28,29]. REAC4 contains UPCC, a potent acid scavenger that aims to verify if it interferes with the charring promoted by Reaguard B-FR/9211. REAC5 has GCC at the same phr as UPCC in REAC4.

Table 1. Inovyn 271 PC is a suspension PVC with a K value of 71 from Inovyn. DINP means Di Iso Nonyl Phthalate; Diplast N is the trade name of Polynt S.p.A. ESBO stands for Epoxidized Soy Bean Oil. Reaflex EP/6 is a Reagens trade name. The used antioxidant is Arenox A10, a Reagens trade name, which is Pentaerythritol tetrakis(3-(3,5-di-tert-butyl-4-hydroxyphenyl)propionate), CAS number 6683-19-8. COS stands for calcium organic stabilizer. RPK B-CV/3038 is a typical stabilizer for 70 °C cables produced by Reagens. Atomfor S and Hydrocarb 95 T are ground milled calcium carbonates, having a stearic acid coating and differing in medium value of particle size distribution (D50), 2.0 and 0.7 microns, respectively. Winnofil S is a UPCC having nanoscale mean particle size [30]. AS-6B is a potent acid scavenger in the condensed phase at high temperatures, produced by Reagens S.p.A, having a D50 of 2.0 microns. Ecopyren 3.5 is uncoated ground milled MDH produced by Europiren, with a D50 of 3.0 microns. Aluprem T GR 4 is a synthetic ATH from Tor Mineral, with a D50 of 2.5 microns (see Supplementary Materials).

Raw Materials	Trade Name	REA1 [phr]	REA2 [phr]	REA3 [phr]	REA4 [phr]	REA5 [phr]	REA6 [phr]	REA7 [phr]	REA8 [phr]	REA9 [phr]
PVC	Inovyn 271 PC	100	100	100	100	100	100	100	100	100
DINP	Diplast N	50	50	50	50	50	50	50	50	50
ESBO	Reaflex EP/6	2	2	2	2	2	2	2	2	2
Antioxidant	Arenox A10	0.1	0.1	0.1	0.1	0.1	0.1	0.1	0.1	0.1
COS	RPK B-CV/ 3038	5	5	5	5	5	5	5	5	5
Sb_2O_3	RI004	0	3	3	3	3	3	3	3	3
$CaCO_3$	Atomfor S	0	0	90	0	0	0	0	0	0
$CaCO_3$	Hydrocarb 95 T	0	0	0	90	0	0	0	0	0
UPCC	Winnofil S	0	0	0	0	90	0	0	0	90
HTAS 2	AS-6B	0	0	0	0	0	90	0	0	0
$Mg(OH)_2$	Ecopyren 3.5	0	0	0	0	0	0	90	0	30
$Al(OH)_3$	Aluprem T GR 4	0	0	0	0	0	0	0	90	0

The ingredient amounts in Tables 1 and 2 are expressed per hundred resin (phr). The formulations have been tested with the apparatuses in Table 3 and according to the test methods indicated in Table 4.

Table 2. Reaguard B-FR/9211 is a commercial flame retardant and smoke suppressant produced by Reagens S.p.A.

Raw Materials	Trade Name	REAC0 [phr]	REAC1 [phr]	REAC2 [phr]	REAC4 [phr]	REAC5 [phr]
PVC	Inovyn 271 PC	100	100	100	100	100
DINP	Diplast N	50	50	50	50	50
GCC	Atomfor S	0	30	30	0	90
$Al(OH)_3$	Aluprem TGR4	0	60	0	0	0
$Mg(OH)_2$	Ecopyren 3.5	0	0	60	0	0
UPCC	Winnofil S	0	0	0	90	0
COS	RPK B-CV/ 3038	3.0	3.0	3.0	3.0	3.0
Flame retardant	Reaguard B-FR/9211	10	10	10	10	10

Table 3. Main test apparatuses utilized.

Test Apparatus	Producer	Model	Additional Information
Calender	Battaggion	MCC/N150X300-E	Temperature 160 °C—Milling Time 3′
Halogen acid gas test apparatus	S.A. Associates	Standard model	Porcelain combustion boats
Multimeter for electric measurements	Mettler Toledo	S213 standard kit	
Conductivity electrode	Mettler Toledo	S213 standard kit	Reference thermocouple adjusting temperature fluctuations
pH electrode	ettler Toledo	S213 standard kit	Reference thermocouple adjusting temperature fluctuations
LOI test apparatus	FTT	Standard model	Test Specimen type IV; ASTM D 2863
Cone calorimeter	FTT	Dual cone calorimeter	ISO 5660-1. Heat flux 50 K.W./m^2, 1 or 3 mm test specimen thicknesses, with grid
Micro combustion calorimeter	FTT	Standard Model	Pyrolizer 1 °C/s, 750 °C, combustor 750 °C, method A of STM D 7309

Table 4. Tests for acidity, flame retardance, and smoke production assessments.

Technical Standard	Measurement	Temperature [°C]	Note
Internal method 3	Multimeter Smoke acidity	40 min to 800 °C +/−10 °C 20 min at 800°C +/−10 °C	DDW, pH, and conductivity. As EN 60754-2 with a heating regime of EN 60754-1
ASTM D 2863	LOI	23 °C	Test specimens type IV. Method B
ISO 5660-1	Time to ignition (TTI), (s) Time to flame out (TTFO) (s) Time to peak (TTP) (s) Peak of heat release rate (pHRR) (kW/m^2) Total heat release (THR) (MJ/m^2) Mass loss (%) Total smoke production (TSP) (m^2) Peak of smoke production rate (m^2/s) Yield of pyrolysis residue, (Yp) (g/g) Fire growth capacity (FGC) (J/g·K) Heat release capacity (η_c) (J/g·K)	755 °C	Sample thicknesses 1 mm and 3 mm, area 88.4 cm^2, sparkling source on
ASTM D 7309	Maximum specific heat release rate (Q_{max}) (J/g) Heat release temperature (T_{max}) (°C) Specific (total) heat release, h_c (J/g) Specific heat of combustions of fuel gases, $h_{c\ gas}$ (J/g)	750 °C combustor 1 °C/min to 750 °C pyrolizer	

Internal method 3, described in Table 4, uses the following materials: double deionized water (DDW) is internally produced by an ion exchange deionizer. The pH of DDW must be between 5.50 and 7.50, and the conductivity must be less than 0.5 μS/mm. Buffer and conductivity standard solutions come from VWR international (pH: 2.00, 4.01, 7.00, 10.00; conductivity: 2.0, 8.4, 14.7, 141.3 μS/mm).

2.2. Test Apparatuses

Table 3 describes the utilized test apparatuses.

2.3. Sample Preparation

The formulations in Tables 1 and 2 were prepared in a turbo mixer producing the dry blends, then processed in the laboratory calender. The foils produced test specimens for internal method 3 and MCC and were shaped in a hydraulic press in plaques with 1.0 and 3.0 mm thicknesses for the cone calorimeter and 3.0 mm plaques for LOI. In Appendix A, Figures A1 and A2 give a schematic diagram with a more detailed description of the sample preparation.

2.4. Internal Tests and International Technical Standards Used

Table 4 shows the technical standards, internal methods, and the main utilized conditions.

Internal method 3 is carried out as EN 60754-2 [31], using the heating regime of EN 60754-1 [32] and following the indications and suggestions highlighted in Ref. [23]. The sample, introduced in the tube furnace at room temperature, was heated for 40 min to 800 °C and then kept at 800 °C for 20 min. The smoke was collected in two bubblers containing DDW. The water from the bubbling devices and the washing procedures was collected in a 1 L volumetric flask filled to the mark. pH and conductivity were measured, and two replicates gave mean value, standard deviation (SD), and coefficient of variation (CV).

LOI was measured following the procedure described in ASTM D 2863 [25], as indicated in paragraph 12, procedure B. Three replicates gave mean and SD. ISO 5660-1 [26] was performed using two replicates, calculating mean values and SD at an incident heat flux of 50 kW/m^2, corresponding to a temperature of 755 °C. According to the standard, the test specimens had dimensions of 100 mm × 100 mm with thicknesses of 1 or 3 mm and an effective exposed area of 88.4 cm^2. FIGRA was calculated, as described in EN 13823 [33], as the maximum multiplied per 1000 of the function HRR/t (t), excluding data corresponding to THR (t) < 0.2 MJ and HRR (t) < 3 kW/m^2. ASTM 7309 [27] was performed on three replicates to calculate the mean and SD, according to method A. Fluxes of 80 mL/min of N_2 in the pyrolizer and 20 mL/min of O_2 in the combustor were set. The temperature of the combustor was adjusted to 750 °C +/− 1 °C, and in the pyrolizer, a heating regime of 1 °C/min was chosen up to 750 °C. The sample's weight was determined, evaluating the oxygen consumption of a trial test. The drop must stay between 20–13% and 20–7%.

In Appendix A, Figure A2 gives a schematic diagram of the conditions used in the test methods.

3. Results

The results of the formulations in Tables 1 and 2 are summarized as follows: Tables 5 and 6 show the pH and conductivity, Tables 7 and 8 report LOI, Tables 9 and 10 summarize cone calorimetry data, and Tables 11 and 12 display MCC measurements.

Table 5. pH and conductivity of the compounds in Table 1 are shown. Internal method 3 has been carried out. The mean values and CV are reported. CVs are below 5%.

Formulation	REA1	REA2	REA3	REA4	REA5	REA6	REA7	REA8	REA9
pH	2.20	2.30	2.60	2.90	3.20	4.20	2.50	2.40	3.40
CV_{pH}	<5.0%	<5.0%	<5.0%	<5.0%	<5.0%	<5.0%	<5.0%	<5.0%	<5.0%
Conductivity (μS/mm)	359.7	328.5	105.7	70.1	31.1	3.8	180.7	205.2	11.8
CV_c	<5.0%	<5.0%	<5.0%	<5.0%	<5.0%	<5.0%	<5.0%	<5.0%	<5.0%

Table 6. pH and conductivity of the compounds in Table 2 are shown. Internal method 3 has been carried out. The mean values, coefficient of variation, and standard deviations are reported.

Formulation	REAC0	REAC1	REAC2	REAC4	REAC5
pH	1.95	2.65	2.74	3.30	2.62
CV_{pH}	<5.0%	<5.0%	<5.0%	<5.0%	<5.0%
Conductivity (μS/mm)	462.1	92.8	76.0	25.1	117.3
CV_c	<5.0%	<5.0%	<5.0%	<5.0%	<5.0%

Table 7. LOIs of the compounds in Table 1 are shown. The mean values, coefficient of variation, and standard deviations are reported.

Formulation	REA1	REA2	REA3	REA4	REA5	REA6	REA7	REA8	REA9
LOI (O_2%)	24.0	29.0	28.0	27.3	22.0	23.0	34.7	34.0	24.0
SD	1.0	0.0	0.0	0.6	0.0	0.6	0.6	0.0	1.0

Table 8. LOIs of the compounds in Table 2 are shown. The mean values, coefficient of variation, and standard deviations are reported.

Formulation	REAC0	REAC1	REAC2	REAC4	REAC5
LOI (O_2%)	25.0	29.3	28.0	21.0	25.0
SD	0.0	1.5	1.0	0.0	0.0

Table 9. Cone calorimetry measurements of the compounds in Table 1 are shown. The mean values, coefficient of variation, and standard deviations are reported. Results are referred to as 3 mm plaques.

Formulation	REA1	REA2	REA3	REA4	REA5	REA6	REA7	REA8	REA9
peak HRR (kW/m^2)	337.5	252.4	192.1	213.0	331.6	394.3	167.7	105.0	254.8
SD	31.0	6.4	9.5	3.3	5.6	13.0	7.7	2.1	10.7
THR (MJ/m^2)	55.0	49.1	43.8	40.0	58.8	45.5	39.4	40.0	53.5
SD	0.7	0.9	1.7	2.0	1.5	1.3	1.9	1.4	3.3
FIGRA (W/s)	4187	3098	2549	3224	4073	5110	1563	1597	3365
SD	147	129	458	83	594	503	146	194	255
TSP (m^2)	28.3	28.1	16.5	17.8	13.8	15.3	10.1	9.6	11.4
SD	0.6	1.3	1.0	1.2	0.5	0.3	1.5	1.8	0.5

Table 10. Cone calorimetry measurements of the compounds in Table 2 are shown. The mean values, coefficient of variation, and standard deviations are reported. Results are referred to as 1 mm plaques.

Formulation	REAC0	REAC1	REAC2	REAC4	REAC5
peak HRR (kW/m^2)	270.4	128.4	200.5	292.6	198.8
SD	33.2	0.5	11.4	1.1	7.4
THR (MJ/m^2)	18.0	20.2	25.4	29.7	23.6
SD	0.5	1.6	2.2	0.1	3.3
FIGRA (W/s)	6239	2616	3986	6035	4316
SD	49	215	402	220	542
TSP (m^2)	6.4	3.9	4.6	6.6	5.1
SD	0.6	0.5	0.1	0.4	0.6

Table 11. MCC measurements of the compounds in Table 1 are shown. The mean values and standard deviations are reported. FGC is the fire growth capacity, HRR means heat release rate, PR is pyrolysis residue, Q max is the maximum of specific HRR, T max is the heat release temperature, h_c is the specific (total) heat release, Y_p the yield of pyrolysis residue, h_c gas is the specific heat of combustion of fuels gases, and Stg means stage.

Formulation	REA1	REA2	REA3	REA4	REA5	REA6	REA7	REA8	REA9
FGC (J/g·K)	156.95	141.42	88.90	90.83	104.72	100.51	75.81	102.43	92.83
SD	5.52	2.41	0.70	0.19	0.23	3.05	2.73	1.63	1.20
η_c (J/g·K)	324.10	326.11	330.20	333.33	338.65	322.50	323.30	321.01	333.03
SD	24.08	8.77	4.94	0.97	5.30	13.23	13.41	7.75	6.71
Qmax (J/g) stg 1	202.00	197.79	135.26	152.50	162.78	144.00	109.86	136.03	147.31
SD	4.78	4.65	0.65	3.33	5.94	4.51	2.13	7.80	2.19
Tmax (°C) stg 1	324.1	326.1	330.2	333.3	338.6	322.5	323.3	321.0	333.0
SD	0.81	1.20	0.30	1.60	0.80	6.20	2.30	1.00	0.20
Qmax (J/g) stg 2	101.61	96.93	51.36	51.37	57.34	51.97	52.62	48.77	59.49
SD	5.69	3.90	0.50	0.54	0.30	1.89	0.38	0.08	1.29
Tmax (°C) stg 2	491.8	493.0	483.5	475.7	480.5	500.6	486.8	478.0	478.8
SD	0.99	1.10	0.16	1.00	0.30	1.70	0.40	2.20	0.90
h_c (J/g) total	17.16	15.42	9.93	10.23	11.76	11.33	9.15	10.38	10.38
SD	0.19	0.17	0.12	0.06	0.03	0.16	0.10	0.09	0.08
h_c (J/g) stg 1	10.31	9.00	5.86	6.31	7.32	6.64	4.74	6.56	6.00
SD	0.18	0.17	0.08	0.06	0.04	0.21	0.09	0.17	0.06
h_c (J/g) stg 2	6.85	6.42	4.07	3.92	4.44	4.69	4.41	3.83	4.38
SD	0.20	0.17	0.16	0.05	0.02	0.11	0.11	0.07	0.10
Yp (g/g)	0.08	0.13	0.35	0.40	0.43	0.48	0.34	0.33	0.46
SD	0.03	0.01	0.02	0.02	0.00	0.02	0.01	0.02	0.02
$h_{c\,gas}$ (J/g) total	18.71	17.84	15.30	16.94	20.65	21.95	13.92	15.73	19.08
SD	0.12	0.27	0.35	0.54	0.11	1.11	0.42	0.32	0.60
$h_{c\,gas}$ (J/g) stg 1	11.24	10.41	8.95	10.45	12.86	12.86	7.22	9.94	11.03
SD	0.10	0.11	0.26	0.35	0.08	0.63	0.20	0.45	0.43
$h_{c\,gas}$ (J/g) stg 2	7.48	7.43	6.35	6.50	7.80	9.09	6.70	5.82	8.05
SD	0.02	0.16	0.09	0.19	0.03	0.48	0.22	0.19	0.17

Table 12. MCC measurements of the compounds in Table 2 are shown. The mean values and standard deviations are reported. FGC is the fire growth capacity, HRR means heat release rate, PR is pyrolysis residue, Q max is the maximum of specific HRR, T max is the heat release temperature, h_c is the specific (total) heat release, Y_p the yield of pyrolysis residue, h_c gas is the specific heat of combustion of fuels gases, and Stg means stage.

Formulation	REAC0	REAC1	REAC2	REAC4	REAC5
FGC (J/g·K)	102.68	83.66	79.99	93.90	76.69
SD	6.25	0.72	1.30	1.67	0.82
η_c (J/g·K)	366.66	212.13	259.66	229.07	287.92
SD	13.40	4.71	4.92	8.83	21.21
Qmax (J/g) stg 1	277.68	123.38	196.29	141.61	166.51
SD	12.84	6.25	8.19	6.65	2.56
Tmax (°C) stg 1	303.4	326.5	314.8	334.1	325.0
SD	0.1	1.7	0.8	1.4	0.8
Qmax (J/g) stg 2	62.13	44.64	51.71	52.57	48.14
SD	3.50	1.00	1.05	1.20	1.25
Tmax (°C) stg 2	481.6	481.2	485.2	482.8	485.9
SD	1.2	2.1	0.8	1.0	2.0
h_c (J/g) total	12.25	9.97	9.60	11.32	9.41
SD	0.27	0.12	0.16	0.15	0.10
h_c (J/g) stg 1	8.06	6.63	5.81	7.34	6.15
SD	0.37	0.13	0.11	0.10	0.03
h_c (J/g) stg 2	4.19	3.33	3.80	3.98	3.27
SD	0.17	0.07	0.10	0.07	0.16
Yp (g/g)	0.18	0.36	0.43	0.44	0.39
SD	0.03	0.01	0.05	0.05	0.03
$h_{c\ gas}$ (J/g) total	15.54	15.74	16.55	20.94	15.70
SD	0.14	0.10	1.45	1.13	0.36
$h_{c\ gas}$ (J/g) stg 1	10.17	10.44	9.81	13.55	10.19
SD	0.14	0.09	1.25	0.86	0.55
$h_{c\ gas}$ (J/g) stg 2	5.36	5.29	6.74	7.38	5.50
SD	0.13	0.07	0.58	0.41	0.16

4. Discussion

4.1. Description of the Impact of Acid Scavengers on pH and Conductivity

Table 5 reports pH and conductivity according to internal method 3 for samples REA1–9, containing ATO as a flame retardant in the gas phase. Internal method 3 is more appropriate than EN 60754-2 in evaluating the smoke acidity in this research due to a heating regime that allows the acid scavenger to interact better with HCl [34]. REA1 and REA2 show the highest smoke acidity (low pH and high conductivity values) since they do not contain any acid scavenger at high temperatures in the condensed phase and have a higher PVC percentage than REA3–9. REA7 and REA8 have ineffective and inert acid scavengers, MDH and ATH; indeed, they show high acidity values because ATH does not react with HCl, while MDH scavenges HCl, but it then decomposes between 350 °C and 550 °C, thus re-releasing HCl [24,28,29]. Both samples show higher acidity than REA3, the formulation with GCC. REA3–5 contain different types of calcium carbonate with different particle size. Atomfor S has a mean particle size of around 2 microns, while Hydrocarb 95 T reaches low values down to 0.7 microns. Winnofil S is a coated UPCC with a mean particle size in nanoscale size [30]. REA6 and 9 give the lowest smoke acidity values due to powerful acid scavengers (ASB-6, REA6) and the synergistic couple MDH/UPCC in REA9 [24].

Table 6 shows pH and conductivity according to internal method 3 for samples REAC0-C5, containing REAGUARD B-FR/9211 as a flame retardant acting in the condensed phase. REAC0 without fillers and acid scavengers displays the highest acidity. REAC5, REAC1, and REAC2 with GCC, ATH, and MDH, respectively, follow in this sequence. REAC4 with

UPCC, as expected, reaches the lowest acidity values. The comparison between REAC4 and REAC5 again shows how profoundly the particle size impacts the smoke acidity.

4.2. Effect of Acid Scavenging on LOI

HCl sequestration impacts the LOI values of the formulations in Table 1, containing ATO acting in the gas phase (Table 7), and the formulations in Table 2 with Reaguard B-FR/9211 acting in the condensed phase (Table 8).

REA1, without a flame retardant, shows 24.0 $\%O_2$ LOI. REA2 containing 3 phr of ATO, gains 5 LOI points reaching 29.0 $\%O_2$. The addition of 90 phr of Atomfor S in REA3 depresses LOI slightly (28.0 $\%O_2$), but the impact becomes more evident as the particle size of $CaCO_3$ decreases and the HCl scavenging efficiency increases: REA3 with 2 microns $CaCO_3$ shows 28.0 $\%O_2$ comparable with REA4 (27.3 $\%O_2$) having 0.7 microns, while REA5 with UPCC has LOI even lower than REA1 without ATO (22.0 $\%O_2$). Using a powerful single-step HCl scavenger such as AS-6B (REA6) or multiple-step such as the couple Winnofil S and MDH (REA9), the trend is the same: REA6 LOI goes down to 23.0 $\%O_2$ and REA9 to 24.0 $\%O_2$. In both formulations containing Winnofil S and AS-6B, the action of ATO is inhibited by HCl scavenging in the gas phase, and LOI values collapse. REA9 has a slightly higher LOI (24.0 $\%O_2$) due to MDH's different mechanism of action as a flame retardant: it acts as a heat sink through an endothermic decomposition, dilutes the flame's fuels, and creates a barrier of MgO in the condensed phase. REA7 and REA8, containing ATH and MDH, boost LOI due to their specific mechanisms as flame retardants [17] and because they do not scavenge HCl. Figure 1 summarizes the data.

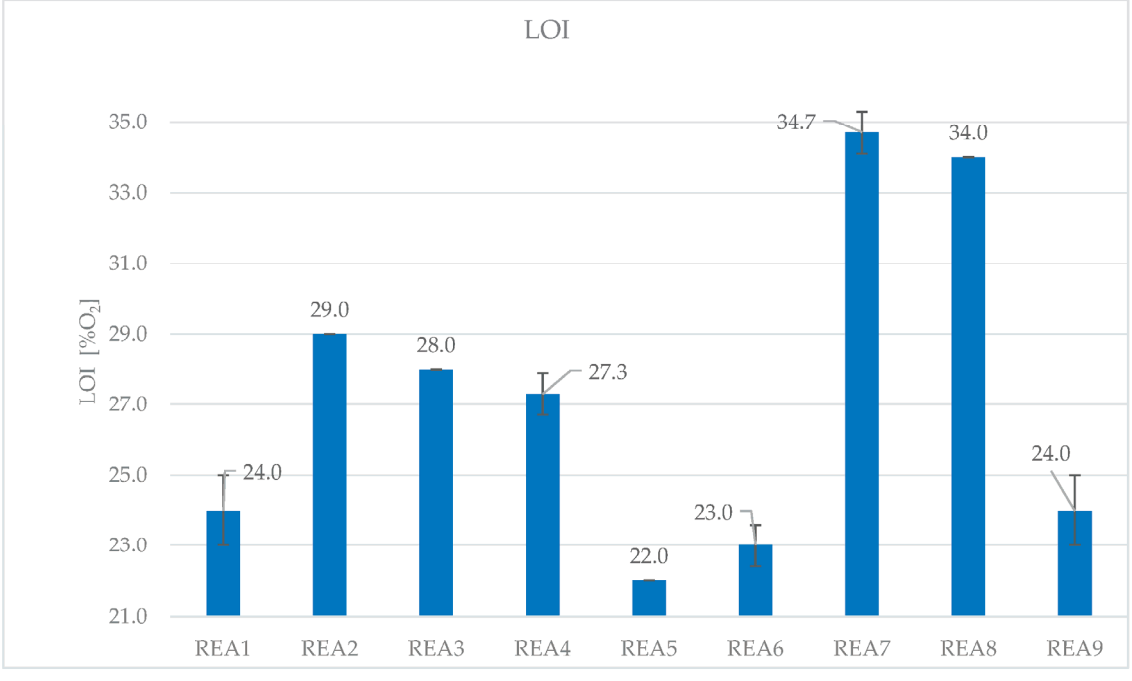

Figure 1. LOI of the formulations in Table 1, REA1–REA9.

HCl scavenging has the same impact when the flame retardant acts in the condensed phase. REAC0 contains only Reaguard B-FR/9211. LOI increases slightly compared to REA1 without a flame retardant (25.0 $\%O_2$ vs. 24.0 $\%O_2$). The introduction of ATH and MDH increases the LOI in REAC1 and REAC2 (29.3 $\%O_2$ and 28.0 $\%O_2$, respectively). As expected, both flame retardant fillers work synergistically with Reaguard B-FR/9211. When

UPCC is in the formulation at 90 phr (REAC4), its scavenging action depresses LOI down to 21.0 $\%O_2$, which is (even) lower than the formulation without flame retardants (REA1). The formulation with GCC, REAC5, shows the same LOI as REAC0. Figure 2 shows the summarized data.

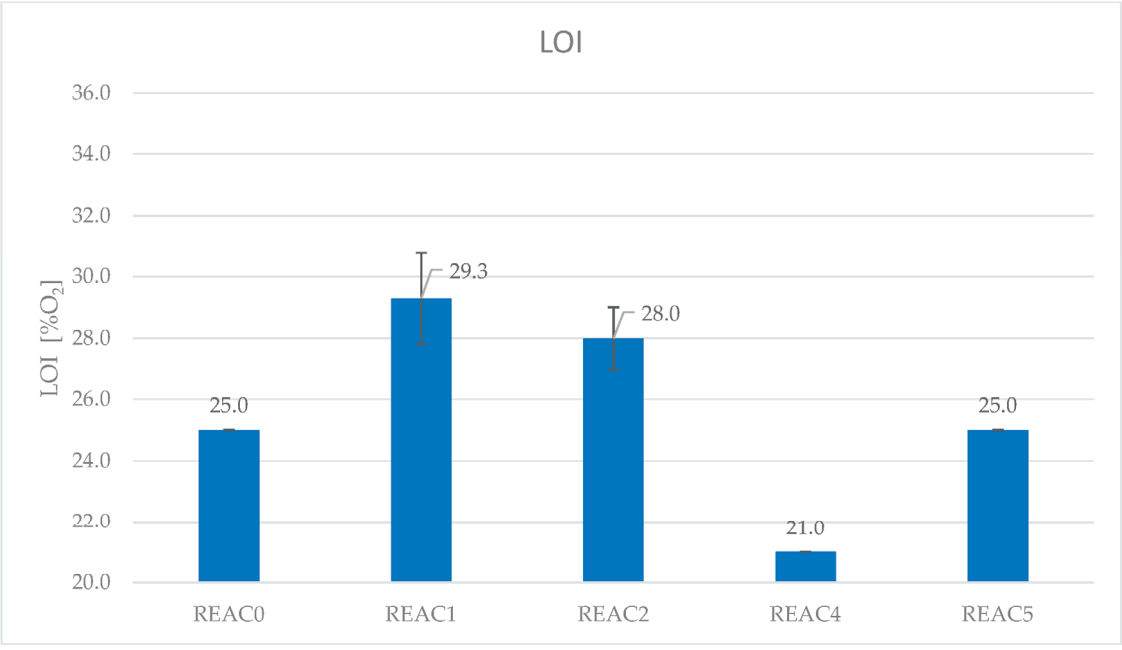

Figure 2. LOI of the formulations in Table 2, REAC0–REAC9.

Finally, the HCl sequestration of a potent acid scavenger depresses the ease of extinction of the formulation imparted by flame retardants acting both in the gas and condensed phase.

4.3. Effect of Acid Scavenging on Heat Release Rate and Smoke Production Measured in Cone Calorimetry

In fire science, the HRR is among the most critical parameter to be evaluated since it can parametrize the "intensity of the fire" [35,36].

The presence of acid scavengers strongly influences the HRR and THR of the formulations reported in Table 1 containing ATO as a flame retardant, as reported in Table 9. pHRR represents the maximum peak of the HRR (t) curve: the higher the peak, the lower the fire performance. Figure 3 clearly shows how acid scavengers at high temperatures affect this measure. REA1 is a formulation that contains neither filler nor ATO and can be considered the lower edge in fire performances. Its peak reached 337.5 kW/m^2, and with the addition of ATO In the formulation REA2, the peak dropped severely to 252.4 kW/m^2. REA3, containing 90 phr of GCC in addition to ATO and, hence, less incombustible material, shows an even lower value of pHRR than REA2. REA3, REA4, and REA5 contain, respectively, GCC, a finer GCC, and UPCC. The finer the particle size, the higher the peak (192.1 kW/m^2, 213.0 kW/m^2, and 331.6 kW/m^2, respectively). REA6, with a powerful acid scavenger, shows a pHRR much higher than the REA1 without flame retardants. REA7 and REA8 contain ineffective and inert acid scavengers, MDH and ATH. Here, HCl is released almost stoichiometrically and stops the action of the radicals feeding the flame. Therefore, because of their extremely low efficiencies in HCl scavenging and their flame retardant action, they show the lowest pHRR values (167.7 kW/m^2 and 105.0 kW/m^2). REA9 contains MDH

and UPCC in the correct ratio for working synergistically in HCl scavenging [23,24]. REA9 shows better fire performances because it contains more incombustible filler (REA9, 130 phr vs. REA6, 90 phr), and one of them, MDH, is capable of working as a flame retardant even in low-acidity conditions. Indeed, REA9 yields a minor smoke acidity (Table 5), but pHRR is lower than REA1, showing that the flame retardancy imparted by MDH is not inhibited by HCl sequestration.

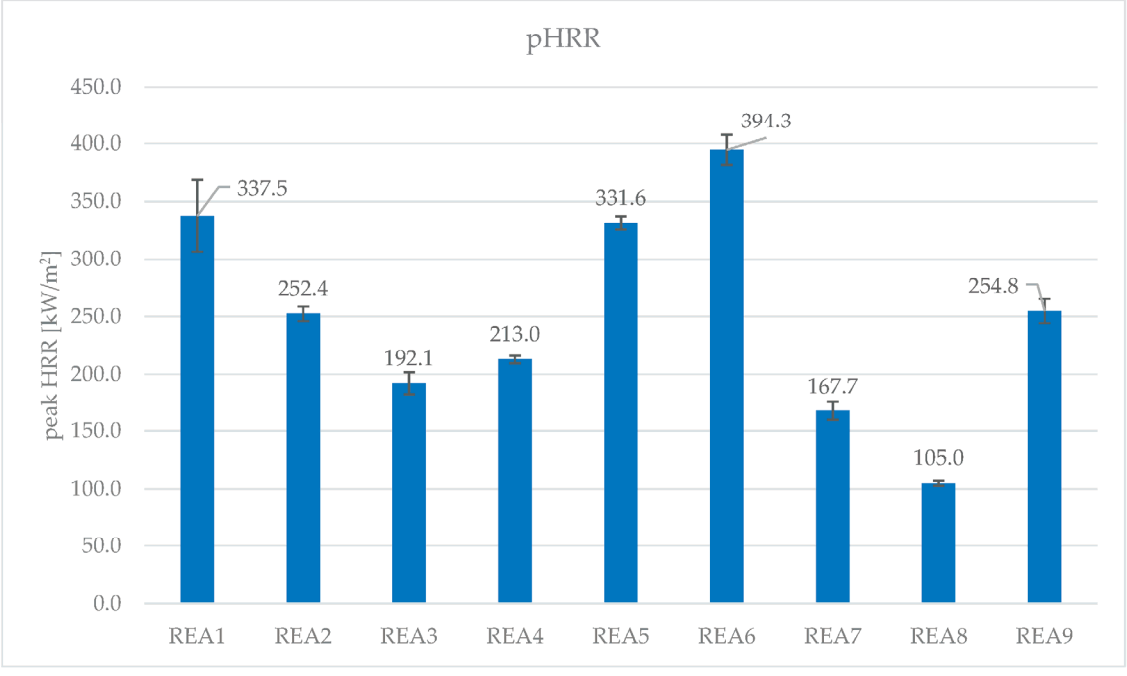

Figure 3. pHRR of the formulations in Table 1, REA1–REA9.

FIGRA is the ratio of the maximum of derivate of the function HRR (t) vs. the time required to reach it; such an index represents the maximum growth rate of the heat release rate and is helpful in ranking the material in terms of potential fire safety. Consequently, the higher the FIGRA, the lower the fire performance of the article. The measurements in Table 9 and Figure 4 indicate the reciprocity between the loss of flame retardance and the HCl availability in the gas phase. REA6, containing a potent acid scavenger, gives a FIGRA much higher than REA1, and the effect of $CaCO_3$ with different particle sizes is highlighted in REA3–REA5, where UPCC in REA5 shows the highest FIGRA in the group. REA7 and REA8, the worst in terms of smoke acidity, provide the best FIGRA of the formulations in Table 1. Again, REA9 compensates for the lack of flame retardance (in REA5) thanks to the presence of MDH and more incombustible flame retardant fillers and acid scavengers.

Total heat release (THR), in Table 9, is the area below the HRR (t) curve and accounts for the heat release in 600 s of the test in the cone calorimetry. Data are summarized in Figures 5 and 6.

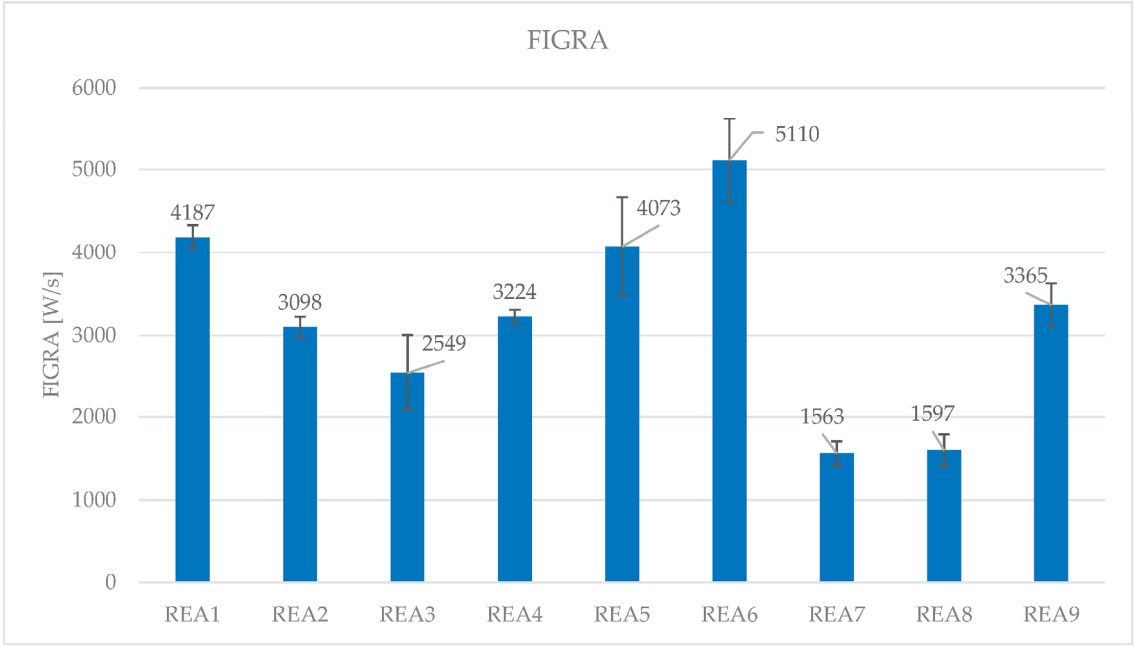

Figure 4. FIGRA of the formulations in Table 1, REA1–REA9.

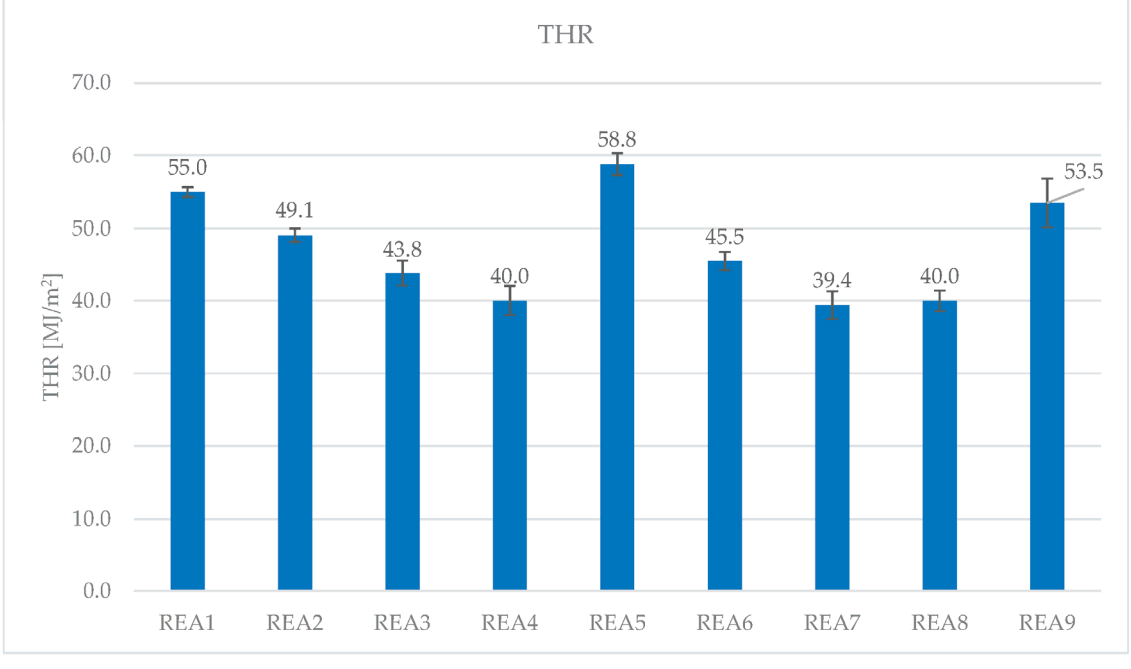

Figure 5. THR of the formulations in Table 1, REA1–REA9.

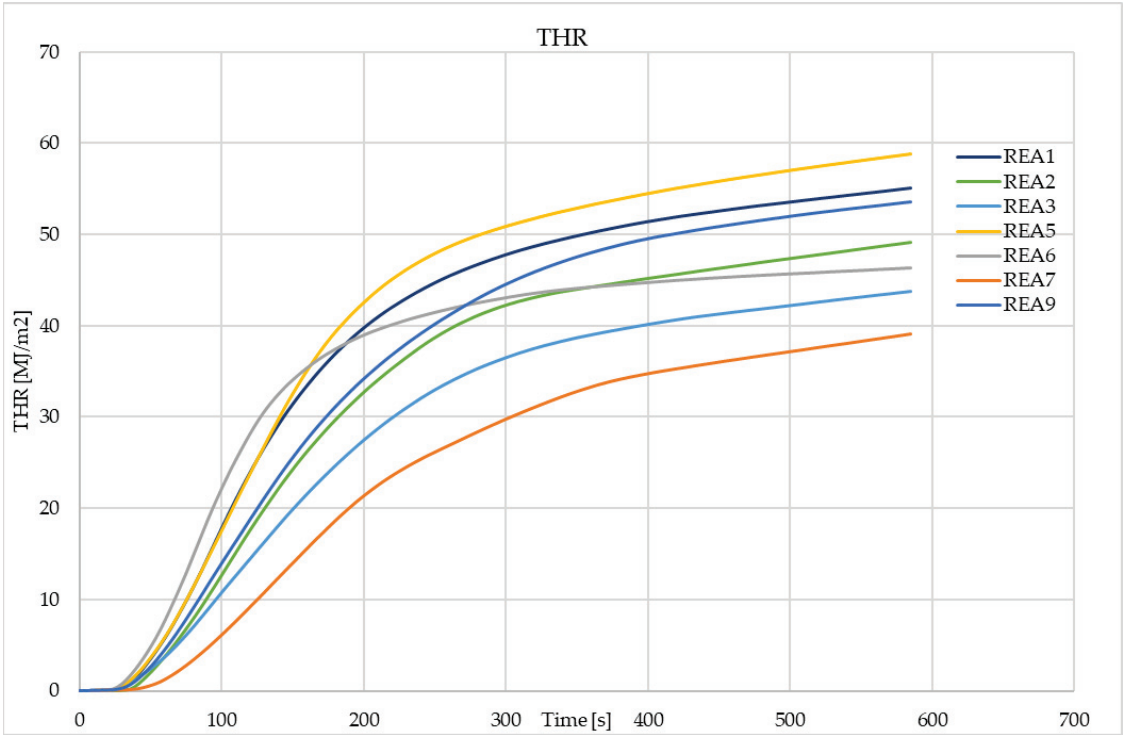

Figure 6. THR (t) of the formulations in Table 1, REA1–REA9.

HCl scavenging seems to have a substantial effect on speeding the velocity at which the heat is released. It also contributes to the intensity of the peak of HRR (t) but to a lesser extent on THR. REA5 shows the highest THR value (58.8 MJ/m^2). REA9 and REA6 follow with peaks higher than REA3 but lower than REA1 and REA2 (Table 9, Figures 5 and 6). In the formulations REA1–9, the flame retardant mechanism in the gas phase is promoted by ATO. In the first stage of the decomposition/combustion, the negative contribution to the flame retardancy by HCl sequestration is given. It is unclear why REA5 shows higher THR values than REA6 (Table 9, Figures 5 and 6), despite yielding more smoke acidity. REA6 seems to release heat faster, but in the end, its THR is lower than REA5. That is probably due to a different scavenging mechanism. REA6 scavenges HCl faster and more efficiently than REA5, reflecting a higher pHRR (Figure 7). However, the reason why REA6 THR is lower than REA5 THR is unknown and difficult to understand with the current measurements and data. However, understanding these differences is out of this paper's scope but is crucial in designing flame retardants, smoke suppressants, and acid scavengers working well together.

In cone calorimetry, a dynamic measure of smoke production is possible. The smoke production rate, SPR (t), is measured, and the area below the curve represents the total smoke production, TSP. Smoke production measures are critical in fire safety because smoke can hamper people involved in fire from escaping unharmed or being rescued by firefighters.

TSP values of the formulations of Table 1 (reported in Figure 8) show that REA1 and REA2 have the worst smoke production performance in the series, with comparable results (REA1 28.3 m^2 and REA2 28.1 m^2, respectively). The analysis of data of the remaining formulations is not easily parameterized. There is no clear correlation between HCl sequestration and smoke, but it should be highlighted that the formulations in Table 1 contain

ATO, which works in the gas phase; therefore, it is a system where smoke production is not inhibited by the presence of substances acting in the condensed phase. It appears that smoke production is just inversely proportional to the content of the fraction burning in the matrix since REA3–9 show fewer TSP than REA1 and REA2. REA7 and REA8 give the lowest values of smoke, probably due to the action of ATH and MDH on smoke production, as Ref. [18] reports.

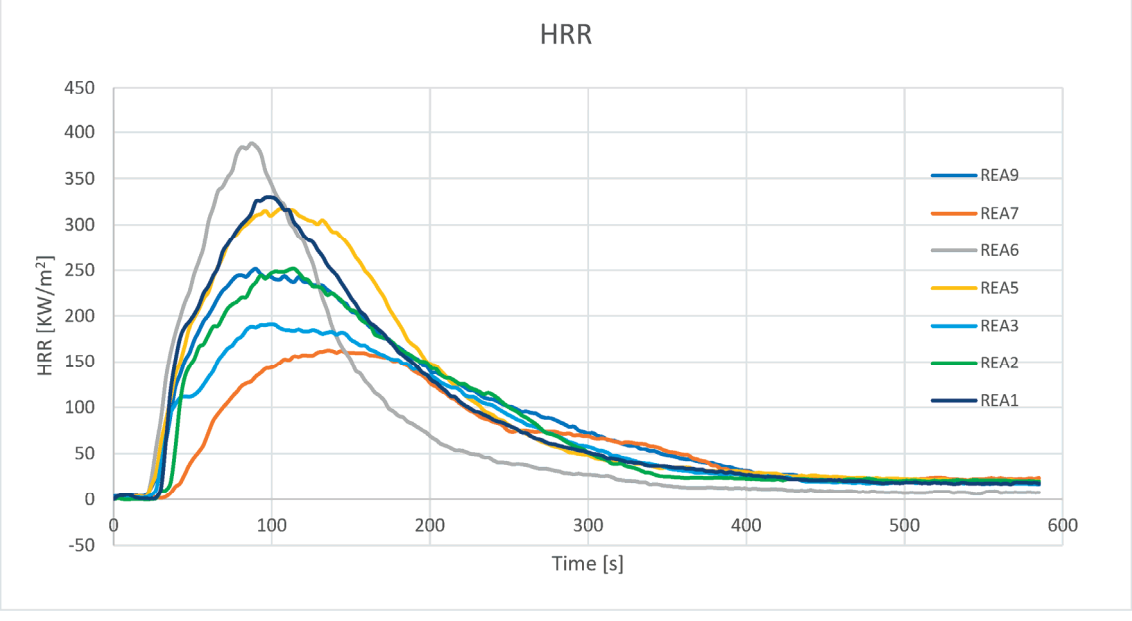

Figure 7. HRR (t) of the formulations in Table 1, REA1–REA9.

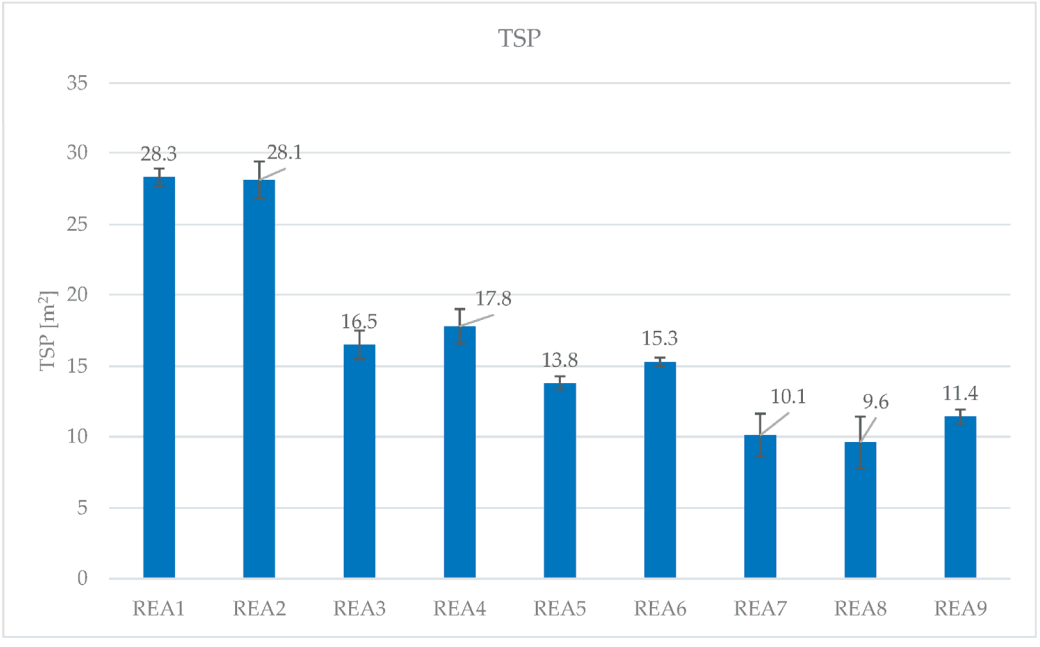

Figure 8. TSP of the formulation REA1–REA9.

In the formulations of Table 2, where the flame retardant acts in the condensed phase, the cone calorimeter measurements (Table 10, Figures 9–15) indicate the interference of HCl sequestration on cross-linking of actual Lewis acid: they clearly show the increase of heat release when HCl scavengers are used.

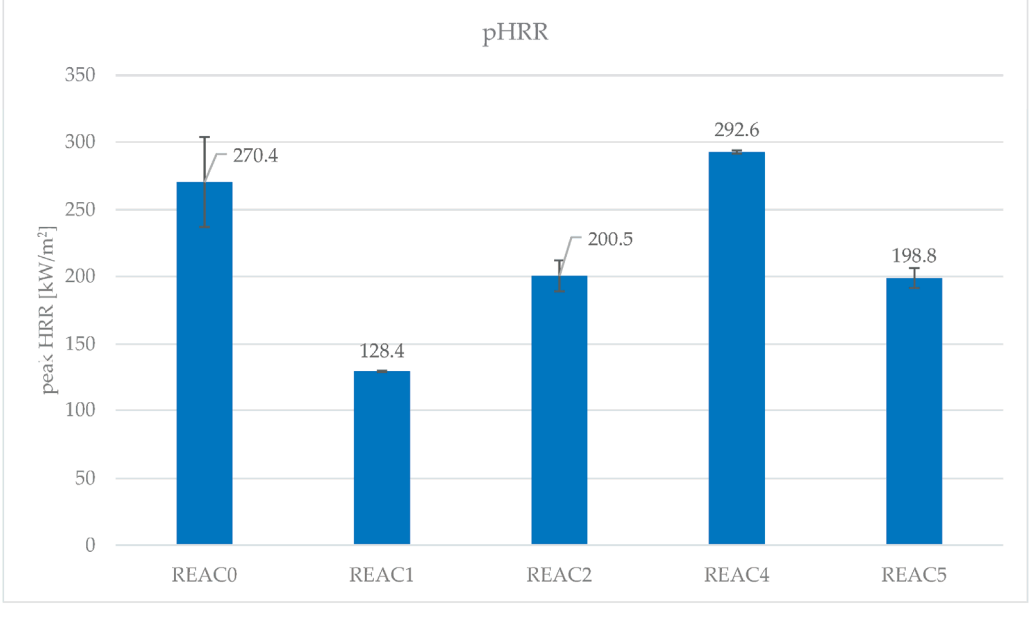

Figure 9. pHRR of the formulations REAC0–5.

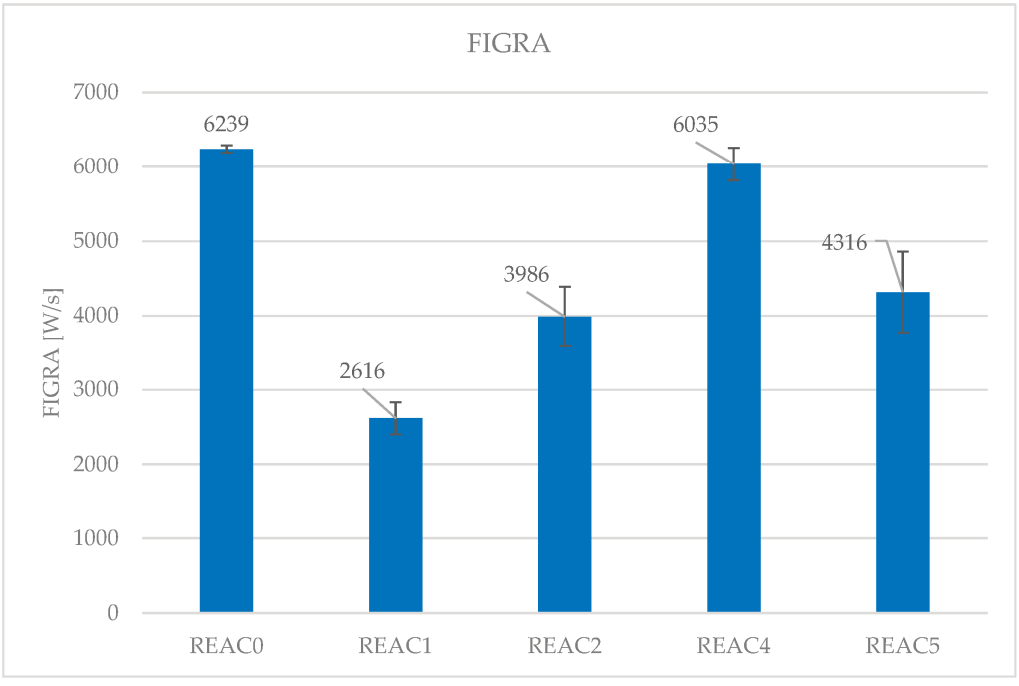

Figure 10. FIGRA of the formulations REAC0–5.

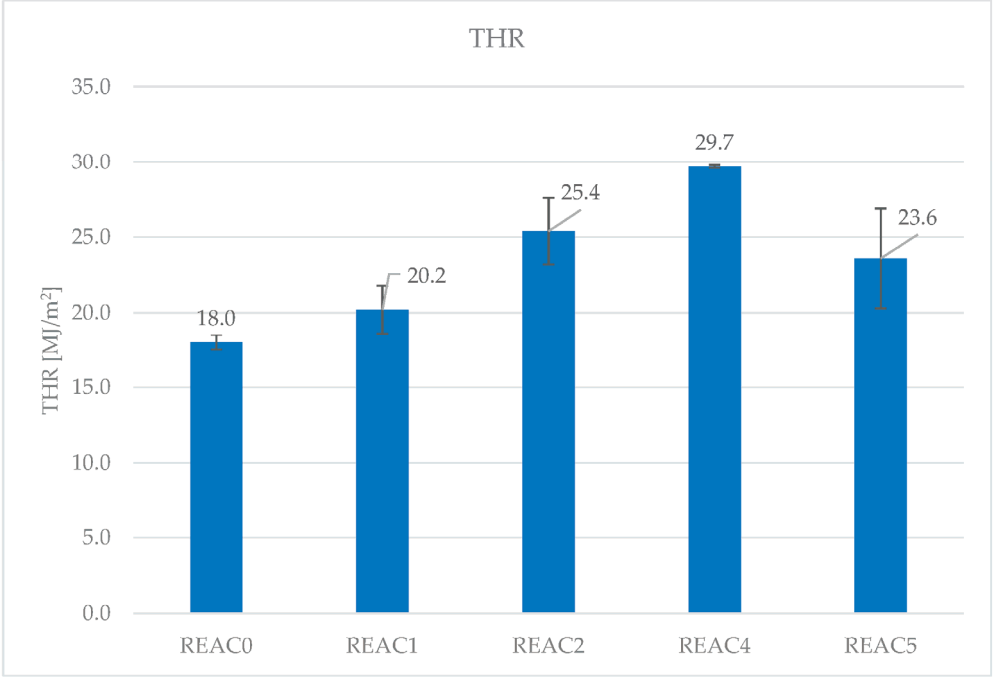

Figure 11. THR of the formulations REAC0–5.

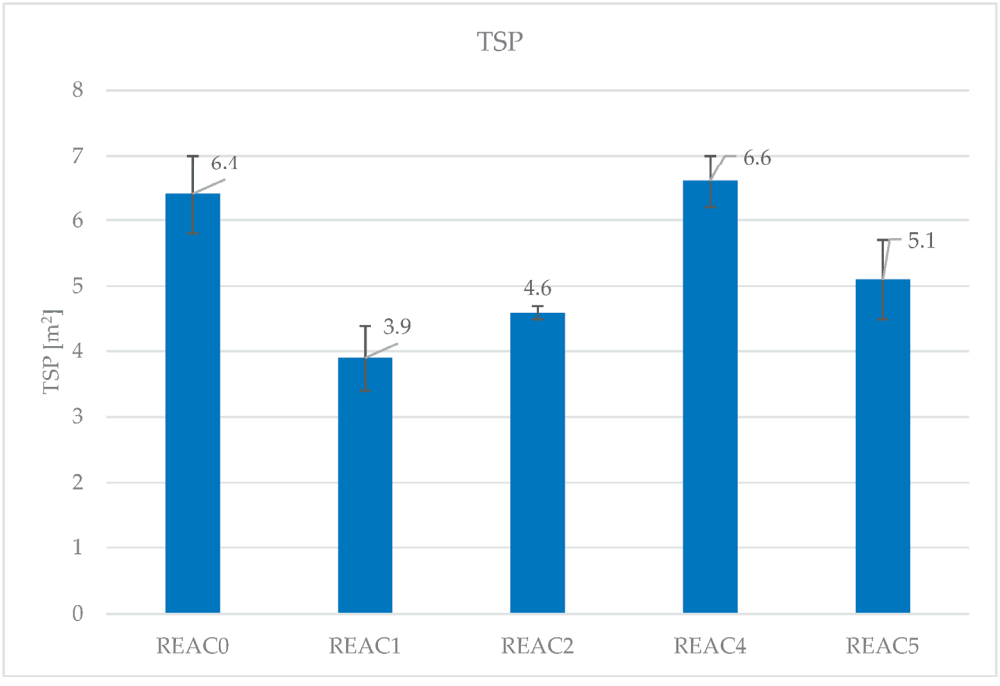

Figure 12. TSP of the formulations REAC0–5.

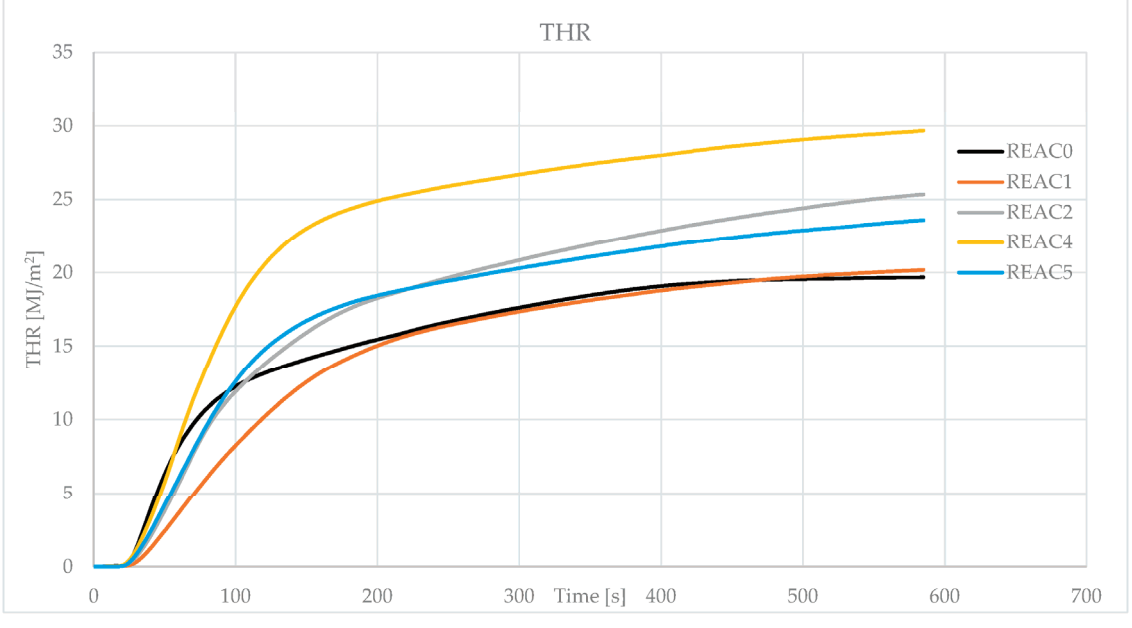

Figure 13. THR (t) of the formulations REAC0–5.

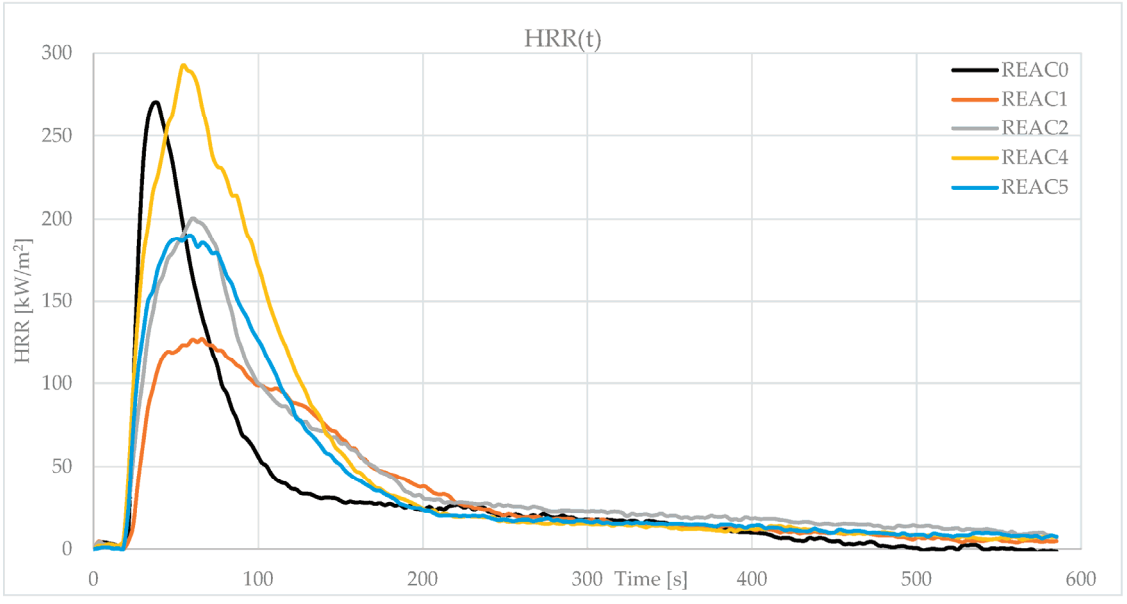

Figure 14. HRR (t) of the formulations REAC0–5.

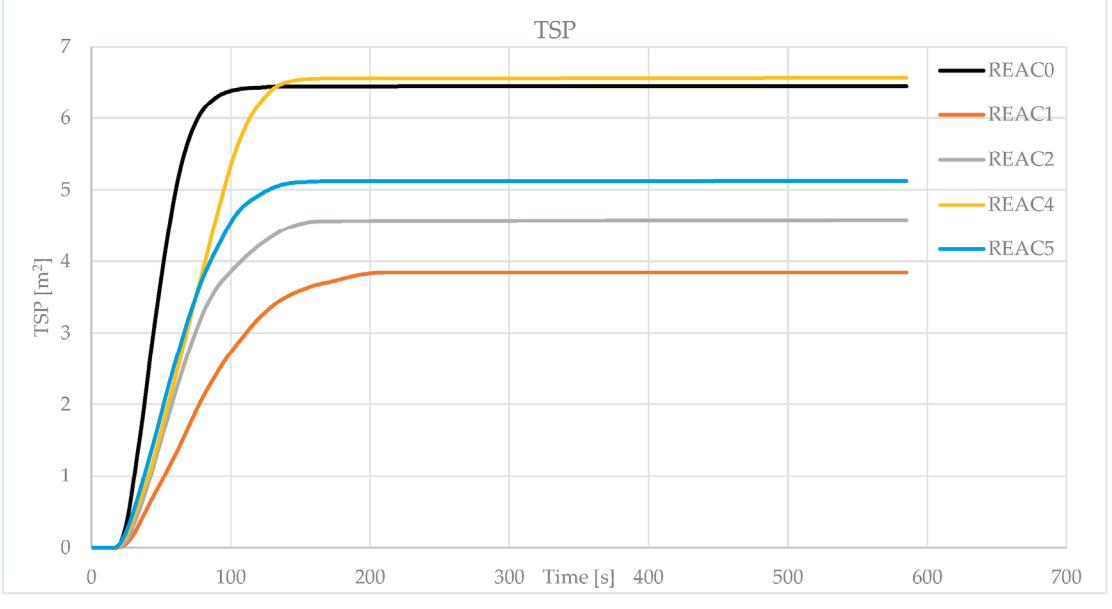

Figure 15. TSP(t) of the formulations REAC0–5.

REAC0 only has Reaguard B-FR/9211. pHRR is 270.4 kW/m^2 (Figure 9), and FIGRA is the highest in the series (Figure 10, 6239 W/s). THR is 18 MJ/m^2, releasing less heat than the others but at a higher speed (Figures 13 and 14). The smoke production evaluation shows that REAC0 has a 6.4 m^2 TSP (Figures 12 and 15). All cone calorimeter measurements indicate a performance improvement in the formulations with the addition of ATH and MDH—respectively, REAC1 and REAC2 (Figures 9–15). For example, FIGRA drops to

2616 W/s with ATH and 3986 W/s with MDH. Furthermore, TSP decreases respectively to 3.9 and 4.6 m^2. In particular, the formulations containing ATH and MDH show the best heat release and smoke production performance of the series. With potent acid scavengers at high temperatures in the condensed phase, such as Winnofil S, both the heat release and the smoke production parameters worsen compared to GCC (REAC5). For example, FIGRA for REAC4 in Figure 10 (6035 W/s) reaches almost the REAC0 rank (6239 W/s), while REAC5 FIGRA is much lower at 4316 W/s. That indicates how the HCl sequestration in REAC4 affects the fire performance of the compound. The same trends are highlighted regarding smoke measures, as indicated in Table 10, Figures 12 and 15. REAC4 has the highest TSP, 6.6 m^2, even more than REAC0. REAC5 containing GCC shows 5.1 m^2, being lower than REAC4 with UPCC. REAC1 and REAC2 give a more substantial smoke reduction, indicating that ATH and MDH work even in withstanding the smoke formation, probably releasing water and reducing the carbon particles, as described in Ref. [18].

The increase in smoke production due to HCl sequestration has also been evidenced by M. Piana in Refs. [37,38], where the smoke was measured as smoke density rating percentage (SDR%) according to ASTM D 2843.

Reaguard B-FR/9211 acts, in the condensed phase, as a flame retardant but also as a smoke suppressant.

The behavior of REAC4 clearly confirms that HCl scavenging also interferes with the action of the incipient Lewis acids in Reaguard B-FR/9211. Indeed, the sequestration of HCl prevents the formation of the potent Lewis acids (metal chlorides), and the pattern bringing to intramolecular rearrangement yielding benzene and soot becomes more probable than intermolecular reactions yielding matrix cross-linking.

4.4. Effect of Acid Scavenging on Measures from MCC

All specific HRR (T) curves show two stages. The first, centered around 260–360 °C, represents the energy released in the flame by the combustion of organic additives in the compound, particularly DINP, which evaporates in the gas phase, where it burns. Coming from intramolecular rearrangement of the polyene sequences, benzene is also combusted in the first stage. In the second stage, around 400–600 °C, the cross-linked polyene sequences release flammable moieties to the combustor, such as aliphatic and alkyl aromatic hydrocarbons, yielding a solid char in the pyrolizer [12]. The additives in the formulation decompose at different temperatures and with different energy, releasing gases such as CO_2 or water and impacting the shape of the specific HRR (T) curve.

The measures, usually taken into consideration in MCC shown in Table 10 and derived by the specific HRR (T), are the following:

- The maximum of the specific HRR (T) (Qmax). It is calculated for stages 1 and 2.
- The heat release temperature (Tmax) corresponds to the Qmax of stages 1 and 2.
- The heat release capacity (η_c) is the maximum rate of heat release divided by the heating rate.
- The specific (total) heat release (h_c). It is derived from the specific HRR (T) integral and represents the total heat released in the test. It calculates the contribution of h_c in stages 1 and 2.
- The specific heat of combustion of the fuel gases is the heat of combustion per gram of fuel burned in the combustor ($h_{c\ gas}$). It accounts for the energy released from the combustion of the fuels in the gas phase. It has also been split as the contribution from stages 1 and 2.
- The fire growth capacity (FGC) is defined in ASTM D7309-21 as a measure considering chemical processes responsible for igniting and burning combustible materials [26]. It is derived from other MCC measures such as η_c, ignition, and burning temperatures. FGC has been built considering the tendency of a material to ignite and spread the flame away from the fire source: ignitability and flame spread. FGC, a measure coming from a flammability micro-scale test, has been correlated to several other

measures from bench-scale tests used by Federal Aviation to discriminate levels of fire performances of the components in the cabin of an aircraft [26,39].
- Char yield. The initial and final weight ratios complete the measures in Table 10.

4.4.1. MCC of the Formulation of Table 1

REA1 is not flame-retarded, and it contains more combustible material than the others. It displays the highest Qmax, h_c, and FGC (Table 11). The addition of 3 phr of ATO in REA2 (LOI 29 $\%O_2$, Table 7) improves flame retardancy, and Qmax, h_c, and FGC decrease, while η_c is more or less comparable in all formulations. The effect of ATO seems more evident comparing LOI (Table 7, REA1 24 $\%O_2$ vs. REA2 29 $\%O_2$) and FIGRA values (Table 9, FIGRA, REA1 4187 W/s vs. REA2 3098 W/s) than in the MCC. That relies on the fact that ATO acts in the gas phase and does not contribute to the char formation in the pyrolysis process of MCC. ASTM D 7309 method A provides a temperature of 900 °C in the combustor. A temperature of 750 °C was chosen to make ATO's gas phase flame retardant action more evident.

REA7 with ATO and MDH (LOI 34.7 $\%O_2$, Table 7, FIGRA 1563 W/s, Table 9) shows how the synergistic action of two flame retardants can decrease the specific heat release in both stages (Table 11, Figure 16). Here, MDH dilutes the fuel in the flame and cools it down, decomposing endothermically between 300 °C and 330 °C. The decomposition of MDH perfectly tunes stage 1 of the decomposition/combustion of PVC compounds (Figure 16).

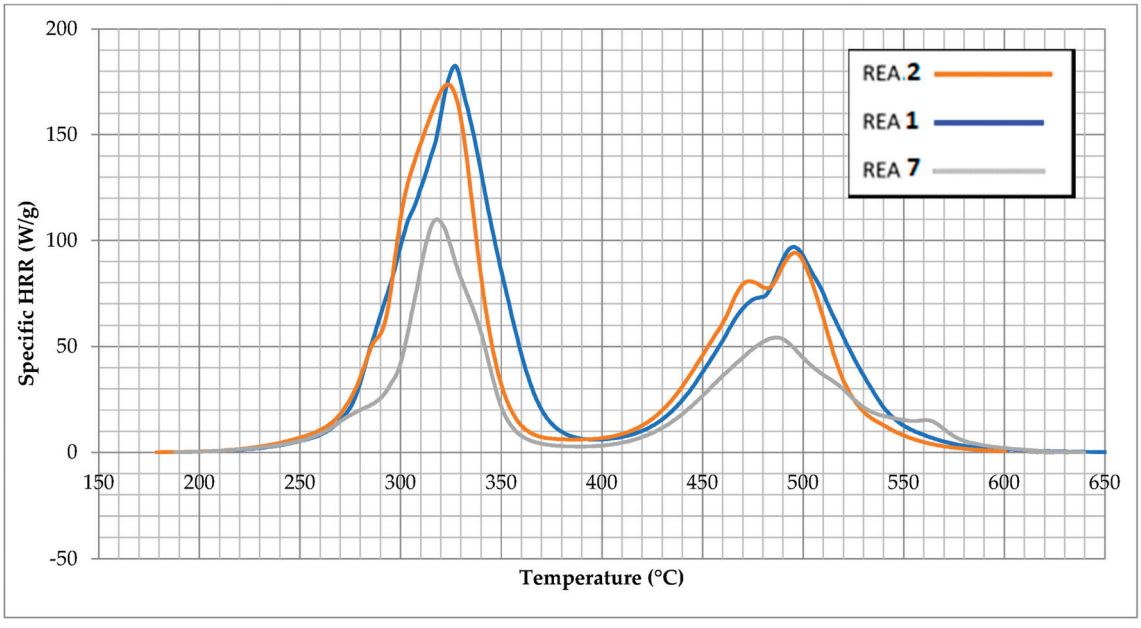

Figure 16. Comparison between REA1 (no flame retardants), REA2 (3 phr of ATO, 90 phr $CaCO_3$), and REA7 (3 phr of ATO and 90 phr of MDH).

Comparing the measures of REA3−5, it is clear how the HCl sequestration decreases the fire performance. REA5 with UPCC gives a higher FGC (104.72 J/g·K), Qmax (162.78 J/g), h_c (11.76 J/g), and $h_{c\ gas}$ (20.65 J/g) than REA3 and REA4. REA4, with a finer particle size $CaCO_3$, shows worst values than REA3, but the differences are near. REA6, containing a potent HCl scavenger, shows FGC 100.51 J/g·K, h_c (11.33 J/g), and $h_{c\ gas}$ (21.95 J/g) comparable with REA5. Qmax of REA6 is lower than REA5 due to a different impact that AS6-B has the shape of the specific HRR (T) curve. The action of the powerful

acid scavenger seems to delay the decomposition temperature and lower the peak of the specific HRR (T) of stage 1 (Table 9).

The $h_{c\ gas}$ shows strong reciprocity with HCl sequestration (Table 11, Figure 17).

The measure considers the energy released per gram of fuel gas combusted in the combustor. REA3 and REA4 containing GCC, which is less reactive with HCl, display overall lower values than REA5 formulated with UPCC. Therefore, REA5 releases more energy during the combustion, even though it releases more incombustible gases such as CO_2 in the first stage due to the fast reaction between HCl and UPCC. REA6 behaves similarly: a potent acid scavenger makes the gases more "flammable." In this case, 21.95 J/g is developed during the combustion of the gases, and the $h_{c\ gas}$ of REA5 and REA6 are even higher than the formulation without a flame retardant and with more plasticizer (REA1).

REA9 shows the synergistic combination of MDH and UPCC in scavenging HCl, lowering the smoke acidity (Table 5), but MDH also starts its function as a flame retardant through its endothermic decomposition releasing water at 300–330 °C. That explains the lower values of $h_{c\ gas}$ in the first stage in REA9 compared with REA5 (11.03 J/g vs. 12.86 J/g), showing that heat sink and fuel dilution are the main mechanisms reducing the $h_{c\ gas}$.

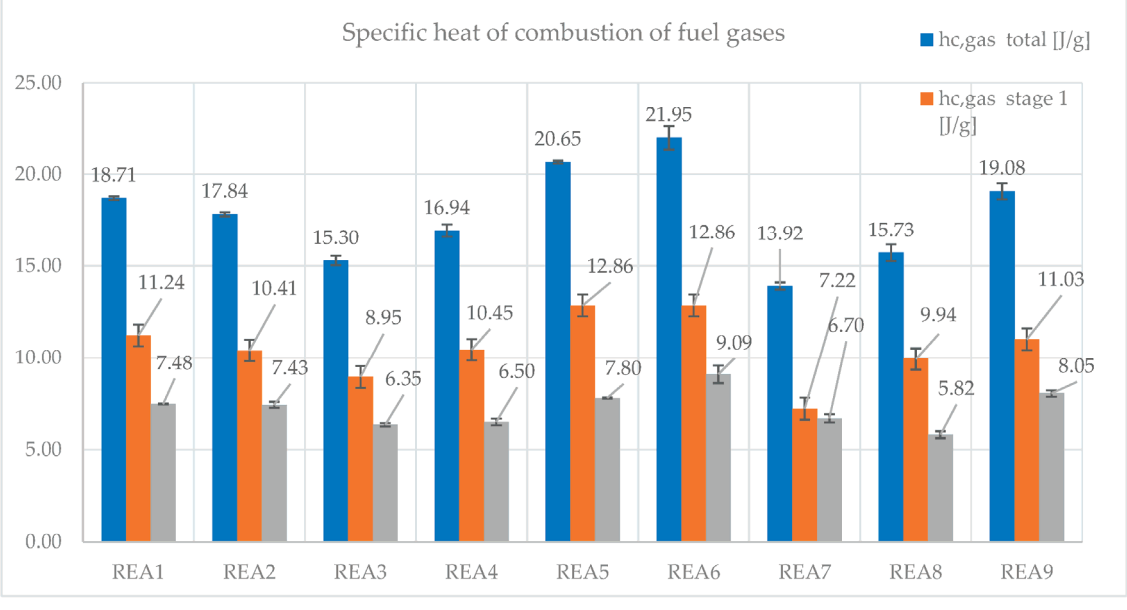

Figure 17. $h_{c\ gas}$ samples REA1–9. Blue column: total; orange: stage 1; grey: stage 2.

$h_{c\ gas}$ from stage 2 seems to worsen in the presence of acid scavengers (REA3, 6.35 J/g, REA4, 6.50 J/g, REA5, 7.80 J/g, REA6 9.09 J/g), and the comparison between REA7 and REA9 seems to confirm it (REA7, 6.70 J/g vs. REA9 8.05 J/g). The acid scavenger probably not only makes the fuel more flammable sequestrating HCl and worsening $h_{c\ gas}$ in the first stage (REA3, 8.93 J/g, REA4, 10.45 J/g, REA5, 12.86 J/g, REA6, 12.86 J/g), but somehow makes the condensation product from polyene sequences more prone to release flammable fuel (see Section 4.4 for entering more into detail of the topic).

4.4.2. MCC of the Formulation of Table 2

From the analysis of the MCC data of the formulations in Table 2 (Table 12), these comments follow. This set combines a powerful charring agent, Reaguard B-FR/9211, with flame retardant fillers such as ATH, MDH, GCC, and UPCC. Therefore, flame retardancy and smoke suppression act mainly in the condensed phase. REAC0 contains no filler

and 10 phr of Reaguard B-FR/9211. It shows the highest FGC, η_c, Q_{max} (102.68 J/g·K, 366.66J/g·K, 277.68 J/g), and the lower T_{max} (303.4 °C). It starts burning before the others and releases more heat. The addition of flame retardant fillers and acid scavengers to Reaguard B-FR/9211 in formulations REAC1, C2, C4, and C5 changes the shape of the specific HRR (T) curve. However, no solid correlation can be established by analyzing FGC, ηc, Q_{max}, T_{max}, and smoke acidity, possibly due to many interplaying factors that are not easily separated as linear functions of single measurable parameters. The only measures of extreme interest that bring correlation are h_c (Figure 18, Table 12) and $h_{c\ gas}$ (Figure 19, Table 12).

In the formulation REAC4 with UPCC, the heat released in the first stage is higher than in REAC5, containing trivial GCC (Figure 18, Table 12). REAC4 shows an h_c of 11.32 J/g, which is much more than REAC5, 9.41 J/g. In the second stage, REAC4 reaches h_c values close to REAC0 (3.98 J/g vs. 4.19 J/g).

REAC4 contributes more to heat in the first stage than in the second (Figure 18). The UPCC in REAC4 scavenges HCl, worsening the item's fire behavior.

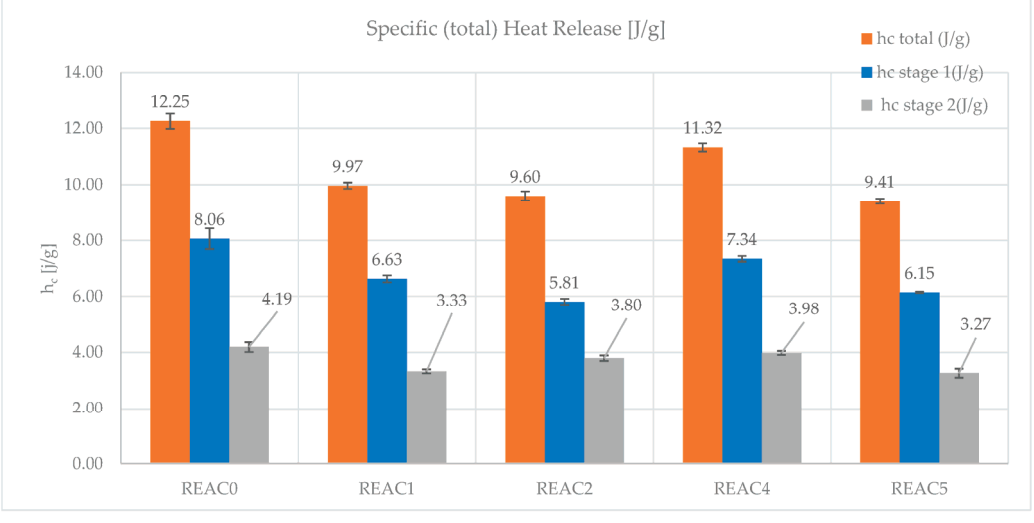

Figure 18. Comparison of h_c in REAC0–REAC5. Specifically, REAC4 contains an HCl scavenger, while REAC5 a trivial GCC.

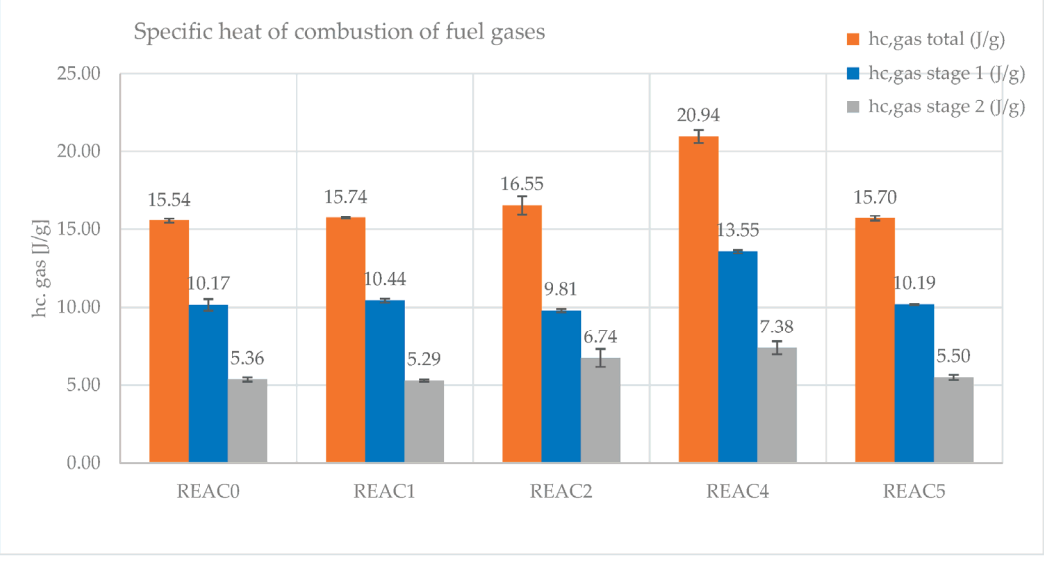

Figure 19. Comparison of $h_{c\ gas}$ in REAC0–REAC5. Specifically, REAC4 contains an HCl scavenger, while REAC5 a trivial GCC.

$h_{c\ gas}$ again gives much information on HCl scavenging. REAC4 with UPCC brings a $h_{c\ gas}$ total of 20.94 J/g against 15.70 J/g of the formulation containing GCC, REAC5 (Figure 19). The contribution is high in the first stage (REAC4, 13.55 J/g vs., REAC5, 10.19 J/g) but also in the second (REAC4, 7.38 J/g vs., REAC5, 5.50 J/g).

h_c and $h_{c\ gas}$ clearly indicate that in REAC4, the sequestration of HCl enhances the flame's energy. Additionally, in stage 2, REAC4 releases more energy than REAC5. Here, the heat comes from fuel combustion from the char in stage 2. It can be viewed as an indirect measure of the consistency of the char. If a powerful acid scavenger captures most of the HCl, it prevents the formation of potent Lewis acids through the reaction between HCl and incipient Lewis acids used in flame retardants and smoke suppressants such as Reaguard B-FR/9211. Therefore, there will be less cross-linking of the polyene sequences and fewer condensation products. What is left will be more prone to lose moieties to the gas phase, which justifies the higher $h_{c\ gas}$ in stage 2 of REAC4 than REAC5 (Figure 19). Furthermore, 9 explains that without potent Lewis acids, the intramolecular reactions of cis–trans polyene sequences yielding benzene will be more probable. As a result, that will bring more soot and smoke, as cone calorimetry actually confirmed.

The analysis of the specific HRR (T) curves in Figure 20 shows how, when CGG is present in the first stage, the combustion starts earlier (REAC5 325 °C vs. REAC4 334.1 °C), with a quicker speed (η_c REAC5 287.92 J/g·K, vs. REAC4 229.07 J/g·K), but the curve is sharper, declining fast to lower specific HRR (T) values.

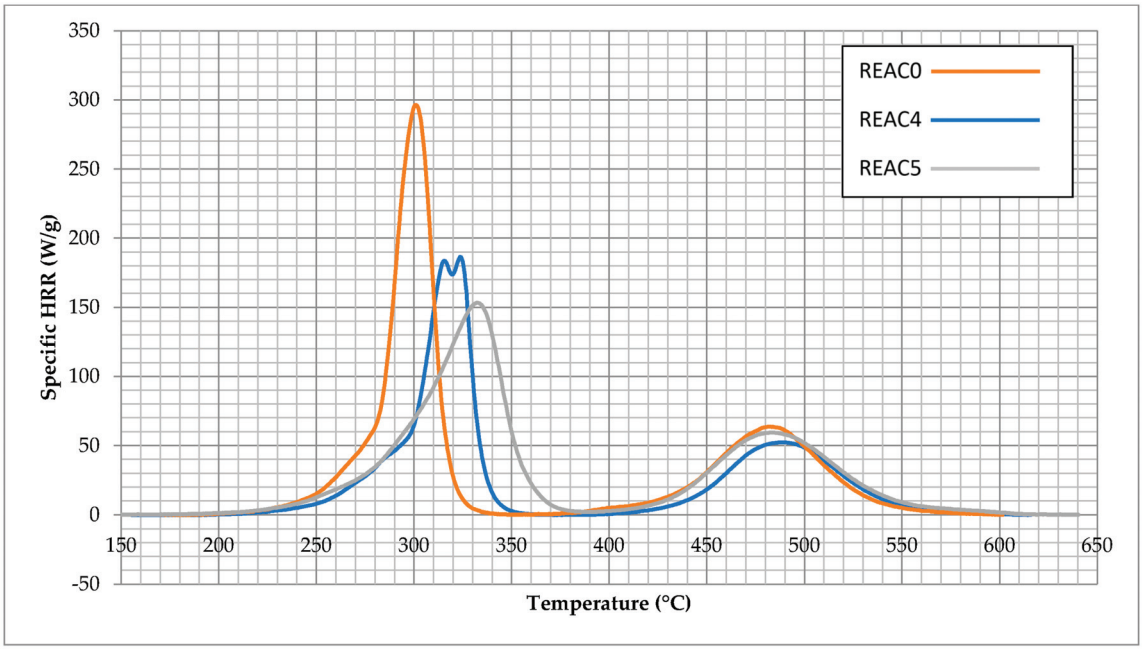

Figure 20. Specific HRR of REAC0 (containing only Reaguard B−FR/9211), REAC4 (containing Reaguard B−FR/9211 and Winnofil S), and REAC5 (containing Reaguard B−FR/9211 and Atomfor S).

The analysis of the data related to REAC2 and REAC3 is also interesting. REAC0 shows the highest value of h_c (12.25 J/g, Figure 12). The addition of flame retardant fillers shows a strong reduction of h_c (REAC1, 9.97 J/g, and REAC2, 9.60 J/g). ATH works better in the second stage, while MDH is in the first. The shapes of the HRR (T) curve of REAC1 and REAC2 are completely different (Figure 21). They differ from REAC0 mainly in η_c (REAC0 366.66 J/g·K, REAC1 212.13, REAC2 259.66 J/g·K, Table 12), in first stage Q_{max} (REAC0, 277.68 J/g, REAC1 123.38 J/g, REAC2 196.29 J/g, Table 12), and T_{max} (REAC0, 303.4 °C, REAC1 326.5 °C, REAC2 314.8 °C, Table 12). Both show a marked flame retardance but with different behavior. While in the second stage Q_{max} and the h_c are lower in REAC1 than REAC2, in stage 1, REAC1 starts the combustion at lower temperatures but with a milder slope than REAC2. In the end, the area of the HRR (T) curve in stage 1 is higher in REAC1, but the speed to the peak, η_c, is higher in REAC2 than REAC1 (Figure 21, Table 12). The reasons are probably in the different temperatures at which ATH and MDH work. ATH decomposes at 190–210 °C, making free water. Probably, water helps the expulsion of plasticizer in the gas phase (probably promoting hydrolysis), but this should be clarified with other instrumentation such as TGA-FTIR.

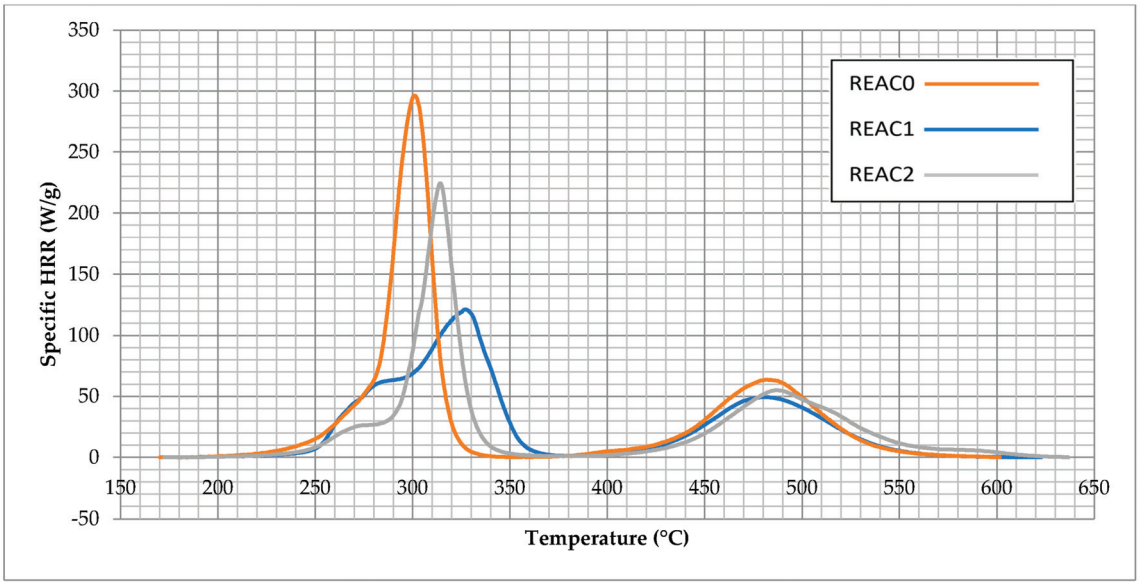

Figure 21. Specific HRR of REAC0 (containing only Reaguard B−FR/9211), REAC1 (containing Reaguard B−FR/9211 and ATH), and REAC2 (containing Reaguard B−FR/9211 and MDH).

If the hypothesis is correct, most combustible fuel from plasticizer moieties will burn at a lower temperature. Water vapor impedes a quick heat release, and the curve flattens and enlarges when the primary flame retardant in the gas phase is wholly consumed.

The data in the second stage show how h_c and $h_{c\ gas}$ decrease more in REAC1 than in REAC2 (Table 12). That is reflected in a more consistent char residue of REAC1, as shown in Scheme 1.

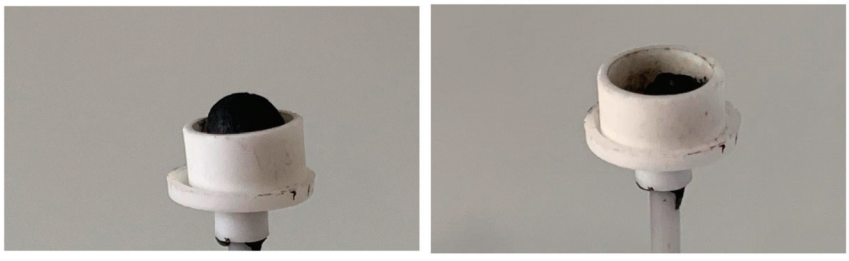

Scheme 1. Left: REAC1 char residue; right: REAC2 char residue.

5. Conclusions

Thermal stability is a measure that must be evaluated in the process stage of PVC items and their useful life. Thermal decomposition of the item must be considered in case of fire when specific additives in the item can affect the chemistry of the flame retardancy and smoke suppression in the condensed and gas phases, contributing negatively or positively to heat release and smoke production. The decomposition/combustion stage can be followed through MCC, plotting the specific HRR versus T, and the shape of HRR (T) is affected by the additives used in the PVC compound. In the decomposition/combustion stage, HCl reaches the gas phase inhibiting the reactions sustaining the flame's energy. However, HCl also creates potent Lewis acids in the condensed phase with the right additives, promoting char formation and decreasing the heat release rate and smoke production.

Acid scavengers at high temperatures trap most of the released HCl, affecting the fire performances of the items; since acid scavengers trap a significant amount of HCl in the condensed phase, HCl cannot reach the gas phase, and therefore its scavenging of the radicals ·OH and ·H in the flame is hindered. Furthermore, the lack of HCl impedes the formation of actual Lewis acid that is responsible for the charring mechanism, passing through the cross-linking of the polyene sequences. Without potent Lewis acids, the more favorable pathway during decomposition is the intramolecular rearrangement of polyene sequences yielding to the benzene formation and, therefore, a substantial increase in smoke production and reduction of flame retardancy. Indeed, without potent Lewis acids, the char is more fragile and prone to release fuels sustaining the flame's energy.

The data also confirm that the actual char promoters are the metal chlorides from the incipient Lewis acids in Reaguard B-FR/9211, as Montaudo showed in Ref. [10], where the polyacetylene thermal decomposition in the presence of metal oxides was explored.

Low-smoke acidity compounds can be essential to introduce PVC cables in classes a_2 or a_1 in high- and medium-risk locations [40]. Such compounds will lose flame retardancy and increase smoke production as much as HCl scavenging is efficient. That issue paves the way for developing a new generation of flame retardants and smoke suppressants working efficiently in low-smoke acidity conditions.

Supplementary Materials: The following are available online at https://www.mdpi.com/article/10.3390/fire6070259/s1, Table S1: commercial additives.

Author Contributions: Conceptualization, G.S.; methodology, G.S., F.D., I.B., C.B., L.M., and E.S.; writing—original draft preparation, G.S.; writing—review and editing, G.S., F.D., I.B., C.B., L.M., and E.S. All authors have read and agreed to the published version of the manuscript.

Funding: This research received no external funding.

Institutional Review Board Statement: Not applicable.

Acknowledgments: The authors would like to acknowledge Ing. Carlo Ciotti, Ing. Marco Piana, all PVC Forum Italia, and the PVC4cables staff.

Conflicts of Interest: The authors declare that there is no conflict of interest regarding the publication of this paper.

Abbreviations

PVC	Poly(vinyl chloride);
HCl	Hydrogen chloride;
EU	European Union;
CPD	Construction Product Directive;
CPR	Construction Product Regulation;
UPCC	Precipitated Calcium Carbonate;
GCC	Ground Calcium Carbonate;
Phr	Part per Hundred Resin;
DINP	Di Iso Nonyl Phthalate;
ESBO	Epoxidized Soy Bean Oil;
COS	Calcium Organic Stabilizer;
DDW	Double Deionized Water;
M	Mean;
SD	Standard Deviation;
CV	Coefficient of variation;
MCC	Micro Combustion Calorimetry

Appendix A. A Schematic Diagram of the Sample Preparation and Testing Process

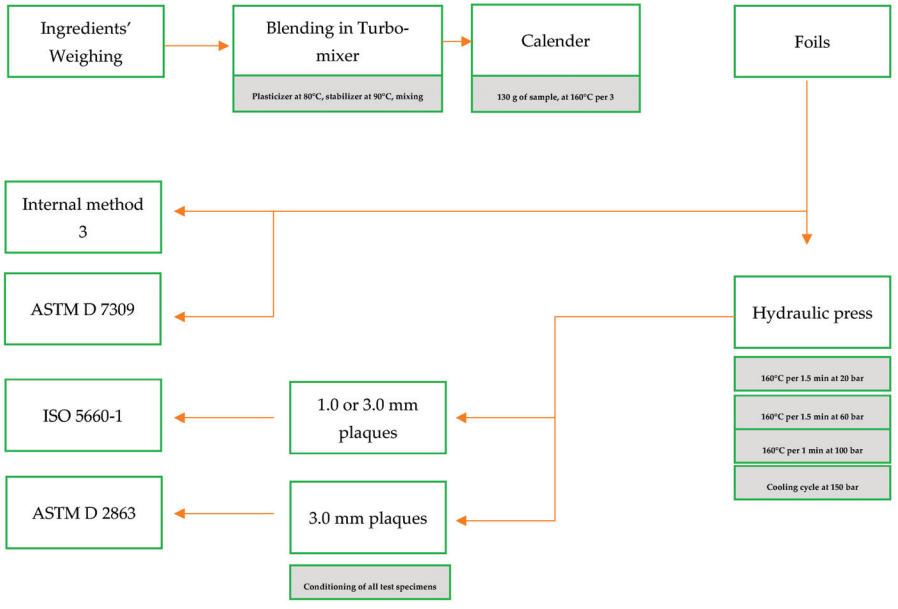

Figure A1. A schematic diagram of the sample preparation.

Figure A2. A schematic diagram of the testing process and main conditions.

References

1. Hjertberg, T.; Sörvik, E.M. Thermal Degradation of PVC. In *Degradation and Stabilisation of PVC*; Owen, E.D., Ed.; Springer: Dordrecht, The Netherlands, 1984. [CrossRef]
2. Starnes, W.H. How and to What Extent Are Free Radicals Involved in the Nonoxidative Thermal Dehydrochlorination of Poly(vinyl chloride). *J. Vinyl Addit. Technol.* **2012**, *18*, 71–75. [CrossRef]
3. Starnes, W.H.; Ge, X. Mechanism of Autocatalysis in the Thermal Dehydrochlorination of Poly(vinyl chloride). *Macromolecules* **2004**, *37*, 352–359. [CrossRef]
4. Starnes, W.H.; Wallach, J.A.; Yao, H. Six-Center Concerted Mechanism for Poly(vinyl chloride) Dehydrochlorination. Requiescat in Pace? *Macromolecules* **1996**, *29*, 7631–7633. [CrossRef]
5. Starnes, W.H. Structural and mechanistic aspects of the thermal degradation of poly(vinyl chloride). *Prog. Polym. Sci.* **2002**, *27*, 2133–2170. [CrossRef]
6. Lynda, P.B. The Dehydrochlorination Mechanism of the Internal Allylic Chloride Structure in Poly(Vinyl Chloride). Dissertations, Theses, and Masters Projects. Master's Thesis, William & Mary, Williamsburg, VA, USA, 2000. [CrossRef]
7. Schartel, B.; Hull, T.R. Development of fire-retarded materials—Interpretation of cone calorimeter data. *FAM* **2007**, *31*, 327–354. [CrossRef]
8. Starnes, W.H.; Edelson, D. Mechanistic Aspects of the Behavior of Molybdenum(VI) Oxide as a Fire-Retardant Additive for Poly(vinylvinyl chloride). *Macromolecules* **1979**, *12*, 797–802. [CrossRef]
9. Starnes, W.H.; Wescott, L.D.; Reents, W.D.; Cais, R.E.; Villacorta, G.M.; Plitz, I.M.; Anthony, L.J. Mechanism of poly(vinyl chloride) fire retardance by molybdenum(vi) oxide. Further evidence in favor of the Lewis acid theory. In *Polymer Additives. Polymer Science and Technology*; Kresta, J.E., Ed.; Springer: Boston, MA, USA, 2007; Volume 26, pp. 237–248. [CrossRef]
10. Montaudo, G.; Puglisi, C. Evolution of aromatics in the thermal degradation of poly(vinyl chloride): A mechanistic study. *Polym. Degrad. Stab.* **1991**, *33*, 229–262. [CrossRef]
11. Wu, C.H.; Wu, C.H.; Chang, C.Y.; Hor, J.L.; Shih, S.M.; Chen, L.W.; Chang, F.W. Two-stage pyrolysis model of PVC. *Can. J. Chem. Eng.* **1994**, *72*, 644–650. [CrossRef]
12. Anthony, G.M. Kinetic and Chemical Studies of Polymer Cross-Linking Using Thermal Gravimetry and Hyphenated Methods. Degradation of Polyvinylchloride. *Polym. Degrad. Stab.* **1999**, *64*, 353–357. [CrossRef]
13. O'Mara, M.M. Combustion of PVC. *Pure Appl. Chem.* **1977**, *49*, 649–660. [CrossRef]
14. Ballistreri, A.; Foti, S.; Maravigna, P.; Montaudo, G.; Scamporrino, E. Effect of metal oxides on the evolution of aromatic hydrocarbons in the thermal decomposition of PVC. *J. Polym. Sci. Polym. Chem. Ed.* **1980**, *18*, 3101–3110. [CrossRef]
15. Fenimore, C.P.; Martin, F.J. The Mechanisms of Pyrolysis, Oxidation, and Burning of Polymers. In *NBS Special Publication 357*; Wall, L.A., Ed.; Executive Agency: Brussels, Belgium, 1972; pp. 159–170. Available online: https://nvlpubs.nist.gov/nistpubs/Legacy/SP/nbsspecialpublication357.pdf (accessed on 1 June 2023).
16. Marcilla, A.; Beltrán, M. Kinetic models for the thermal decomposition of commercial PVC resins and plasticizers studied by thermogravimetric analysis. *Polym. Degrad. Stab.* **1996**, *53*, 251–260. [CrossRef]
17. Laoutid, F.; Bonnaud, L.; Alexandre, M.; Lopez-Cuesta, J.-M.; Dubois, P. New prospects in flame retardant polymer materials: From fundamentals to nanocomposites. *Mater. Sci. Eng. Rep.* **2009**, *63*, 100–125. [CrossRef]
18. Edelson, D.; Kuck, V.J.; Lum, R.M.; Scalco, E.; Starnes, W.H.; Kaufman, S. Anomalous behavior of molybdenum oxide as a fire retardant for polyvinyl chloride. *Combust. Flame* **1980**, *38*, 271–283. [CrossRef]
19. Pike, R.; Starnes, W.H.; Jeng, J.P.; Bryant, W.S.; Kourtesis, P.; Adams, C.W.; Bunge, S.D.; Kang, Y.M.; Kim, A.S.; Kim, J.H.; et al. Low-Valent Metals as Reductive Cross-Linking Agents: A New Strategy for Smoke Suppression of Poly(vinyl chloride). *Macromolecules* **1997**, *30*, 6957–6965. [CrossRef]
20. Li, B.; Wang, J. A Cone Calorimetric Study of Flame Retardance and Smoke Emission of PVC. I. The Effect of Cuprous and Molybdic Oxides. *J. Fire Sci.* **1997**, *15*, 341–357. [CrossRef]
21. Li, B. A study of the thermal decomposition and smoke suppression of poly(vinyl chloride) treated with metal oxides using a cone calorimeter at a high incident heat flux. *Polym. Degrad. Stab.* **2002**, *78*, 349–356. [CrossRef]
22. Morley, J.C.; Grossman, R.F. Flame Retardants and Smoke Suppressants. In *Handbook of Vinyl Formulating*, 2nd ed.; Grossman, R.F., Ed.; John Wiley & Sons Inc.: Hoboken, NJ, USA, 2007; pp. 403–414. [CrossRef]
23. Sarti, G. A New Perspective on Hydrogen Chloride Scavenging at High Temperatures for Reducing the Smoke Acidity of PVC Cables in Fires. I: An Overview of the Theory, Test Methods, and the European Union Regulatory Status. *Fire* **2022**, *5*, 127. [CrossRef]
24. Sarti, G. A New Perspective on Hydrogen Chloride Scavenging at High Temperatures for Reducing the Smoke Acidity of PVC Cables in Fires. II: Some Examples of Acid Scavengers at High Temperatures in the Condensed Phase. *Fire* **2022**, *5*, 142. [CrossRef]
25. *ASTM D 2863:2019*; Standard Test Method for Measuring the Minimum Oxygen Concentration to Support Candle-Like Combustion of Plastics (Oxygen Index). ASTM International: West Conshohocken, PA, USA, 2019. Available online: www.astm.org (accessed on 1 June 2023).
26. *ISO 5660-1:2015*; Reaction-to-Fire Tests—Heat Release, Smoke Production and Mass Loss Rate—Part 1: Heat Release Rate (Cone Calorimeter Method) and Smoke Production Rate (Dynamic Measurement). ISO: Geneva, Switzerland, 2015. Available online: https://www.iso.org/standard/57957.html (accessed on 1 June 2023).

27. *ASTM D 7309:2019*; Standard Test Method for Determining Flammability Characteristics of Plastics and Other Solid Materials Using Microscale Combustion Calorimetry. ASTM International: West Conshohocken, PA, USA, 2019. Available online: www.astm.org (accessed on 1 June 2023).
28. Kipouros, G.J.; Sadoway, D.R. A thermochemical analysis of the production of anhydrous $MgCl_2$. *J. Light Met.* **2001**, *1*, 111–117. [CrossRef]
29. Galwey, A.K.; Laverty, G.M. The thermal decomposition of magnesium chloride dihydrate. *Thermochim. Acta* **1989**, *138*, 115–127. [CrossRef]
30. Commercial PCC Purchased by Imerys. Available online: https://www.imerys-performance-minerals.com/system/files/2021-02/DATPCC_Winnofil_S_LSK_EN_2019-07.pdf (accessed on 1 June 2023).
31. *EN 60754-2:2014/A1:2020*; Test on Gases Evolved during Combustion of Materials from Cables—Part 2: Determination of Acidity (by pH Measurement) and Conductivity. CENELEC: Brussels, Belgium, 2020.
32. *EN 60754-1:2014/A1:2020*; Test on Gases Evolved during Combustion of Materials from Cables—Part 1: Determination of the Halogen Acid Gas Content. CENELEC: Brussels, Belgium, 2020.
33. *EN 138523:2022;* Reaction to Fire Tests for Building Products—Building Products Excluding Floorings Exposed to the Thermal Attack by a Single Burning Item. CEN: Brussels, Belgium, 2022. Available online: https://store.uni.com/en-13823-2020-a1-2022 (accessed on 1 June 2023).
34. Bassi, I. Characterization of PVC Compounds and Evaluation of Their Fire Performance, Focusing on the Comparison between EN 60754-1 and EN 60754-2 in the Assessment of the Smoke Acidity. Master's Thesis, University of Bologna, Bologna, Italy, 2021. Available online: https://www.pvc4cables.org/images/assessment_of_the_smoke_acidity.pdf (accessed on 1 June 2023).
35. Hirschler, M. Poly(vinyl chloride) and its fire properties. *FAM* **2017**, *41*, 993–1006. [CrossRef]
36. Babrauskas, V.; Richard, D. Peacock, Heat release rate: The single most important variable in fire hazard. *Fire Saf. J.* **1992**, *18*, 255–272. [CrossRef]
37. Sarti, G.; Piana, M. New formulations and test comparison for the classification of PVC cables under EU regulation n 305/2011 for construction products. In Proceedings of the AMI Cables 2019, Duesseldorf, Germany, 5–7 March 2019.
38. Sarti, G.; Piana, M. PVC cables and smoke acidity: A review comparing performances of old and new compounds. In Proceedings of the AMI Cables 2020, Duesseldorf, Germany, 3–5 March 2020.
39. DOT/FAA/TC-22/22 Federal Aviation Administration William, J. Hughes Technical Center Aviation Research Division Atlantic City International Airport New Jersey 08405. Final Report Microscale Flammability Criterion for Constituents of Aircraft Cabin Materials. 2022. Available online: https://www.fire.tc.faa.gov/pdf/TC22-22.pdf (accessed on 1 June 2023).
40. Sarti, G.; Piana, M. PVC in cables for building and construction. Can the "European approach" be considered a good example for other countries? *Acad. Lett.* **2022**, 5453. [CrossRef]

fire

MDPI

Article

A New Perspective on Hydrogen Chloride Scavenging at High Temperatures for Reducing the Smoke Acidity of PVC Cables in Fires V: Comparison between EN 60754-1 and EN 60754-2

Iacopo Bassi [1], Claudia Bandinelli [1], Francesca Delchiaro [1], Marco Piana [2] and Gianluca Sarti [1,*]

[1] Reagens S.p.A., Via Codronchi, 4, 40016 San Giorgio di Piano, Italy; iacopo.bassi@reagens-group.com (I.B.); claudia.bandinelli@reagens-group.com (C.B.); francesca.delchiaro@reagens-group.com (F.D.)
[2] PVC Forum Italia, Via Giovanni da Procida, 11, 20149 Milano, Italy; marcopiana@pvcforum.it
* Correspondence: gianluca.sarti@fastwebnet.it

Abstract: Regulation (EU) No 305/2011 lays down harmonized conditions for marketing construction products in the European Union. One of its consequences has been the introduction of the product standard EN 50575 and standard EN 130501-6, concerning power, control, and communication cables permanently installed in buildings to prevent the risk of a fire and its consequences. EN 13501-6 provides the reaction to fire classifications for cables, the test methods to be performed, the requirements to meet a specific reaction to fire, and additional classifications for smoke production, flaming droplets, and acidity. It requires EN 60754-2 as the technical standard to assess acidity, and it defines three classes: a_1, a_2, and a_3 (the less performant). Due to the release of hydrogen chloride during the combustion, acidity is the weak point of PVC cables, which are not yet capable of achieving the a_1 or a_2 classes required for specific locations according to fire risk assessments. EN 13501-6 does not include EN 60754-1, used in harmonized standards outside the scope of Regulation (EU) No 305/2011. EN 60754-1 and EN 60754-2 are common standards for determining halogen gas content, and acidity/conductivity, respectively. While they involve the same type of test apparatus, they differ in heating regimes, final temperatures, and detection methods. In particular, EN 60754-2 requires testing at temperatures between 935–965 °C in the tube furnace, where the sample burns, the smoke is collected in bubblers, and pH and conductivity are measured as an indirect assessment of acidity. On the other hand, the temperature regime of EN 60754-1 is a gradual heating run, followed by isothermal heating at 800 °C. The paper shows that when potent acid scavengers are used in PVC compounds, performing EN 60754-2 with the thermal profile of EN 60754-1 or at 500 °C in isothermal conditions, the evolution of hydrogen chloride changes significantly up to 10 times less than the test performed in isothermal at 950 °C. The reason lies behind the kinetic of hydrogen chloride release during the combustion of PVC compounds: the higher the temperature or faster the heat release, the quicker hydrogen chloride evolution and the lower the probability for the acid scavenger to trap it. Thus, these findings emphasize the "fragility" of EN 60754-2 as a tool for assessing risks associated with the release of hydrogen chloride during fires.

Keywords: acid scavengers; PVC; cables; smoke acidity; acidity; construction product regulation

Citation: Bassi, I.; Bandinelli, C.; Delchiaro, F.; Piana, M.; Sarti, G. A New Perspective on Hydrogen Chloride Scavenging at High Temperatures for Reducing the Smoke Acidity of PVC Cables in Fires V: Comparison between EN 60754-1 and EN 60754-2. *Fire* **2023**, *6*, 326. https://doi.org/10.3390/fire6080326

Academic Editors: Ying Zhang, Xiaoyu Ju, Xianjia Huang and Fuchao Tian

Received: 24 July 2023
Revised: 10 August 2023
Accepted: 16 August 2023
Published: 21 August 2023

1. Introduction

1.1. The Additional Classification for Acidity and the Role of Acid Scavengers

In the European Union (EU), cables permanently installed in buildings must also be classified for acidity, and current PVC cables cannot meet the most stringent classifications required in some locations. This paper shows how acid scavengers work at different temperatures and temperature regimes and how they impact technical standards based on tube furnaces for assessing the hydrogen chloride (HCl) released in the gas phase during the combustion of PVC compounds for cables. These kinds of research play a crucial role

in the competition with halogen-free cables, intending to protect and improve the market of PVC compounds for cables.

1.2. The Background. Regulatory Context and Test Methods for Assessing the Acidity

The regulatory framework of building and construction works is laid down by the Regulation (EU) No 305/2011 (Construction Products Regulation, or CPR) that sets harmonized rules for evaluating the requirements of items permanently installed in residential and public buildings, considering the impacts on the environment and people's health and safety [1]. According to CPR, one of the basic requirements of construction works is safety in case of fire. In this context, a harmonized classification regarding reaction to fire and additional classifications for smoke production, flaming droplets, and acidity have been adopted [2–4]. Flooring, linear insulation for pipes, panels, wall coverings, and other items commonly found in buildings do not require tests and requirements for assessing the release of acid gases in case of fire [2]. However, cables are the only building and construction products for which an additional classification for acidity is needed [3].

EN 13501-6 provides the test methods and requirements for evaluating the reaction to fire classification of cables and their additional classifications [3]. EN 60754-2, originally developed to determine the corrosivity, is the technical standard used for assessing the acidity according to CPR [5], with the methodology also explained in detail in [6,7]. It is carried out by burning 1 g of test specimen in a tube furnace. The effluents are then collected in two bubblers with double deionized water (DDW), where pH and conductivity are measured. Weighted pH and conductivity values for the cable are calculated considering the non-metallic material per unit length of the cable, according to paragraph 8.3 of the standard [5]. Class a_1 cable requires the pH to be more than 4.3 and the conductivity less than 2.5 μS/mm, class a_2 requires the pH to be more than 4.3, and the conductivity less than 10 μS/mm and class a_3 are those materials that are neither class a_1 nor class a_2.

EN 60754-2 is performed under isothermal conditions between 935 °C and 965 °C. On the other hand, EN 60754-1, the technical standard performed for determining the halogen acid gas content in contexts outside CPR [8], is carried out with this heating regime: 40 min from room temperature to 800 °C and 20 min in isothermal conditions at 800 °C. In EN 60754-1, temperature increases at about 20 °C/min, covering the typical temperatures of ignition and the developing stage of the fire, then exceeding the typical flashover temperatures (600–650 °C) [9], and finally reaching 800 °C.

It should be highlighted that EN 60754-2 and EN 60754-1 are bench-scale tests. They do not consider all variables of a real fire scenario that could affect the concentration of HCl in the gas phase.

1.3. Fire Hazards: The Role of Flame Retardants, Smoke Suppressants, and Acid Scavengers

Flame retardants and smoke suppressants are crucial in designing PVC compounds for cables capable of delaying flashover, and decreasing smoke production, to meet the main goals of fire safety strategy, i.e., the reduction of fatalities and injuries, conservation of property, protection of environment, preservation of heritage, and continuity of business operations in case of fire. For evaluating the performance of flame retardants and smoke suppressants, different external heat fluxes can be chosen in bench-scale fire tests [9–11], to understand how to reduce the fire hazard, strictly linked to parameters like ignitability, flammability, heat release (amount and rate), flame spread, smoke production, and its toxicity [12]. For example, in cone calorimetry, flame retardants and smoke suppressants are usually tested in external heat fluxes typical of pre-flashover stages of a fire [9]. Among the parameters mentioned above, the heat release rate is considered "the single most important variable in fire hazard" [13], while the toxicity of the effluents is dominated by carbon monoxide (CO) and HCl plays a minor role in fire safety [14].

When a PVC cable burns, HCl is released from the polymer's thermal decomposition; therefore, it is one of the effluents in case of fire. However, in a real fire scenario, its concentration in the gas phase decays, absorbed by common materials found in buildings [14].

This behavior has two consequences: the HCl concentration in the gas phase is less than expected, and HCl does not travel far from where the fire originates. The presence of acid scavengers at high temperatures in PVC compounds for cables can decrease further the concentration of HCl in the gas phase in case of fire, but their use can interfere with flame retardants and smoke suppressants' action, as explained in [15].

1.4. Acid Scavengers, Their Behavior at Different Temperatures and Novel Low Smoke Acidity PVC Compounds for Cables

Current PVC cables in the market can only meet class a_3. Thus, the research in new low-smoke acidity compounds is paramount for making PVC cables, working in specific locations where the best additional classifications for acidity are needed [6,16]. A new generation of low-smoke acidity PVC compounds has been recently developed with the aim of manufacturing cables to meet the best additional classifications for acidity [17–19]. Despite improving the acidity, they failed to meet the class a_1 or a_2. These compounds contain acid scavengers that act at high temperatures in the condensed phase, efficiently trapping HCl in the char and reducing its evolution in the gas phase.

However, the acid scavengers' efficiency drops significantly at temperatures over 900 °C, according to the theory and data exhaustively reported in Parts I and II of this article [6,7]. In fact, at 950 °C, trivial coated ground calcium carbonate (GCC) has more or less the same performances as the more performant acid scavenger used in that research. In summary, their performance in dropping down the smoke acidity is strictly linked to the efficiency of the acid scavengers, and the efficiency depends on the kinetics of scavenging and whether acid scavengers or their reaction products are stable in the range of temperatures where we need them to work. Therefore, as described in [6], temperatures, heating regimes, and the chemical nature of the acid scavengers play a crucial role in their efficiency. Also, the acid scavengers' particle size and the dispersion level they can reach in the matrix, getting as much as possible intimate contact with PVC chains is paramount. Hence, the research in novel low-smoke acidity compounds at the laboratory level will be decisive, but the right choice of production systems able to reach a high dispersion level for acid scavengers will also be crucial. Cable manufacturers willing to do research aiming to produce PVC cables in class a_1 or a_2 must consider all these variables.

1.5. The Impact of Acid Scavengers when EN 60754-2 Is Run at Different Thermal Profiles

EN 60754-2 is run isothermally at temperatures between 935 °C and 965 °C. It is interesting and never shown before to see what happens when it is performed with different heating regimes in the presence and absence of acid scavengers to see their impacts when gradual heating runs are used or when isothermal temperatures below the flashover are applied. That emphasizes if the acid scavengers can show good efficiency at the temperatures typical of the stages of fires when a safe escape is possible.

1.6. The Aim of the Research

In this article, the acidity of several PVC compounds for cables has been tested by comparing the following test methods:

(1) EN 60754-2 has been carried out isothermally at 950 °C, and EN 60754-2 with the heating regime of EN 60754-1 (internal method 3).
(2) EN 60754-2 has been conducted at isothermally 950 °C, and EN 60754-2 isothermally at 500 °C (internal method 2).

The heating regime of EN 60754-1 is as follows: 40 min to 800 °C from room temperature and further heating of 20 min at 800 °C.

The aim has been to verify if different heating regimes could affect the concentration of HCl in the gas phase and to explore the role of the HCl scavengers in this context. In particular, it has been evaluated whether the acidity is reduced when the heating regime of EN 60754-1 is run and a pre-flashover temperature of 500 °C is chosen.

The high temperatures acid scavengers used in this research act in the condensed phase.

In this paper, "acidity" and "smoke acidity" are considered interchangeable terms.

The subsequent sections of this paper present the experimental material and methods, results, and discussion, followed by the conclusion and implications.

2. Materials and Methods

2.1. Materials

The tested formulations have been divided into four series to verify if the internal methods 2 and 3 give different results from EN 60754-2. Table 1 displays the first series and intends to show the impact of different acid scavengers at high temperatures on acidity, performing EN 60754-2, internal methods 2 and 3. FR50.0 is a typical PVC compound for non-flame retarded jackets, with a coated GCC with a low HCl scavenging efficiency like Riochim [20]. FR50.1 contains a synthetic $Al(OH)_3$ (ATH, from Nabaltec, Schwandorf, Germany), an inert acid scavenger, which does not reduce smoke acidity. FR50.2 has $Mg(OH)_2$ (MDH, from Europiren, Schiedam, The Netherlands) as uncoated brucite, an ineffective acid scavenger fixing HCl as $MgCl_2$ but then rereleasing it due to its decomposition [6,7,21,22]. FR50.3 includes coated ultrafine precipitated calcium carbonate (UPCC), Winnofil S from Imerys [23], a potent acid scavenger which efficiently captures HCl as $CaCl_2$ in a single-step reaction, currently used for reducing the acidity of the PVC compounds' effluents in case of fire [6,7]. FR50.4 and FR50.5 show the action of two potent acid scavengers from Reagens, AS-1B and AS-6B. They are the new generation of acid scavengers at high temperatures, acting in the condensed phase.

Table 1. First series of formulations: DINP means Di Iso Nonyl Phthalate. ESBO stands for Epoxidized Soy Bean Oil. The used antioxidant is Arenox A10, which is Pentaerythritol tetrakis(3-(3,5-di-tert-butyl-4-hydroxyphenyl)propionate), CAS number 6683-19-8. COS stands for Calcium Organic Stabilizer. UPCC means Ultrafine Precipitated Calcium Carbonate. HTAS stands for High Temperature Acid Scavengers.

Raw Materials	Trade Name	FR50.0 [phr]	FR50.1 [phr]	FR50.2 [phr]	FR50.3 [phr]	FR50.4 [phr]	FR50.5 [phr]
PVC	Inovyn 271 PC	100	100	100	100	100	100
DINP	Diplast N	50	50	50	50	50	50
ESBO	Reaflex EP/6	2	2	2	2	2	2
Antioxidant	Arenox A10	0.1	0.1	0.1	0.1	0.1	0.1
COS	RPK B-CV/3037	3	3	3	3	3	3
$CaCO_3$	Riochim	90	0	0	0	0	0
$Al(OH)_3$	Apyral 40 CD	0	90	0	0	0	0
$Mg(OH)_2$	Ecopyren 3.5	0	0	90	0	0	0
UPCC	Winnofil S	0	0	0	90	0	0
HTAS 1	AS-1B	0	0	0	0	90	0
HTAS 2	AS-6B	0	0	0	0	0	90

Tables 2–4 show typical formulations with low values of acidity, where acid scavengers work in multiple-step reactions in fixing HCl in the condensed phase. These kinds of reactions are explained in [6,7]. The primary and secondary acid scavengers are dosed in different ratios giving different scavenging efficiencies, and the impacts on the measurements carried out with EN 60754-2 and internal 3 are evaluated. RPK B-NT/8014 is an anti-pinking additive from Reagens commonly used to switch off discoloration when large quantities of MDH are introduced in PVC compounds. AS0-B is a potent acid scavenger produced by Reagens. Cabosil H5 is a fumed silica from Cabot, RI004 antimony trioxide from Quimialmel, and Kisuma 5A, a synthetic coated MDH produced by Kisuma.

Table 2. Second series of formulations: DINP means Di Iso Nonyl Phthalate. ESBO stands for Epoxidized Soy Bean Oil. The used antioxidant is Arenox A10, which is Pentaerythritol tetrakis(3-(3,5-di-tert-butyl-4-hydroxyphenyl)propionate), CAS number 6683-19-8. COS stands for Calcium Organic Stabilizer. HTAS means High Temperature Acid Scavengers.

Raw Materials	Trade Name	FR50.6 [phr]	FR50.7 [phr]	FR50.8 [phr]	FR950.9 [phr]
PVC	Inovyn 271 PC	100.0	100.0	100.0	100.0
DINP	Diplast N	50.0	50.0	50.0	50.0
ESBO	Reaflex EP/6	2.0	2.0	2.0	2.0
$Mg(OH)_2$	Kisuma 5A	30.0	30.0	30.0	30.0
Antioxidant	Arenox A10	0.1	0.1	0.1	0.1
COS	RPK B-CV/3037	3.0	3.0	3.0	3.0
HTAS 1	AS-1B	123.0	123.0	0.0	0.0
HTAS 2	AS-6B	0.0	0.0	123.0	123.0
Anti Pinking	RPK B-NT/8014	0.0	6.0	0.0	6.0

Table 3. Third series of formulations: DINP means Di Iso Nonyl Phthalate. ESBO stands for Epoxidized Soy Bean Oil. The used antioxidant is Arenox A10, which is Pentaerythritol tetrakis(3-(3,5-di-tert-butyl-4-hydroxyphenyl)propionate), CAS number 6683-19-8. COS stands for Calcium Organic Stabilizer. UPCC means Ultrafine Precipitated Calcium Carbonate. HTAS High Temperature Acid Scavenger.

Raw Materials	Trade Name	FR50.10 [phr]	FR50.11 [phr]	FR50.12 [phr]	FR950.13 [phr]
PVC	Inovyn 271 PC	100.0	100.0	100.0	100.0
DINP	Diplast N	50.0	50.0	50.0	50.0
ESBO	Reaflex EP/6	2.0	2.0	2.0	2.0
Antioxidant	Arenox A10	0.1	0.1	0.1	0.1
COS	RPK B-CV/3037	3.0	3.0	3.0	3.0
$Mg(OH)_2$	Kisuma 5A	30.0	30.0	30.0	30.0
UPCC	Winnofil S	90.0	90.0	0.0	0.0
Fumed Silica	Cabosil H5	0.0	15.0	0.0	15.0
HTAS 3	AS-0B	0.0	0.0	123.0	123.0

Table 4. Forth series of formulations: DINP means Di Iso Nonyl Phthalate. ESBO stands for Epoxidized Soy Bean Oil. The used antioxidant is Arenox A10, which is Pentaerythritol tetrakis(3-(3,5-di-tert-butyl-4-hydroxyphenyl)propionate), CAS number 6683-19-8. COS stands for Calcium Organic Stabilizer. ATO means antimony trioxide and HTAS High Temperature Acid Scavenger.

Raw Materials	Trade Name	FR50.14 [phr]	FR50.15 [phr]	FR50.16 [phr]	FR50.17 [phr]
PVC	Inovyn 271 PC	100.0	100.0	100.0	100.0
DINP	Diplast N	50.0	50.0	50.0	50.0
ESBO	Reaflex EP/6	2.0	2.0	2.0	2.0
$Mg(OH)_2$	Ecopyren 3.5	30.0	30.0	30.0	30.0
Antioxidant	Arenox A10	0.1	0.1	0.1	0.1
COS	RPK B-CV/3037	3.0	3.0	3.0	3.0
ATO	RI004	10.0	10.0	10.0	10.0
$CaCO_3$	Riochim	0.0	0.0	0.0	65.0
HTAS 1	AS-1B	123.0	0.0	0.0	0.0
HTAS 2	AS-6B	0.0	123.0	0.0	0.0
HTAS 3	AS-0B	0.0	0.0	123.0	0.0

EN 60754-2 and internal methods 2 and 3 use DDW internally produced by the ion exchange deionizer in Table 5 with the quality according to the standard (pH between

5.50 and 7.50, and conductivity less than 0.5 μS/mm). Buffer and conductivity standard solutions from VWR International are the following:

- pH: 2.00, 4.01, 7.00, and 10.00,
- conductivity: 2.0, 8.4, 14.7, 141.3 μS/mm

2.2. Test Apparatuses

Table 5 gives the employed test apparatuses.

Table 5. Main test apparatuses utilized.

Test Apparatus	Producer	Model	Additional Info's
Torque Rheometer	Brabender	Plastograph EC	50 CC chamber, 30 rpm, 60 g sample mass, 160 °C per 10 min.
Halogen Acid Gas test apparatus	SA Associates	Standard model	Porcelain combustion boats.
Multimeter	Mettler Toledo	S213 standard kit	
Conductivity electrode	Mettler Toledo	S213 standard kit	Reference thermocouple adjusting temperature fluctuation.
pH electrode	Mettler Toledo	S213 standard kit	Reference thermocouple adjusting temperature fluctuation.
Ion Exchange Deionizer	Culligan Pharma	System 20	

2.3. Sample Preparation

The formulations in Tables 1–4 were prepared in a turbo mixer, making the dry blends and then processing them in a torque rheometer. Dry blends were produced as follows. PVC and all additives, except plasticizer, were mixed up to 80 °C. Then plasticizer was added slowly until its complete "absorption." When the temperature reached 105 °C, the dry blend was unloaded in PE bags and left there for a full "maturation" of 24 h, then, 60 g of the dry blend were processed in the torque rheometer for 10 min Appendix A in Figures A1 and A2 details sample preparation, test apparatuses, and conditions.

The test specimens for EN 60754-2 and internal methods 2 and 3 have been derived from the kneaders.

2.4. Internal Tests and International Technical Standards Used

Table 6 shows the technical standards and the main utilized conditions.

Table 6. Tests for assessing acidity.

Technical Standard	Measurement	Temperature	Note
EN 60754-2	pH and conductivity	Isothermal at 950 °C	The general method, according to the 2014 version.
Internal method 2	pH and conductivity	Isothermal at 500 °C	The general method, according to the 2014 version.
Internal method 3	pH and conductivity	23–800 °C in 40 min 800 °C per 20 min	EN 60754-2 carried out with the thermal profile of EN 60754-1

The procedures and the precautions in performing EN 60754-2 and internal methods 2 are described in detail in the technical standard [5], and Parts I and II of this paper [6,7].

Internal method 3 follows this specific procedure: an empty combustion boat is introduced into the tube furnace through the sample carrier. The airflow is set between 290 and 310 mL/min, depending on the quartz tube geometry. The thermocouple is placed at the center of the tube furnace, the initial ramp is chosen, the heater is started, and the time is measured with a stopwatch. The ramp is selected to reach 800 ± 10 °C in 40 ± 5 min and to maintain an isothermal condition of 800 ± 10 °C for 20 ± 1 min. The heating rate is adjusted accordingly if temperatures and times exceed the above ranges. The conductivity of the water in the bubblers is checked to verify the possibility of contamination from previous tests. After determining the quartz tube's heating regime and cleaning status, the sample is weighed in the combustion boat (1.000 ± 0.001 g of material) and introduced into the tube furnace at room temperature through the sample carrier. The

heater is switched on, and the stopwatch monitors the ramp. After 1 h, the connectors are opened, the water from the bubbling devices and washing procedures is collected in a 1 L volumetric flask filled to the mark, and then pH and conductivity are measured as follows. The multimeter is calibrated with standard solutions before each measurement. The pH is calibrated at two points (4.01 and 7.00) while conductivity is at 1 point at 141.3 μS/mm. Then pH and conductivity of the quotes from the flask are measured. The solutions closer to the measured values are used as correction standards, and the measurements are corrected accordingly. pH and conductivity electrodes have a reference thermocouple that adjusts the temperature fluctuation. The method measures three replicates to calculate the mean value, standard deviation (SD), and coefficient of variation (CV).

Appendix A, Figures A1 and A2 provide a schematic diagram of the sample preparation, conditions, and testing process.

Supplementary Materials file provides additional information regarding materials (Table S1), test apparatuses (Table S2), and standards (Table S3) in Section S1, sample preparation in Section S2, and test procedures in Section S3.

3. Results

Tables 7–9 show pH and conductivity of the formulations in Table 1 measured according respectively to EN 60754-2 at 950 °C, internal methods 3 and 2.

Table 7. pH and conductivities of the formulation in Table 1, according to EN 60754-2 at 950 °C. The mean values, standard deviations, and coefficient of variation are reported.

Formulation	FR50.0	FR50.1	FR50.2	FR50.3	FR50.4	FR50.5
pH	2.62	2.27	2.27	2.74	2.89	2.79
SD_{pH}	0.03	0.10	0.02	0.06	0.08	0.02
CV_{pH} [%]	1.15	4.41	0.88	2.19	2.77	0.72
Conductivity [μS/mm]	97.3	221.5	224.3	74.0	70.1	70.1
SDc	3.7	8.4	3.1	1.6	0.7	2.0
CVc [%]	3.8	3.8	1.4	2.2	1.0	2.9

Table 8. pH and conductivity of the formulation in Table 1, according to internal method 3. The mean values, standard deviations, and coefficient of variation are reported.

Formulation	FR50.0	FR50.1	FR50.2	FR50.3	FR50.4	FR50.5
pH	2.51	2.29	2.28	3.32	3.56	3.29
SD_{pH}	0.02	0.04	0.02	0.00	0.00	0.02
CV_{pH} [%]	0.80	1.75	0.88	0.00	0.00	0.61
Conductivity [μS/mm]	135.7	224.7	228.0	25.5	11.6	22.8
SDc	4.4	6.1	1.5	0.7	0.2	0.1
CVc [%]	3.2	2.7	0.7	2.7	1.7	0.4

Table 9. pH and conductivity of the formulation in Table 1, according to internal method 2 at 500 °C. The mean values, standard deviations, and coefficient of variation are reported.

Formulation	FR50.0	FR50.1	FR50.2	FR50.3	FR50.4	FR50.5
pH at 500 °C	2.48	2.41	2.41	3.73	3.70	3.69
SD_{pH}	0.04	0.03	0.09	0.10	0.15	0.13
CV_{pH} [%]	1.61	1.24	3.73	2.68	4.05	3.52
Conductivity at 500 °C [μS/mm]	139.1	177.2	177.3	7.7	8.2	8.6
SDc	1.2	2.5	6.2	0.3	0.4	0.3
CVc [%]	0.9	1.4	3.5	3.9	4.9	3.5

Table 10 gives the pH and conductivity of the formulations in Table 2 measured according to EN 60754-2 at 950 °C. Table 11 pH and conductivity performing internal method 3.

Table 10. pH and conductivity of formulations in Table 2, according to EN 60754-2 at 950 °C. The mean values, standard deviations, and coefficient of variation are reported.

Formulation	FR50.6	FR50.7	FR50.8	FR50.9
pH	4.17	4.18	4.31	4.14
SD_{pH}	0.08	0.11	0.07	0.17
CV_{pH} [%]	1.92	2.63	1.62	4.11
Conductivity [μS/mm]	3.2	2.8	2.5	3.9
SDc	0.1	0.4	0.1	1.0
CVc [%]	3.1	14.3	4.0	25.6

Table 11. pH and conductivities of formulations in Table 2, according to internal method 3. The mean values, standard deviations, and coefficient of variation are reported.

Formulation	FR50.6	FR50.7	FR50.8	FR50.9
pH	4.29	4.46	4.73	4.44
SD_{pH}	0.01	0.09	0.35	0.28
CV_{pH} [%]	0.23	2.02	7.40	6.31
Conductivity [μS/mm]	1.8	1.8	1.3	2.3
SDc	0.0	0.4	0.3	0.7
CVc [%]	0.0	22.2	23.1	30.4

Table 12 brings the pH and conductivity of the formulations in Table 3 measured according to EN 60754-2 at 950 °C. Table 13 gives pH and conductivity obtained by performing internal method 3.

Table 12. pH and conductivity of formulations in Table 3, according to EN 60754-2 at 950 °C. The mean values, standard deviations, and coefficient of variation are reported.

Formulation	FR50.10	FR50.11	FR50.12	FR50.13
pH	3.29	3.12	3.65	3.69
SD_{pH}	0.01	0.06	0.17	0.07
CV_{pH} [%]	0.30	1.92	4.66	1.90
Conductivity [μS/mm]	24.2	34.3	11.0	8.1
SDc	2.1	2.3	3.9	2.1
CVc [%]	8.7	6.8	35.2	25.9

Table 13. pH and conductivity of formulations in Table 3, according to internal method 3. The mean values, standard deviations, and coefficient of variation are reported.

Formulation	FR50.10	FR50.11	FR50.12	FR50.13
pH	4.10	3.62	4.33	4.35
SD_{pH}	0.04	0.06	0.07	0.08
CV_{pH} [%]	0.98	1.66	1.62	1.84
Conductivity [μS/mm]	3.9	10.7	2.1	2.0
SDc	0.3	1.6	0.7	0.2
CVc [%]	7.7	15.0	33.3	10.0

Table 14 shows the pH and conductivity of the formulations in Table 4 measured according to EN 60754-2 at 950 °C. Table 15 displays the pH and conductivities, performing internal method 3.

Table 14. pH and conductivities of formulation in Table 4, according to EN 60754-2 at 950 °C. The mean values, standard deviations, and coefficient of variation are reported.

Formulation	FR50.14	FR50.15	FR50.16	FR50.17
pH	4.18	4.20	4.03	2.63
SD_{pH}	0.08	0.09	0.08	0.10
CV_{pH} [%]	1.91	2.14	1.99	3.80
Conductivity [μS/mm]	3.0	3.2	4.0	92.8
SDc	0.5	0.2	0.5	3.2
CVc [%]	16.7	6.3	12.5	3.4

Table 15. pH and conductivities of formulation in Table 4, according to internal method 3. The mean values, standard deviations, and coefficient of variation are reported.

Formulation	FR50.14	FR50.15	FR50.16	FR50.17
pH	4.31	4.59	4.62	2.66
SD_{pH}	0.01	0.01	0.02	0.07
CV_{pH} [%]	0.23	0.22	0.43	2.63
Conductivity [μS/mm]	1.7	1.1	1.1	91.6
SDc	0.0	0.1	0.1	0.9
CVc [%]	0.0	9.1	9.1	1.0

4. Discussion

Figure 1a,b compares pH and conductivity achieved by formulations FR50.0–FR50.5 of Table 1 (results reported in Tables 7 and 8) when performing EN 60754-2 at 950 °C and internal method 3. FR50.0, representing a typical non-flame retarded PVC jacket compound for cables, contains a GCC, which is a grade not actually good as an acid scavenger. Internal method 3 and EN 60754-2 differ slightly in pH and conductivity. In particular, for FR50.0, EN 60754-2 only shows a slightly better smoke acidity compared to internal method 3. The phenomenon has been observed in Ref. [7], probably due to the formation of CaO, which more likely occurs at 950 °C than in the heating conditions of EN 60754-1. However, this effect disappears as particle size decreases and $CaCO_3$ increases its efficiency.

FR50.1 and FR50.2, containing ATH and MDH, respectively an inert and an ineffective acid scavenger, show high and comparable smoke acidity with both methods. Hence, the results obtained for FR50.0, FR50.1, and FR50.2 indicate that internal method 3 and EN 60754-2 work similarly when formulations are free of efficient acid scavengers. Nevertheless, the behavior in FR50.3, FR50.4, and FR50.5 is different. All these formulations contain potent acid scavengers at high temperatures that act in the condensed phase. In this case, the differences between the two heating regimes are significant, with EN 60754-2 showing rather higher smoke acidity than internal method 3.

Figure 2a,b compares the pH and conductivity achieved by formulations FR50.6–FR50.9 of Table 2 (results reported in Tables 10 and 11 when performing internal method 3 and EN 60754-2). In this case, the measurements concern the effect on acidity from AS-1B and AS-6B, which are potent acid scavengers at high temperatures, in combination with synthetic MDH. The compounds have high pH and low conductivity, and internal method 3 clearly shows low acidity, confirming the behavior of the samples FR50.3–FR50.5 in Table 1, which also contain potent acid scavengers. It is essential to highlight that as soon as the conductivity reaches values below 10 μS/mm, obtaining values with less than 5% of the coefficient of variation, as requested by EN 60754-2 (Tables 10 and 11), becomes complex. In fact, the standard has many manual procedures and other sources of errors, exhaustively

explained in [6,7], severely affecting the small values of the conductivity obtained with these formulations.

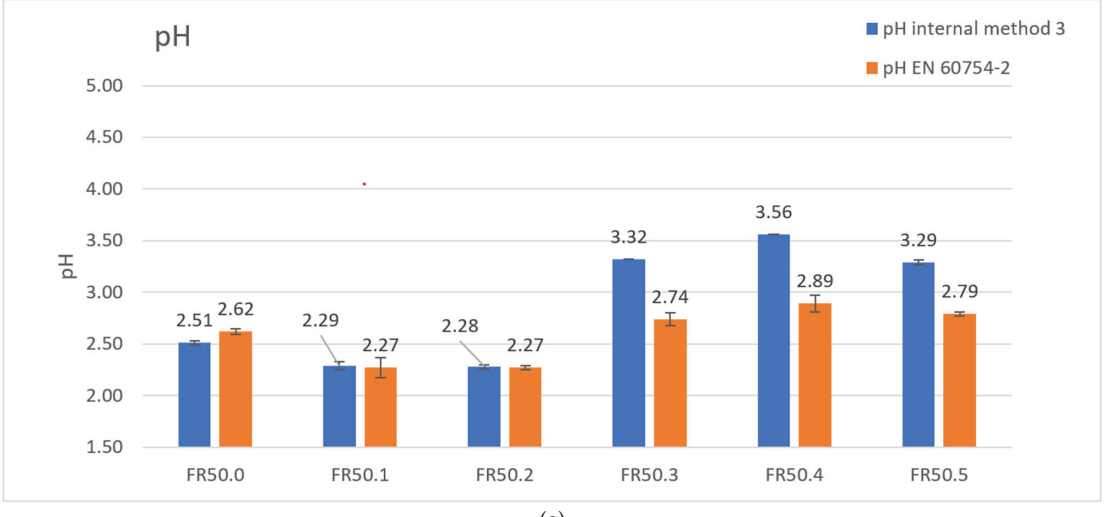

(**a**)

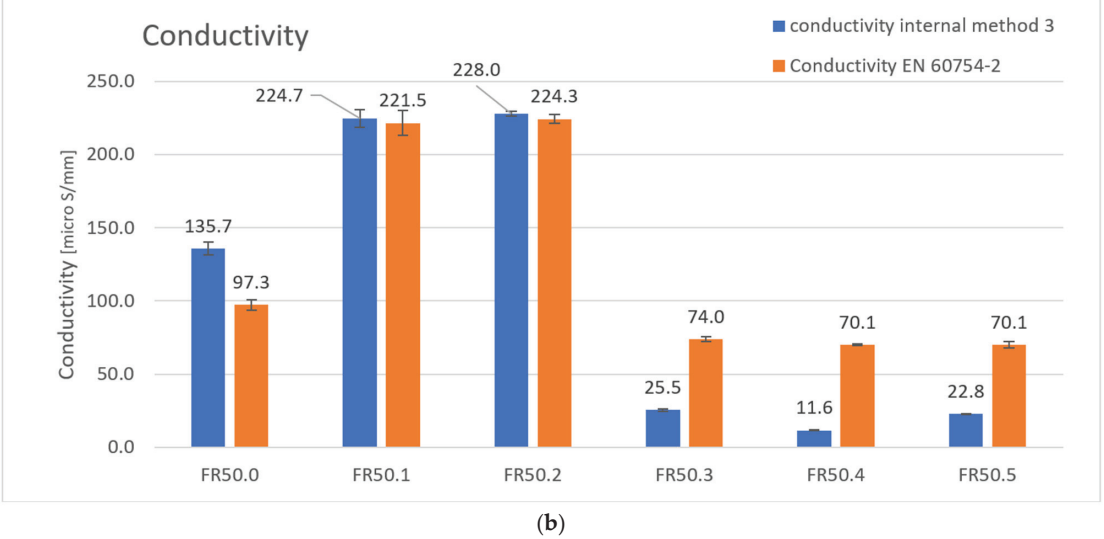

(**b**)

Figure 1. Comparison of pH (**a**) and conductivity (**b**) of formulations FR50.0–FR50.5 measured with internal method 3 (blue bars) and EN 60754-2 (orange bars). SD is reported. FR50.0–FR50.2 without efficient acid scavengers, FR50.3–FR50.5 with efficient acid scavengers.

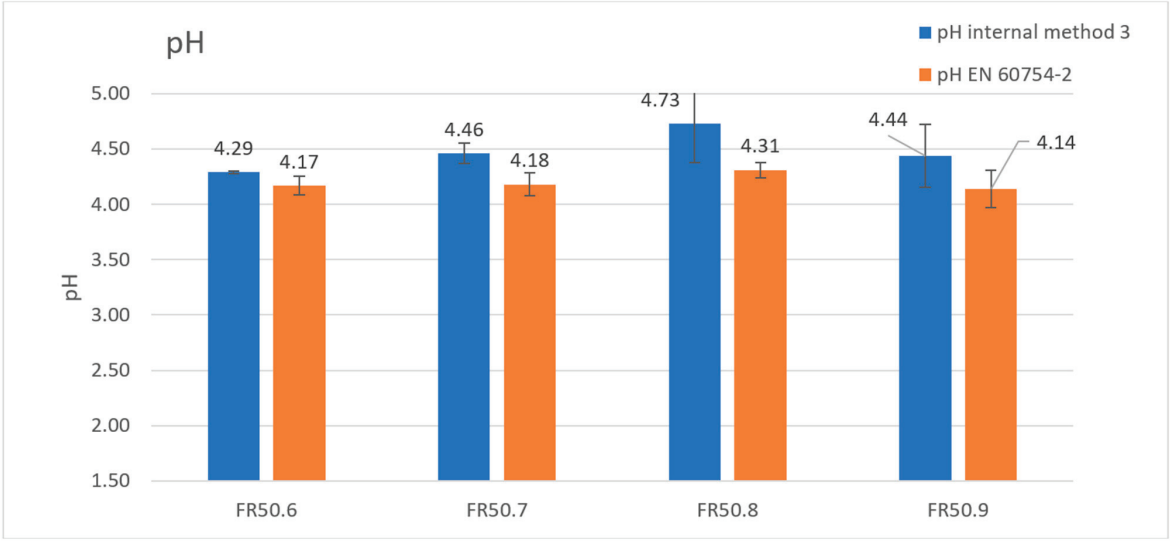

(**a**)

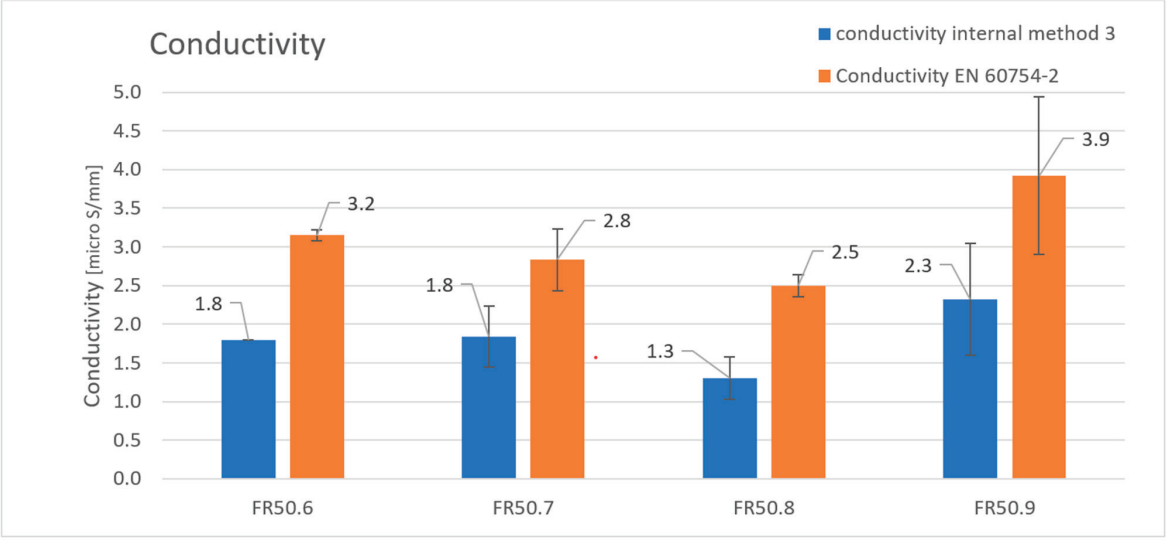

(**b**)

Figure 2. Comparison of pH (**a**) and conductivity (**b**) of formulations FR50.6–FR50.9 measured with internal method 3 (blue bars) and EN 60754-2 (orange bars). SD is reported.

Figure 3a,b compares the pH and conductivity achieved by formulations FR50.10–FR50.13 of Table 3 (results reported in Tables 12 and 13), performing internal method 3 and EN 60754-2 at 950 °C. In this set of formulations, UPCC and AS-0B, potent acid scavengers at high temperatures, are tested in combination with synthetic MDH, Kisuma 5A, and fumed silica. All formulations show extremely low acidity, reflecting the synergistic effect of UPCC and AS-0B with MDH in multiple-step reactions, as described in [6,7]. AS-0B behaves better than UPCC. The use of fume silica, aiming to help the dispersion, is unsuccessful.

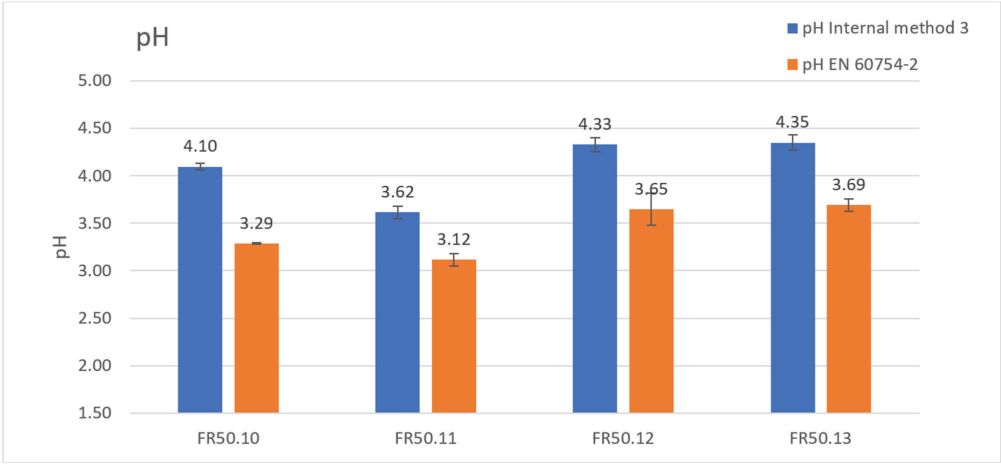

(**a**)

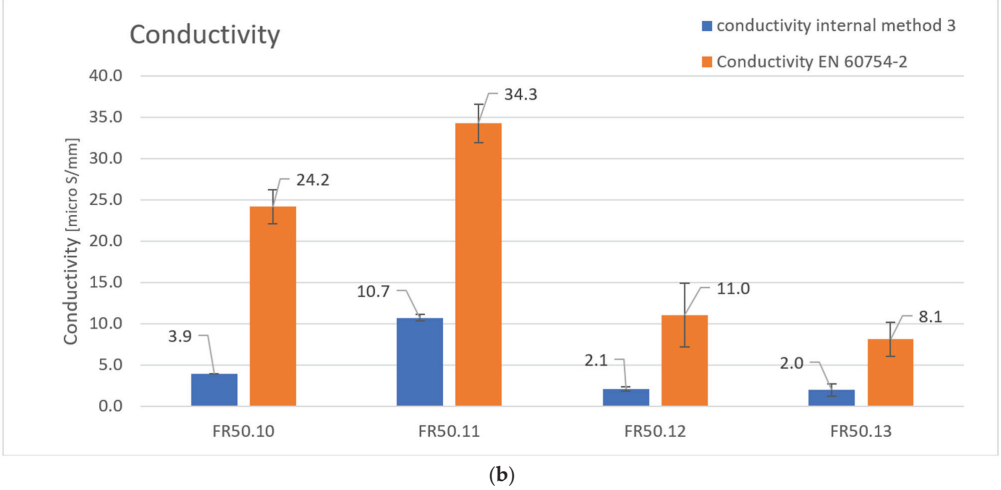

(**b**)

Figure 3. Comparison of pH (**a**) and conductivity (**b**) of formulations FR50.10–FR50.13 measured with internal method 3 (blue bars) and EN 60754-2 (orange bars). SD is reported.

As for the formulations of the first two series (Tables 1 and 2), internal method 3 and EN 60754-2 again show significant differences due to the different temperature regimes and final temperatures, with EN 60754-2 measuring higher acidity than internal method 3.

Figure 4a,b compares the pH and conductivity achieved by formulations FR50.14–FR50.17 of Table 4 (results reported in Tables 14 and 15), performing internal method 3 and EN 60754-2 at 950 °C. In this series, AS-0B, AS-1B, and AS-6B, potent acid scavengers at high temperatures, are tested with milled brucite (FR50.14, FR50.15, and FR50.16). As with synthetic MDH, with brucite, the smoke acidity is also low, suggesting its synergistic effect between AS-0B, AS-1B, and AS-6B. Again, the internal method 3 and EN 60754-2 differences are considerable. On the other hand, FR50.17 is a typical CPR jacket compound used for matching the classification Cca s3 d1 a3 in PVC cables. Figure 4a,b and Tables 14 and 15 show that the new low-smoke acidity compounds exhibit acidity values of some orders below standard grade compounds for cable currently on the market. In this last case, being

the compound free of potent acid scavengers, internal method 3 and EN 60754-2 give comparable measurements in terms of pH and conductivity.

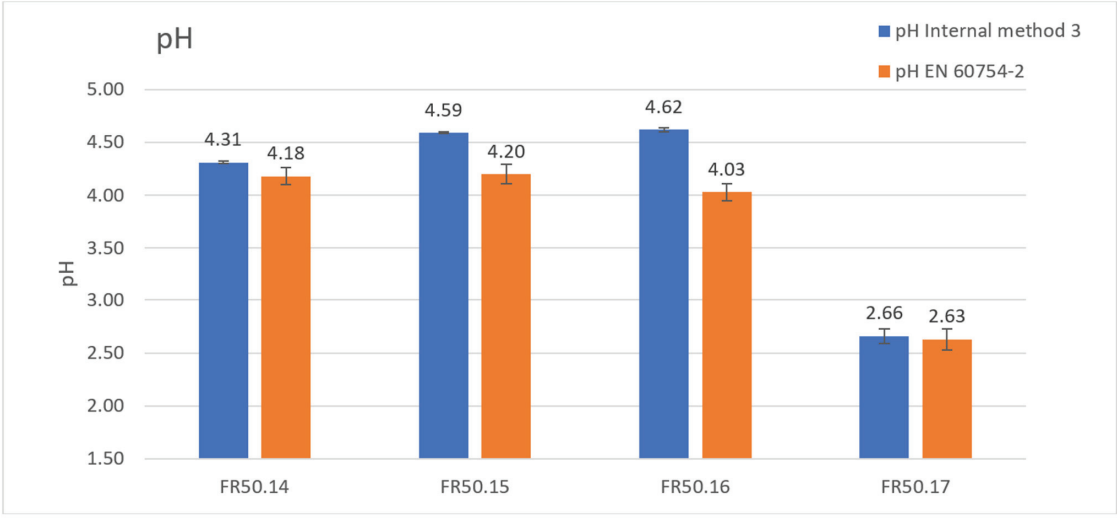

(**a**)

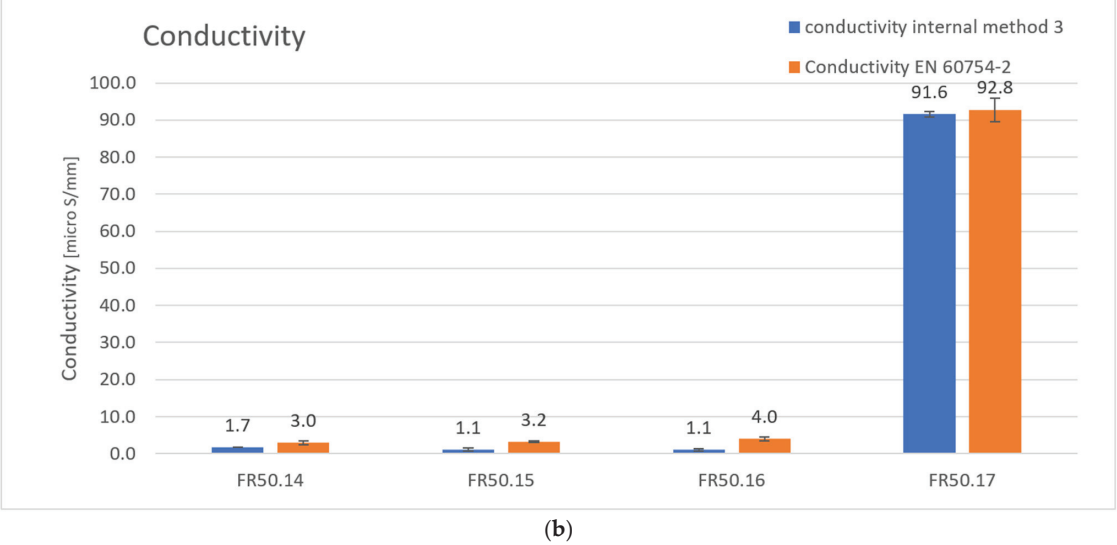

(**b**)

Figure 4. Comparison of pH (**a**) and conductivity (**b**) of formulations FR50.14–FR50.17 measured with internal method 3 (blue bars) and EN 60754-2 (orange bars). SD is reported.

Figure 5a,b compares the pH and conductivity (Table 9) achieved by formulations FR50.0–FR50.5 of Table 1, performing internal method 2 and EN 60754-2. The measurements have been performed in isothermal conditions, respectively, at 500 °C and 950 °C and clearly show that applying a lower temperature of 500 °C, in the presence of effective acid scavengers, the HCl in the gas phase is highly reduced (see FR50.3–FR50.5). The behavior of FR50.0 in isothermal conditions at 500 °C resembles that observed with the internal method 3. The formation of CaO at 500 °C is unlike, and the efficiency at 950 °C is higher.

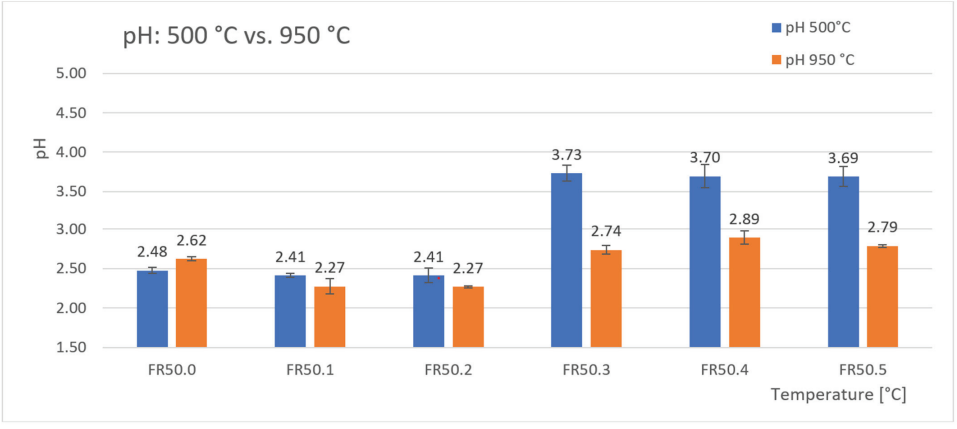

(**a**)

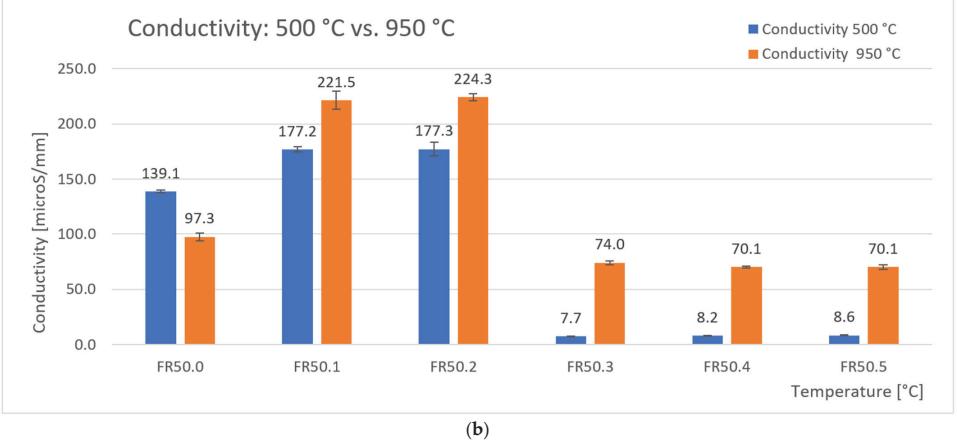

(**b**)

Figure 5. Comparison of pH (**a**) and conductivity (**b**) of formulations FR50.0–FR50.5 measured with internal method 2 at 500 °C (blue bars) and EN 60754-2 (orange bars) at 950 °C. SD is reported.

All these data clearly indicate that if a powerful acid scavenger has time to react with HCl, as it happens at lower temperatures (internal method 2, isothermal) and lower temperatures with a slower heating regime (internal method 3), it can trap HCl in the condensed phase with higher efficiencies. On the other hand, the higher temperatures and fast heating regimes of EN 60754-2 hinder its action: the acid scavenger at high temperatures cannot compete with the rapid HCl evolution during PVC compound combustion, and HCl escapes quickly into the gas phase, decreasing the pH and increasing the conductivity of the solutions in the bubblers. In the absence of effective acid scavengers, both standards show comparable values.

The interference of heating regimes and final temperatures in tube furnace tests for determining HCl was well explained in [24] in 1986. Here Chandler, Hirschler, and Smith highlighted that humidity, soot formation, dimensions of the combustion boat, and temperature regimes could affect the results of the method. In the paper, the acid scavenger in PVC compounds was $CaCO_3$, but no information regarding its particle size was given. Isothermal conditions at 650 °C, 700 °C, 800 °C and 950 °C were applied, showing an increase in the emission of HCl as temperature increases. The scavenging efficiency in isothermal was also lower than performing a temperature gradient of 10 °C per minute. All these aspects confirmed that $CaCO_3$, as an acid scavenger, suffers from high temperatures and fast heating rates. They justified the behavior with these specific phrases.

"*It is clear that the higher the temperature at which the tube furnace test is carried out, the higher the HC1 emission will be*".

"*The lower efficiency during isothermal runs (after 3 weight loss stages) than during gradual heating runs. . .., coupled with the fact that there is a significantly larger weight loss in the first stage of the isothermal runs, indicates that there is a much greater likelihood of HCI being emitted before it has had the opportunity of reacting with the filler*".

The acid scavengers used in our paper, currently used such as UPCC or novel such as AS-XB series, confirm the same behavior with a collapse of their efficiencies as temperature increases and when the heating regime accelerates.

5. Conclusions

Acidity is the weak point of PVC, and currently, no PVC cables can meet classes a_1 or a_2, performing EN 60754-2. For this reason, the research on novel acid scavengers capable of decreasing acidity is crucial. In this context, exploring different heating regimes in EN 60754-2 in the presence and absence of acid scavengers is also interesting, particularly when performed with the milder heating regime of EN 60754-1 and in isothermal conditions below flashover (500 °C).

The paper actually highlighted that when an acid scavenger, acting in the condensed phase at high temperatures, is added to the PVC compound, EN 60754-2 performed at 950 °C assesses higher smoke acidity than internal method 3, with a heating regime up to 800 °C. On the contrary, if acid scavengers are absent, inert, or ineffective, both tests show comparable acidity values. Depending on the acid scavengers in the formulations, the gap between EN 60754-2 and internal 3 can become significant. For example, in Figure 1b, FR50.3 gives a value about 3 times lower in conductivity when the gradual heating regime of EN 60754-1 is set, becoming even about 10 times less when EN 60754-2 is run isothermally at 500 °C, using internal method 2 (Figure 5b). This gap is evident for an acid scavenger, such as UPCC, commonly used in PVC compounds for cables to reduce the effluents' acidity in many standards out of the scope of CPR and also for the novel acid scavengers (AS-XB series) studied in this paper in several kinds of formulations.

This behavior confirms what [7] reports, where the efficiencies of some acid scavengers were measured in isothermal conditions at different temperatures. What speeds up the evolution of HCl, such as high temperatures and quick heating regimes, hinders the action of the acid scavengers during PVC compound combustion. Therefore, acid scavengers cannot trap HCl released quickly in the gas phase, increasing the effluents' acidity. Thus, the higher the temperature or faster the heating regime, the quicker the evolution and lower the probability of acid scavenger trapping HCl, as shown also in [24,25].

It must be highlighted that room fires can have different stages with different temperatures and heat flows. Temperatures can rise from 300 °C to 600 °C in the ignition and developing fire stages, capable of reaching from 650 °C up to 1100 °C in the fully developed stage [9,11]. As emerged in this paper and [7], the temperatures and heating regime of EN 60754-2 obliterate entirely the action of the powerful HCl scavengers in low-smoke acidity compounds for cables. Acid scavengers, on the other hand, work efficiently (even up to 10 times better) when a heating regime or pre-flash-over temperatures are used.

In our opinion, the implications of these results and the considerations on room fire temperatures show how EN 60754-2 is weak in its indirect assessment of acidity. It is probably a useless device to foresee if the material of an item can be a real problem in terms of its capability of releasing HCl in the gas phase. That is not only because in real fire scenarios, HCl decays, generating less acidity than expected, and travels only a short distance from where the fire originated [14]. But also because EN 60754-2 assesses the acidity at typical temperatures of fully developed fires, and a different heating regime should probably be adopted. Full-scale fire tests comparing the evolution of HCl of PVC cables of different classes could definitely clarify this aspect.

Supplementary Materials: The following supporting information can be downloaded at: https://www.mdpi.com/article/10.3390/fire6080326/s1, Table S1: commercial additives. Table S2: test apparatuses. Table S3: standards. Section S2: sample preparation. Section S3: test procedures.

Author Contributions: Conceptualization, G.S.; methodology, G.S., F.D., I.B., M.P. and C.B.; writing—original draft preparation, G.S.; writing—review and editing, G.S., F.D., I.B., M.P. and C.B. All authors have read and agreed to the published version of the manuscript.

Funding: This research received no external funding.

Institutional Review Board Statement: Not applicable.

Informed Consent Statement: Not applicable.

Data Availability Statement: Not applicable.

Acknowledgments: The authors want to acknowledge Carlo Ciotti, Emma Sarti, all PVC Forum Italia, and the PVC4cables staff.

Conflicts of Interest: The authors declare that there is no conflict of interest regarding the publication of this paper.

Abbreviations

PVC	Poly(vinyl chloride)
HCl	Hydrogen chloride
EU	European Union
CPD	Construction Product Directive
CPR	Construction Product Regulation
UPCC	Precipitated Calcium Carbonate
GCC	Ground Calcium Carbonate
Phr	Part per Hundred Resin
DINP	Di Iso Nonyl Phthalate
ESBO	Epoxidized Soy Bean Oil
COS	Calcium Organic Stabilizer
DDW	Double Deionized Water
M	Mean
SD	Standard Deviation
CV	Coefficient of variation

Appendix A. A Schematic Diagram of the Sample Preparation and Testing Process

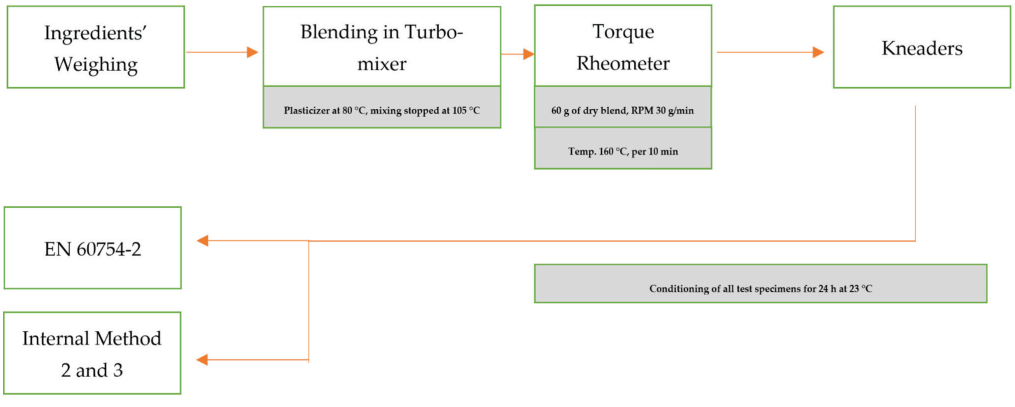

Figure A1. A schematic diagram of the sample preparation.

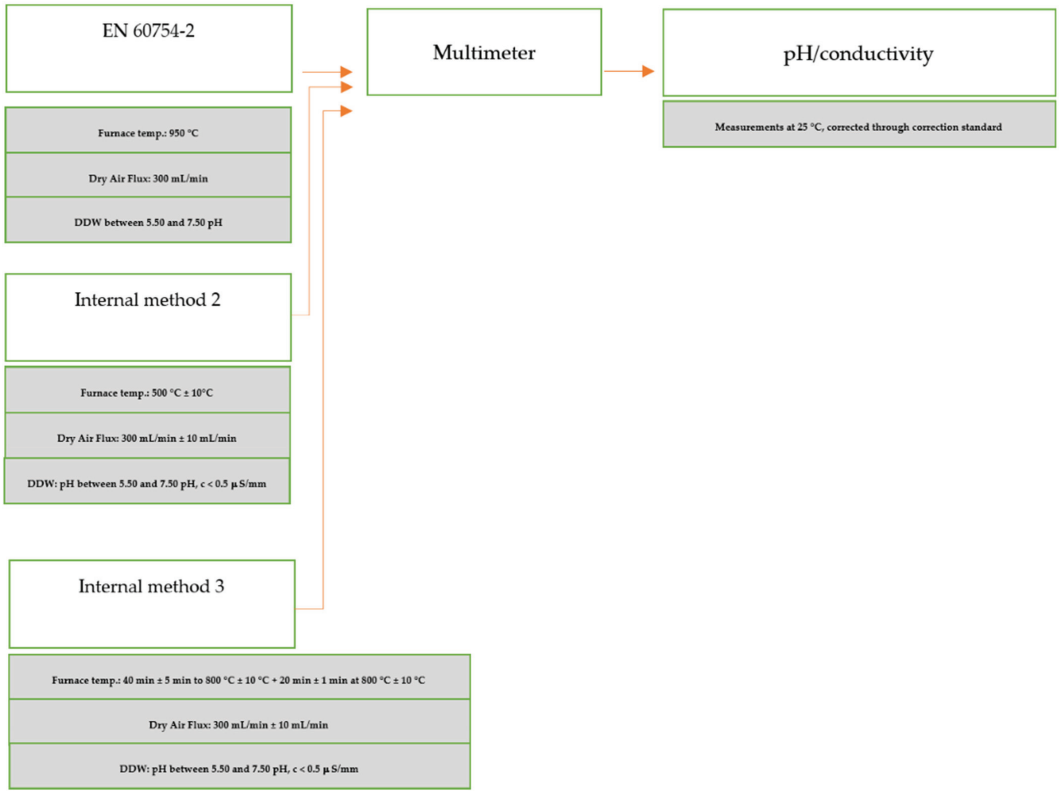

Figure A2. A schematic diagram of the testing process and main conditions.

References

1. Regulation (EU) No 305/2011 of the European Parliament and of the Council of 9 March 2011 Laying Down Harmonised Conditions for the Marketing of Construction Products and Repealing Council Directive 89/106/EEC. Consolidate Version. Available online: https://eur-lex.europa.eu/legal-content/EN/TXT/?uri=CELEX%3A02011R0305-20210716 (accessed on 10 June 2023).
2. *EN13501-1:2018*; Fire Classification of Construction Products and Building Elements—Part 1: Classification Using Data from Reaction to Fire Tests. CEN: Brussels, Belgium, 2019. Available online: https://store.uni.com/ (accessed on 10 June 2023).
3. *EN 13501-6:2018*; Fire Classification of Construction Products and Building Elements. Classification Using Data from Reaction to Fire Tests on Power, Control and Communication Cables. CEN: Brussels, Belgium, 2018. Available online: https://store.uni.com/ (accessed on 10 June 2023).
4. *EN 50575:2014+A1:2016*; Power, Control and Communication Cables—Cables for General Applications in Construction Works Subject to Reaction to Fire Requirements. CENELEC: Brussels, Belgium, 2016. Available online: https://my.ceinorme.it/home.html (accessed on 10 June 2023).
5. *EN 60754-2:2014/A1:2020*; Test on Gases Evolved during Combustion of Materials from Cables—Part 2: Determination of Acidity (by pH Measurement) and Conductivity. CENELEC: Brussels, Belgium, 2020. Available online: https://my.ceinorme.it/home.html (accessed on 10 June 2023).
6. Sarti, G. A New Perspective on Hydrogen Chloride Scavenging at High Temperatures for Reducing the Smoke Acidity of PVC Cables in Fires. I: An Overview of the Theory, Test Methods, and the European Union Regulatory Status. *Fire* **2022**, *5*, 127. [CrossRef]
7. Sarti, G. A New Perspective on Hydrogen Chloride Scavenging at High Temperatures for Reducing the Smoke Acidity of PVC Cables in Fires. II: Some Examples of Acid Scavengers at High Temperatures in the Condensed Phase. *Fire* **2022**, *5*, 142. [CrossRef]
8. *EN 60754-1*; Test on Gases Evolved during Combustion of Materials from Cables—Part 1: Determination of the Halogen Acid Gas Content. CENELEC: Brussels, Belgium, 2014. Available online: https://my.ceinorme.it/home.html (accessed on 1 August 2022).
9. Schartel, B.; Hull, T.R. Development of fire-retarded materials—Interpretation of cone calorimeter data. *FAM* **2007**, *31*, 327–354. [CrossRef]
10. Babrauskas, V. Specimen Heat Fluxes for Bench-scale Heat Release Rate Testing. *Fire Mater.* **1995**, *19*, 243–252. [CrossRef]

11. Schartel, B.; Kebelmann, K. *Fire Testing for the Development of Flame Retardant Polymeric Materials from: Flame Retardant Polymeric Materials, a Handbook*; CRC Press: Boca Raton, FL, USA, 2019. Available online: https://www.routledgehandbooks.com/doi/10.1201/b22345-3 (accessed on 10 June 2023).
12. Hirschler, M. Poly(vinyl chloride) and its fire properties. *FAM* **2017**, *41*, 993–1006. [CrossRef]
13. Babrauskas, V.; Peacock, R.D. Heat release rate: The single most important variable in fire hazard. *Fire Saf. J.* **1992**, *18*, 255–272. [CrossRef]
14. Hirschler, M. Fire safety, smoke toxicity, and acidity. In Proceedings of the Flame Retardants—Interscience Communications, London, UK, 14–15 February 2006.
15. Bassi, I.; Delchiaro, F.; Bandinelli, C.; Mazzocchetti, L.; Salatelli, E.; Sarti, G. A New Perspective on Hydrogen Chloride Scavenging at High Temperatures for Reducing the Smoke Acidity of PVC Cables in Fires, IV: The Impact of Acid Scavengers at High Temperatures on Flame Retardance and Smoke Emission. *Fire* **2023**, *6*, 259. [CrossRef]
16. Sarti, G.; Piana, M. PVC in cables for building and construction. Can the "European approach" be considered a good example for other countries? *Acad. Lett.* **2022**, 5453. [CrossRef]
17. Sarti, G.; Piana, M. PVC cables and smoke acidity: A review comparing performances of old and new compounds. In Proceedings of the AMI International Wire and Cable Conference, Duesseldorf, Germany, 3–5 March 2020.
18. Sarti, G.; Piana, M. Smoke acidity and a new generation of PVC formulations for cables. In Proceedings of the AMI PVC Formulation Conference, Cologne, Germany, 16–18 September 2021.
19. Sarti, G. Developing and improving fire performance and safety in PVC. In Proceedings of the Future of PVC Compounding, Production & Recycling, AVLANTE, Online Conference, 24–25 February 2022.
20. Commercial GCC Purchased by Umbriafiller. Available online: https://elastomeri-polimeri.hu/pdf/umbria/riochim.pdf (accessed on 1 June 2023).
21. Kipouros, G.J.; Sadoway, D.R. A thermochemical analysis of the production of anhydrous $MgCl_2$. *J. Light Met.* **2001**, *1*, 111–117. [CrossRef]
22. Galwey, A.K.; Laverty, G.M. The thermal decomposition of magnesium chloride dihydrate. *Thermochim. Acta* **1989**, *138*, 115–127. [CrossRef]
23. Commercial PCC Purchased by Imerys. Available online: https://www.imerys-performance-minerals.com/system/files/2021-02/DATPCC_Winnofil_S_LSK_EN_2019-07.pdf (accessed on 1 June 2023).
24. Chandler, L.A.; Hirschler Smith, G.F. A heated tube furnace test for the emission of acid gas from PVC wire coating materials: Effects of experimental procedures and mechanistic considerations. *Eur. Polym. J.* **1987**, *23*, 51–61. [CrossRef]
25. Bassi, I. Characterization of PVC Compounds and Evaluation of Their Fire Performance, Focusing on the Comparison between EN 60754-1 and EN 60754-2 in the Assessment of the Smoke Acidity. Master's Thesis, University of Bologna, Bologna, Italy, October 2021. Available online: https://www.pvc4cables.org/images/assessment_of_the_smoke_acidity.pdf (accessed on 1 June 2023).

fire

MDPI

Article

An Experimental Study for Deriving Fire Risk Evaluation Factors for Cables in Utility Tunnels

Hyun Jeong Seo *, Yon Ha Chung and Tae Jung Song

Department of Research Planning Division, KIT Valley, Seoul 08512, Republic of Korea; yonhas@naver.com (Y.H.C.); tjsong73@gmail.com (T.J.S.)
* Correspondence: sincedeni@naver.com; Tel.: +82-2-2624-3550

Abstract: In this study, we performed three tests to measure the fire-retardant performance of power cables installed in utility tunnels. The standards we applied for testing are ISO 5660-1, NES 713, and IEEE 1202. Specifically, we performed a cone calorimetric analysis, calculated the toxicity index, and measured the flame spread length on material surfaces. Even though the same fire-retardant chemical composites were applied, various differences in fire-retardant performance were found depending on the chemical properties of the cable sheath and insulation. We also found that gaseous substances generated during the burning of cables can serve as important risk assessment factors in fires. We determined that, in addition to the heat generated when the cable burns, the toxic gases emitted at this time can also be a risk factor. This is because it is important to consider any potential risk to a person entering as part of an initial response to an event or accident involving cables installed in utility tunnels. Moreover, in the event of a fire in the cable, there is a risk of hazardous substances flowing into the city center as toxic gases are released. Therefore, we determined that the risk of hazardous gases emitted during cable fire should be reflected in the fire-retardant performance standard.

Keywords: cable fire; toxicity index; fire characteristics; utility tunnels; risk assessment

Citation: Seo, H.J.; Chung, Y.H.; Song, T.J. An Experimental Study for Deriving Fire Risk Evaluation Factors for Cables in Utility Tunnels. *Fire* **2023**, *6*, 342. https://doi.org/10.3390/fire6090342

Academic Editors: Ying Zhang, Xiaoyu Ju, Xianjia Huang and Fuchao Tian

Received: 3 August 2023
Revised: 24 August 2023
Accepted: 29 August 2023
Published: 1 September 2023

1. Introduction

A utility tunnel is a facility that includes various types of infrastructure such as power cables, communication cables, water and sewage pipes, and waste transport pipes. Utility tunnels are increasingly being used to optimally arrange supply piping, water supply, and sewage pipes, and other pipelines to improve city roads, traffic conditions, and urban planning [1–4]. However, there are certain dangerous situations that can arise after installing a utility tunnel underground [3,4]. For example, utility tunnels are particularly vulnerable to various disasters, and to fire in particular [4–6]. This is because utility tunnels house many combustible materials that can easily become ignition sources, such as cables, distribution panels, gas supply facilities, and communication facilities. Among these combustible materials, cables are most vulnerable to fire, and they can be a major ignition source [3,4]. Moreover, since the space is sealed in a utility tunnel, the extinguishing activities available in the event of a fire are very limited.

When a fire breaks out in a utility tunnel, a city's communication function, power supply function, gas supply function, etc., can be interrupted, thus resulting in paralysis of the city's main functions [3,6–8]. Most studies examining fires in utility tunnels have mainly focused on the temperature inside the space [7,8]. Additionally, partial fire characteristics were reflected by establishing a theoretical model that simplified the internal structure of the field and utility tunnels. Partial fire properties are related to the propagation of flames on the surface of a material. The flame spread length is the only such property that is currently reflected in the cable's fire-retardant performance standard. It is important to more comprehensively evaluate the fire risk of cables installed in utility tunnels, as overloading of cables represents the main cause of fires in utility tunnels. In addition to

disrupting a city's communication network and power supply, cable fires also generate toxic gases from the burning of the cable sheath, which interfere with firefighting activities [9,10]. These harmful gases are also released to the outside through ventilation, which may harm local residents.

Despite these risks, there are currently no specific evaluation criteria for the fire risk of cables installed in utility tunnels. The existing fire-retardant performance regulations of cables stipulates that they cannot be used below a certain performance level, which is ascertained by conducting a fire-retardant performance evaluation test [9–11]. However, when only the performance level is used as a criterion, only the flame is considered, so such an evaluation is limited by not considering all the risk factors of a cable fire. Issues such as the amount of heat released in the event of a cable fire and the type and amount of toxic gases are currently not included in regulations related to the fire-retardant performance of cables [11–13]. It is therefore necessary to update the risk factors that are included in these regulations to allow for the safer installation of cables in utility tunnels.

Analyzing previous studies shows that existing research related to cable fires applied to utility tunnels has mainly been focused on the methods that can be used to calculate the amount of heat generated from a flame or suppress the spread of a flame [2–10]. Bian et al. [2] designed a system using a sensor that detects initial heat in the event of a fire in cables. Ye et al. [3] designed fire accident scenarios in utility tunnels and simulated the fire spread speed. In this work, the important factors were considered to be the vertical and horizontal temperature, and the temperature flow of the smoke was also analyzed to identify the safe section in the tunnel. An et al. [6] tried to demonstrate the relationship between the combustion characteristics (HRR, THR, and MLR) and heat flux of an optical cable applied within the cable through a cone calorimeter analysis. Studies examining the toxicity of combustion products of cables in enclosed spaces have also been conducted [14–16]. Those studies analyzed the thermal characteristics and components of the hazardous gases of combustion products by utilizing power cables with specifications applied to utility tunnels. However, for power cables, which are the main source of ignition in the event of a fire in a tunnel, the standards regulating the fire-retardant performance have limitations in that the harmfulness of gas and the characteristics of thermal decomposition due to combustion are not reflected.

In this study, experiments were conducted to analyze the characteristics of cable fires, including the heat release rate, the types of toxic gases and emissions, and flame spread characteristics. Further, by analyzing the results, we summarized the risk factors of specific cable fires. The results of this study are expected to help conceptualize the fire risk evaluation factors of cables and be useful as basic research data.

2. Materials and Methods

2.1. Materials

The two cables used in this experiment represent those used for power and control in utility tunnels, power plants, and other facilities. Such cables are made up of a sheath, insulation, and core (electrical wires). The sheath of both cables in this experiment was made of polychloro rubber. The insulation components were different, as one was made using ethylene propylene rubber (EPR) material whereas the other was made using cross-linked polyethylene (XLPE). The core of both cables was made of copper. Table 1 lists the physical specifications of the cable specimens.

The test specimens were prepared by making three types of samples: First, the cable specimens were manufactured according to the ISO 5660-1 [11] and ISO 19702 [12] standards in sizes of 100 mm $\times$ 100 mm $\times$ 25 mm. Second, the cable specimens were fabricated by cutting three to five sheaths and accompanying insulation with a mass of 1 $\pm$ 0.025 g to meet the NES 713 [13] standard. Third, seven cable specimens with a cable diameter of 25 mm were prepared according to the IEEE 1202 [14] standard, and the length of each specimen was cut to 3.5 m.

Table 1. Physical specifications of the experimental specimens.

Materials		**CR/EPR Cable**	**CR/XLPE Cable**
Application		Power and control	Control
Power capacity (kV)		0.6	0.6
Thermal characteristics		Thermosetting	Thermosetting
Cable diameter (mm)		25	25
Fire-retardant treatment		FR	FR
Characteristics of physical composition	Sheath	Polychloro rubber (CR)	Polychloro rubber (CR)
	Insulation	Ethylene propylene rubber (EPR)	Cross-linked polyethylene (XLPE)
	Core (Electric wires)	Copper	Copper

2.2. Methods

Cable fire performance evaluation tests can generally be divided into four categories: heat resistance, flame retardancy, fire resistance, and toxicity determination. In Korea, the "IEEE Standard for Flame Testing of Cables for Use in Cable Tray in Industrial and Commercial Occupancies (IEEE Std 1202-1991)" is applied as a regulation related to proof of the fire retardancy of power and control cables. However, since IEEE Std 1202 (1991) only evaluates the spread of the flame, it has a limitation in that it does not reflect other combustion characteristics.

In the present study, three experiments were conducted to identify the fire characteristics of cables. First, cone calorimetric analysis was performed based on the ISO 5660-1 standard to identify the amount of heat released and the combustion characteristics in a fire. This experiment allows for the measurement and analysis of the heat release rate (HRR), total heat release (THR), time to ignition (TTI), and mass loss rate (MLR). To analyze the heat release from the cable covering material, insulation material, and copper wire as well as the emission characteristics of the combustion products, the temperature in the laboratory was set and maintained at 25 ± 2 °C with a relative humidity of 50 ± 5%. The test was performed under conditions of a cone heater heat flux of 50 kW/m^2 and an exhaust flow rate of 0.024 ± 0.002 m^3/s. The test was conducted a total of three times for 20 min each time, and the results were summarized as the average value obtained. This experiment conformed to the ISO 5660-1 standard.

The second experiment was a quantitative toxic gas emission measurement experiment measuring the combustion products of the test specimens. The "Naval Engineering Standard (NES) 713 (1985)" is a technical standard that can be applied to the calculation of the combustion gas toxicity index of non-metallic materials such as small materials and cable components including the sheath and insulation materials. The size of the chamber in this experiment was 0.6 m^3, while the gas mixing ratio was set at 2 L/min for methane gas and 15 L/min for air. The flame height of the burner was maintained at approximately 100 mm, while the flow rate was adjusted so that the temperature of the flame was 1150 ± 25 °C. The test specimens exposed to the flame maintained a continuous flame contact state until reaching complete combustion. After combustion, the burner flame was ignited and the mixing fan was operated for 30 s to detect and sample the combustion gas in the chamber through each detector tube. After gas sampling, the residues inside the chamber were immediately discharged through a forced discharge device; this discharge lasted over three minutes.

Finally, an experiment was conducted to measure the flame spread properties of the test specimens. IEEE 1201 is a cable vertical tray test standard, and in this experiment, pre-treatment was performed for more than three hours at a temperature of 18 °C or higher in a constant temperature and humidity room before the test specimens were installed on the tray according to the corresponding standard. A vertical tray was installed

in a 2.4 m × 2.4 m × 2.4 m firebrick chamber, while the test specimens were fixed on a 30 cm × 2.4 m tray at 1/2 intervals of the cable diameter. The air flow rate was set to 1280 cm^2/s and the flame source was applied at 20 kW (approximately 70,000 BTU/h). The flame application time was set to 20 min in total, and the experiment was conducted.

Figure 1 shows the tray and equipment used for the cable flame test as specified by the IEEE. We provide explanations for specific sequences for the cable tray test below.

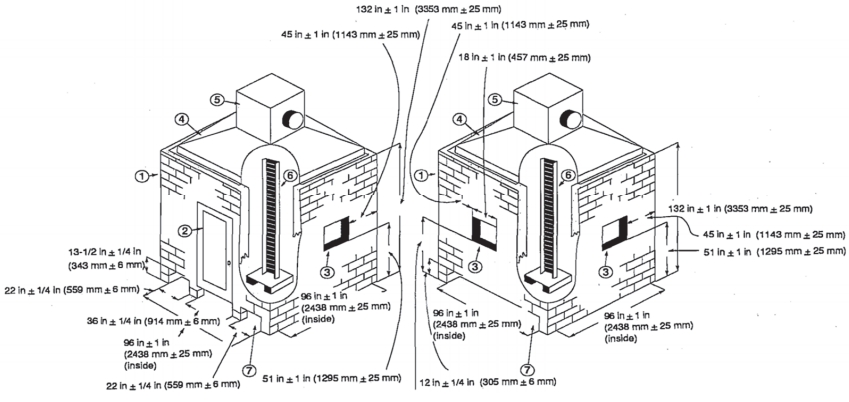

Figure 1. Flame Test Facility [14].

We provided a detailed explanation of the process by which the experiment is performed in Figure 1. First, this is an explanation of cables and cable trays. The cables are attached to the cable trays and pretreatment is performed. The tray is installed parallel to the wall of the chamber, and the cable is installed such that the end of the sample touches the top of the burner. Second, the flow rate of the exhaust duct is adjusted to be 0.65 $m^3/s \pm 0.02$ m^3/s. Third, the burner is installed horizontally at an angle of 20 degrees and separated by 75 mm from the sample surface. This propane flow is theoretically equivalent to a 20 kW heat release, but the actual heat release is lower due to incomplete combustion of the burner. Fourth, the airflow rate is set to 1280 $cm^3/s \pm 80$ cm^3/s under standard temperature and pressure. Finally, the flame of the burner continues to ignite the sample for 20 min. When the test is finished, the flame of the burner is turned off and the cable is left burning until it is self-extinguished.

3. Results

This section presents this study's findings regarding the combustion properties, toxicity gases emission characteristics, and flame spread length on the cable surface. First, the combustion properties obtained by analyzing the results of the cone calorimetry analysis experiment are presented. Following the ISO 5660-1 standard, this experiment was conducted three times with two test specimens, and the average value of these results is presented in this paper. Following the NES 713 standard, gaseous substances were collected through a total of two tests, after which the amount of gas emitted was measured and the toxicity index was calculated. The results of the experiment are presented as the average of two measurements and calculations. In this study, this was also applied and the average of the experimental results and calculated values was presented in this paper.

3.1. Combustion Properties

Two types of test specimens were used in this study. Specifically, cable E was classified as having an insulation material of EPR (ethylene propylene rubber) whereas cable X was classified as having an insulation material of XLPE (cross-linked polyethylene). Table 2 presents the cone calorimetry test results for these two types of cables.

Table 2. Results of cone calorimetric analysis.

Parameter	Cable E	Cable X
PHRR (kW/m^2)	149.06	124.65
tPHRR (s)	69	70
THR (MJ/m^2)	52.77	32.10
Total oxygen consumed (g)	31.13	18.73
Time to ignition (s)	38	36
Initial mass (g)	714.98	703.73
Mass lost (g)	58.77	38.48
Remaining mass (g)	656.21	665.25
Mass loss rate (%)	8.22	5.47

For the HRR, the peak of the HRR (PHRR) did not exceed 200 kW/m^2 for either of the test specimens. The times at which PHRR appeared (tPHRR) were 69 s for Cable E and 70 s for Cable X, which were almost identical. The THR value for Cable X was 32.10 MJ/m^2, which was 20 MJ/m^2 lower than that of Cable E. The ignition time (TTI) on the surface of the test specimens was 38 s for Cable E and 36 s for Cable X, thus showing no significant difference.

However, Cable E exhibited higher released heat values than Cable X. These results are attributed to the different insulation components of EPR and XLPE. Both cables were treated with fire-retardant additives on the sheath and insulation. No significant difference was observed in terms of the sheath, because the sheaths of both test specimens belonged to the CR series, but the degree of combustion was determined to be different due to the difference in insulation components [15,16]. Figure 2 shows the HRR and THR graphs obtained after the cone calorimetry analysis. From the graphs, it can be seen that two peaks appear in the HRR curve. This suggests a phenomenon wherein heat release is delayed due to the formation of a char layer after an increase in heat release due to the evaporation of volatile substances in the initial cable material. Then, as the surface of the char is broken, combustion proceeds again, and the heat release rate increases, which is the meaning of the second peak.

The results shown in the cable HRR curve confirm that the HRR of Cable E was not constant after the PHRR, as change occurred from 200 s until the end of the experiment. By contrast, Cable X's HRR curve showed no significant change after one PHRR. This heat release characteristic was also reflected in the THR curve. This is attributed to the EPR-based cable insulation.

EPR-based and XLPE-based insulation types are mainly used for manufacturing cables for utility tunnels or power plants because of their excellent heat and fire resistance. When making cables using these materials, vulcanizing agents such as sulfuric acid and bromine are added as fire-retardant chemical composites [9,10]. EPR has a low degree of deterioration, good flexural properties, and self-extinguishing properties because of the organic-group (R) attached to the Si-O framework. However, the mixing of a fire-retardant filler with a vulcanizing agent during cable manufacturing causes the affinity of the EPR insulation material to be lower than that of XLPE, so the non-uniformity of the material can serve as an obstacle to improving its fire-retardant performance [9,16].

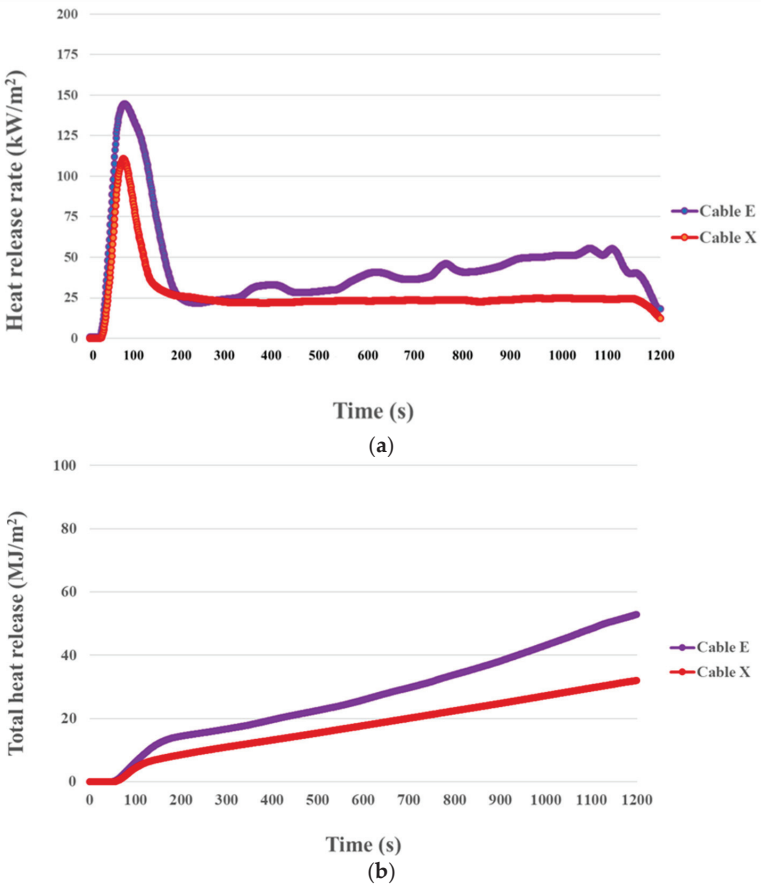

Figure 2. HRR and THR test results after the cone calorimeter test: (**a**) HRR results; (**b**) THR results.

Since the HRR represents the amount of heat released from the surface of a material, it may have limitations in terms of its ability to determine the degree of improvement in fire-retardant performance based on the size of the value. Therefore, we additionally compared the consumption of oxygen, which is a combustible gas that is used when the materials are burned. The oxygen consumption was 31.13 g, and the value consumed by Cable E was found to be higher than that of Cable X. When comparing the MLR values of the two specimens, the MLR value of Cable X was confirmed to be lower than that of Cable E. Although both types of cables were treated with fire-retardant additives, the fire-retardant performance differed depending on the components of the material itself.

3.2. Toxic Gas Emission Characteristics

To subdivide the risk by calculating the toxicity index (TI) of the gas generated during combustion, an experiment was conducted in accordance with the NES 713 standard. The test results were analyzed in accordance with the MIL-DTL standard [17,18]. The standard set by MIL-DTL is the TI, where the maximum value is 5.0 for the cable sheath and 1.5 for the cable insulation. In NES 713, the TI value is presented by applying the limit set by the MIL-DTL standard. Moreover, the critical values of thirteen gas components are set in detail. The specific types of gas are as follows: carbon dioxide (CO_2), carbon monoxide (CO), phenol (C_6H_5OH), ammonia (NH_3), hydrogen sulfide (H_2S), sulfur dioxide (SO_2), formaldehyde

(HCHO), hydrogen chloride (HCl), hydrogen bromide (HBr), hydrogen cyanide (HCN), nitrogen oxides (NO_X), hydrogen fluoride (HF), and acrylonitrile (CH_2CHCN).

Table 3 presents the combustion gases detected in Cable E and Cable X in this experiment.

Table 3. Combustion gas toxicity test results of experiment conducted in accordance with NES 713.

Parameter	Cr (Critical Limit, ppm)	Cable E		Cable X	
		Sheath	Insulation	Sheath	Insulation
Carbon dioxide (CO_2)	100,000	83,333	41,687	34,649	40,222
Carbon monoxide (CO)	4000	7321	6402	8373	6608
Hydrogen sulfide (H_2S)	750	0	0	0	0
Ammonia (NH_3)	750	0	0	0	0
Formaldehyde (HCHO)	500	30	119	29	115
Hydrogen chloride (HCl)	500	60	30	46	86
Acrylonitrile (CH_2CHCN)	400	12	36	23	40
Sulfur dioxide (SO_2)	400	655	30	144	57
Nitrogen oxides (NO_X)	250	149	71	87	230
Phenol (C_6H_5OH)	250	0	0	0	0
Hydrogen cyanide (HCN)	150	18	30	29	34
Hydrogen bromide (HBr)	150	20	10	15	29
Hydrogen fluoride (HF)	100	0	0	0	0

In total, nine toxic gases were emitted from Cable E and Cable X: dioxide, carbon monoxide, formaldehyde, hydrogen chloride, acrylonitrile, sulfur dioxide, nitrogen oxides, hydrogen cyanide, and hydrogen bromide. Comparing the combustion gases emitted from the cable sheath, the amount of carbon dioxide emitted from Cable E was higher than that emitted from Cable X. By contrast, the amount of carbon monoxide emitted from Cable X was higher than that emitted from Cable E. Carbon monoxide is produced during incomplete combustion, and its production indicates higher fire-retardant performance. Regarding the emissions of sulfur dioxide and nitrogen oxides, higher values were measured in Cable E. This was attributed the difference in the component ratios of the fire-retardant chemical composites processed on the cable sheath.

Among the released toxic gases, HCl can cause eye or upper airway mucosal irritation and airway damage, which can lead to suffocation [9,19,20]. As thermal decomposition progresses during the combustion of materials that contain components such as polyethylene and polyvinyl chloride, HCL is considered to be a product that is generated by organic acids and aromatic substances, among the chemical species included in the cable sheath [21,22].

Both cable sheaths are composed of polychloroprene, but there was confirmed to be a difference in the combustion products. This was attributed to the types of additives that are additionally used when polychloroprene is applied to the cable sheath. Polychloroprene is mainly used as a cable sheath because of its excellent insulation and fire-retardant properties. However, since it hardens at low temperatures, certain amounts of additives, typically sulfuric acid or bromine, are used to improve the durability of materials. When these additives are applied, a synergy effect is expressed in the fire-retardant effect [23]. However, when these components are burned, they can cause the emission of toxic gases such as hydrogen sulfide, sulfur dioxide, and hydrogen bromide. Therefore, it was determined that the additives used in the manufacture of cable sheaths require additional hazard consideration.

The combustion gas of the cable insulation was found to be similar to that of the cable sheath in terms of hazardous components. The amount of carbon monoxide emitted among the hazardous components exceeded the critical limit. Moreover, the emission of

formaldehyde from the cable insulation was found to be higher than that from the cable sheath. Notably, a large amount of nitrogen oxide was detected in the insulation of Cable X. Since the critical limit value stipulated in NES 713 is 250 ppm, the detection amount of nitrogen oxides in this experiment is not a problem in terms of regulations. However, in terms of the risk of nitrogen oxides, we determined that the 230 ppm detected in this experiment was dangerous because it was very close to the critical limit. Table 4 presents the combustion gas toxicity index calculation results.

Table 4. Toxicity index of the cable specimens.

Parameter	Cable E		Cable X	
	Sheath	Insulation	Sheath	Insulation
Carbon dioxide (CO_2)	0.83	0.42	0.35	0.40
Carbon monoxide (CO)	1.83	1.60	2.09	1.65
Hydrogen sulfide (H_2S)	0.00	0.00	0.00	0.00
Ammonia (NH_3)	0.00	0.00	0.00	0.00
Formaldehyde (HCHO)	0.06	0.24	0.06	0.23
Hydrogen chloride (HCl)	0.12	0.06	0.09	0.17
Acrylonitrile (CH_2CHCN)	0.03	0.09	0.06	0.10
Sulfur dioxide (SO_2)	1.64	0.08	0.36	0.14
Nitrogen oxides (NO_X)	0.60	0.28	0.35	0.92
Phenol (C_6H_5OH)	0.00	0.00	0.00	0.00
Hydrogen cyanide (HCN)	0.12	0.20	0.19	0.23
Hydrogen bromide (HBr)	0.13	0.07	0.10	0.19
Hydrogen fluoride (HF)	0.00	0.00	0.00	0.00

3.3. Flame Spread Characteristics

The carbonized lengths of Cable E and Cable X were measured. In detail, the cable specimens were exposed to flame for a total of five times, for 20 min each time. Upon completion of the flame exposure test, the carbonization length was measured. The average carbonization length of Cable E was approximately twice that of Cable X. Based on this result, it was determined that the fire-retardant performance of Cable X was better than that of Cable E in terms of flame spread among fire-retardant performances. These results are attributed to the component characteristics of the cable specimens. Among the components of cable insulations used as fire-resistant fillers, XLPE does not lose the insulation properties of cables and can exhibit resistance to extreme fire. Although the EPR of Cable E also has fire resistance, its combustion progressed relatively more than that of Cable X because XLPE has stronger resistance to thermal decomposition due to cross-linking. Table 5 shows the results of flame spread tests.

Table 5. Results of flame spread experiments.

Category		Carbonization Length (mm)		
		Test 1	Test 2	Test 3
Cable E	Cable E-1	900	910	935
	Cable E-2	1010	910	1010
	Cable E-3	1020	910	1010
	Cable E-4	1000	910	1005
	Cable E-5	970	760	990

Table 5. *Cont.*

Category		Carbonization Length (mm)		
		Test 1	**Test 2**	**Test 3**
Cable X	Cable X-1	580	560	485
	Cable X-2	570	560	500
	Cable X-3	575	605	530
	Cable X-4	595	650	550
	Cable X-5	560	670	560

4. Conclusions and Implications

In this study, we measured and analyzed the fire characteristics of power cables used in utility tunnels and the toxicity of combustion gases. To measure the fire characteristics of cable specimens, cone calorimeter analysis was performed, and to measure the toxicity index of combustion products, the NES 713 standard was applied for the absorption of combustion gases using the Drager tube. We also measured the carbonization length to confirm the characteristics of flame spread on the surface of cable test specimens. Based on an analysis of the experimental results obtained in this study, we have derived the following implications:

First, when determining the fire-retardant level of power cables applied to utility tunnels, it is important for fire characteristics of cables to be specifically reflected. This is because the fire-retardant performance of a cable varies depending on the chemical composites of the sheath and insulation that make up the cable. According to the components of these chemical composites, we confirmed through experiments that fire resistance can differ even when using the same fire-retardant additives for treatment. It is also necessary to check the temperature at which the cable burns and the temperature at which it deteriorates, rather than simply considering the amount of heat emitted.

We determined that there is a limit to determining improvements in fire-retardant grade by simply considering reductions in the flame spread on the material surface or reductions in the carbonization length in the case of cable fire. We thought it should be considering maintaining or losing the function of power cables. The current fire-retardant performance standard of cables has a limitation in that it does not consider situations in which various functions, such as the power supply of cables, maintenance of facility functions, and maintenance of networks with the outside, might be lost. Considering these factors, the secondary risk due to functional loss is as dangerous as the temperature of the fire. Therefore, it is necessary to subdivide the grade by considering the chemical composites of the cable, the system, and the functions.

Second, the toxicity of combustion products should be considered when distinguishing fire-retardant levels in cable fires. When a fire occurs in utility tunnels, hazardous gases are generated, and workers inspecting the inside of the tunnel may be exposed to these harmful gases. These risks can lead to emergencies. Moreover, the release of a large amount of harmful gas can cause problems that affect firefighter safety during firefighting. We also note that utility tunnels are installed in downtown areas, and that it is important to consider that dangerous situations may occur if the air inside the utility tunnel leaks to the outside through the ventilation, thus harming people in the city.

Although we derived the above implications, our study has some limitations. First, while burning the cables, we measured the amounts of toxic gases emitted for 30 min, but time-series data on how the combustion gases were emitted in real time could not be confirmed. We determined that time-series data related to combustion gas emission are an important concept because plans for evacuation from utility tunnels or fire suppression plans can be set up differently depending on whether a lot of gaseous substances are released at the beginning of combustion or after some period of time. Further, since the toxicity index is a calculated result for an enclosed space, it is necessary to conduct

experiments that consider various space conditions. Since certain sections of utility tunnels are straight sections and involve mechanical ventilation, the spread of smoke or flame is an important risk assessment factor. Moreover, due to the spatial characteristics of utility tunnels, in the case of spaces such as T-shaped vents or natural ventilation vents, there are differences in airflow, so we determined that simulations reflecting spatial conditions would be necessary.

While carrying out this study, we were able to secure data on the derived fire characteristics of power cables in utility tunnels and the emission characteristics of hazardous gases. In future studies, we plan to perform modeling and fire simulations targeting utility tunnels based on the data obtained in this study. The data acquired in this study are expected to help elucidate the characteristics of the flow and diffusion of heat and smoke according to the internal shape of the utility tunnels.

Author Contributions: Conceptualization, H.J.S. and Y.H.C.; methodology, H.J.S.; software, H.J.S. and Y.H.C.; validation, H.J.S., Y.H.C. and T.J.S.; formal analysis, H.J.S.; investigation, Y.H.C.; resources, Y.H.C. and T.J.S.; data curation, Y.H.C. and T.J.S.; writing—original draft preparation, H.J.S., writing—review and editing, Y.H.C. and T.J.S.; visualization, Y.H.C.; supervision, H.J.S.; project administration, T.J.S.; funding acquisition, T.J.S. All authors have read and agreed to the published version of the manuscript.

Funding: This research was supported by the Institute of Information & Communications Technology Planning & Evaluation (IITP), with a grant funded by the Korea government (MSIT, MOIS, MOLIT, and MOTIE) (No. 2020-0-00061, Development of integrated platform technology for fire and disaster management in underground utility tunnel based on digital twin).

Institutional Review Board Statement: Not applicable.

Informed Consent Statement: Not applicable.

Data Availability Statement: Not applicable.

Conflicts of Interest: The authors declare no conflict of interest.

References

1. Pan, R.; Zhu, G.; Liang, Z.; Zhang, G.; Liu, H.; Zhou, X. Experimental study on the fire shape and maximum temperature beneath ceiling centerline in utility tunnel under the effect of curved sidewall. *Tunn. Undergr. Space Technol.* **2022**, *99*, 103304. [CrossRef]
2. Bian, H.; Zhu, Z.; Zang, X.; Luo, X.; Jiang, M. A CNN Based Anomaly Detection Network for Utility Tunnel Fire Protection. *Fire* **2022**, *5*, 212. [CrossRef]
3. Ye, K.; Tang, X.; Zheng, Y.; Ju, X.; Peng, Y.; Liu, H.; Wang, D.; Cao, B.; Yang, L. Estimating the two-dimensional thermal environment generated by strong fire plumes in an urban utility tunnel. *Saf. Environ. Prot.* **2021**, *148*, 737–750. [CrossRef]
4. Chung, Y.H.; Kim, S.D.; Seo, H.J.; Lee, H.; Song, T.J. Establishment of Complex Disaster Scenario on the Utility Tunnel Study for Digital Twin System Application. *J. Soc. Disaster Inf.* **2022**, *18*, 861–872. [CrossRef]
5. Ko, J. Study on the Fire Risk Prediction Assessment due to Deterioration contact of combustible cables in Underground Common Utility Tunnels. *J. Korea Soc. Disaster Inf.* **2015**, *11*, 135–147. [CrossRef]
6. An, W.; Sun, X.; Tang, Y.; Wang, T.; Wang, Z. Experimental study on fire performance of optical cables used in utility tunnel: Influence of cable spacing and heat flux. *Fire Mater.* **2023**, 1–8. [CrossRef]
7. Sun, B.; Xu, Z.D. Automatic Data Generation Method for Precise Ceiling Temperature Prediction of Cables Fire in the Utility Tunnel and Full-Scale Experimental Verification. *Fire Technol.* **2022**, *58*, 2847–2869. [CrossRef]
8. Zheng, X.; Cai, G.; Guo, J.; Gao, W.; Huang, Y.; Tong, X. Combustion characteristics and thermal decomposition mechanism of the flame-retardant cable in urban utility tunnel. *Case Stud. Therm. Eng.* **2023**, *44*, 102882. [CrossRef]
9. Seo, H.J.; Kim, N.K.; Lee, M.C.; Lee, S.K.; Moon, Y.S. Investigation into the toxicity of combustion products for CR/EPR cables based on aging period. *J. Mech. Sci. Technol.* **2020**, *34*, 1785–1794. [CrossRef]
10. Seo, H.J.; Kim, N.K.; Jo, J.M.; Lee, M.C.; Lee, S.K.; Moon, Y.S. A Study on the Human Toxicity of Combustion Products for Non Class 1E Cables. *J. Korean Soc. Hazard Mitig.* **2018**, *18*, 215–222. [CrossRef]
11. *ISO 5660-1*; Reaction-to-Fire Tests—Heat Release, Smoke Production and Mass Loss Rate—Part 1: Heat Release Rate (Cone Calorimeter Method) and Smoke Production Rate (Dynamic Measurement). International Organization for Standardization (ISO): Geneva, Switzerland, 2015.
12. *ISO 19702*; Toxicity Testing of Fire Effluents—Guidance for Analysis of Gases and Vapours in Fire Effluents Using FTIR Gas Analysis. International Organization for Standardization (ISO): Geneva, Switzerland, 2006.

13. NES 713*Determination of the Toxicity Index of the Products of Combustion from Small Specimens of Materials*; Ministry of Defense: London, UK, 2000.
14. *IEEE 1202*; IEEE Standard for Flame Testing of Cables for Use in Cable Tray in Industrial and Commercial Occupancies. IEEE: Montreal, QC, Canada, 1991. [CrossRef]
15. Seo, H.J.; Lee, M.C.; Kim, N.K.; Lee, S.K.; Moon, Y.S. An Experimental Study on the Combustion Characteristics of Non Class 1E Cables. *J. Korean Soc. Comb.* **2019**, *24*, 15–24. [CrossRef]
16. Kim, H.K. Radiation Ray Stress Characteristics of EPDM Insulation Cable for Nuclear Power Plant. Ph.D. Thesis, Department of Electrical Engineering, Chosun University, Gwangju, Republic of Korea, 2002.
17. MIL-DTL-24640/15D*Cable, Electric, 600 Volts, Lightweight, Multi-Pair, AWG 22, Type 2XSAW (Including Variation Type 2XSAOW)*; Departments and Agencies of the Department of Defense: Arlington County, VA, USA, 2002.
18. *MIL-DTL-24643B*; Cables and Cords, Electric, Low Smoke, for Shipboard Use General Specification for 22 August 2002. EverySpec: Gibsonia, PA, USA, 2002. Available online: http://everyspec.com/MIL-SPECS/MIL-SPECS-MIL-DTL/MIL-DTL-24643B_35771/ (accessed on 22 August 2002).
19. Han, S.B. A Study on the Toxic Gases Released from Interior Upholstery Fires. Ph.D. Thesis, Hoseo University, Asan, Republic of Korea, 2001.
20. Kim, Y.T. A Study on the Combustion of Car Interior Materials. Ph.D. Thesis, Kangwon National University, Chuncheon, Republic of Korea, 2009.
21. Lee, D.H.; Choi, H.J.; Kim, D.S.; Lee, B.H. Distribution Characteristics of Pyrolysis Products of Polyethylene. *Polym. Korea* **2008**, *32*, 157–162.
22. Seo, H.J.; Son, D.W. Hazard Assessment of Combustion Gases from Interior Materials. *Fire Sci. Eng.* **2015**, *4*, 49–56. [CrossRef]
23. Sallet, D.; Mailhos-Lefievre, V.; Martel, B. Flame retardancy of polyamide 11 with a decabromodiphenyl-antimony trioxide mixture. A bromine-antimony-nitrogen synergism. *Polym. Degrad. Stab.* **1990**, *30*, 29–39. [CrossRef]

fire

MDPI

Article

Research on the Fire Hazard of Different Cables Based on Cone Calorimetry

Bobo Shi *, Chenyang Yang and Haifan Long

School of Safety Engineering, China University of Mining and Technology, Xuzhou 221116, China; ts20120106p31@cumt.edu.cn (H.L.)
* Correspondence: shibobo@cumt.edu.cn

Abstract: In recent years, due to the extensive application and inherent fire hazard of cable materials, the combustion characteristics of frequently used cables, including electrical cables, wires, optical fibers, and network cables have been studied based on ISO 5660 cone calorimetry. The fire hazard associated with these cables under different radiation intensities was explored in this study, with parameters such as time to ignition (TTI), heat release rate per unit area (HRRPUA), peak heat release rate (PHRR), total heat release (THR), and mass loss rate (MLR) being investigated for each cable type. Based on an experimental analysis, the risk of fire for all four cable types was augmented by an increase in the external radiation intensity, with electrical cables considered as posing the greatest risk. Regarding smoke toxicity, the lowest risk of smoke toxicity was demonstrated by the network cable, with an FED (fractional effective dose) of 0.0203, followed by optical fibers, with an FED of 0.0507; electrical wires, with an FED of 0.0417; and electrical cables, with an FED of 0.0501. Notably, no significant distinctions were exhibited by the other three cable types, and the smoke toxicity of all four cables did not reach lethal concentration levels in humans. Consequently, considering both thermal hazard and smoke toxicity, it became evident that electrical cables posed the greatest overall fire hazard.

Keywords: cables; combustion characteristics; cone calorimeter; fire hazard

Citation: Shi, B.; Yang, C.; Long, H. Research on the Fire Hazard of Different Cables Based on Cone Calorimetry. *Fire* **2023**, *6*, 431. https://doi.org/10.3390/fire6110431

Academic Editors: Ying Zhang, Xiaoyu Ju and Xianjia Huang

Received: 20 September 2023
Revised: 5 November 2023
Accepted: 8 November 2023
Published: 9 November 2023

1. Introduction

Recently, the widespread utilization of electronic and electrical devices has led to a surge in electrical fire incidents. Among the primary causes of electrical fires, cable malfunction, and ignition were prominent, accounting for over half of all electrical fire accidents in China [1,2]. Consequently, given the extensive application scenarios and significant fire risks associated with cables [3], numerous scholars from both domestic and international academic circles have undertaken extensive research on cable combustion behavior.

Advanced apparatuses, such as cone calorimeters, flash point testers, and flame propagation calorimeters, have been utilized to investigate this subject. In a study on halogen-free flame-retardant cables under external heat radiation intensities ranging from 25 to 75 kW/m^2, Fontaine et al. [4] observed a reduction in cable ignition time with an increase in applied radiation intensity. Specifically, when the external radiation was increased from 25 kW/m^2 to 75 kW/m^2, the ignition time decreased by 802 s. Zheng et al. [5] conducted a comprehensive investigation of the ignition, expansion charring, pyrolysis, and combustion behavior of ZRC-YJV22 flame-retardant cables from both the macroscopic and microscopic perspectives. They employed multiple criteria to assess the cable's hazardous nature and conducted a detailed analysis of the burning product characteristics and pyrolysis reaction mechanisms of the flame-retardant cable. The research outcomes had the potential to establish an integrated fire engineering database and comprehensive utility tunnel standards. Elliot et al. [6] explored the cone calorimeter testing method for insulation wires, a relatively simple, cost-effective method that exhibited good repeatability and

provided quantitative data on wire combustibility. The results revealed significant differences between halogen-free flame-retardant wires and their equivalent halogen-containing counterparts. Barnes et al. [7] analyzed the fire performance of halogen-containing and halogen-free polymeric cable sheath materials. They found that flame-retardant cables and halogen-containing polymer cable sheaths demonstrated resistance to ignition and reduced heat release rates. However, they exhibited unfavorable factors, such as low smoke visibility and high toxicity. Tang et al. [8] conducted a comparative study on the combustion characteristics and fire hazards of two types of cables used in nuclear power plants, utilizing cone calorimetry and cable tray fire tests. The experimental findings demonstrated that the fire performance of the NPP flame-retardant cable was notably affected by external radiation intensity. A single peak in the heat release rate was exhibited under low radiation intensities, while two peaks were observed under high radiation intensities. On the other hand, the heat release rate curve of the conventional flame-retardant cable displayed three peaks, with the maximum heat release rate peak surpassing that of the NPP flame-retardant cable by 108 kW/m^2. Matheson et al. [9] researched halogenated and non-halogenated polymer materials, revealing that halogen-containing materials exhibited superior electrical properties compared with non-halogenated flame-retardant materials.

Various testing methods have also been explored to determine the combustion characteristics of cables. Hirschler [10] summarized the advantages and limitations of various testing methods for cables and wires in fires of different scales. Additionally, he proposed using thermal power to assess the hazardous nature of cables and applying deep learning techniques to predict the effectiveness of cable fire tests. Kaczorek-Chrobak et al. [11] conducted fire experiments on power cables at radiation intensities of 10, 20, 30, 40, and 50 kW/m^2. They compared the results with those of large-scale cable fire experiments and analyzed the cone calorimeter test results based on the Quintiere theory, substantiating the feasibility of using cone calorimetry as a substitute for large-scale fire tests. Sun-Yeo Mun et al. [12] investigated the thermal decomposition characteristics of five types of flame-retardant cables composed of various materials using thermogravimetric analysis. They observed that different cables exhibited similar thermal decomposition temperatures. However, significant differences were observed in the decomposition rates during combustion. Shi et al. [13] explored the relationship between fire source power and the combustion characteristics of flame-retardant coatings on subway cables. The researchers subjected cables with various flame-retardant properties to radiation heat fluxes ranging from 20 to 40 kW/m^2 using a cone calorimeter. The results indicated a positive correlation between a cable's burning rate and the rate of harmful gas generation with increasing radiation intensity. Moreover, the increase in the amount of flame-retardant coating extended the ignition time of the cable. Zhang et al. [14] conducted thermogravimetric experiments on the outer sheath material of low-voltage flame-retardant cables using a simultaneous thermal analyzer at three different heating rates. The findings indicated a two-stage thermal decomposition process for the cable's outer sheath, and with an increase in the heating rate, the peak mass loss rate shifted towards higher temperature regions. Sun [15] conducted research on the combustion characteristics of cables, focusing on the ignition time and heat release rate through experiments with radiation intensities of 45 kW/m^2 and 50 kW/m^2.

In summary, despite both domestic and international scholars having conducted some research on the combustion characteristics and fire hazards of cables using apparatuses like the cone calorimeter, the flame propagation calorimeter, and the simultaneous thermal analyzer, most of these studies have focused solely on electrical cables. However, in many scenarios, besides electrical cables, a significant amount of electrical wires, network cables, and optical fibers can also be present. Therefore, it is imperative to employ a cone calorimeter to study the combustion characteristics of these other materials, including their heat release rate, ignition time, and smoke release rate, and to subsequently analyze their level of fire hazard (thermal hazard and smoke toxicity).

Compared with previous studies on cable materials, this article not only investigates the combustion characteristics of cables but also examines the smoke toxicity generated

during cable combustion. Through a comprehensive analysis of the experimental results, the conclusion that electrical cables pose the greatest fire hazard was drawn. Furthermore, this study can serve as a guideline for the selection of appropriate cable materials in specific scenarios.

2. Experimental Methods

2.1. Experimental Equipment

A cone calorimeter was used in this experiment as it effectively replicates real-life fire scenarios, exhibits high repeatability, and allows for acquiring much combustion characteristic data on the test material in a single experiment [16].

2.2. Methods

Two variables were considered in the cable combustion experiment. (1) Cable types: Different cable types have different materials, structures, and combustibility, which can result in diverse combustion characteristics and fire hazard levels. Hence, cable types were treated as an experimental variable. (2) External radiation intensity: This variable was used to investigate how different combustion characteristic parameters and fire hazard levels change in different fire scenarios.

In choosing the experimental methods, we considered the international standard EN50399. However, after careful examination, we found that this standard was primarily intended for use in the European region. It was commonly used for testing cable fire resistance, as well as measuring heat release and smoke production from cables. Additionally, the material requirements specified in this standard differed significantly from those of our prepared materials. Taking into account the specific conditions in our region, we ultimately adopted the measurement standard for cable combustion characteristics outlined in ISO5660 [16].

The cables were prepared as 100 mm $\times$ 100 mm specimens, following the cone calorimeter's instructions. Aluminum foil was used to protect five sides of each specimen, while an irradiated surface was left exposed; the foil did not exceed the specimen's surface by more than 3 mm, as shown in Figure 1. Additionally, a wire mesh securely held the cables in place during combustion to prevent deformation. The experiments were conducted under controlled environmental conditions, maintaining an oxygen concentration of 20.95%, a temperature of 25.0 °C, and a relative humidity of 50%. Before each experiment, diligent calibration of the instruments was performed.

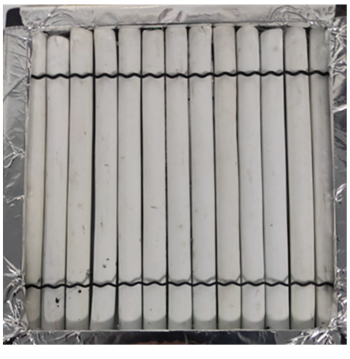

Figure 1. Effect of experimental material treatment.

The experiment involved conducting combustion tests on four types of cables: YJV cables, BV wires, Cat6 ethernet cables, and OM3 optical fibers. These cables were subjected to four different thermal radiation intensities: 30 kW/m^2, 40 kW/m^2, 50 kW/m^2, and 60 kW/m^2. The manufacturers and dimensions of these four cable types are presented in

Table 1. Furthermore, on the 100 mm × 100 mm test fixture, approximately 13 cables were used in each test, with each cable trimmed to a length of 100 mm and a width of around 7.7 mm. Our primary objective was to investigate the combustion characteristics and fire hazards of the cables when exposed to varying levels of heat from external radiation. As a result, a total of 16 different test conditions were examined, as detailed in Table 2.

Table 1. Material manufacturers and sizes.

Type	Manufacturer	Size
Electrical cable	Kangpu Technology Co., Ltd. (Suzhou, China)	100 mm
Wire	Henggong Technology Co., Ltd. (Taizhou, China)	100 mm
Network cable	Kangpu Technology Co., Ltd. (Suzhou, China)	100 mm
Optical fiber	Youpuguang Technology Co., Ltd.(Shenzhen, China)	100 mm

Table 2. Experimental condition setting for cone calorimeter combustion test.

NO.	Cable Type	Outer Sheath	Insulating Layer	Intensity of External Heat Radiation (kW/m^2)
T-1	Electrical cable	Flame-retardant PVC	XLPE	30
T-2				40
T-3				50
T-4				60
T-5	Wire	Flame-retardant PVC	None	30
T-6				40
T-7				50
T-8				60
T-9	Network cable	LSZH	HDPE	30
T10				40
T-11				50
T-12				60
T-13	Optical fiber	PVC	None	30
T-14				40
T-15				50
T-16				60

3. Results and Analysis

3.1. Time to Ignition

Table 3 presents the time to ignition (TTI) of the four cable types under varying external radiation intensities. The analysis of Table 2 indicated that the ignition time of the materials decreased as the external radiant heat intensity increased. This was because, as the external heat radiation intensity applied to the cable increased, the heat transfer from the heater to the specimen's surface intensified. This accelerated the thermal degradation rate of the specimen's outer sheath, leading to a reduction in the time for the generation of combustible gases and ultimately resulting in the specimen igniting at an earlier stage. However, the rate of reduction diminished with time. This phenomenon could be attributed to the fact that, when the external radiation intensity reached higher levels (ranging from 50 to 60 kW/m^2 in this study), the accelerated thermal degradation effect due to the increased external radiant heat diminished. Consequently, the rate of ignition time reduction became less pronounced. Meinier et al. [17] observed similar patterns in their experimental investigations of halogen-free flame-retardant cables, and Chen [18] reported comparable findings regarding the combustion characteristics of flame-retardant EPDM rubber. Notably, the optical fiber exhibited a significantly shorter ignition time than the other cables under all four radiation intensities, with a mere 8 s. Therefore, in terms of ignition time alone, the flame retardancy ranking for the four cables was as follows: Cat6 ethernet cable > BV wire > YJV cable > OM3 optical fiber. As shown by the experiment, the LSZH materials demonstrated superior

flame retardancy compared with the flame-retardant PVC materials, with ordinary PVC materials displaying the poorest flame-retardant performance in this ranking.

Table 3. Summary of ignition time of different types of cables.

TTI(s)	Intensity of External Heat Radiation			
	30 kW/m^2	40 kW/m^2	50 kW/m^2	60 kW/m^2
Electrical cable	37	25	18	15
Wire	54	33	20	13
Network cable	151	77	49	46
Optical fiber	19	12	8	8

3.2. Heat Release Rate and Total Heat Release

3.2.1. Heat Release Rate

Figure 2 illustrates the variation in the heat release rate per unit area (HRRPUA) over time for the four cable types under four different external radiation intensities. HRRPUA was a crucial parameter for assessing the fire hazard of cables [19]. The HRRPUA curves for the cables remained relatively consistent under different intensities of external radiation, as demonstrated by the graph. However, with an increase in external radiation intensity, the curves shifted toward the left. This phenomenon occurred because higher external radiation heat levels resulted in the cables receiving a greater amount of radiative energy from the cone heater. Consequently, the surface temperature of the cable's outer sheath rose rapidly, leading to the thermal decomposition of the outer layer material. Compared with lower external radiation levels, this faster combustion reaction caused an accelerated increase in heat release, leading to a more rapid elevation in the heat release rate per unit area. During the combustion phase, the HRRPUA curves of different cable types exhibited variations. Optical fibers displayed a single peak, electrical cables showed an increase in heat release rate after a decrease in fire intensity with a curve featuring two peaks, and network cables and electric wires exhibited three distinct peaks. These differences arose due to a combination of factors, including cable material, flame-retardant properties, structure, and the formation of char during the combustion process.

The primary objective of this experiment was to measure the peak heat release rate (PHRR) and the average heat release rate (ave-HRR) during the onset of combustion up to 1 min, 3 min, and 5 min, denoted as ave-HRR1, ave-HRR3, and ave-HRR5, respectively [20]. The average and peak values of the heat release rate for each condition, along with the time to reach the peak (T_p), are presented in Table 3.

Table 4 clearly shows that an increase in the external radiation intensity led to a decrease in the time required for all four cable types to reach their maximum heat release rate (T_p), while their peak heat release rates increased by varying degrees. This phenomenon could primarily be attributed to higher external radiation intensities, resulting in faster material decomposition rates, more intense combustion, and greater heat emission. Consequently, a corresponding increase in the peak heat release rate and a gradual reduction in the time required to reach it were observed. The data in Table 4 indicate that electric wires had the greatest variation in T_p, while electrical cables had the smallest variation, with network cables and optical fibers falling in between. The differences in peak heat release rates were also pronounced across various radiation intensities, with network cables having shown the largest increase and electric wires having displayed the smallest increase, while cables and optical fibers lay in between. Furthermore, significant disparities were seen in the average heat release rates among the different cable types. Notably, at an external radiation intensity of 40 kW/m^2, the ave-HRR1 values for cables and optical fibers surpassed the ave-HRR3 and ave-HRR5 values, indicating that cables and optical fibers released a substantial amount of heat in the early stages of a fire. Moreover, at an external radiation intensity of 60 kW/m^2, network cables demonstrated the highest peak heat release rate among all conditions, reaching 676.3 kW/m^2 and requiring 213 s to reach

this peak. Optical fibers achieved their peak heat release rate much faster, in just 31 s, but their peak value was only 242.87 kW/m^2. Despite having achieved the fastest peak heat release rate, the heat release rate of optical fibers was merely 35.9% of that observed for network cables, indicating that optical fibers posed a lower level of risk compared with network cables.

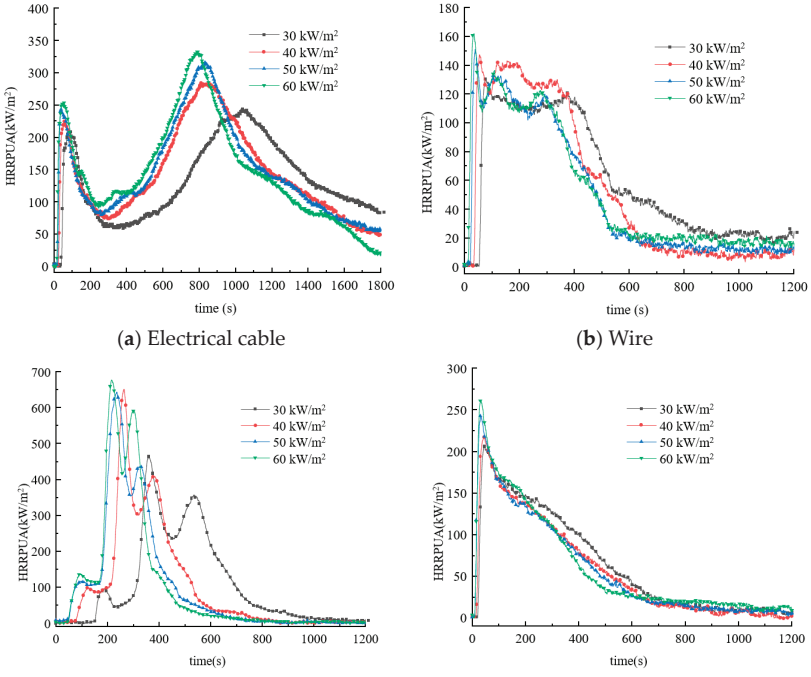

Figure 2. HRRPUA curves of cables under different radiation powers.

Table 4. Peak heat release rate and average heat release rate under different operating conditions.

NO.	Type	Intensity of External Heat Radiation (kW/m^2)	PHRR (kW/m^2)	T_P (s)	ave-HRR$_1$	ave-HRR$_3$	ave-HRR$_5$
T-1	Electrical cable	30	243.98 ± 1.28	1038	166.55	145.47	114.84
T-2		40	284.14 ± 1.31	826	198.10	153.93	124.98
T-3		50	316.08 ± 2.73	837	204.67	156.97	128.88
T-4		60	333.74 ± 2.63	792	216.71	177.71	146.89
T-5	Wire	30	130.67 ± 1.52	76	110.62	112.49	112.12
T-6		40	147.33 ± 1.33	55	117.50	130.83	129.35
T-7		50	151.83 ± 3.29	39	114.35	121.06	117.01
T-8		60	162.73 ± 2.73	33	120.52	121.06	118.46
T-9	Network cable	30	463.59 ± 3.46	360	53.03	75.07	180.10
T10		40	653.03 ± 5.17	264	69.48	144.08	247.42
T-11		50	644.63 ± 2.89	235	90.65	190.67	296.59
T-12		60	676.31 ± 3.68	213	95.29	213.88	325.40
T-13	Optical fiber	30	206.51 ± 1.89	46	165.90	161.01	150.87
T-14		40	217.36 ± 1.74	44	170.56	159.79	145.38
T-15		50	242.87 ± 2.65	31	192.27	167.41	148.99
T-16		60	261.72 ± 2.56	32	202.46	179.65	158.29

3.2.2. Total Heat Release

Table 5 provides a summary of the total heat release (THR) of cables under different external radiation intensities. Upon comparing the total heat release of cables at various radiation intensities after combustion, the average THR for cables was 258.49 MJ/m^2, while for wires, it was 65.02 MJ/m^2; for network cables, it was 122.90 MJ/m^2; and for optical fibers, it was 72.75 MJ/m^2. Overall, with the increase in external radiation intensity, the total heat release of the electrical cables tended to increase relative to that at 30 kW/m^2. When the external radiation intensity was raised from 30 kW/m^2 to 60 kW/m^2, the total heat release increased by 16.80 MJ/m^2.

Table 5. Total heat release of cables under different radiation intensities.

THR (MJ/m^2)	**Intensity of External Heat Radiation**			
	30 kW/m^2	**40 kW/m^2**	**50 kW/m^2**	**60 kW/m^2**
Electrical cable	245.47	259.33	266.89	262.26
Wire	71.88	65.07	59.63	63.49
Network cable	127.21	120.33	121.77	122.31
Optical fiber	77.13	69.41	70.74	73.71

3.3. Mass Loss and Residual Mass

3.3.1. Mass Loss

Figure 3 illustrates that, with an increase in external radiation intensity, the mass loss rate (MLR) of all four cable types accelerated, with the most significant changes being observed in wires and network cables. Additionally, for cables, wires, and network cables, the increase in MLR was more pronounced at low to moderate radiation intensities compared with the increment observed at moderate to high intensities. This behavior could be attributed to the flame-retardant properties of cables. At radiation intensities exceeding 40 kW/m^2, the flame-retardant capabilities of cables, wires, and network cables were compromised during the initial stages of a fire. However, at radiation intensities below 40 kW/m^2, the flame-retardant properties of the cables played a role in delaying the combustion of materials.

3.3.2. Residual Mass

Figure 4 presents summarized data on the combustion residual mass of cables under different external radiation intensities. Analyzing the combustion residues revealed that, for the same type of cable, the differences in residual mass under various external radiation influences remained within 1%. However, significant variations in combustion residues existed among the different types of cables. For instance, at an external radiation intensity of 60 kW/m^2, the cable and wire experienced mass losses of 26.05% and 13.74%, respectively, while the network cable and optical fiber encountered mass losses of 43.88% and 67.97%, respectively. The maximum difference between them was 54.23%. This was due to differences in the composition of the cable materials. The copper cores in the electrical cables and wires accounted for a significant portion of the mass, with relatively fewer combustible materials in the outer sheath and insulation layers. Under the specified radiation intensity, cables and wires experienced less mass loss during thermal decomposition and combustion. In contrast, network cables had a lower mass proportion of copper cores, and optical fibers involved combustion in both the outer sheath and the inner core. So, it could be concluded that network cables and optical fibers contained lower metal components, resulting in a higher rate of mass loss. In terms of residual mass, network cables and optical fibers exhibited greater combustibility. Compared to electrical cables and wires, network cables and optical fibers had significantly lower non-combustible component percentages, resulting in a higher rate of mass loss.

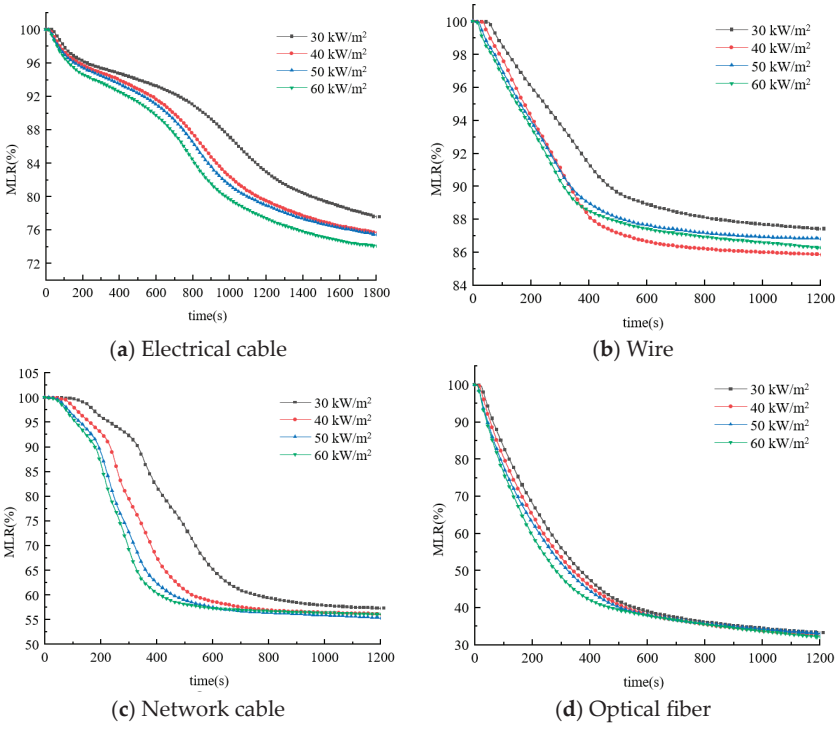

Figure 3. Mass loss of cables under different radiation intensities.

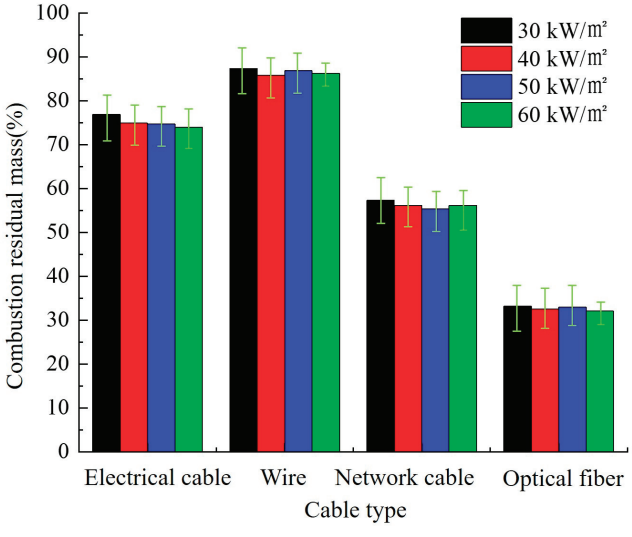

Figure 4. Residual mass of cables under different radiation intensities.

3.4. Comprehensive Fire Risk Analysis

3.4.1. Thermal Hazard Analysis

The use of combustion characteristics such as ignition time, heat release rate per unit area, peak heat release rate, and mass loss had limitations and allowed only a rough estimation of the combustion behavior of the four types of cables. Consequently, this

approach fell short of providing a comprehensive assessment of which material posed the greatest overall fire hazard. To address this limitation and to investigate the overall fire hazard of different cables under various radiation intensities, this study adopted two parameters from Petrella's fire hazard rating system [21]: total heat release and parameter X_0. Table 6 presents Petrella's fire hazard rating system based on parameter X_0. The formula for calculating X_0 is given in the following Equation (1).

$$X_0 = \frac{PHRR}{TTI} \quad (1)$$

The comprehensive evaluation table for the thermal hazards of different types of cables was computed and is presented in Table 7. As shown in Table 7, it became apparent that, for the same cable type, the X_0 parameter values increased with the increase in radiation intensity, indicating a corresponding escalation in the risk of fire. When using X_0 as the benchmark for assessing various cables, it was evident that fiber optic materials exhibited the greatest flashover hazard. Based on the total heat released, the different types of cables posed varying degrees of risk. Among them, electrical cables posed the highest risk for total heat release, indicating the highest level of danger. Following closely were the network cables and fiber optics, which released relatively lower amounts of total heat during the entire combustion process. Overall, a moderate to high level of fire hazard was presented by all four types of cables in the data center once the external radiation intensity had surpassed 30 kW/m^2. Among them, electrical cables exhibited the greatest overall risk of fire, followed by fiber optics and network cables, while wires posed the least danger.

Table 6. Petrella thermal hazard assessment.

Value	Total Heat Release (THR)	X_0 Parameter
0.1–1	Ultra-low risk	Low risk
1–10	Low risk	Medium risk
10–100	Medium risk	High risk
100–1000	High risk	--

Table 7. Comprehensive assessment form for cable thermal hazard.

NO.	Type	Intensity of External Heat Radiation (kW/m^2)	TTI (s)	THR (MJ/m^2)	X_0 Parameter	Overview
T-1	Electrical cable	30	37	245.47 ± 1.26 high risk	6.59 medium risk	Medium to high risk
T-2		40	25	259.33 ± 1.28 high risk	11.37 high risk	high risk
T-3		50	18	266.89 ± 2.11 high risk	17.56 high risk	high risk
T-4		60	15	262.26 ± 2.34 high risk	22.25 high risk	high risk
T-5	Wire	30	54	71.88 ± 0.57 medium risk	2.42 medium risk	medium risk
T-6		40	33	65.07 ± 0.82 medium risk	4.46 medium risk	medium risk
T-7		50	20	59.63 ± 1.58 medium risk	7.59 medium risk	medium risk
T-8		60	13	63.49 ± 2.10 medium risk	12.52 high risk	Medium to high risk

Table 7. *Cont.*

NO.	Type	Intensity of External Heat Radiation (kW/m^2)	TTI (s)	THR (MJ/m^2)	X_0 Parameter	Overview
T-9	Network cable	30	151	127.20 ± 1.07 high risk	3.07 medium risk	Medium to high risk
T10		40	77	120.33 ± 1.82 high risk	8.48 medium risk	Medium to high risk
T-11		50	49	121.77 ± 2.42 high risk	13.16 high risk	high risk
T-12		60	46	122.31 ± 2.26 high risk	14.74 high risk	high risk
T-13	Optical fiber	30	19	77.13 ± 1.52 medium risk	10.87 high risk	Medium to high risk
T-14		40	12	69.41 ± 1.95 medium risk	18.21 high risk	Medium to high risk
T-15		50	8	70.74 ± 2.49 medium risk	30.36 high risk	Medium to high risk
T-16		60	8	73.70 ± 2.76 medium risk	32.71 high risk	Medium to high risk

3.4.2. Smoke Toxicity Analysis

The toxicity of smoke produced during cable combustion was comprehensively assessed using the smoke production rate, CO release rate, and FED method. Certainly, during the combustion process of cables, the main component of the flame-retardant outer sheath, PVC, produces harmful chlorine gas. However, our experimental equipment at that time could not accurately measure chlorine gas data. This limitation was primarily due to technical constraints of the equipment and the limited availability of facilities for monitoring this specific gas in our region. Therefore, our toxicity analysis primarily focused on parameters we could accurately measure, such as smoke generation and CO/CO_2 emissions.

(1) Smoke production rate

The smoke production rate (SPR) was obtained by comparing the specific extinction area (SEA) with the mass loss rate (MLR). Figure 5 illustrates the smoke production rate (SPR) curves of the four cable types under different external heat radiation intensities. From the graph, it can be observed that the trends in the smoke generation rate curve and the heat release rate curve are similar. In the initial stage of material combustion, the smoke generation rate increased with an increase in external radiation. However, the smoke generation rate curve exhibited significant fluctuations, and the period of rapid smoke release coincided with the stage of high heat release rate. This indicates that the cable generated a substantial amount of smoke during the combustion phase, with the fire growing and the amount of smoke increasing simultaneously. Furthermore, the network cable exhibited the lowest smoke production rate. Under the influence of 30 kW/m^2 thermal radiation, there was minimal smoke production during the initial 80 s after ignition, with SPR1 having remained below 0.007 m^2/s. Additionally, following the attenuation of the fire, there was another period of approximately 150 s with almost no smoke generation. Even after 300 s, the peak smoke production rate was still under 0.035 m^2/s. The network cable demonstrated effective smoke suppression characteristics during the combustion experiment.

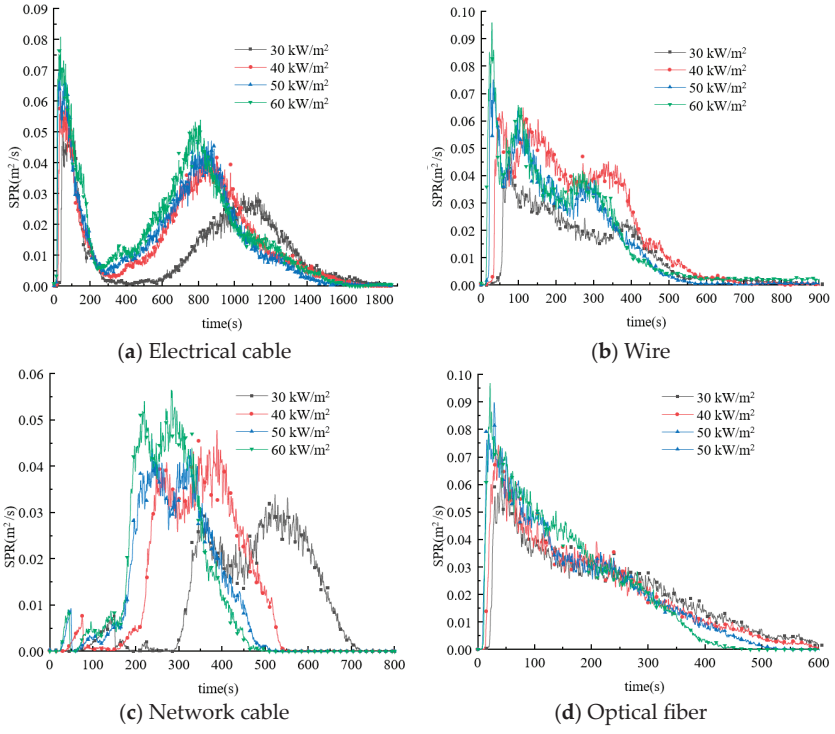

Figure 5. Smoke production rate of cables under different radiation intensities.

(2) Carbon monoxide release rate

Figure 6 illustrates the CO release rate curves of the four cable types under different radiation intensities. It was evident from the graph that the CO release rate curve of the cables followed a similar pattern to that of the unit area heat release rate curve, with an increase in toxic gas emissions as the heat release intensity rose. Moreover, there were notable differences in the CO generation rates among the various cables. The network cable exhibited a significantly lower CO release rate compared with the others, with only an approximately 0.0217% CO release rate under the influence of 60 kW/m^2 external heat radiation. In contrast, the CO release peaks of the other cables were generally in the range of 0.03% to 0.035%. The reason for this discrepancy was attributed to the superior smoke suppression effect of the LSZH sheathing material employed in the network cable, leading to a relatively lower CO release rate. As for the other three cable types, the distinctions in their CO release rates were less pronounced.

(3) FED method

The FED method enabled the calculation of smoke toxicity based on the composition and concentration of the combustion gases produced by the samples. In the FED testing related to CO and CO_2 gases, our primary focus was CO emissions because CO posed a greater risk to human health. In this study, the concentrations of toxic components in the cable combustion products were measured using a cone calorimeter, and a mathematical model for smoke toxicity was established to quantitatively analyze the risk of cable fires. The overall smoke toxicity was computed by considering the cumulative toxicity of each component [22].

$$FED = \sum \frac{\int_0^i C_i dt}{LC_{50}(i)t} \quad (2)$$

where FED is the fractional effective dose;

C_i is the concentration of toxic component i, μL/L;
$LC_{50}(i)t$ is the LC_{50} value of gas i, ppm.

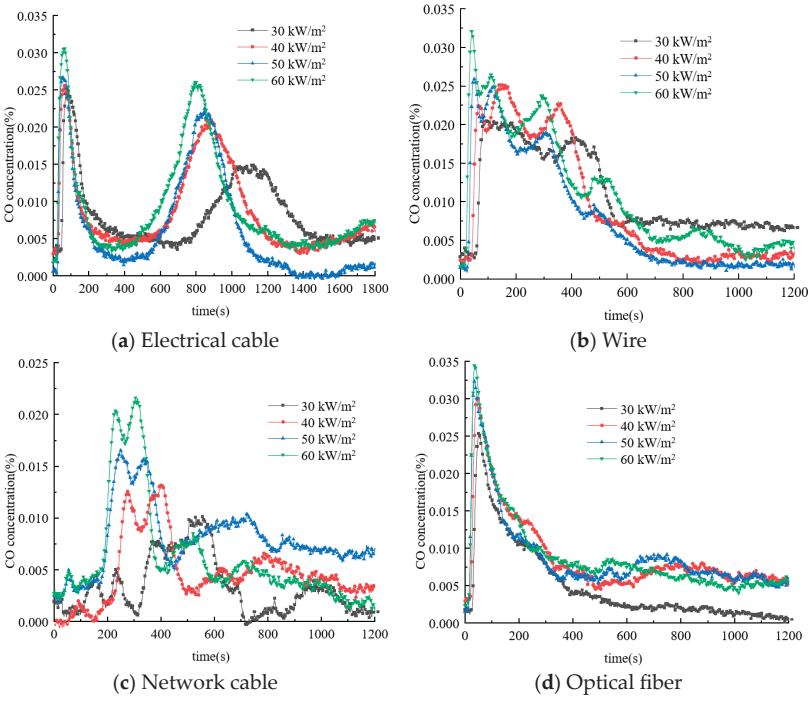

(**a**) Electrical cable (**b**) Wire

(**c**) Network cable (**d**) Optical fiber

Figure 6. Carbon monoxide release rate of cables under different radiation intensities.

As the toxic gases primarily detected in the cone calorimeter combustion experiment were CO and CO_2, Equation (3) can be simplified to the following:

$$FED = \frac{[CO]}{LC_{CO}} + \frac{[co_2]}{LC_{CO_2}} \tag{3}$$

The FED method was utilized to assess the toxicity of the smoke based on the calculated fractional effective dose. Since the measured CO_2 concentration was much lower than LC_{CO_2}, the value of $\frac{[co_2]}{LC_{CO_2}}$ became extremely small, allowing for further simplification of the formula to the following:

$$FED = \frac{[CO]}{5000} \tag{4}$$

The FED calculations under different radiation intensities are presented in Table 8, It was observed that the FED values of the four cable types at four different external radiation intensities, 30 kW/m^2, 40 kW/m^2, 50 kW/m^2, and 60 kW/m^2, ranged from 0.0203 to 0.06938, well below 1 (the FED value that would cause animal death), and did not reach a level of danger that would be fatal to humans. However, in practical scenarios, the potential risk posed by the generated toxic gases cannot be overlooked, given the number of cables involved. Table 8 indicates that, as the external radiation intensity increases, the toxicity of the smoke produced by the burning cables also increases, with the FED value of the network cable consistently remaining at the lowest level.

Table 8. Smoke toxicity of cable combustion under different operating conditions.

NO.	Type	Intensity of External Heat Radiation (kW/m^2)	CO Peak (ppm)	FED = [CO]/5000
T-1	Electrical cable	30	250.7 ± 1.50	0.0501
T-2		40	256.5 ± 1.28	0.0513
T-3		50	269.3 ± 2.11	0.0539
T-4		60	308.3 ± 2.08	0.0617
T-5	Wire	30	208.4 ± 1.02	0.0417
T-6		40	253.2 ± 1.54	0.0506
T-7		50	262.9 ± 2.17	0.0526
T-8		60	322.8 ± 3.01	0.0646
T-9	Network cable	30	101.5 ± 1.21	0.0203
T10		40	133.4 ± 1.36	0.0267
T-11		50	168.4 ± 2.27	0.0337
T-12		60	217.3 ± 2.51	0.0435
T-13	Optical fiber	30	253.5 ± 1.23	0.0507
T-14		40	302.8 ± 1.55	0.0606
T-15		50	328.0 ± 1.87	0.0656
T-16		60	346.9 ± 2.14	0.0694

4. Conclusions

This study examined the combustion characteristics and overall fire risk of four frequently employed cable types under distinct external radiation levels using a cone calorimeter. The principal conclusions are outlined as follows.

Regarding the combustion characteristics of the cable, the findings revealed that, with the increase in external radiation intensity, the TTI of all four cables decreased, but the rate of reduction gradually diminished over time. Among them, the ignition time for optical fibers was the shortest, with a TTI of merely 8 s. Additionally, the heat release rate per unit area (HRRPUA) of the four cables remained relatively unchanged but reached their first peak earlier. This phenomenon was attributed to the cables experiencing higher external heat radiation, causing a rapid increase in the surface temperature and promoting thermal decomposition of the outer layer materials, leading to accelerated combustion reactions and an increase in heat release, resulting in a faster rise in the heat release rate per unit area. Furthermore, the peak heat release rate (PHRR) of the four cables showed varying degrees of increase. The total heat release (THR) for the cable exhibited a slight rise. Moreover, the mass loss rate (MLR) for all four cables was accelerated, and the proportion of mass loss for cables and wires was lower compared with those of network cables and optical fibers, with a maximum difference of 54.23%. This discrepancy primarily arose from the larger proportion of non-combustible components in cables and wires.

Our ability to determine the overall risk of fire of cables is limited when relying solely on an analysis of cable fire hazards based on their combustion characteristics. Therefore, to comprehensively evaluate the fire hazards of different types of cables, it was necessary to consider both their thermal hazards and smoke toxicities. As the external radiation intensity increased, the overall thermal hazard of all four cables increased, with electrical cables presenting the greatest risk, followed by network cables and optical fibers, and finally, wires. In the assessment of smoke toxicity, the lowest level of overall smoke toxicity among the four cable types was exhibited by network cables, while no significant difference was shown by the other three. Additionally, none of the materials reached toxic gas concentrations that could cause human fatalities. Therefore, electric cables pose the greatest overall risk of fire.

In this study, considering both thermal hazards and smoke toxicity, we ascertained that electrical cables pose the greatest risk of fire, supported by experimental data for these cables under different radiation intensities. This study provides valuable data that support the study of cable combustion characteristics in scenarios where cable hazards need to be considered.

Author Contributions: Conceptualization, B.S.; methodology, B.S. and H.L.; validation, B.S. and C.Y.; investigation, B.S. and H.L.; resources, B.S.; data curation, H.L.; writing—original draft preparation, C.Y. and H.L.; writing—review and editing, B.S. and C.Y.; visualization, H.L.; supervision, B.S.; project administration, B.S.; funding acquisition, B.S. All authors have read and agreed to the published version of the manuscript.

Funding: This research was supported by the National Natural Science Foundation of China (Grant No. 52074277) and the Natural Science Foundation of Jiangsu Province (Grant No. BK20211585).

Institutional Review Board Statement: Not applicable.

Informed Consent Statement: Not applicable.

Data Availability Statement: Data are contained within the article.

Conflicts of Interest: The authors declare no conflict of interest.

Abbreviations

TTI	time to ignition
HRRPUA	heat release rate per unit area
ave-HRR	average heat release rate
PHRR	peak heat release rate
THR	total heat release
MLR	mass loss rate
SPR	smoke production rate
SEA	smoke extinction area
FED	fractional effective dose

References

1. Xue, Y. Experimental Research on Fire Spread of PE and ETFE Conductors under Low-Pressure Conditions. Ph.D. Thesis, University of Science and Technology of China, Hefei, China, 2017.
2. Zhu, K. Research on Horizontal and Inclined Fire Spread Behavior of Inner Core Wires with Different Thermal Conductivity under Low-Pressure Conditions. Ph.D. Thesis, University of Science and Technology of China, Hefei, China, 2019.
3. Huang, X.; Nakamura, Y. A Review of Fundamental Combustion Phenomena in Wire Fires. *Fire Technol.* **2020**, *56*, 315–360. [CrossRef]
4. Fontaine, G.; Ngohang, F.E.; Gay, L.; Bourbigot, S. Investigation of the Contribution to Fire of Electrical Cable by a Revisited Mass Loss Cone. In *Fire Science and Technology 2015: The Proceedings of 10th Asia-Oceania Symposium on Fire Science and Technology*; Springer: Singapore, 2017; pp. 687–693.
5. Zheng, X.; Cai, G.; Guo, J.; Gao, W.; Huang, Y.; Tong, X. Combustion Characteristics and Thermal Decomposition Mechanism of the Flame-Retardant Cable in Urban Utility Tunnel. *Case Stud. Therm. Eng.* **2023**, *44*, 102887. [CrossRef]
6. Elliot, P.; Whiteley, R. A Cone Calorimeter Test for the Measurement of Flammability Properties of Insulated Wire. *Polym. Degrad. Stab.* **1999**, *64*, 577–584. [CrossRef]
7. Barnes, M.A.; Briggs, P.J.; Hirschler, M.M.; Matheson, A.F.; O'Neill, T.J. A Comparative Study of the Fire Performance of Halogenated and Non-Halogenated Materials for Cable Applications. Part I Tests on Materials and Insulated Wires. *Fire Mater.* **1996**, *20*, 17–37. [CrossRef]
8. Tang, K.; Zhang, Y.; Jiang, S.; Li, C.; Ma, C.; Liu, G.; Zhang, H.; Yuan, B. A Comparative Study on Fire Hazards of Cables Used in Nuclear Power Plants Based on Small- and Large-Scale Experiments. *J. Therm. Anal. Calorim.* **2022**, *147*, 14659–14671. [CrossRef]
9. Matheson, A.F.; Charge, R.; Corneliussen, T. Properties of PVC Compounds with Improved Fire Performance for Electrical Cables. *Fire Saf. J.* **1992**, *19*, 55–72. [CrossRef]
10. Hirschler, M.M. Survey of Fire Testing of Electrical Cables. *Fire Mater.* **1992**, *16*, 107–118. [CrossRef]
11. Kaczorek-Chrobak, K.; Fangrat, J.; Papis, B.K. Calorimetric Behavior of Electric Cables. *Energies.* **2021**, *14*, 1007. [CrossRef]
12. Mun, S.Y.; Hwang, C.H. Experimental and Numerical Studies on Major Pyrolysis Properties of Flame Retardant PVC Cables Composed of Multiple Materials. *Materials* **2020**, *13*, 1712. [CrossRef] [PubMed]
13. Shi, C.; Qian, X.; Zhang, Y.; Jing, J.; Ren, F.; Li, J. Research on the Combustion Characteristics of ZR-YJLV Cables Based on Flame Propagation Calorimetry. *China Saf. Prod. Sci. Technol.* **2020**, *16*, 17–21.
14. Zhang, J.; Guo, Y.; Feng, R.; Li, K.; Huang, Y.; Shang, F. Characteristics and Reaction Mechanism of Pyrolysis Solid Gas Products of Typical Substation Flame-Retardant Low-Voltage Cable Outer Sheath Materials under Fire Conditions. *J. Tsinghua Univ. (Nat. Sci. Ed.)* **2022**, *62*, 33–42.
15. Sun, Z. *Experimental Analysis and Numerical Simulation of Radiation Ignition Behavior of Subway Cables*; Capital University of Economics and Business: Beijing, China, 2019.

16. *ISO 5660-1*; Reaction-to-Fire Tests-Heat Release, Smoke Production and Mass Loss Rate-Part1 Release Rate (Cone Calorimeter Method) and Smoke Production Rate (Dynamic Measurement). International Organization for Standardization (IOS): Geneva, Switzerland, 2015.
17. Meinier, R.; Sonnier, R.; Zavaleta, P.; Suard, S.; Ferry, L. Fire Behavior of Halogen-Free Flame Retardant Electrical Cables with the Cone Calorimeter. *J. Hazard. Mater.* **2018**, *342*, 306–316. [CrossRef] [PubMed]
18. Chen, R. *Research on Pyrolysis and Combustion Characteristics of Typical Interior Materials of Subway Trains*; University of Science and Technology of China: Hefei, China, 2016.
19. Zhou, Q. Comparison of Experimental Methods for Fire Response of Materials. *Fire Sci. Technol.* **2007**, *2007*, 34–37.
20. Shu, Z.; Xu, X.; Li, X. *Fire Combustion Performance Evaluation of Polymer Materials: Cone Calorimeter Test Method*; Chemical Industry Press: Beijing, China, 2007.
21. Petrella, R. The Assessment of Full-Scale Fire Hazards from Cone Calorimeter Data. *J. Fire Sci.* **1994**, *12*, 14–43. [CrossRef]
22. Mao, Y. *Research on Fire Protection Development System of Passenger Cars Based on Fire Risk Analysis*; University of Science and Technology of China: Hefei, China, 2019.

fire

MDPI

Article

Simulation of Damage Caused by Oil Fire in Cable Passage to Tunnel Cable

Feng Liu [1], Jiaqing Zhang [2], Mengfei Gu [3], Yushun Liu [2], Tao Sun [2] and Liangpeng Ye [2,*]

[1] State Grid Anhui Electric Power Co., Ltd., No. 9 Huangshan Road, Baohe District, Hefei 230061, China; ahdky_st@163.com
[2] Electric Power Research Institute, State Grid Anhui Electric Power Co., Ltd., 299 Ziyun Road, Economic and Technological Development Zone, Hefei 230601, China; dkyzjq@163.com (J.Z.); silencelys@163.com (Y.L.); xkssun@163.com (T.S.)
[3] Hefei Power Supply Company, State Grid Anhui Electric Power Co., Ltd., No. 133 Susong Road, Baohe District, Hefei 230022, China; 18855165990@163.com
* Correspondence: 15551180972@163.com

Abstract: In order to evaluate the damage to tunnel cables caused by fire caused by leakage of transformer oil into a cable channel, the fire characteristics of different volumes of transformer oil flowing into a cable channel were analyzed by numerical simulation. The results show that when the total leakage of transformer oil is less than or equal to 3 L, the fire will end within 120 s, and when the total leakage is greater than or equal to 5 L, the fire duration will exceed 900 s. When the leakage amount is 1 L, the cable only burns slightly, and when the leakage amount is 3~12 L, the cable burns obviously. The combustion of the cable is mainly concentrated between 15 s and 75 s, and the overall combustion rate of the cable increases first and then decreases. When the total leakage is greater than or equal to 8 L, the damage distance of the middle and lower layer cable is the smallest. When the total leakage is less than or equal to 5 L, the damage distance of the lower layer cable is the smallest, and the damage distance of the lower layer cable, middle and lower layer cable, and middle and upper layer cable is less than half of the length of the cable channel.

Keywords: cable channel; transformer oil; cable fire; cable damage; fire

Citation: Liu, F.; Zhang, J.; Gu, M.; Liu, Y.; Sun, T.; Ye, L. Simulation of Damage Caused by Oil Fire in Cable Passage to Tunnel Cable. *Fire* **2024**, *7*, 147. https://doi.org/10.3390/fire7040147

Academic Editors: Grant Williamson, Ying Zhang, Xiaoyu Ju, Xianjia Huang and Fuchao Tian

Received: 18 December 2023
Revised: 8 April 2024
Accepted: 10 April 2024
Published: 19 April 2024

1. Introduction

With the development of the economy and the increase in urban residents, the demand for industrial production and daily electricity in various regions of China is also increasing. The transmission lines arranged in the past cannot meet the demand for electricity today, so it is urgent to add more transmission lines to ensure the normal operation of social and economic life. In the past, power transmission lines were often laid as overhead lines. However, due to the development of urban construction and the increasing density of population distribution in China's cities, there is a serious shortage of land resources, leading to a direct contradiction between power transmission resources and land resources. Therefore, the method of transmitting power in the form of cable channels has gradually come into people's view. On one hand, overhead lines occupy ground space and are prone to problems such as aging, damage, and difficult maintenance due to exposure to the open air and height. On the other hand, compared to overhead lines, underground cable channels have the advantages of convenient power operation and maintenance, minimal ground space occupation, and reduced risk of cable damage, leading to an increase in the construction of underground cable channels.

The increase in the number of cable channels has also brought attention to the fire hazards associated with cable channels. Currently, a large number of power cables and communication cables are laid through underground cable channels, and some cable channels are arranged near transformers due to site and power transmission requirements,

such as the terminal and end of transmission and transformation, which inevitably require proximity to transformers. However, transformer fires occur frequently [1,2], and due to limitations in current technology, transformers worldwide still use oil storage for insulation and cooling, posing a risk of oil ignition. Once deflagration occurs, burning transformer oil may flow into the cable channel and ignite the cables concentrated within, potentially leading to the spread of fire along the cable channel.

Due to the high cost of physical experiments on the spread of fire in cable passages, numerical simulation methods are primarily used for research [3–8]. Relevant scholars at home and abroad have carried out some research on cable passage fires, but the research scenarios are mostly limited to cable fault combustion in common cable passages and cable combustion in underground pipe corridors, and there are relatively few studies on the combustion of oil, especially transformer oil, into cable passages. In view of this situation, this paper uses numerical simulation to simulate fire in a cable channel caused by transformer oil, taking a cable channel as an example, in order to evaluate the damage to the tunnel cable caused by the fire caused by leaking transformer oil into the cable channel.

2. Model Building

2.1. Cable Channel Prototype and Simplified Physical Model

2.1.1. Cable Tunnel Prototype

The prototype to be studied is a cable channel near a transformer in China, and its cross-section design is shown in Figure 1. The section size of the cable channel is 1 m × 1.1 m. Eight cables are placed, and four cables are arranged on the left and right sides. The four layers of cables are defined as the lower layer cables, lower layer cables, upper layer cables, and upper layer cables from the bottom up. Two drainage ditches for ventilation are provided on the lower side of the cable passage. A firewall is installed every 60 m in the cable channel, so every 60 m is a fire protection zone. The cable is a crosslinked polyethylene (XLPE) flame retardant cable, and the flame retardant cable is placed in the cable channel in the form of a cable bundle with multiple cables, as shown in Figure 1.

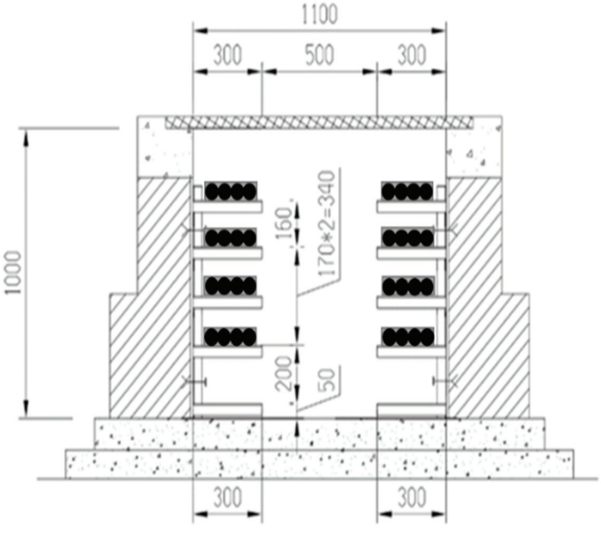

Figure 1. Cable channel size and cable layout.

2.1.2. Physical Model

A fire protection zone is considered, so the cable channel model length is 60 m, the section size is 1000 mm × 1100 mm, and the cable bracket width is 300 mm. The main fuel in the cable channel is the cable. Ignore other facilities in the cable channel. Considering the

drainage ditch and its ventilation function, the equivalent area method is used to simplify the cable trench and cable. The physical simplification model is shown in Figure 2.

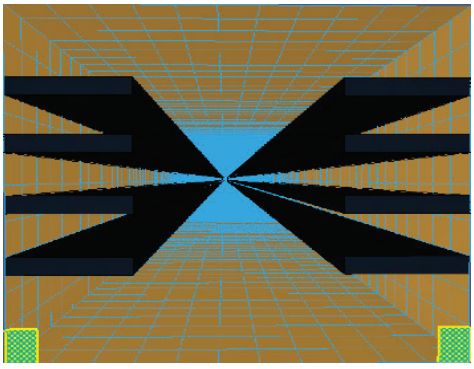

Figure 2. Section diagram of the cable channel model.

2.2. Cable Channel Prototype and Simplified Physical Model

The FDS (Fire Dynamics Simulator) software developed by NIST of the United States Institute of Standards and Technology (Gaithersburg, MD, USA) is used for simulation. FDS can describe the problem of low Mach number gas flow and can well solve the problems of temperature, heat flux, heat release rate, visibility, and combustion product concentration changes with the development of fire. Based on the three conservation equations of mass (component), momentum, and energy, as well as basic fluid dynamics equations such as the ideal gas equation, the region in the calculation grid is calculated, and the Arrhenius formula is used to calculate the combustion chemical reaction [9]. The details are as follows:

$$\frac{\partial \rho}{\partial t} + \nabla \cdot \rho u = 0 \tag{1}$$

$$\frac{\partial}{\partial t}(\rho \vec{u}) + \nabla \cdot \rho u u + \nabla \cdot p = \rho g + f + \nabla \cdot \tau_{ij} \tag{2}$$

$$\frac{\partial}{\partial t}(\rho h) + \nabla \cdot \rho h u = \frac{Dp}{Dt} + \dot{q}^m - \nabla \cdot \dot{q}^n + \varnothing \tag{3}$$

$$p = \frac{\rho R T}{\overline{W}} \tag{4}$$

$$r_s = \left(\frac{\rho_{s,i}}{\rho_{s0}}\right)^{n_s} A \cdot exp\left(\frac{-E}{RT_S}\right) \tag{5}$$

where ρ is gas density (kg/m^3); u is the velocity vector (m/s); g is the gravitational acceleration (m/s^2); f is the external force vector (N); τ_{ij} is the Newtonian viscous stress tensor (N); h is the sensible enthalpy (J/kg); p is the pressure (Pa); $\dot{q}^m$ is the heat release rate per unit volume (W/m^3); $\dot{q}^n$ is the heat flux vector (W/m^2); T is the temperature (K); $\varnothing$ is the dissipation function; R is the ideal gas constant; $\overline{W}$ is the relative molecular mass of the gas mixture; ρ_{s0} is the initial density of the s layer (kg/m^3); $\rho_{s,i}$ is the density of component i in the s layer (kg/m^3); A refers to the pre-factor (1/s); E is the activation energy (kJ/mol); n_s is the mass fraction index of the s layer; and T_S indicates the temperature of layer s (°C).

2.3. Fire Scenario Analysis

Consider burning transformer oil leaking into the cable channel and causing a fire. The leakage of burning transformer oil into the cable channel is caused by transformer deflagration, splashing, jets, and other uncertain situations, so the leakage location, leakage

area, and leakage amount of burning transformer oil into the cable channel are difficult to determine. Therefore, in this study, it is assumed that the leakage center of the transformer oil burned in each working condition is the center of the cable channel (30 m away from one end of the channel), the diffusion area of the transformer oil is 1 m^2, the leakage rate is equal to the burning rate of the transformer oil in an area of 1 m^2, and the total leakage of the transformer oil increases from 1 L to 12 L according to different working conditions. They are 1 L, 3 L, 5 L, 8 L, 10 L, and 12 L. Since the diffusion area is constant, the total leakage can be controlled by the thickness change of the transformer oil.

2.4. Fire Source and Combustion Model

Assuming that the only possible combustibles in the cable channel are cables and the transformer oil leaking into the cable channel, the simulated initial fire source is the transformer oil, and other combustibles in the cable channel are cables.

The transformer oil in the transformer near a cable channel is KI50X transformer oil, and the heat of evaporation and combustion are 364.9 KJ/kg and 4.51 MJ/kg, respectively [10,11]. The combustion process of transformer oil is simplified to a process in which transformer oil evaporates into oil steam and oil steam continues to burn, and the combustion chemical reaction adopts the Arrhenius formula [9].

Most of the cables laid in the cable channel are flame-retardant crosslinked polyethylene cables, so their reactants are mainly crosslinked polyethylene. Therefore, referring to previous results [12], the ratio of copper to XLPE is assumed to be 6:4, and the specific heat capacity, thermal conductivity, and density of copper and XLPE are set according to [13]. For chemical reaction kinetic parameters, referring to previous experimental results [14], the pre-factor, apparent activation energy, and mass fraction index were set as 2 × 1022 (1/s), 317 (KJ/mol), and 0.8, respectively. The location of the cable bundle is the same as in the simulation prototype.

2.5. Grid Sensitivity Analysis

In FDS, the size of the grid determines the simulation accuracy and calculation time, and the simulation accuracy and calculation time are inversely proportional to the mesh size. In order to make the grid size set more reasonable, it is necessary to analyze the sensitivity of the grid to make the simulation results reasonable enough. According to the calculation method in The FDS User Guide [9], a more reasonable range of mesh size can be obtained, and the relevant formula is as follows:

$$D^* = \left(\frac{\dot{Q}}{\rho_\infty c_p T_\infty \sqrt{g}} \right)^{\frac{2}{5}} \tag{6}$$

where ρ_∞ is the ambient air density, which is 1.1164 kg/m^3 in this study; c_p is the specific heat capacity of air in the environment, which is 1.013 kJ/(kg·K) in this study; T_∞ is the temperature of the environment, which is 293 K in this study; g is the acceleration of gravity, which is 9.8 m/s^2 in this study; $\dot{Q}$ is the heat release rate of the fire source—the size is set according to the fire source, and the unit is kJ/s (kW); and D^* is the characteristic diameter of the fire, expressed in m.

$$\frac{\delta x}{D^*} = \frac{1}{R} \tag{7}$$

where δx represents the size of the grid, and R is the recommended coefficient, generally between 4 and 16.

Since the transformer oil simulated into the cable channel is KIX50 transformer oil, according to the experimental data [15,16], the maximum heat release rate per unit area of a 100 mm × 100 mm oil pan is HRRPUA = 783.26 kW/m^2. Since the area of the transformer oil in the simulation is 1 m, the heat release rate of the fire source $\dot{Q}$ is 783.26 kW. By bringing the data into the above equation, it can be concluded that D^* is about 0.879 m

and 0.05 m $\leq \delta x \leq$ 0.21 m. In order to improve the simulation accuracy, the mesh size in this study is set to 0.1 m × 0.1 m. In particular, it should be noted that in this paper, the cable will have a combustion reaction, and the combustion process is controlled by the above parameters.

3. Results and Discussion

3.1. Influence of Leakage on the Fire Process of Cable Passage

The influence of leakage on the fire process of the cable channel is analyzed through the heat release rate, the change in average oxygen concentration, the burning rate of the cable, and the burning rate of the transformer oil. The change in heat release rate and average oxygen concentration in each working condition is shown in Figure 3, and the burning rate of the cable and transformer oil in each working condition is shown in Figure 4.

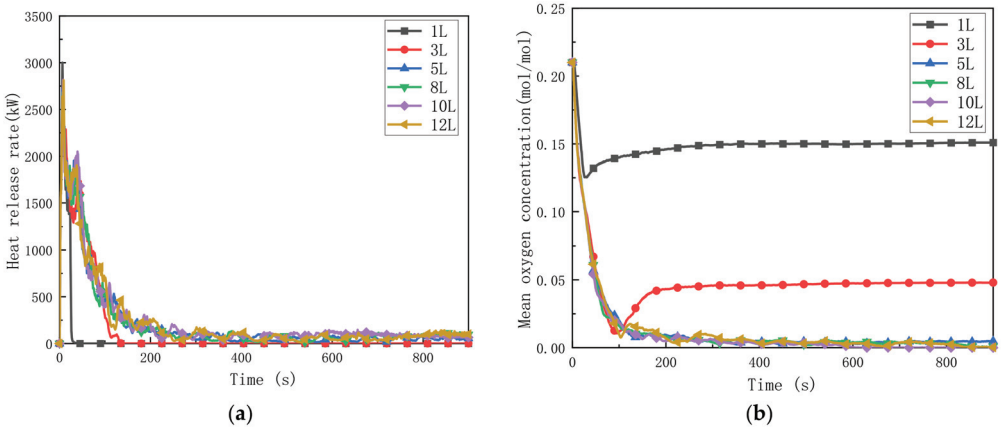

Figure 3. Diagram of variation in heat release rate and average oxygen concentration under various working conditions: (**a**) variation diagram of heat release rate under different working conditions; (**b**) variation diagram of average oxygen concentration under different working conditions.

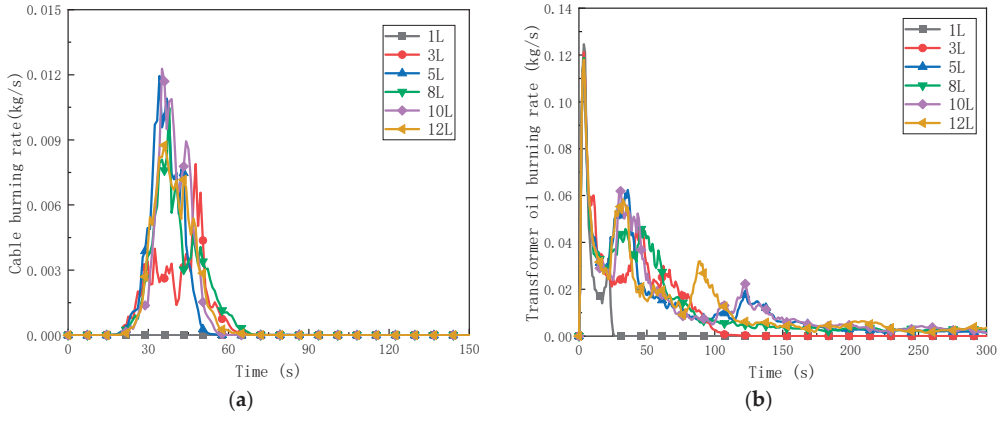

Figure 4. Diagram of cable burning rate and transformer oil burning rate variation under various working conditions: (**a**) variation diagram of cable burning rate under different working conditions; (**b**) transformer oil burning rate variation diagram under different working conditions.

According to the curve of heat release rate, the fire under each working condition did not have an obvious full combustion period after a short growth period but directly entered a decline period, and the heat release rate reached about 2800 KW at the beginning

of the simulation and then dropped rapidly. When the leakage amount is 3~12 L, the heat release rate will rise by about 500 KW after the decline and then continue to decline, but when the leakage amount is 1 L, the heat release rate does not rise significantly and continues to decline. When the leakage amount is 1 L and 3 L, respectively, the heat release rate decreases to 0 about 30 s and 120 s after the simulation, indicating that there is no combustion in the cable channel with this leakage amount. When the leakage amount is 5 L, 8 L, 10 L, and 12 L, the heat release rate decreases to below 100 kW after 160 s, 180 s, 210 s, and 230 s, and then starts to fluctuate up and down until the end of the simulation. According to the change in heat release rate, when the leakage amount of the transformer oil is less than or equal to 3 L, the fire will end within 120 s, and when the leakage amount is greater than or equal to 5 L, the duration of the fire will exceed 900 s.

As can be seen from the average oxygen concentration curve, when the leakage is 1 L and 3 L, the oxygen concentration on the whole first drops to the lowest value and then slowly rises to the end of the simulation. When the leakage is 1 L and 3 L, the oxygen concentration decreases to about 0.12 mol/mol and 0.015 mol/mol at about 20 s and 100 s, respectively. Then it slowly rose to about 0.15 mol/mol and 0.05 mol/mol, respectively, until the end of the simulation. When the leakage is 5 L, 8 L, 10 L, and 12 L, respectively, the oxygen content in the entire cable channel gradually decreases with the combustion of the cable, and the oxygen concentration decreases from 0.21 mol/mol to about 0.01 mol/mol after 130 s, 120 s, 110 s, and 105 s, respectively, and then begins to fluctuate up and down until the end of the simulation.

From the point of view of the cable burning rate, when the leakage is 1 L, the cable burning rate is very low, and only slight combustion occurs. When the leakage amount is 3~12 L, the cable appears to have obvious combustion; the combustion of the cable is mainly concentrated between 15 s and 75 s, and the overall burning rate of the cable shows a trend of first rising and then decreasing.

From the point of view of the burning rate of the transformer oil, at the beginning of the fire, the burning rate of the transformer oil in each working condition rapidly increased to about 0.12 kg/s, then quickly dropped to 0.3 kg/s, showing a slight recovery, and then began to continue to decline in volatility until the end of the simulation. When the leakage amount is 1 L and 3 L, respectively, the burning rate of the transformer oil is reduced to 0 kg/s at about 28 s and 110 s, respectively. When the leakage is 5~12 L, the burning rate of the transformer oil slowly decreases to about 0.01 kg/s and fluctuates up and down until the end of the simulation.

By comparing the burning rate of the cable and the transformer oil, it can be found that the burning time of the cable is within 75 s after the fire, and the main fuel in the subsequent fire is the transformer oil. Combined with the heat release rate curve and the change in average oxygen concentration, we can see the development process of the fire caused by the transformer oil entering the cable channel. Due to the combustion of the transformer oil, the oxygen near the transformer oil is rapidly consumed. If the transformer oil is insufficient, the cable will only burn slightly after the transformer oil is exhausted. If the transformer oil is sufficient, it will ignite the cable in the cable channel. With the reduction in oxygen concentration, the combustion of the cable and the transformer oil is suppressed, and after a period of time, the cable no longer burns, and only the transformer oil burns in the cable channel.

3.2. Assessment of Cable Damage Range Caused by Fire

Cable channels are mostly unmanned places, so it is only necessary to pay attention to the economic losses caused by the burning transformer oil entering the cable channels. The main combustible material in the cable channel is the cable. According to the previous research [17,18], the damage to the cable starts with pyrolysis at about 250 °C, so the area with the highest temperature above 250 °C is identified as the area where the cable may be damaged. Therefore, this study can analyze the fire loss caused by the combustion of the external transformer oil entering the cable channel by analyzing the temperature changes

at different horizontal and vertical positions in the simulated working conditions. The highest temperature at different horizontal and vertical positions from one end of the cable channel in each simulated working condition is shown in Figure 5.

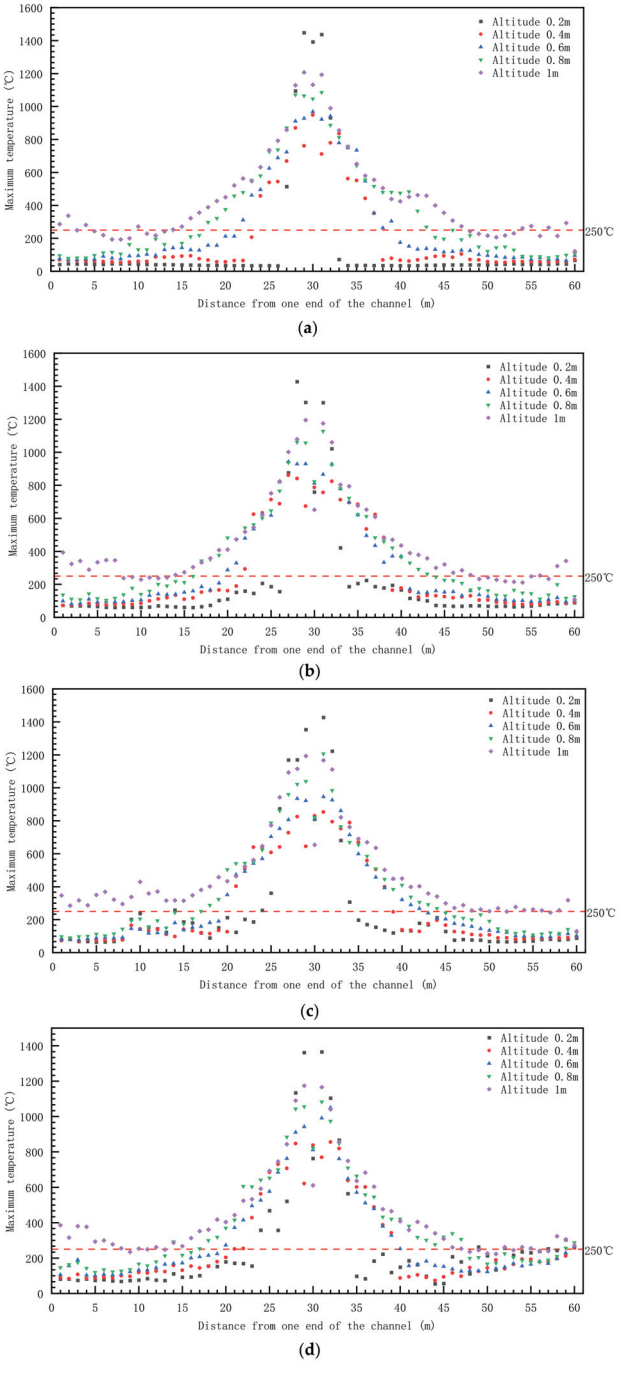

Figure 5. *Cont.*

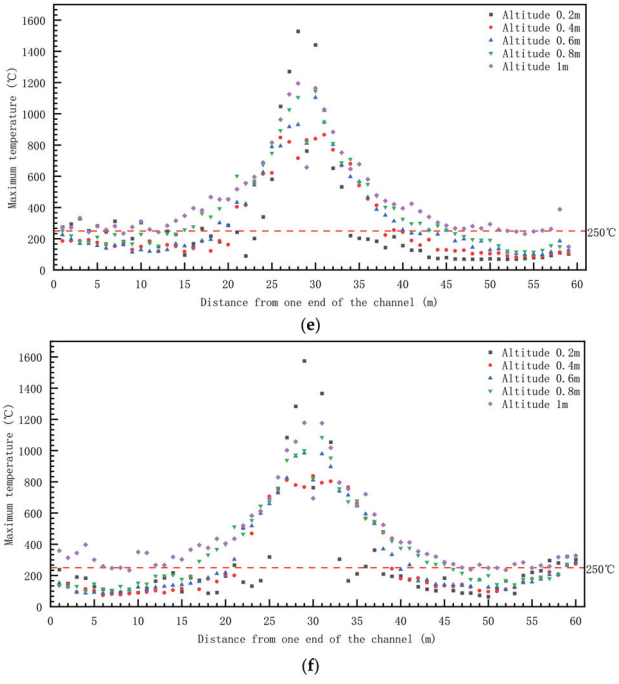

Figure 5. Maximum temperature variation diagram at different horizontal and vertical positions under different working conditions: (**a**) maximum temperature diagram at each horizontal position and height when the leakage amount is 1 L; (**b**) maximum temperature diagram at each horizontal position and height when the leakage amount is 3 L; (**c**) maximum temperature diagram at each horizontal position and height when the leakage amount is 5 L; (**d**) maximum temperature diagram at each horizontal position and height when the leakage amount is 8 L; (**e**) maximum temperature diagram at each horizontal position and height when the leakage amount is 10 L; (**f**) maximum temperature diagram at each horizontal position and height when the leakage amount is 12 L.

In particular, it should be noted that although the combustion model of the cable in this paper is set, the damage to the cable and the combustion of the cable are not the same concept. When the cable is at 250 °C, the mechanical properties and insulation properties will decline, and melting (non-combustion) will also occur. Therefore, in this paper, the cable reaching 250 °C is used as the judgment standard for cable damage instead of using cable burning as the criterion for judging cable damage.

The maximum temperature of each simulated condition in the horizontal direction takes 30 m as the origin, and the temperature decreases gradually along the position far from the origin until it rises slightly near the end of the cable channel. When the leakage amount is 1 L to 5 L, the slight rise in temperature at one end of the cable channel does not exceed 250 °C, except for at a height of 1 m. When the leakage is 8 L to 12 L, the slight rise in temperature at one end of the cable channel exceeds 250 °C, which increases the length of the cable that may be damaged. In the vertical direction, the maximum temperature of each horizontal position increases with the increase in height, except where the height of one end of the channel is 0.2 m (there is a vent).

As can be seen from FIG. 5, when the leakage volume is 1 L, the maximum spacing between each position with temperatures greater than 250 °C in the cable channel at heights of 0.2 m, 0.4 m, 0.6 m, 0.8 m, and 1 m is 7 m, 15 m, 18 m, 27 m, and 59 m, respectively. When the leakage volume is 3 L, the maximum spacing between temperatures above 250 °C at heights of 0.2 m, 0.4 m, 0.6 m, 0.8 m, and 1 m is 8 m, 18 m, 22 m, 29 m, and 59 m, respectively. When the leakage volume is 5 L, the maximum spacing between temperatures

above 250 °C in the cable channel at heights of 0.2 m, 0.4 m, 0.6 m, 0.8 m, and 1 m is 22 m, 20 m, 24 m, 29 m, and 59 m, respectively. When the leakage amount is 8 L, the maximum spacing between temperatures above 250 °C in the cable channel at heights of 0.2 m, 0.4 m, 0.6 m, 0.8 m, and 1 m is 27 m, 39 m, 39 m, 44 m, and 60 m, respectively. When the leakage volume is 10 L, the maximum spacing between temperatures above 250 °C in the cable channel at heights of 0.2 m, 0.4 m, 0.6 m, 0.8 m, and 1 m is 34 m, 20 m, 28 m, 45 m, and 59 m, respectively. When the leakage volume is 12 L, the maximum spacing between temperatures above 250 °C in the cable channel at heights of 0.2 m, 0.4 m, 0.6 m, 0.8 m, and 1 m is 40 m, 39 m, 40 m, 42 m, and 60 m, respectively.

Since the height of each layer of cable in the simulated working condition is between 0.2 m and 0.4 m, 0.4 m and 0.6 m, 0.6 m and 0.8 m, and 0.8 m and 1 m, the highest temperature at different horizontal positions of each layer of cable is the highest temperature in the corresponding interval. The damage distance in the horizontal direction is the maximum distance between the two ends of the channel above 250 °C. Through data analysis, the damage distance of cables in different working conditions and layers can be obtained, as shown in Table 1. Cable damage distance can measure the extent of cable damage.

Table 1. Cable damage distance table for each layer in each working condition.

Leakage (L)	Cable Damage Distance (m)			
	Bottom Cable	Middle and Bottom Cable	Upper-Middle Cable	Top Cable
1	15	18	27	59
3	18	22	29	59
5	22	24	29	59
8	39	39	44	60
10	34	28	45	59
12	40	40	42	60

It can be seen from the data in the above table that the damage distance of the upper layer cable in each working condition is the largest, and the damage distance is very close to the length of the cable channel. The maximum damage distance of the bottom cable, middle and bottom cable, middle and upper cable, and upper cable in each working condition is between 15 m and 40 m, 18 m and 41 m, 27 m and 45 m, and 59 m and 60 m. When the leakage amount is 1~8 L, the damage distance of each layer of cable gradually increases with the increase in height, and the damage distance between the lower layer cable and the middle and lower layer cable is small. With the increase in transformer oil thickness, the damage distance of each layer of cable also increases.

4. Conclusions

In evaluating the impact of transformer oil leaks on tunnel cables and the ensuing fire characteristics within cable channels, this study leverages numerical simulations. The findings lead to the following conclusions:

(1) Fire Duration and Transformer Oil Leakage

Under the specified study conditions, when the transformer oil leakage is 3 L or less, the fire ceases within 120 s. Conversely, when the leakage exceeds or equals 5 L, the fire's duration surpasses 900 s.

(2) Cable Combustion Rates

In this study's operational context, a leakage amount of 1 L results in a very low combustion rate for the cable, with only slight combustion occurring. For leakage amounts ranging from 3 L to 12 L, noticeable cable combustion is observed, predominantly concentrated between 15 s and 75 s. The overall cable burning rate exhibits an initial increase followed by a subsequent decrease.

(3) Fire Development Process

Analyzing the fire's development process caused by transformer oil leakage into the cable channel reveals rapid oxygen consumption near the transformer oil due to combustion. If the transformer oil becomes depleted, the cable experiences only minimal burning. Conversely, if there is an ample supply of transformer oil, it ignites the cable in the channel. As oxygen concentration diminishes, both cable and transformer oil combustion are suppressed. After a certain duration, the cable ceases burning, leaving only the transformer oil to burn within the cable channel.

(4) Damage Distance Ranges

Under this study's operational conditions, the damage distance range for each cable layer is delineated. When the total transformer oil leakage falls between 1 L and 12 L, the maximum damage distance for the bottom, middle and bottom, middle and upper, and upper cables ranges from 15 m to 40 m, 18 m to 41 m, 27 m to 45 m, and 59 m to 60 m, respectively.

(5) Layer-specific Damage Distances

In this study's operational context, the upper layer cable exhibits the largest damage distance. When the total transformer oil leakage equals or exceeds 8 L, the lower layer cable manifests the smallest damage distance. Conversely, when the total leakage is 5 L or less, the damage distances for the lower layer cable, middle and lower layer cable, and upper layer cable do not surpass half the length of the cable channel (30 m).

Since such an underground cable passage structure is widely used in practical engineering, these conclusions can provide technical references for practical engineering applications, such as power operation and maintenance personnel, who can estimate the duration of the fire caused by the leakage of transformer oil in the transformer near the cable passage and estimate the length of cable damage to replace the cable in the most economical way. For fire prevention and control, since the amount of transformer oil entering the cable channel has a great impact on cable damage and fire development, operation and maintenance personnel can open channels on both sides of the underground cable channel near the transformer to make transformer oil flow into it rather than into the cable channel. It can also be designed in the transformer, the oil-bearing part of the layout, so that when deflagration occurs, there is an expected direction of leakage.

These comprehensive conclusions derived from numerical simulations provide valuable insights into the intricate dynamics of fire propagation and damage patterns within cable channels affected by transformer oil leakage.

Author Contributions: Resources, F.L.; Software, M.G.; Supervision, T.S.; Writing—original draft, L.Y.; Writing—review & editing, J.Z. and Y.L. All authors have read and agreed to the published version of the manuscript.

Funding: This paper is supported by the Science and technology project of Anhui Electric Power Co., Ltd., State Grid. The project name is the key technology and application of fire spread mechanism, monitoring, prevention and control of power cabin in integrated pipe gallery (52120523001C).

Institutional Review Board Statement: Not applicable.

Informed Consent Statement: Not applicable.

Data Availability Statement: The original contributions presented in the study are included in the article material, further inquiries can be directed to the corresponding author.

Conflicts of Interest: The authors declare no conflict of interest.

References

1. Mao, Z. Study and Feasibility Analysis of Bulk Strong Oil Drainage Scheme in ULTRA-High Pressure Rheological Change Fire. Ph.D. Thesis, South China University of Technology, Guangzhou, China, 2019.
2. Chen, T.; Zhao, L.; Fu, X.; Zhang, J.; Wang, Q.; Hu, C.; Bao, Z.; Li, B.; Li, G. Fire accident characteristics and firefighting solutions of large converter transformer. *Fire Sci. Technol. Fire Prot.* **2020**, *39*, 1138–1141.
3. Tao, L.; Zeng, Y.; Liu, Z.; Peng, J.; Zhou, X. Study on the influence of air curtain on fire temperature and flow field in subway tunnel. *China Saf. Sci. J.* **2021**, *31*, 157–163.
4. Mi, H.; Zhang, X.; Yang, W.; Wang, W.; Liu, Y.; Jiao, Y. Fire probability analysis method of cable cabin in urban utility tunnel. *China Saf. Sci. J.* **2021**, *31*, 165–172.
5. Liu, S.R.; Hu, Y.X.; Zheng, J.K.; Su, X.T.; Xu, Y. Dynamics simulation of 10 kV cable tunnel fire for single-phase arc grounding fault. *High Volt. Eng.* **2021**, *47*, 4341–4348. [CrossRef]
6. Matala, A.; Hostikka, S. Probabilistic Simulation of Cable Performance and Water Based Protection in Cable Tunnel Fires. *Nucl. Eng. Des.* **2011**, *241*, 5263–5274. [CrossRef]
7. Hao, G. Simulation Study on Fire Smoke in Cable Compartment of Integrated Pipe Gallery. Ph.D. Thesis, Xi'an University of Architecture and Technology, Xi'an, China, 2017.
8. Li, X. Numerical Simulation and Optimization Design of Ventilation System After Cable Cabin fire in Integrated Pipe Gallery. Ph.D. Thesis, Xi'an University of Architecture and Technology, Xi'an, China, 2018.
9. McGrattan, K.; Hostikka, S.; McDermott, R.; Floyd, J.; Weinschenk, C.; Overholt, K. *Fire Dynamics Simulator User's Guide*; National Institute of Standards and Technology: Gaithersburg, MD, USA, 2013.
10. Wang, Y.; Li, C.; Zhang, J.; Shang, F.; Lu, S.; Fan, M.; Cheng, D. Fire characteristic parameter analysis of KI50X UHV transformer oil. *J. Saf. Environ.* **2020**, *20*, 1361–1369.
11. Anonymous. Material Safety Data Sheet of KI50X DC Transformer Oil. Available online: http://kunlunlube.cnpc.com.cn/klrhy/msdstzy/201606/fa791152f8794a6199c7ba19fa8cfd7f/files/1740388a6a3d42e69e033aa95a89db5e.pdf (accessed on 3 June 2020).
12. Kai, L. Study on Fire Spreading Behavior and Smoke Flow Characteristics of Urban Underground Comprehensive Pipe Corridor. Ph.D. Thesis, China University of Mining and Technology, Xuzhou, China, 2020.
13. Hamins, A.; Maranghides, A.; Johnsson, R.; Donnelly, M.; Yang, J.; Mulholland, G.; Anleitner, R.L. *NIST Special Publication 1013-1. Report of Experimental Results for the International Fire Model Benchmarking and Validation Exercise #3*; NIST: Gaithersburg, MD, USA, 2005.
14. Tang, X. Study on Pyrolysis Kinetics And Radial One-Dimensional Thermal Expansion Model of Flame Retardant Cable. Ph.D. Thesis, University of Science and Technology of China, Langfang, China, 2018.
15. Wang, Y.; Li, C.; Zhang, J.; Shang, F.; Lu, S.; Fan, M.; Wang, L. Research on characteristics and countermeasures of oil-immersed transformer fire accident. *Saf. Environ. Eng.* **2019**, *26*, 166–171.
16. Wang, Y.; Li, C.; Zhang, J.; Shang, F.; Lu, S.; Fan, M.; Wang, L. Experimental Study on Combustion Characteristics of Insulating Oil of Typical Converter Transformer Based on Flame Spread Meter. *Saf. Environ. Eng.* **2020**, *27*, 190–196.
17. Shen, T. Research on Fire Risk of Metro Tunnel Wire and Cable. Ph.D. Thesis, Capital University of Economics and Business, Beijing, China, 2018.
18. Zhang, Z.; Wei, B. Preparation and Thermal degradation kinetics of palygorskite/silane crosslinked polyethylene composites. *J. Northwest Norm. Univ. (Nat. Sci. Ed.)* **2013**, *49*, 63–69.

MDPI AG
Grosspeteranlage 5
4052 Basel
Switzerland
Tel.: +41 61 683 77 34

Fire Editorial Office
E-mail: fire@mdpi.com
www.mdpi.com/journal/fire

MDPI

Academic Open
Access Publishing

mdpi.com

ISBN 978-3-7258-2516-5